UILU-ENG 89-3602

Report No. 148

A PLASTICITY THEORY OF METALS BASED ON THE DISLOCATION SUBSTRUCTURES

by

Shiing-Hwa Doong
Materials and Design Division
Department of Mechanical and Industrial Engineering

A Report of the
MATERIALS ENGINEERING - MECHANICAL BEHAVIOR
College of Engineering, University of Illinois at Urbana-Champaign
February 1989

A PLASTICITY THEORY OF METALS BASED ON THE DISLOCATION SUBSTRUCTURES

Shiing-Hwa Doong, Ph.D.
Department of Mechanical and Industrial Engineering
University of Illinois at Urbana-Champaign, 1988

ABSTRACT

A cyclic plasticity model developed from the microscopic deformation mechanism of metals is suggested. In the development of such a mechanistic model, the dislocation substructure of metals under different loadings is studied. Based on the observed substructure, the deformation mechanism of metals is described. The mechanisms that control the macroscopic mechanical behavior of materials are the change of dislocation substructures, the movement of active dislocations and the change in atomic spacing. By making quantitative assumptions for these mechanisms, a plasticity model is established. When compared to the experimental result, the model is found to be capable of predicting the mechanical behavior of metals under highly complicated loading conditions.

ACKNOWLEDGMENT

This study was conducted in Materials Research Laboratory and Material Engineering Research Laboratory of the University of Illinois at Urbana-Champaign and was supported by U.S. Department of Energy under contract DE-AC02-76ER 01198.

Professor D. F. Socie, thesis advisor, is gratefully acknowledged for his advice and encouragement. Special thanks are extended to Professor I. M. Robertson, Dr. P. Kurath, J. Bannantine, E. Liang and D. Jones for their assistance with experiments and stimulating discussions.

A special thanks is to Fan-Lin for her love and encouragement.

TABLE OF CONTENTS

Page

LIST OF TABLES

LIST OF FIGURES

LIST OF SYMBOLS

$\underset{\sim}{e}_t$	Total Deviatoric Strain Tensor
$\underset{\sim}{\varepsilon}_p$	Plastic Strain Tensor
$\underset{\sim}{\varepsilon}_c$	Strain Tensor Defining the Center of Elastic Region
$\underset{\sim}{\varepsilon}_a$	Strain Tensor Defining the Translation Direction of Elastic Region
$\underset{\sim}{s}$	Deviatoric Stress Tensor
$\underset{\sim}{n}$	Unit Tensor Defining the Plastic Direction
$\underset{\sim}{l}$	Unit Tensor Defining the Translation Direction of Elastic Region
σ_{eff}	Effective Stress
σ_L	Limit Stress
Cp	Plastic Compliance
A	Ellipse Area
ρ	Anisotropic Ratio
ϕ	Major Axis Orientation of Ellipse Model
E	Young's Modulus
G	Shear Modulus
ε_y	Effective Yield Strain
ν	Poisson Ratio

1. INTRODUCTION

The plastic deformation behavior of engineering metals has interested numerous investigators over the last several decades. Studies on this subject can be classified into three categories. The first kind of study emphasizes the quantitative description of the stress-strain relation [1-8]. Mathematical models or constitutive laws which can be used in engineering calculations are developed. Generally speaking, this approach has reached maturity over the last 30 years and many sophisticated plastic deformation details can be accurately modeled [9-13]. The second type of study investigates the dislocation substructure of the deformed material [14,15]. Through these studies the relation between the microstructure and the material strength is understood. An attempt of relating the substructure to the stress-strain curve in a quantitative way did not succeed because of the complexity of microstructures [16]. Study in the third category tries to derive the macroscopic stress-strain relation from the slip mechanism of metal crystals [17,18]. In this respect, mathematical theories are based on the knowledge about the kinematics of dislocation motion. Although this approach is very attractive from either a mechanical or physical viewpoint, its development is limited by the simplicity of assumptions regarding the slip mechanism and crystal structure [19].

Several problems still exist in the plasticity model currently used for the structural analysis. The advance of material testing technologies has greatly increased the information on the deformation behavior of metals [20-23]. In order to accommodate these new findings, the mathematical model has become increasingly complicated [9-12]. However, even with such high complexity, there are still many features which cannot be modeled successfully [12,13]. Moreover, it is uncertain if a model is capable of modeling the material behavior under a loading condition which cannot be achieved with current experimental techniques. A reason for this uncertainty is because the current plasticity models are not developed from deformation principles such as the slip, twinning, diffusion, and so on. They are based upon an artificial description of the experimentally observed stress-strain curve, usually the uniaxial case. By reviewing the development of these models, it can be found that little attempt has been made to understand why the stress-strain curve of a material will exhibit one particular feature before the mathematical model is established [3,4,6,8]. As a result, the mechanistic meaning of the variables and constants in the model are not clear and no rule can be followed when modifications for new observations are added.

Ideally, deriving the macroscopic stress-strain relation from the dislocation behavior is a very logical way of modeling metal plasticity. As mentioned earlier, the major problems of this approach are the assumptions about the crystal structure and slip mechanisms. The crystal structure of metals is much too complex to be assumed as a simple lattice. For instance, an FCC crystal can have 12 slip systems. How one dislocation moves in the crystal is dependent on the applied loading path, the slip mode, the grain size, etc. Many different explanations about the experimentally observed dislocation substructures also suggest that the current understanding about dislocation behavior is still far away from being capable of making quantitative assumptions at the microscopic level [24-30]. As such, developing a reliable mathematical plasticity model from this approach is quite unfeasible at this time.

A possible way of approaching the plasticity problem is to develop a semi-empirical model in which the slip mechanism and the experimentally observed dislocation substructure are utilized in establishing the modeling concept while material constants are still determined from the macro stress-strain curve. With this approach, each assumption of the constitutive model has a mechanistic basis and the validity of modeling a particular loading condition can be assured. If the reason for a feature of the stress-strain curve can be found and compared with the dominant material property, the material constant for a new material may be predicted without testing. The necessity of some expensive tests can be greatly reduced.

The purpose of this study is to pursue a mechanistic plasticity model. Although the capability of modeling the material behavior in a quantitative manner is the major goal of the proposed model, the mechanism for several important features in the stress-strain curve will be discussed. In particular, three deformation characteristics will be studied. The first one is nonproportional cyclic hardening behavior. It has been widely observed that the cyclic strain hardening under nonproportional loading is much more significant than that under proportional loading for materials like copper and stainless steels [20-23]. On the other hand, materials such as the 6061-T6 aluminum alloy was found to have no such differences in the cyclic hardening behavior [31]. A possible mechanism will be proposed to explain the material dependence of this phenomenon. Another characteristic is the change of the plastic modulus during the unloading and reloading process. In many nonlinear plasticity models [6,7,13], a major concern is the capability of describing features like the cyclic creep in the direction of the mean stress by unsymmetric stress cycles, the mean stress relaxation by unsymmetric strain cycles and the memory of the prior loading after material is cycled with a small strain amplitude. A general strategy for simulating these behaviors is changing the plastic modulus by introducing more variables in the calculation. Although many models have claimed success in simulating some of these features, there is still no model which can describe all of the features without a complex discrete memory code [13]. A possible mechanism which is responsible for all these features will be addressed. The last deformation characteristic to be studied is the cyclic hardening and softening of materials under symmetric strain or stress cycles. Although it is suggested that the observed hardening stage of the stress-strain curve results from a balance between the hardening and softening effects [32], the mechanism of these effects is still not clear. Without a physical understanding of these effects, it is quite easy to define variables and constants which are duplicative in their physical meaning and, therefore, increase the unnecessary complexity of the model. In this study, a model for the dislocation substructure will be used to explain the possible reason of material hardening and softening under complex loadings.

2. EXPERIMENTS

2.1 Material Properties

Polycrystalline OFHC copper, 1100 aluminum and 310 stainless steel tubular specimens were machined from round bars. Specimen details are shown in Ref. [33]. Prior to testing, aluminum was found to have elongated grains along the longitudinal axes of the specimens. Copper and 310 stainless steel showed equiaxial grains with an average size of 0.56 mm and 0.013 mm respectively. The dislocation substructures of these materials before testing are shown in Figs. 1 to 3.

2.2 Testing and Results

A tension-torsion test frame was used to perform biaxial strain controlled tests at room temperature. Twelve 1100 aluminum, five copper and six 310 stainless steel specimens were tested by either torsion or 90° out-of-phase tension-torsion. The axial strain applied ranged from 0.0007 to 0.0035 and the shear strain ranged from 0.0009 to 0.0061. All specimens were cycled to failure which was defined as a 10% load drop from the stabilized condition. Results of these tests are shown in Table 1 to 3. The stabilized stress values reported were recorded at half the cycles required for failure.

The stabilized shear stress is also plotted as a function of the shear strain in Figs. 4 to 6. Additional data on the 304 stainless steel and the 7075 aluminum alloy, which were tested by Kurath [34], Bannantine [35] and Jones [36], were collected for comparison. The compositions and properties of these materials are given in Ref. [34] and [35]. Figures 7 and 8 show the relation between the stabilized shear stress and the shear strain of these materials. Since a 90° phase difference is found between the axial stress and shear stress when the material is cycled by the 90° out-of-phase loading, the amount of hardening can be represented by the stabilized shear stress.

In order to examine the plasticity model, two aluminum and four 310 stainless steel specimens were tested by either biaxial or uniaxial strain controlled loadings. The biaxial loading paths include squares and stairs of different step sizes, see Figs. 9 to 15. The uniaxial test is a tensile test of changing amplitude, Fig. 16. The biaxial stress-strain response is presented by four kinds of diagrams: axial strain vs. shear strain, axial stress vs. shear stress, axial strain vs. axial stress and shear strain vs. shear stress. In the axial strain vs. shear strain diagram, both the total strain and plastic strain histories are plotted. The plastic strain is evaluated from the recorded total strain and stress by assuming

$$\varepsilon_p = \varepsilon_t - \sigma/E, \tag{2.1}$$

and

$$\gamma_p = \gamma_t - \tau/G \tag{2.2}$$

in which ε_t and γ_t are the total axial and shear strains, ε_p and γ_p are the plastic axial and shear strains, E is the Young's modulus and G is the shear modulus. σ and τ are the axial and shear stresses. Similar test results on 304 stainless steel are also presented in Figs. 17 to 20 [35,36].

2.3 Microstructural Examination

After failure, small samples suitable for electron microscopy were cut from the bulk region of the tubular specimens by using a diamond blade saw. These samples were then mechanically polished to about 0.2 mm and, finally, jet-electropolished to produce areas suitable for examination in the transmission electron microscope. A Phillips EM400T electron microscope operating at 120V was used to examine the dislocation substructures. In addition to the three materials tested in this study, the dislocation substructures of 304 stainless steel and 7075 aluminum alloy were also examined. Tables 4 and 5 list the testing results of the specimens chosen for this substructural investigation. Figs. 21 to 34 are the observed dislocation substructures. Table 6 is a summary of the dislocation substructures observed for different materials.

3. DISLOCATION SUBSTRUCTURES

The formation of dislocation substructures represents the physical change of metals during plastic cycling. To develop a mechanistically based plasticity theory, this physically observed change in metals has to be understood. In this chapter, the current understanding about the dislocation substructure will be reviewed briefly. The results of the microscopic observations made in this study will be presented and discussed. A possible mechanism for the nonproportional cyclic hardening of metals will be suggested.

3.1 Background

Over the last several decades, dislocation substructures in metals under proportional cyclic loading have been extensively studied by transmission electron microscopy [15,24-30,37-46]. Generally speaking, these substructures can be classified into five categories - planar dislocations, matrix veins, ladders or walls, cells and labyrinths [24-26]. Structures consisting of only planar dislocations occur in low stacking fault energy materials. Matrix veins are tangles of edge dislocations along major slip planes. Between these tangles, channels free of dislocations are also formed by the movement of screw dislocations. Ladders are bands with cleared channels and dense walls. It is believed that the ladders and walls are formed by small-scale secondary glide in the matrix veins when a critical dislocation density is reached [27,28]. The formation of cell structures was found to be associated with multiple slip systems [28]. The strong light-dark contrast across cell walls is normally used to differentiate cells from walls. Labyrinth structures are perpendicularly orientated walls formed when many slip systems are activated [29,30].

The dislocation substructures were also compared to the slip mode of materials [37,38]. In the study of a Cu-Zn alloy, Lukas and Klensnil [37] found that, as the slip mode changed from wavy to planar slip, the dislocation substructure changed from cells and ladders to planar dislocations. A similar result was reported for a Cu-Al alloy by Saxena and Antolovich [38]. Together with the understanding about the slip systems involved in various structures, these observations clearly indicate that dislocation structures are determined by the number of active slip systems which is dependent on the slip mode of the material.

The observed substructures are also affected by the applied strain range, the number of cycles applied, the distance from the grain boundary, the depth beneath the specimen surface, etc. An increase in the strain range tends to form more cell structures in copper [37]. Ackermann, et al. [25] suggested an evolution procedure for copper crystals cycled at high strain levels. In general, increased accumulated plastic strain during cycling activates more secondary slips and, therefore, results in multi-slip structures. Figueroa and Laird [39] showed that multi-slip structures might form in the region adjacent to the grain boundary when the interior substructure was walls. Winter, et al. [26] compared several samples of polycrystalline copper at different depths. Although no obvious difference was observed in their structures, dislocation-free zones were reported at grain boundaries and surfaces.

3.2 Experimental Results and Discussion

The dislocation substructures observed for each material will be illustrated separately. As the purpose of this study is to compare the substructures of materials resulting from different loading paths and relate the microstructures to the macroscopic stress-strain curves, only the general features of these substructures will be described. Discussion will be focused on the effects of changing the maximum shear planes by nonproportional loadings. More detailed understanding of the formation procedures of these substructures requires further investigations.

3.2.1 1100 Aluminum

The dislocation substructures of aluminum under proportional loading have been found to be either dipoles or cells [15,40]. The strain ranges for forming these structures have been suggested by Grosskietz and Waldow [40]. A transition from dipoles to cells was found when the applied strain range was about 10^{-4}. Increasing the strain range starts to decrease the cell size. Figure 21 shows the dislocation cells formed in 1100 aluminum cycled with a shear strain of 0.0017. Similar structures, Fig. 22, were observed in specimens loaded with 90° out-of-phase tension-torsion loading. For the strain range studied, no major difference in cell size was observed although a higher contrast between cells for the latter case was noticed. This difference may be attributed to local rotation between the cells.

A comparison of the stable stress response for proportionally and nonproportionally loaded cases is shown in Fig. 35. The strain range for the formation of each substructure proposed by Grosskietz and Waldow [40] is also given. The substructures are not changed by the loading path. This consistency in the substructures can be explained by the wavy slip mode of aluminum. Under in-phase torsional loading, even though the maximum shear planes are fixed, the stresses from the dislocation interactions and the constraint of grain boundaries can easily cause slip in all directions so that equiaxial cell structures are formed. Although 90° out-of-phase tension-torsion loadings can activate many slip systems by changing the maximum shear planes, the number of active slip systems is nearly the same for both cases and the dislocation substructures are, therefore, unchanged. The similarity in cell sizes also suggests that similar mechanisms are responsible for forming these cells.

3.2.2 OFHC Copper

Five kinds of dislocation substructures have been observed in copper [24,26]. With increasing plastic strain range, these substructures are matrix veins, ladders, walls, cells and labyrinths. For torsional cases, dislocation substructures are basically the same as those for uniaxial tension. Structures like ladders, Fig. 23, walls and cells, Fig. 24, are observed. For 90° out-of-phase loading, uncondensed cells, Fig. 25, are observed at very low strain ranges. Labyrinths, Fig. 26, walls, Fig. 27, and cells, Fig. 28, are the major substructures at higher strain levels.

In comparing the substructures in copper produced by the different loading paths, two differences are noticed. First, multi-slip structures such as cells and labyrinths are found in nonproportionally loaded specimens at strain levels much lower than those observed in proportionally loaded specimens, Fig. 36. Second, the size of cells formed by 90° out-of-phase loadings, Fig. 28, are smaller than those observed in torsionally cycled specimens, Fig. 24.

Since copper is a wavy/planar slip material, dislocations cannot cross slip as easily as in aluminum. In the case where the major slip plane is unchanged by the applied loading, such as the proportional loading condition, the amount of secondary slip depends on the strain range applied. An increased amount of secondary slip will be activated as the strain range increases. Associated with this increase of secondary slip is the transition of the substructure of copper from a single-slip to a multi-slip structure. The formation of multi-slip structures at the lower strain levels indicates that the rotation of maximum shear planes have formed more active slip systems. Since higher plastic strain ranges have been found to result in smaller cell sizes by increasing the secondary glide, the decrease in the cell size in this case may also result from the increase in the number of active slip systems. The effect of rotating maximum shear planes by nonproportional loadings is, therefore, to decrease the required strain range of forming multi-slip structures in copper.

3.2.3 Stainless Steels

Extensive studies of the dislocation substructures in stainless steels after cyclic tension have been performed at different temperatures [42-44]. The observations made by Abdel-Raouf, et al. [42]

indicates that planar dislocations are the major substructures in 304 stainless steel at room temperature. Dislocation cells and subgrains were found at elevated temperature. It is suggested by Challenger and Moteff [43] that the transition from cells to subgrains occurs at a test temperature between 650 and 816°C.

In this investigation, no difference was found between the substructure of 304 and 310 stainless steels. During proportional loading, stainless steels exhibit planar dislocations, Fig. 29, and walls. Tangles of dislocations, Fig. 30, are the major substructures in stainless steels cycled with proportional loadings at low strain ranges. As the strain range increases, walls, Fig. 31, cells, Fig. 32, and labyrinths, Fig. 33, are observed. Substructures with combined features were quite often found.

A comparison of the substructures in stainless steels suggests that a material showing single slip structures under proportional cycling will exhibit multi-slip structures if the major slip plane is rotated by nonproportional loading paths. This feature also occurs in copper except that more cross slips are involved in the substructures of proportionally cycled copper. The planar-slip material is, therefore, more sensitive to the loading path than wavy and wavy/planar slip materials.

3.2.4 7075 Aluminum Alloy

Homogeneously distributed dislocation tangles, as shown in Fig. 34, were found to be the major feature in 7075 aluminum alloy under both torsion and 90° out-of-phase tension-torsion. A comparison with the microstructure before testing indicates that dislocation substructure remains unchanged even though the specimen has been cycled to failure. Two possible reasons are used to explain why little change was observed. First, the applied plastic strain ranges are so small that the deformation is basically elastic. Second, the observation made in this study only represents the substructure in the bulk region of the material which is responsible for the macroscopic stress-strain response. Fatigue failure is initiated from the persistent slip bands which have been observed in areas close to the surface and crack tip even when the applied stress is far below the yield stress [45,46]. Tests at higher strain level may be necessary to examine how the nonproportional loading path affects the substructure.

3.3 Nonproportional Hardening

It has been widely observed that the cyclic strain hardening under nonproportional loading is more significant than that under proportional loading for materials like copper and stainless steels. The work by Krempl and Lu [22] showed that, among various nonproportional loading paths, 90° out-of-phase tension-torsion cycling exhibited the strongest hardening behavior. On the other hand, a material such as aluminum alloy 6061-T6 does not exhibit such differences in the cyclic hardening behavior [31].

For the materials tested in this study, different cyclic hardening behavior is also observed. As shown in Fig. 35, 1100 aluminum shows no difference in the cyclic hardening level between torsion and 90° out-of-phase tension-torsion loading. Copper and stainless steels, however, exhibit a 30 and 50 percent increase in the saturated stress when loaded nonproportionally, see Fig. 36 and Fig. 37.

Kanazawa et al. [21] suggested that, when materials were cycled by nonproportional loadings, the rotation of the principal strain axes during each cycle prevented the material from forming stable dislocation substructures so that the stress-strain curves for out-of-phase loadings were above those for in-phase loadings. It is, however, not understood why the aluminum alloy 6061-T6 does not show this behavior. The interpretation of more dislocation interactions due to the change of maximum shear planes cannot explain the material dependence of this cyclic hardening phenomenon.

McDowell et al. [47] studied the deformation products of type 304 stainless steel subjected to nonproportional loadings. In their study, the directional distributions of slip bands and transformed materials were found to be more homogeneous for nonproportionally loaded specimens. Although this observation could be related to the rotation of principle strain axis directly, no quantitative relationship was identified. The micromechanical interpretation suggested in that study followed the same concept as that proposed by Kanazawa et al. [21] Why additional cyclic hardening is material dependent remained unanswered.

The difference in the cyclic hardening behavior can be easily explained by the change of dislocation substructures. Since 1100 aluminum exhibits cell structures under both torsion and 90° out-of-phase tension-torsion, there is no difference in its hardening levels. Copper and stainless steels which change their slip mechanisms under nonproportional loading exhibit additional cyclic hardening. Cells and subgrains have been observed in stainless steels at high temperatures. These results suggest that stainless steels will have no additional hardening under nonproportional cycling if the temperature is high enough for the cross slip to occur under proportional loading.

The argument that the increase of cyclic stress results from the change of dislocation substructure from single slip to multiple slip is further supported by earlier tests on copper crystals. Jin and Winter [29] showed that labyrinth structures could be formed in copper crystals if the tensile axis was along the [001] direction. When compared to the ladder structures formed by single slips, labyrinth structures exhibit a 40 percent increase in the saturated stress. With a similar change in the microstructures, copper and stainless steels increase their hardening levels under nonproportional loading.

Although it is believed that the slip mode of dislocations plays an important role in the cyclic hardening behavior of metals, other factors such as the stress-induced phase transformation in some stainless steels and persistent slip band formation in precipitated materials still need to be studied. A comparison between the cyclic stress-strain relations of 304 and 310 stainless steels in Fig. 37 shows no major difference in their hardening behavior. However, measurements of Bannantine [35] show up to 6 percent of the 304 stainless steel undergoes a stress-induced phase transformation to martensite after cycling. Similar measurements on 310 stainless steel specimens do not show such a phase transformation. These limited results indicate that the martensite phase transformation does not play a major role in the nonproportional hardening of 304 stainless steel.

4. THEORETICAL BASIS

The large scale computing capability of the modern computer system has greatly changed the direction of the research on plasticity. Before 1970, most of the researchers were concerned about the thermodynamic principles and the mathematical theory of plasticity. The loading condition that was actually modeled in that period was quite simple. As the technology of computation and material testing improved quickly in the 1970's, the development of the plasticity theory was to meet the industrial requirement in which the accuracy and efficiency of the model were important. A large number of plasticity models which dealt with complicated loading conditions were developed.

Although many different models have been proposed, they are either directly or indirectly based on a theory that was fully established in the 1950's. This theory, sometimes called the classical plasticity theory, is the basis of studying plasticity modeling. Searching for a mechanistic modeling method, this chapter starts with a brief review of the classical plasticity theory. After that, the classical theory is compared to the micro deformation mechanism of metals. A possible plasticity modeling method developed from a mechanistic point of view is suggested. In the end, a comparison is made between the proposed method and the classical plasticity theory. Implementation and comparison of the model with the experimental result are performed in the next chapter.

4.1 The Classical Plasticity Theory

Reviewing classical plasticity theory is not an easy task as it has been intensively studied from many different viewpoints and several modifications have been made in the progress of this theory. Since this study is concerned with the application of plasticity theory, discussion will be focused on the aspect that directly influences the philosophy of constitutive modeling, i.e. assumptions for the yield surface, the flow rule and the hardening rule. In particular, emphasis of the discussion will be placed on the assumptions related to the deformation mechanisms. Mathematical formulation of various models is listed in the Appendix.

4.1.1 The Yield Surface

The yield surface is a scalar function in stress space that defines the state of stress at which the material starts to deform plastically. According to Drucker's second postulate [48], the yield surface has to be convex toward the origin of the stress space. A material is said to be elastically deformed if the stress tensor remains inside the yield surface. Otherwise, the material has plastic deformation.

Different formulations have been suggested to define the configuration of the yield surface. The most well-known yield surface functions for metals are the von Mises and Tresca yield criteria [49]. Since the von Mises yield criterion is simpler than the Tresca criterion, it has been widely used in the plasticity modeling.

Extensive research has been conducted to determine the yield surface experimentally [50-52]. In general, the yield surface of metals falls between the Tresca and von Mises yield criteria before the metal is plastically deformed. After plastic deformation, the yield surface is found to undergo translation, rotation and distortion [50]. Many researchers also reported corners on the subsequent yield surface [50,51]. Because different methods are used to define the yield point, no conclusion is made regarding the behavior of the yield surface after plastic deformation.

To account for the observed change of the yield surface, mathematical formulation for the yield surface has also been modified. The most important modifications are changes in the size of the yield surface, called isotropic hardening [1], and the translation of the yield surface, called kinematic hardening [3]. Methods that account for the distortion of the yield surface have also been suggested [53].

4.1.2 The Flow Rule

A flow rule is used to define the relation between the stress and the plastic strain. In the incremental plasticity theory, this relation is given as an equation which relates the stress tensor (or stress rate tensor) to the plastic strain rate tensor.

In the classical plasticity theory, there exists a generalized theorem about the behavior of plastic flow [1]. It is believed that the plastic flow of materials can be described by a thermodynamic potential, called the loading function. Physically, the loading function can be viewed as a potential difference resulting from the applied loading and the material resistance. The plastic flow is said to be along the direction that is defined by the derivative of the loading function with respect to the stress. The plastic strain increment tensor is obtained by multiplying a unit tensor of that direction with a scalar representative of the magnitude of the increment.

The loading function is different from the yield function from both theoretical considerations and experimental observations [54]. However, these two functions are assumed the same in most constitutive models [6-9]. A plasticity model is called associated if the loading function is the same as the yield function. For this case, the plastic flow has the same direction as the outward normal of the yield surface. A plastic model which has the loading function different from the yield function is called nonassociated [49].

4.1.3 The Hardening Rule

In developing the flow rule of plasticity theory, it has been implicitly assumed that, when the material starts yielding, the external loading is larger than the material resistance. Like a fluid, the material is expected to deform continuously even if the applied loading remains unchanged. However, this assumption is not valid as most metals exhibit a limited amount of plastic deformation after yielding. This discrepancy is believed to be associated with certain changes in the material that increase the material resistance after yielding. The purpose of the hardening rule is to describe this kind of change in the material.

The number of hardening rules depends on the loading function used. Each of the variables that define the material resistance can be modified to account for the related change in the material resistance. For associated models, the loading function is the same as the yield function. Changes in the material resistance are, therefore, same as changes in the shape of the yield surface. As a result, the kinematic and isotropic hardening rules which have been used to describe changes of the yield surface also describe the associated changes in the material resistance.

Mathematic formulation of the hardening rule varies between models. In fact, this is the major reason that plasticity models are different from each other. Since changes of the material resistance result from the plastic deformation, most of the hardening rules are functions of the plastic strain [5,7]. A scalar like the effective yield stress, or size of the yield surface, can be easily assumed to be a function of the accumulated plastic strain, or plastic work. The detailed relation between these two quantities is normally determined from experimental data. For a tensorial variable such as the back stress, or center of the yield surface, both the direction and magnitude of the change has to be specified. The assumption for the translation direction is particularly important for nonproportional plasticity models as the location of yield surface influences the direction of plastic flow. It has been concluded by McDowell [55] that the Mroz kinematic hardening rule can predict the flow direction better than others. In general, material constants are necessary in determining this change.

4.1.4 The Consistency Condition

Upon loading of a hardening material, both the applied loading and the material resistance increase. For a given stress level, the material will deform to an equilibrium state at which the applied force equals the material resistance. If not, the material becomes unstable and failure occurs. This equilibrium condition is used to determine the amount of plastic deformation for a plasticity model considering strain hardening. An equation describing this condition is called the consistency equation.

Mathematically, the equilibrium condition is described by taking the derivative of the loading function with respect to stress [49]. Because the value of the loading function remains constant, its derivative is zero. The consistency equation is, therefore, a derivative equation of the loading function in which the variable for the material resistance has often been assumed as a function of the accumulated plastic strain.

4.2 A Critical Review of the Classical Plasticity Theory

Under the general frame work laid out by the classical plasticity theory, engineers face the following difficulties. First, the number of material constants continue to increase when new findings have to be accommodated. It is still unknown how many constants are required to predict all the possible features of the stress-strain curve. Second, there is no direct connection between the mathematical plasticity theory and the deformation mechanism. It is quite difficult to understand the theory from a mechanistic point of view. Consequently, instead of being a model for the physical phenomenon, plasticity theory has become a mathematical puzzle for many engineers and students. Third, using classical plasticity theory, it is generally difficult to predict the material behavior without performing a detailed series of experiments to validate the plasticity model for a given material.

The difficulties of classical plasticity theory arise from the lack of understanding about the complex mechanism of plastic deformation. Plasticians have argued that classical plasticity theory is a phenomenological approach which is based on the observation of experimental results [13]. Material testing and data acquisition technologies were, however, very limited during the early development period of plasticity theory. Many essential assumptions of that theory were developed from the stress-strain response of materials under highly simplified loading conditions. Although the hardening rule of the theory has been modified after the early development period, assumptions such as the yield surface and the flow rule have not been changed. The plasticity model which is used to deal with today's complicated loading conditions is still based on several over-simplified testing results produced in the early days.

In view of the difficulties in the current development of a plasticity model, it is suggested that all the assumptions made in the classical plasticity theory be examined and compared to testing results for complex loadings and microstructural observations. A critical review of classical plasticity theory from such an examination is presented in the following sections.

4.2.1 The Concept of Yielding

The existence of a yield surface which is defined by a scalar function in stress space is the most essential assumption for classical plasticity theory. Both the flow rule and the hardening rule are based on this assumption. However, definition of the yield point and function of the yield surface have not been clearly specified in the classical plasticity theory.

Two possible methods of defining the yield stress are shown in Fig. 38a. In the first choice, the yield stress is assumed to be the point where the stress-strain curve departs from the linear elastic portion. It can be found that, with this choice, it is usually difficult to specify how the yield stress may change during cyclic loading. Another choice is defining the yield stress by the intersection of the linear elastic stress-strain curve with a line tangent to the nonlinear stress-strain curve at a higher stress level. In this case, the yield stress is dependent on the hardening behavior at the higher stress level that, in many models, is defined by other variables. The yield stress is, therefore, not a variable independent from others.

Definition of the yield stress is found to be highly dependent on the purpose of usage. For example, if the yield stress is used to define the upper limit of elasticity analysis, the 0.2% yield point seems to be a reasonable choice. For an elastic-linear plastic model, the yield point could be defined as the intersection of two linear curves. In many nonlinear models, the radius of the yield stress has been used to account for the hardening of the material. However, based on the experimental data, Lamba [56] has concluded that the portion of the stress-strain curve where the slope is extremely small is more important than the shape of the yield surface. Dafalias and Popov [57] proposed that it was possible to treat almost any material as having no purely elastic region by developing a function which was linear for the range that would otherwise be defined as elastic. The purpose of defining the yield surface is, therefore, very confusing for the nonlinear elasto-plastic model.

From a micromechanical point of view, the meaning of yield stress is also unclear. For many commercial metals, a large number of dislocations already exist before they are plastically deformed. The stress required for a dislocation to slip depends on the crystal orientation, the arrangement of inactive and active dislocations, etc. In one particular grain, dislocations may start to slip at one stress level because of the suitable crystal orientation when dislocations in other grains still remain immobile. After the dislocation starts to slip, further plastic deformation may become easier by creating many mobile dislocations through various dislocation resources or the movement of dislocation may stop as a result of the increased interactive stress between dislocations and grain boundaries. For this reason, it is almost impossible to define a stress level at which the material can be said as to start yielding from a microscopic point of view. The smooth transition of the stress-strain curve from the linear elastic region to the nonlinear plastic portion is a reasonable response for most materials. The case where the yield point is clearly defined by a sharp corner in the stress-strain curve only occurs in materials such as carbon steel. This results from the pinning of dislocations by a second phase and should be looked as a special case for the plasticity modeling of metals.

4.2.2 The State Variables

The idea of using state variables has been introduced in plasticity and creep modeling of materials [8,58,59]. The state variable is a scalar or tensorial variable that quantitatively describes the deformation state of the material after plastic deformation. Although different methods have been suggested to define the state variables of metals, they are still based on the observation of the macroscopic stress-strain curve [58,59]. Generally, it is not possible to relate those variables to the microstructure of the material [16].

In the classical plasticity theory, every variable that is used to define the material resistance in the loading function can be viewed as a state variable. For a simple model with only isotropic and kinematic hardening, the state variables are the yield and back stresses. In many nonlinear models, additional parameters are introduced to adjust the plastic modulus so that more sophisticated features of the stress-strain curve can be modeled [8]. These parameters should also be viewed as state variables. The number of state variables required to simulate all the possible features of the stress-strain curve remains unknown.

A major problem in the current plasticity model is whether or not their state variables are independent. Ideally, a model can introduce an infinite number of variables in order to fit the data successfully. However, a good engineering model should include a minimum number of variables while being capable of simulating complex loading conditions. It is postulated that these kinds of state variables can only be obtained from a good understanding about the deformation mechanism of materials instead of the observation of the macroscopic stress-strain curve. If a variable is developed from macroscopic observation, it should also be verified by the deformation mechanism of the material.

In examining the state variables of the classical plasticity theory, two difficulties arise. First, the state variables defined in the classical plasticity theory are all stress related quantities. Since stress is not a physically observable quantity, interpretation of those variables require further assumptions about the stress field of the substructure. Usually, the validity of those assumptions cannot be verified. Second, the deformation substructure can only provide general information about the hardening level. For example, Kayali and Plumtree [15] showed that the peak cyclic stress was inversely related to the cell size. If the cell size of a material is measured and used as a state variable, the amount of hardening can be defined. The cell size, however, cannot be used to indicate the level of yield stress which, in the classical plasticity theory, has been used to specify the amount of material hardening. As mentioned earlier, the concept of the yield stress is to define the stress at which the plastic deformation starts. A material can have a large amount of hardening but a low yield stress. On the other hand, a material with no strain hardening may have a relatively high yield stress. For this reason, it is quite difficult to develop a microstructural explanation for the yield surface. Clarification for the mechanistic meaning of the back stress is even more complicated. Since the back stress is a tensorial quantity, establishing a relation between the microstructure and the stress tensor requires many assumptions and simplifications about the crystal structure and the behavior of dislocations. The validity of such assumptions is also difficult to verify. A possible reason that the major state variables of the classical plasticity theory have not been successfully explained by the microstructure of materials may result from their stress-defined character.

4.2.3 The Flow Rule

The flow rule of the classical plasticity theory is derived from two approaches. The first approach assumes that the plastic work is always positive [48]. By assuming the existence of the yield surface, the plastic flow is found to be along the outward normal direction of the yield surface. Another approach is from the concept of thermodynamic potential [1]. With this approach, the plastic flow direction is obtained by differentiating the loading function with respect to stress.

Although each of the approaches mentioned above has its theoretical background, experimental verification of them can not be easily accomplished. In the first approach, the existence of a yield surface in stress space must be assumed. According to the previous discussion, most metals do not show a boundary that clearly separates the stress space into either plastic or elastic. As the assumption of a clearly defined yield surface is very critical in proving the normality property of the flow rule [48], the applicability of this approach to the material which has a vague yield surface is still questionable. Difficulties for the microstructural examination of the second approach arises from the definition of the loading function. Loading functions are abstract quantities that can not be easily verified by the observed substructure without many assumptions. The continuous modification of the definition of the loading function also increases the difficulty of choosing a correct formulation. Perhaps, further research on the thermodynamics of solids is necessary to determine the appropriate form of the loading function.

4.3 A Mechanistically Based Model

According to the observed dislocation substructure and the deformation mechanism of metals, it is suggested that a mechanistic plasticity model should consider at least three mechanisms. The first mechanism is the change of the dislocation substructure during plastic deformation. Since the dislocation substructure is generally formed by inactive dislocations, the geometry of these substructures influences the hardening level of materials. Appropriate variables and evolution rules which describe the observed substructure should be chosen in defining the deformation state of the material. The second mechanism is the fact that, when a metal is deformed, a certain amount of strain is accomplished by adjusting the atomic spacing. Strain formed by this mechanism is linear and elastic. As only a limited amount of strain can be accommodated by this mechanism, a stress or strain range in which this mechanism is dominant has to be specified. The third mechanism considers plastic flow formed by the slip mechanism. In general, this mechanism is associated with the active dislocations which slip between the inactive dislocation substructure. A schematic diagram describing the relation between the active and inactive dislocations, which is motivated from the interpretation of the dislocation substructure by Laird [41] and Mughrabi et al. [60], is shown in Fig. 39. A smaller distance between the inactive dislocations increases the interactive stress among active dislocations and, therefore, the level of cyclic hardening. The configuration of the dislocation substructure can also be changed by the movement of active dislocations particularly when a large deformation or force is applied. These changes, however, occur at a slower rate than that of the active dislocations. Details of the hysteresis loop are determined by the behavior of these active dislocations.

To construct a plasticity model, quantitative assumptions have to be made for each of the mechanisms mentioned previously. The accuracy and efficiency of the model depend on the assumptions of these mechanisms. In this section, a possible set of assumptions which can be made for each mechanism are discussed. Equations based on these assumptions are also presented.

4.3.1 The Dislocation Substructure

For the purpose of plasticity modeling, it is normally necessary to define certain features of the deformed material in a quantitative way so that the mechanical properties can be defined. Although the experimentally observed dislocation substructure provides direct information about the deformation state of metals, they have not been used in the plasticity modeling. Since the purpose of this study is to develop a plasticity model that is as close to the deformation mechanism of metals as possible, the dislocation substructure is used as a major state variable of the material. In the following, a method of defining the dislocation substructure of materials under biaxial loadings will be presented. The relation between the substructure and the material strength will be discussed. Evolution of the substructure under several loadings of changing path is described with experimental results.

4.3.1.1 Description of the Dislocation Substructure

Description of the dislocation substructure formed by biaxial loadings is based on the geometry of the dislocation-free zone. Two features of these zones are considered important: the size and anisotropy. To simulate these two characteristics, an ellipse defined by its area, major/minor axis ratio and major axis direction is suggested. The physical meaning of this model can be visualized by comparing a cell to a ladder. In Fig. 40, it can be seen that the geometry of a cell is close to a circle which is just an ellipse with its major/minor axis ratio equal to one. A ladder is geometrically similar to an ellipse which has the major/minor axis ratio larger than one. The choice of using the ellipse area as a variable allows the cell size to be explicitly defined.

For other substructures, the physical meaning of the ellipse model cannot be defined by purely geometrical comparison. Interpretation of the variables has to be based on the formation of the substructure.

Since a single-slip structure such as the planar dislocation and matrix vein usually has a major slip direction, the stress required for the dislocation to slip is a function of direction as the level of interaction between dislocations is direction dependent. For wall structures, anisotropic behavior can be expected as a higher stress is required for the dislocation to cross the wall than along the wall. Although it is quite difficult to estimate how the stress may change with direction for each substructure, the over-all anisotropy of the mechanical properties of materials can always be viewed as an ellipse with an appropriate major/minor axis ratio.

In fact, a quantitative model for each kind of substructure is unnecessary. For most polycrystalline metals, the change of the crystal orientation from grain to grain, the effect of grain boundaries and material processing procedures make all kinds of substructures possible in the material. The ellipse suggested here is a qualitative estimate for the relative amount of each substructure in the material.

Because the ellipse is used to symbolize the deformation state of the material, assumptions have been made as simple as possible. From a mechanical point of view, two perpendicular orientated ellipses may be necessary as there are always two maximum shear planes under two dimensional loading conditions. However, because one ellipse is enough to characterize the anisotropic properties of the material, a transformation is suggested to relate the model to the physical substructure of materials. As shown in Fig. 41, a geometry of two perpendicularly orientated ellipses can be transformed into one ellipse if the rotation coordinate is doubled. For the biaxial case, the model with one single ellipse can be directly used in a strain based formulation to determine the material strength in each direction. It will be seen later that many important features in the stress-strain curves are better explained by one ellipse rather than two.

4.3.1.2 The Strength of Material

The strength of a material is defined as the stress required for the material to undergo a certain amount of plastic deformation. Because the stress is very sensitive to the strain when the plastic strain is small, it would be more appropriate to define the material strength by choosing a stress at which the stress-strain curve approaches a constant stress value. The constant used to define the exponent of the power law stress-strain curve can also be used as a measure of the material strength.

According to previous discussions, the stress required for a dislocation to slip is dependent on the substructure of the material. Because the distribution of inactive dislocations is not uniform for most single-slip structures, the strength of material is generally a function of the slip direction. Using the concept that the interactive stress increases as the dimension of dislocation-free zone reduces, the stress, S, required for slip to occur along a direction, θ, can be related to the ellipse by

$$S \propto \frac{1}{D(\theta)} \tag{4.1}$$

where $D(\theta)$ is the dimension of the ellipse along the slip direction. With this assumption, the material strength associated with a particular dislocation substructure is determined.

4.3.1.3 Evolution of the Dislocation Substructure

The evolution of the substructure in the material during the cyclic loading can be described by changing the variables which define the ellipse, i.e. the ellipse area, the major/minor axis ratio and the major slip direction.

For an annealed polycrystalline material, the deformation state is represented by a circle with a relatively large radius. If this material is plastically deformed, the ellipse area which represents the cell size should decrease and approach a stable value as the accumulated plastic strain or plastic work increases. The stabilized area is a function of the number of slip systems activated in the material. More active slip systems result in a smaller ellipse area as the dislocation density increases. The nonproportionality of the loading path is a major factor in determining the number of active slip systems. As the amount of cross slip may be increased by increasing the strain range, the stabilized ellipse area is also a function of the strain range. The major/minor axis ratio of the ellipse is related to the number of slip planes activated in the material. If slip is activated along all possible directions, the anisotropic ratio is one. Otherwise, it becomes larger than one. In this case, direction of the major axis has to be defined. The direction along which most active slip systems occur is the major slip direction. In two-dimensional strain plane, the major axis of the ellipse is orientated in the direction with the most plastic strain.

Since the dislocation density cannot be decreased by increasing the accumulated plastic strain, the ellipse area is a monotonically decreasing function of the accumulated plastic strain. In contrast, the major/minor axis ratio and the major axis orientation are dominated by the loading condition of the last several cycles. In other words, the major/minor axis ratio and the major axis orientation are "temporary" memory and can be "washed out" by changing the loading direction. Several examples are given to illustrate the change of dislocation substructures by different loadings.

1) Aluminum Under Proportional and Nonproportional Loadings

Fig. 42 describes how the deformation state of aluminum changes during torsion and 90° out-of-phase tension-torsion cycling. Under the annealed condition, the deformation state can be symbolized by a circle with a large area. As the accumulated plastic strain increases, the ellipse area becomes smaller as the cell size decreases. Since multi-slip structures are formed in aluminum under both loading conditions, the major/minor axis ratio is always one. The material has a constant strength along all directions.

2) Stainless Steel Under In-Phase Tension-Torsion

Under proportional tension-torsion, the deformation state of the annealed stainless steel starts with a circle and then evolves into an ellipse with a smaller area as shown in Fig. 43. The substructure implied by the ellipse is planar dislocations. It can be seen that there are two components influencing the hardening level. The decrease of the ellipse area represents the hardening effect resulting from the accumulation of dislocations. The increase of the major/minor ratio represents the softening effect as the inactive dislocations are arranged in such a way that the slip along the major slip direction becomes easier than other directions. Since the slip direction remains unchanged, the macroscopically observed stress is a result of the balance between the hardening and softening effects.

3) Stainless Steel Under 90° Out-Of-Phase Tension-Torsion

Under 90° out-of-phase tension-torsion, multi-slip structures such as cells and labyrinths are formed in the stainless steel. Assuming an annealed initial condition, the deformation procedure of the stainless steel is a circle with decreasing area which is similar to that of aluminum shown in Fig. 42. Since the substructure is basically isotropic, the hardening level is the same along all possible loading directions. A higher peak stress is observed as the stabilized area of the ellipse is smaller than that by proportional loadings. The softening effect which occurs during proportional loading does not occur for this case.

4) Planar-Slip Material Under An Abrupt Change of Loading Direction

The cross hardening effect and its associated hardening behavior is best described by McDowell's [61] test results on the stainless steel, see Figs. 44 and 45. After cyclic stabilization, a single-slip structure which is described by an ellipse is formed along the loading direction. With a sudden change of the loading direction, the stress level increases abruptly as the diameter of the ellipse along the new slip direction is small. After additional cycles are applied along this new direction, the ellipse first reduces its anisotropic ratio and, then, evolves into an ellipse which has a new major axis orientation and a smaller area. The combination of the reduced area and the anisotropic ratio along the new direction causes the peak stress to decrease gradually after the change of loading direction.

The physical change that might happen to the dislocation substructure under this loading case is described in Fig. 46. Before the change of loading direction, most of the grains consist of single-slip structures such as the planar dislocation, matrix veins and ladders as a result of the proportional cycling. The sudden change of loading direction forces the dislocation to slip along the new direction and results in the modification of substructures. Depending on the grain orientation and the existing substructure, substructures in one grain may change faster than others. The resultant substructure in each grain can also vary. Some grains may end up with multi-slip substructures while others still show single-slip structures with the major axis along the new direction. Since the ellipse model is to describe the effect from all possible substructures, the circle which may occur in the process of transition, as shown in Fig. 46, represents the status that the material has about the same number of single-slip structures along the old and new directions. The smaller ellipse area at the final stage results from of the increased number of multi-slip structures after the change of loading path.

5) Planar-Slip Material Under A Slow Change of Loading Direction

Figures 47 and 48 illustrate the change of deformation state and hardening level when the loading direction is changed slowly. Starting with a large circle, the deformation state of the material gradually becomes an ellipse with the area decreasing and the major axis rotating. Because the radius that determines the required stress remains a relatively fixed angle from the major axis orientation, a smooth transition of hardening level is observed. The recovery of the peak stress does not occur as the macroscopically observed hardening is only modeled by the decrease of ellipse area.

The possible change of the dislocation substructure is shown in Fig. 49. In the beginning, relatively few dislocations exist in the material. After the first cycle, single-slip structures are formed in those grains which have the crystal orientation matching the loading direction. For grains in which the crystal orientation is not suitable for single slip, the substructure has either a mixed feature or a major slip direction slightly different from the loading direction. The effect of the following cycles is to form structures which have their major slip directions close to the new loading direction while destroying the structure in which slip along the new direction is difficult. As the cycling continues, the number of multi-structures in the material also increases. The combined effect of these changes is a rotating ellipse with a decreasing area.

4.3.2 The Elastic Range

Most metals undergo plastic deformation as a result of dislocation slip. The formation of dislocations requires certain changes in the atomic arrangement. The strain observed in metals may also result from change of the space between atoms. The strain resulting from this kind of mechanism is the elastic strain. Because higher energy is required to increase the spacing between atoms, stress is required to maintain the elastic strain. The elastic strain reduces to zero when the stress is removed as atoms always return to the location where the energy can be minimized.

In general, any amount of strain that is measured from a deformed metal involves changes in both the atomic spacing and the atomic arrangement, i.e. both the elastic and plastic strain. The amount of strain formed by each mechanism is, however, dependent on the total deformation. When the deformation is small, most of the strain comes from the elastic deformation. If the deformation of materials gets larger, the contribution of the plastic deformation increases. To consider the condition in which the elastic deformation is dominant, a strain or stress range, which is defined as the elastic range, has to be specified.

Since the experiments conducted in this study are strain controlled tests, a plasticity formulation in deviatoric strain space is employed. Figure 50 illustrates the relation between the total strain, the plastic strain and the elastic strain. For a strain controlled loading condition, the problem of plasticity modeling is to find the change of plastic strain associated with a given increment of the total strain. After the plastic strain increment is calculated, the stress is determined by the elastic strain which is the difference between the total and the new plastic strain. The elastic range is a region defined in the strain space so that, whenever the total strain is in that range, no change occurs to the plastic strain, i.e. the plastic strain increment is zero.

A possible way of defining the elastic range starts with the study of the experimental results. Based on the experimental data, it has long been observed that the stress range in which the material exhibits linear stress-strain relation may undergo translation, distortion and rotation. Although those observations have been interpreted as either isotropic or kinematic hardening in stress space, a similar formulation can also be done in strain space. In fact, a formulation in strain space provides deeper insight into the mechanism of those phenomena.

Figure 50 shows the relation between the elastic range and the total strain. The most significant assumption is that the elastic range is always adjacent to the total strain. This assumption, which results in the consistency condition in the classical plasticity theory, represents that, regardless how the material is deformed, there always exists a direction along which a small change of total strain can be obtained by adjusting atomic spacing of the material. In other words, a plastically deformed material can always be further deformed without the plastic deformation mechanism be involved if the loading direction is appropriate.

Before plastic deformation, the elastic range is normally isotropic and has the center located at the origin of the strain space. After that, the material behavior usually becomes so complicated that it is quite difficult to estimate the location and shape of the elastic range. From the uniaxial hysteresis loop, it can be concluded that the elastic range cannot cover the region toward which the plastic strain tensor moves. This region is shown by the shaded area in Fig. 50. The exact location of the elastic range during nonproportional cycling cannot be determined from the uniaxial test result. A detailed examination of biaxial nonproportional testing results shows that, during nonproportional cycling, there does not exist a range in which the plastic strain increment is exactly zero. Relatively small changes in the plastic strain are observed when the total strain tensor moves along a direction between the reverse direction of the total strain increment and the reverse direction of the elastic strain. The elastic range plotted in Fig. 50 is a good estimation for the location of the elastic region.

From a mechanistic point of view, the atomic spacing of the material is stretched most along the direction of the elastic strain. A deformation change that tends to decrease the elastic strain can be easily obtained by reducing the atomic spacing. The change of plastic strain is, therefore, small as the total strain increment is along the reverse direction of the elastic strain. On the other hand, the arrangement of the dislocations can also affect the location of the elastic range. If many dislocations are formed along one direction, the total strain change that tends to activate dislocations to slip across those previously formed dislocations should have a smaller plastic strain change as a higher stress is required to overcome the effect of interaction. Since the ease of cross slip is dependent on the slip mode of materials, location of the elastic range may also depend on the material.

Estimation of the shape and size of the elastic range is more complicated than that of the location. As mentioned earlier, there does not exist a range in which the plastic strain change is really zero. Definitions for the shape and size of the elastic range requires a criterion for the amount of the plastic strain change. As in classical plasticity theory, the elastic range defined by this approach is likely to become highly dependent on the criterion used. In view of these difficulties, it is suggested that definitions chosen for the shape and size of the elastic range be as simple as possible. In fact, the accuracy of the shape and size of the elastic range should be determined by considering the role it plays in the model. In the classical plasticity theory, the yield surface is used to define the amount of hardening and the direction of plastic flow. In particular, since the plastic flow is believed to be along the outward normal direction of the yield surface, the exact shape of the yield surface is quite important. The reason that the elastic range is defined in this model is only to specify a region in which the change of plastic strain is small. For this purpose, a function such as the von Mises criterion is good enough to approximate the shape of this range. The elastic range is, therefore, defined as

$$[(\underset{\sim}{e}_t - \underset{\sim}{\varepsilon}_c) : (\underset{\sim}{e}_t - \underset{\sim}{\varepsilon}_c)]^{\frac{1}{2}} - \varepsilon_y = 0 \qquad (4.2)$$

where $\underset{\sim}{\varepsilon}_c$ is a tensor defining the center of this range and ε_y is the effective yield strain defined as the uniaxial yield strain divided by $\sqrt{2}$.

In order to make the elastic range be located in the expected region, the incremental direction of the elastic range center, $\underset{\sim}{\varepsilon}_c$, is assumed to be along a direction $\underset{\sim}{l}$, which is defined as

$$\underset{\sim}{l} = \frac{\underset{\sim}{\varepsilon}_a - \underset{\sim}{\varepsilon}_c}{|\underset{\sim}{\varepsilon}_a - \underset{\sim}{\varepsilon}_c|} \tag{4.3}$$

where

$$\underset{\sim}{\varepsilon}_a = (\underset{\sim}{e}_t + d\underset{\sim}{e}_t) + \frac{(\underset{\sim}{\varepsilon}_p + d\underset{\sim}{\varepsilon}_p) - (\underset{\sim}{e}_t + d\underset{\sim}{e}_t)}{|(\underset{\sim}{\varepsilon}_p + d\underset{\sim}{\varepsilon}_p) - (\underset{\sim}{e}_t + d\underset{\sim}{e}_t)|} \zeta \, \varepsilon_y, \tag{4.4}$$

ε_y is the effective yield strain which defines the size of the elastic range and ζ a material constant with a value between 0 and 1. Assuming that $d\eta$ is the magnitude of the elastic range center increment, i.e.

$$d\underset{\sim}{\varepsilon}_c = d\eta \underset{\sim}{l}, \tag{4.5}$$

its value can be related to the total deviatoric strain increment, $d\underset{\sim}{e}_t$, and the effective yield strain increment, $d\varepsilon_y$, by

$$d\eta = \frac{(\underset{\sim}{e}_t - \underset{\sim}{\varepsilon}_c) : d\underset{\sim}{e}_t - \varepsilon_y \, d\varepsilon_y}{(\underset{\sim}{e}_t - \underset{\sim}{\varepsilon}_c) : \underset{\sim}{l}} . \tag{4.6}$$

Note that Eq. (4.6) is obtained by substituting Eq. (4.5) into the derivative of Eq. (4.2). The size of the elastic range may be assumed as a constant or it may expand or decrease. If the size of the elastic range is allowed to change, the value of $d\varepsilon_y$ in Eq. (4.6) can be determined by any evolution function similar to the isotropic hardening rule used in the classical plasticity model. The total deviatoric strain increment, $d\underset{\sim}{e}_t$, is a given quantity for the strain controlled case.

4.3.3 The Plastic Flow

Modeling of the plastic flow, or the plastic strain increment tensor, is divided into two parts. The first part considers the direction of plastic flow which is defined as a tensor in the deviatoric strain space that has its second invariant equal to one. The second part discusses the magnitude of plastic strain increment. Like other tensors, its value is defined as the second invariant of the plastic strain increment tensor.

4.3.3.1 The Direction of Plastic Flow

In order to develop the assumption for the plastic flow direction, the experimental result is once again reviewed. Although this observation can be performed in either stress or strain space, it is found that the strain space provides more information than the stress space does. A comparison is done for the biaxial case in Fig. 51. In the strain plane, both the total strain and the plastic strain histories can be plotted. The elastic strain, which is the difference between the total and plastic strain, also indicates the direction and magnitude of the stress. In contrast, the only information which can be easily shown by the stress plane is the stress history. Although the plastic flow direction has been compared in the stress plane by earlier researchers, discussions on the plastic flow direction will refer to the strain plane in this study.

The experimental results show that the plastic flow cannot be along both the direction of the total strain increment and the direction of stress. In Fig. 18a, it can be seen that the plastic flow follows the direction of the total strain increment and the stress only if the loading is proportional, point A to point B. Once the loading becomes nonproportional, the plastic flow direction is between the direction of the total strain increment and the direction of stress.

A possible way of assuming the plastic flow direction is using the difference between the total deviatoric strain tensor and the plastic strain tensor, see Fig. 50. With this assumption, the plastic flow can have a direction between the total strain increment direction and the stress direction when the loading path is nonproportional. However, this assumption is found incapable of predicting the behavior of materials which have a strong Bauchinger effect. As the schematic diagram shown in Fig. 52, the plastic flow increment becomes negative when the material is unloaded from point M to point N. Because the difference between the current total strain and the previous plastic strain can be nonnegative within this range, it cannot describe the flow direction of this case correctly.

The experience obtained from the classical plasticity theory suggests that the plastic flow direction may be defined by the elastic range. In view of the difficulty of defining the shape of the elastic range, assumptions using shape of the elastic range are avoided. The method suggested uses the difference between the total strain and the elastic range center, i.e.

$$\underset{\sim}{n} = \frac{(\underset{\sim}{e}_t + d\underset{\sim}{e}_t) - \underset{\sim}{\varepsilon}_c}{|(\underset{\sim}{e}_t + d\underset{\sim}{e}_t) - \underset{\sim}{\varepsilon}_c|} \tag{4.7}$$

where $\underset{\sim}{n}$ is the tensor defining the direction of plastic flow. Note that, conceptually, this assumption is very close to the flow rule developed in the classical plasticity theory if the von Mises yield criterion is used as the loading function.

4.3.3.2 The Magnitude of Plastic Flow

According to the discussion about the dislocation substructure, the material strength is a function of the plastic flow direction. After the flow direction is determined, the level of hardening, or the ease of slip, can be estimated from the ellipse model with Eq. (4.1). The magnitude of the plastic strain increment is related to the hardening level estimated in this manner. Since the material strength has been defined as the stress at which the stress-strain curve approaches a constant value, an analytical function has to be assumed to determine details of the stress-strain curve before it reaches the limit stress. This function describes the stress-strain curve between the yield point and the saturated portion.

By looking at the uniaxial test result shown in Fig. 38b, it is found that there are three kinds of stress-strain relation. The first one is represented by curve A along which the plastic modulus first equals infinity at the yield point and, then, continues to decrease to a value of almost zero as the stress increases. The second kind is the elastic unloading case represented by curve B. For this case, the stress-strain curve exhibits a sharp corner as it turns from the linear behavior to the portion that has a plastic modulus of the controlling loop. The third kind of stress-strain relation, curve C, has a combined feature of curves A and B. Right after yielding, the plastic modulus decreases in a manner similar to that of the first kind. When the stress-strain curve approaches the controlling loop, the plastic modulus decreases at a higher rate and becomes almost the same as that of the controlling loop.

The macroscopic stress-strain relation observed in Fig. 38b can be related to the motion of active dislocations that have been mentioned earlier. A general equation that relates the plastic strain to the dislocation can be written as

$$\Delta\varepsilon_p = N\, b\, \Delta x \tag{4.8}$$

where $\Delta\varepsilon_p$ is the plastic strain increment, N is the number of the mobile dislocations along the slip direction, b is the Burger's vector and Δx is the average slip distance of dislocations. In this equation, b is a constant. Both N and Δx can be functions of stress. From the observations in Fig. 38b, it is known that the magnitude of the plastic strain increment becomes very large when the stress approaches the limit value. Due to the existence of the inactive dislocation substructure, it can be argued that the average slip distance has a finite value. The number of mobile dislocations may, therefore, be the controlling factor for the magnitude of plastic strain increment. If it is assumed that the plastic compliance, inverse of the plastic modulus, is proportional to the number of active dislocations in the material, the observed stress-strain relation can be explained by the micro mechanism. Fig. 53(a) shows the possible dislocation arrangement at point P_0 of Fig. 38b. When the applied stress reaches the yield stress, a small number of the active dislocations starts to slip. Due to the increased interactive stress between these mobile dislocations and the dislocation wall, Fig. 53(b), their movements do not continue unless a higher stress is applied. The continuous decrease of the plastic modulus results from the increase of the number of mobile dislocations that can be activated by the increased applied stress. If a the applied stress drops slightly, such as from point P_1 to P_2, the change of strain may result from reducing the atomic space only. Since the arrangement of mobile dislocations has not been changed during the unloading period, the plastic modulus is the same as the major loop when the stress reaches the level at which unloading happens, i.e. point P_1. If the decrease of stress is so large that some of the mobile dislocations have to move backward during the unloading period, these dislocations, having a lower interactive stress against the reloading direction, are easier to activate if the applied loading increases again. The smooth transition of the plastic modulus during the unloading and reloading periods results from the movement of these dislocations, Fig. 53(c). As the majority of the mobile dislocations remain unchanged, the stress-strain curve still approaches the major loop when the applied stress approximates the unloading stress level. The smoothness of the transition of the stress-strain curve results in a larger strain at the unloading stress level which is responsible for the cyclic creep of the unsymmetric stress cycling and the mean stress relaxation of the unsymmetric strain cycling.

Observations made so far are limited to the uniaxial condition. For the nonproportional loading case, such as the biaxial testing result shown in Figs. 9 to 11, the direction of unloading and reloading cannot be easily defined. Particularly, a dislocation activated for one direction may become inactive as the loading turns to other directions. As such, a function capable of describing all possible details of the multiaxial loading path is unlikely to be simple.

In this study, three features are considered important in determining details of the stress-strain curve. First, the plastic modulus has to be infinity at the yield stress and decreases to almost zero at the limit stress. Second, if elastic unloading occurs, the stress-strain curve has to show a discontinuous point and follow the major loop upon reloading. Third, the ease of plastic flow has to decrease continuously as the flow direction changes from the major slip direction of the mobile dislocations to a fully reversed direction. To meet these three requirements the plastic compliance, C_p, i.e. $|d\underset{\sim}{\varepsilon}_p|/d\sigma_{eff}$, is calculated as

$$C_p = g(\sigma_L, \sigma_{eff})\, d\sigma_{eff} + k\, C_p^o \qquad (4.9)$$

where $g(\sigma_L, \sigma_{eff})$ is a function of the applied stress and the limit stress, C_p^o is the value of $|d\underset{\sim}{\varepsilon}_p|/d\sigma_{eff}$ before the application of $d\sigma_{eff}$ and k is a factor due to the change loading direction. The specific equation assumed for function $g(\sigma_L, \sigma_{eff})$ is

$$g(\sigma_L, \sigma_{eff}) = \frac{c}{(\sigma_L - \sigma_{eff})^2} \tag{4.10}$$

and the assumption for k is

$$k = \underset{\sim}{n} : \underset{\sim}{n}^o \tag{4.11}$$

where $\underset{\sim}{n}$ is the tensor defining the plastic flow direction due to $d\sigma_{eff}$ and $\underset{\sim}{n}^o$ is the plastic flow direction before the application of $d\sigma_{eff}$. The value of k is arbitrarily assumed to be zero if Eq. (4.11) gives a negative value. The effective stress, σ_{eff}, is defined as

$$\sigma_{eff} = (\underset{\sim}{s}:\underset{\sim}{s})^{1/2} \tag{4.12}$$

After taking derivative, it becomes

$$d\sigma_{eff} = \frac{\underset{\sim}{s}:d\underset{\sim}{s}}{\sigma_{eff}} \tag{4.13}$$

Note that for the uniaxial case with no unloading, k has a value of one. Equations (4.9) and (4.10) give an exponential stress-strain relation after integration.

So far, the plastic flow direction, $\underset{\sim}{n}$ and the plastic compliance, C_p, which are associated with a change in the total deviatoric strain increment, $d\underset{\sim}{e}_t$ have been defined. To determine the magnitude of the plastic strain increment, the assumption that the total strain consists of the plastic and elastic strain additively, i.e.

$$\underset{\sim}{e}_t - \underset{\sim}{e}_e + \underset{\sim}{\varepsilon}_p \qquad (4.14)$$

has to be used. The elastic deviatoric strain, $\underset{\sim}{e}_e$, is related to the deviatoric stress by

$$\underset{\sim}{s} = 2\ G\ \underset{\sim}{e}_e. \qquad (4.15)$$

The magnitude of plastic strain increment, $d\lambda$, is defined as

$$d\lambda = (d\underset{\sim}{\varepsilon}_p : d\underset{\sim}{\varepsilon}_p)^{\frac{1}{2}}. \qquad (4.16)$$

By combining Eqs. (4.12) and 4.16, $d\lambda$ can be written as

$$d\lambda = \frac{(\underset{\sim}{e}_t - \underset{\sim}{\varepsilon}_p) : d\underset{\sim}{e}_t}{\frac{\sigma_{eff}}{4G^2 C_p} + (\underset{\sim}{e}_t - \underset{\sim}{\varepsilon}_p) : \underset{\sim}{n}}\ . \qquad (4.17)$$

This is the equation used to calculate the magnitude of plastic strain increment associated with an given change in the total deviatoric strain.

4.4 Comparison and Comments

The model developed in the last section is closely related to the classical plasticity theory. In fact, most of the mathematic formulation follows the same procedure as that of the classical plasticity theory. The model is, however, initiated from a viewpoint which is different from the classical theory. The classical plasticity theory starts with the assumption of a yield surface and thermodynamic principles. On the other hand, the proposed model emphasizes the deformation mechanism and experimental results. Figure 54 is a diagram showing the difference between the proposed model, the classical plasticity theory and the crystal plasticity theory. The suggested model uses the information obtained from the microstructural observation to make assumptions at a macroscopic level. The classical plasticity theory focuses at the macroscopic level, while the crystal plasticity theory starts with assumptions at the crystal level. With such a difference in viewpoints, the proposed model has a number of features that should be further discussed.

Definition of the state variables is one of the major differences between the proposed model and the classical plasticity theory. In the classical plasticity theory, the location and shape of the yield surface are the main variables which determine the plastic flow direction and the hardening level of the material. Since the yield surface can only define the elastic region, additional variables are necessary for modeling nonlinear region of the stress-strain curve. Up to date, there is still no universal method to define variables for nonlinear portion of the stress-strain curve as no fundamental theory has been developed regarding the principle of nonlinear deformation behavior of the material. The proposed model has three kinds of state variables. The first kind of variables are concerned with the arrangement of inactive dislocation substructures, the ellipse model that describes the geometrical configuration of the dislocation substructure. From this kind of variables, the limit stress, or the hardening level, is defined. The second kind of variables are related to the number and direction of the active dislocation. As active dislocations are assumed to move in the region confined by the dislocation substructure, these variables are used to describe the stress-strain curve bounded by the limit stress. The third kind of state variables define the region in which change of the atomic spacing is the major mechanism for deformation. Elastic behavior is expected if the total strain tensor lies in this region. The proposed model has, therefore, a complete description about the deformation state and mechanism of the material under plastic deformation.

The shape of the yield surface is conceptually important for the classical plasticity theory as it defines the plastic flow direction. Although the proposed model also uses the center of the elastic range to define the plastic flow direction, the shape of the elastic range is not as important as that of the classical theory. In the development of the model, it has been mentioned that, experimentally, the relative location of the elastic range is normally easier to estimate than its configuration. This approach avoids the difficulty of searching for the shape of the elastic range. Instead, a material constant, ζ, is introduced to account for the possible material dependence of the flow direction.

Another major difference is the space of defining the state variable and developing the mathematic assumption. It is found that the proposed model might be able to explain the corner of the subsequent yield surface which have been reported by early researchers. In the classical plasticity theory, it has been assumed that the yield surface is a scalar function of stress. For this reason, the yield point remains unchanged regardless the loading direction. The proposed model suggests that the stress change associated with a given total strain increment is dependent on the plastic flow direction. It has been observed that the plastic flow direction is generally different from the direction of stress. The yield point, which is normally assumed as the point having a small amount of plastic strain, may depend on the loading direction. If so, the yield surface cannot be defined as a scalar function of stress. Since the major variables used in the proposed model are defined by strain, the material behavior that might be predicted by proposed model cannot be easily compared to the early experimental work on the yield surface. A detailed study of this possibility requires further experimental data conducted with appropriate loading paths.

5. MODELING AND RESULTS

Implementation of the proposed model will be divided into two parts. The first part considers the stabilized material behavior under biaxial strain controlled cycling. In this part, the loading path is unchanged from cycle to cycle. The purpose of the model is to describe the stress-strain relation after the hysteresis loop is stabilized. The second part deals with transient material behavior. For this case, the loading path is changed during the cycling. The purpose of the model is to simulate the evolution of the hardening level during such changes.

5.1 The Stabilized Behavior

According to previous discussions, a plasticity model has to include a complete description about the evolution of the dislocation substructure, the mechanism of the elastic deformation and the behavior of mobile dislocations. Among them, the dislocation substructure determines the limit stress or the amount of hardening during cyclic loading. Since the dislocation substructure of the material does not change after the material behavior is stabilized, how the substructure reaches the stabilized stage is normally unimportant for the description of the stabilized stress-strain curve. As such, the ellipse model, which has been proposed to model the dislocation substructure, can be neglected as far as the limit stress of the loading path can be estimated. In order to simplify the calculation, it is suggested that the limit stress be estimated from the loading path and the material property without using the ellipse model. An easy method of determining the limit stress of a biaxially cycled metal is presented. This method is then combined with the formulation for the elastic range and the plastic flow to simulate the stabilized stress-strain response of the stainless steel and aluminum under several strain-controlled loading paths. The stress and plastic strain responses predicted by the model are compared to the experimental results. The purpose of this modeling work is to examine the accuracy of the detailed stress-strain relation predicted by the model.

5.1.1 Mathematical Formulation

The Limit Stress

For wavy slip materials, the limit stress is independent of the loading path as an equiaxial dislocation substructure is expected for both proportional and nonproportional loading paths. The limit stress is, therefore, only a function of the applied strain range. A uniaxial stress-strain curve is enough to estimate the limit stress. As shown in Fig. 38a, the limit stress can be obtained by extrapolating the experimentally obtained stress-strain curve to the region where the strain is relatively large. Since the limit stress is insensitive to the strain, it can also be approximated by the peak stress of any stress-strain curve that has a relatively large strain range. A power law or linear function can be assumed as the relation between the limit stress and the applied strain range. Experimental results shown in Fig. 35 suggest that the stabilized limit stress of aluminum is almost independent of the applied strain range. A constant value is used to approximate the limit stress of this material.

For wavy and wavy/planar slip materials, the limit stress is dependent on both the loading path and the applied strain range. Figure 55 shows the relation between the limit stress and the strain range of stainless steel under both uniaxial and 90° out-of-phase tension-torsion loadings. From Fig. 36, it can be found that the stabilized peak stress of copper increases suddenly as the plastic strain amplitude reaches 0.001. This behavior cannot be described by a simple function such as the power law. Assuming that the 90° out-of-phase tension-torsion loading path has the highest hardening and that the proportional loading path has the lowest hardening, the limit stress of an arbitrary loading path can be obtained by interpolation between these two limits. Fig. 55 shows an example of such an estimation.

Although it has been concluded that the nonproportionality of a loading path is determined by the plastic strain history, the total strain path, which is the input variable for the strain-controlled case, can still be used to estimate this quantity. For a total strain path shown in Fig. 56, it can be assumed that all the small "perturbations" observed in the total strain history result from the elastic deformation mechanism. The plastic strain path follows the over-all trend of the total strain path. An easy way of estimating the degree of nonproportionality is drawing a "wide" line along the total strain path. The width of this line should have the order of the effective yield strain. Since the plastic strain increment can have a component normal to the major loading direction whenever the total strain increment is not tangent to the major loading direction, the width of this line should be less than the effective yield strain. In this study, the width of the this line is arbitrarily assumed to have a value of the uniaxial yield strain divided by the square root of two. The maximum difference in the incremental direction of this line, $\Delta\psi$, divided by 90° is defined as the nonproportionality of the loading path, β, i.e.

$$\beta = \frac{\Delta\psi}{90} \, . \tag{5.1}$$

The limit stress is calculated as

$$\sigma_L = \beta[\sigma_L^{90}[\Delta\varepsilon/2) - \sigma_L^{0}(\Delta\varepsilon/2)] + \sigma_L^{0}(\Delta\varepsilon/2) \tag{5.2}$$

where $\sigma_L^{90}(\Delta\varepsilon/2)$ and $\sigma_L^{0}(\Delta\varepsilon/2)$ are the limit stresses with a strain amplitude of $\Delta\varepsilon/2$ for the 90° out-of-phase tension-torsion and the uniaxial tension cases. Note that, in Eq. (5.2), a linear relation has been assumed between the directional difference and the degree of nonproportionality. Depending on the experimental results, it may be necessary to develop an empirical nonlinear relation between these two parameters.

The Elastic Range

Since the elastic range is not used to define the amount of strain hardening for the proposed model, the size of the elastic range does not have to be changed during the plastic deformation of materials. In view of the fact that the experimental determination of the yield point is quite difficult for the multiaxial cyclic loading case, the size of the elastic range is assumed constant for simplification. As this range is defined in strain, its value equals the strain at which the stress-strain curve departs from the elastic region. The shape of the elastic range is also assumed unchanged as the plastic flow direction is not defined by the configuration of this range.

Equation (4.2) of the last chapter defines the elastic range for the proposed model. To determine its moving direction, Eqs. (4.3) and (4.4) are used. For the calculation in which a continuous loading path is approximated by a number of discrete points, a problem arose when Eqs. (4.5) and (4.6) are used for estimating the movement of the elastic range. Since discrete points used to approximate the strain path normally don't include the strain at which the material starts yielding, an incremental equation such as Eq. (4.6) may result in a constant error in the location of the elastic range. For this reason, Eq. (4.5) is substituted into Eq. (4.2) to solve for the magnitude of movement directly. The magnitude of the elastic range center increment associated with a total deviatoric strain change, $d\underset{\sim}{e}_t$, is written as

$$d\eta = b - (b^2 - c)^{\frac{1}{2}} \tag{5.3}$$

where

$$b = (\underset{\sim}{e}_t + d\underset{\sim}{e}_t - \underset{\sim}{\varepsilon}_c) : \underset{\sim}{1} \tag{5.4}$$

and

$$c = (\underset{\sim}{e}_t + d\underset{\sim}{e}_t - \underset{\sim}{\varepsilon}_c):(\underset{\sim}{e}_t - d\underset{\sim}{e}_t - \underset{\sim}{\varepsilon}_c) - \varepsilon_y{}^2. \tag{5.5}$$

The Plastic Flow

The amount of plastic flow is calculated by the procedure proposed in the last chapter. Equation (4.7) is used to determine the direction of flow. Constant ζ is obtained by fitting the stress-strain history of the 90° out-of-phase tension-torsion case. Eqations (4.9) and (4.17) are used to calculate the plastic modulus and the magnitude of plastic strain increment. Because Eqs. (4.9) and (4.17) are first order approximations of the exact stress-strain curve, computational error may become significant when stress approaches the limit stress. To solve this problem, a procedure similar to that of solving the change of elastic range center is used. When the stress calculated from Eq. (4.17) is close to or larger than the limit stress, the magnitude of plastic strain increment is calculated as

$$d\lambda = b - (b^2 - c), \tag{5.6}$$

in which

$$b = (\underset{\sim}{e}_t + d\underset{\sim}{e}_t - \underset{\sim}{\varepsilon}_c):\underset{\sim}{n} \tag{5.7}$$

and

$$c = (\underset{\sim}{e}_t + d\underset{\sim}{e}_t - \underset{\sim}{\varepsilon}_p):(\underset{\sim}{e}_t - d\underset{\sim}{e}_t - \underset{\sim}{\varepsilon}_p) - (\sigma_L/2G)^2. \tag{5.8}$$

The value of $d\lambda$ calculated from Eq. (4.17) is negative for some combi nations of $\underset{\sim}{n}$ and $d\underset{\sim}{e}_t$. This situation happens when the sign of $(\underset{\sim}{e}_t - \underset{\sim}{\varepsilon}_p):d\underset{\sim}{e}_t$ is different from that of $(\underset{\sim}{e}_t-\underset{\sim}{\varepsilon}_p):\underset{\sim}{n}$. Since a negative of $d\lambda$ is not allowed in the model, $d\lambda$ is assigned to be zero when it occurs.

The loading condition of the biaxial test conducted on the tubular specimen is not exactly a strain controlled case. Instead, the variables controlled by the testing machine involve both strain and stress. The major input data are the normal strain along the longitudinal axis of the specimen, ε_{zz}, and the shear strain tangent to the surface of the specimen, $\varepsilon_{z\theta}$, see Fig. 57. Since the tubular specimen is assumed to have a plane stress loading condition, the normal strain along other two axes, ε_{rr} and $\varepsilon_{\theta\theta}$, are not known while the normal stress of those directions, σ_{rr} and $\sigma_{\theta\theta}$, are assumed zero. Since Eqs. (4.17) and (5.6) assume a full knowledge of the total strain change, they cannot be used to calculate the magnitude of plastic strain increment directly. An iterative scheme is used to solve this problem. Initially, strain increments $d\varepsilon_{rr}$ and $d\varepsilon_{\theta\theta}$ are calculated with an assumption of no plastic deformation, i.e.

$$d\varepsilon_{rr} = d\varepsilon_{\theta\theta} = -\nu\, d\varepsilon_{zz}, \tag{5.9}$$

where ν is the Poisson ratio. These quantities are substituted into Eqs. (4.17) and (5.6) to calculate the magnitude of plastic strain increment, $d\lambda$. After $d\lambda$ is determined, $d\varepsilon_{rr}$ and $d\varepsilon_{\theta\theta}$ are corrected by considering the condition that $d\sigma_{rr}$ and $d\sigma_{\theta\theta}$ are zero, which is

$$d\varepsilon_{rr} = d\varepsilon_{\theta\theta} = -\nu\, d\varepsilon_{zz} + \frac{1-2\nu}{3}\, d\lambda\, n_{22} \tag{5.10}$$

The correct values of $d\varepsilon_{rr}$ and $d\varepsilon_{\theta\theta}$ are obtained by continuing this calculation until $d\lambda$ approaches a constant value. During this iterative calculation, the plastic modulus is also modified to have a value closer to the exact value. Using this method, the value of $d\lambda$ is found to have an error less than one percent after a few iterations. Figure 58 is the flow chart for such calculations.

5.1.2 Results and Discussion

A computer program written in C is used to implement the proposed model. This program is used to model the behavior of aluminum and stainless steel. The loading path for aluminum is the strain controlled uniaxial path shown in Fig. 16. Material constants for aluminum are shown in Table 7. The stress-strain response predicted by the proposed model is compared to the experimental result in Fig. 59. The loading paths for the stainless steel are the biaxial paths shown in Figs. 9 to 11 and Figs. 17 to 19. Material constants for the stainless steel are shown in Table 8. Comparisons of the predicted paths to the experimental results are shown in Figs. 60 to 65. The limit stress of these loading paths is estimated by the procedure discussed in the last section.

In comparing the predicted stress-strain histories to the experimental results, it is found that the proposed model can predict the stabilized response of materials successfully. Fig. 59 shows that the stress-strain curve under various unloading and reloading conditions can be reasonably approximated by Eqs. (11) to (13). Figure 18 shows that, when the total strain path has a sudden change in its incremental direction, the instantaneous change of the plastic flow direction is less than that of the total strain. If the total strain continues to increment along the new direction, the plastic flow turns to that direction gradually. If the increment direction of the total strain keeps changing as in the 90° out-of-phase tension-torsion case, Fig. 17, the plastic flow direction can not reach the new increment direction of the total strain. A constant difference exists between the plastic flow and the total strain increment direction. For this case, the plastic flow direction also deviates from the direction of stress by a constant angle. Figures 60 to 65 show that the assumption made for the plastic flow direction can simulate this feature correctly.

There are also a number of features which the model cannot predict well. For a square strain path shown in Fig. 18, the effective stress at the corner is larger than the stress between corners by almost 30%. Although this difference can be easily related to the difference of the effective strain between those two points, the loading path of this case does not involve a clear unloading and reloading procedure such as that of the uniaxial test. A detailed examination of the experimental data shows that the plastic strain continues to increment along the previous flow direction when the total strain increment direction has turned to the new direction. This behavior persists for a short period and results in the sudden drop of the effective stress which can be observed in Fig. 18. A similar test conducted on aluminum shows that this effect is less obvious for aluminum than stainless steel, see Fig. 14. It is quite possible that this feature is related to the time-dependent behavior of the stainless steel. Limited to the assumption of time-independence, the proposed model cannot predict this behavior correctly.

The simplified method of estimating the limit stress is found not accurate for some of the loading paths. Particularly, the predicted maximum stress of the two-stair path loading case, Fig. 63, has an twenty two percent error when compared to that of the experimental data. This error is believed to be the major reason for the inaccuracy of predicting the plastic strain history in Fig. 63. The method is relatively accurate in estimating the limit stress of the four-stair and eight-stair path. The "wide" line method of estimating the limit stress is accurate only if the total strain path is close to proportional.

Another source of error comes from the assumption of the elastic range. As mentioned earlier, there does not exist a range in which the plastic strain increment is exactly zero. This is particularly true for the nonproportional path. Assuming zero plastic strain increment in the elastic range makes the predicted stress increases faster than the experimental result when the elastic strain increases. The over estimated stress in the predicted result of the stair path tests, Figs. 63 to 65, is a good example of this effect.

5.2 The Transient Behavior

In order to simulate the transient material behavior due to the change of the loading path between cycles, the ellipse model has to be included in the plasticity modeling. The ellipse that describes the change of the dislocation substructure in the material is used to determine the limit stress of each cycle. As the formulation for the elastic deformation and the plastic flow remains unchanged, this section will focus on the mathematic assumptions of the ellipse model. The purpose of this section is to present a possible way of including the change of dislocation substructures in the plasticity modeling.

5.2.1 Mathematical Formulation

In the last chapter, the relation between the ellipse model and the cyclic hardening behavior of the material has been explained in a qualitative manner. In this section, this relation will be quantified by a number of mathematic assumptions regarding the definition and evolution of the ellipse. These assumptions are developed from a purely empirical approach with no theoretical consideration.

The Ellipse Area

Formulation for the ellipse model starts with the assumption that the limit stress before the plastic deformation, σ_L^i, is given. Assuming that the major/minor axis ratio equals one at the beginning, the initial ellipse area, A_i, is π if the limit stress is normalized by the initial limit stress. The limit stress can, then, be related to radius of the ellipse, $r(\theta)$, by

$$\sigma_L = \frac{\sigma_L^i}{r(\theta)} \tag{5.11}$$

where θ is the loading direction. For the two-dimensional biaxial case, the direction of loading is defined as

$$\theta = \tan^{-1}\left(\frac{\underset{\sim}{n}:\underset{\sim}{n}^{u}}{\underset{\sim}{n}:\underset{\sim}{n}^{t}}\right) \tag{5.12}$$

where $\underset{\sim}{n}^{u}$ and $\underset{\sim}{n}^{t}$ are the plastic flow direction tensors resulting from the axial and torsion loadings.

In view of the cyclic stress-strain relation shown in Fig. 37, the stabilized limit stress is assumed to be dependent on the plastic strain amplitude through an exponential function. Assuming the stabilized limit stress at zero plastic strain amplitude, σ_L^{o}, and the stabilized limit stresses at infinite plastic strain amplitude under uniaxial loading, σ_L^{u}, and 90° out-of-phase tension-torsion, σ_L^{90}, be given as material constants, the stabilized ellipse areas at those limits are

$$A_L^{o} = \left(\frac{\sigma_L^{i}}{\sigma_L^{o}}\right)^2 \pi, \tag{5.13}$$

$$A_L^{u} = \left(\frac{\sigma_L^{i}}{\sigma_L^{u}}\right)^2 \frac{\pi}{\rho^{u}} \tag{5.14}$$

and

$$A_L^{90} = \left(\frac{\sigma_L^{i}}{\sigma_L^{90}}\right)^2 \pi \tag{5.15}$$

where ρ^{u} is the stabilized major/minor axis ratio for the uniaxial case. The stabilized ellipse area with a maximum plastic strain amplitude of $\Delta\varepsilon_p$ under the uniaxial loading, A_s^{u}, and 90° out-of-phase tension-torsion, A_s^{90}, are

$$A_s^{u} = A_L^{u} + (A_L^{u} - A_L^{o})\, e^{-\Delta\varepsilon_p/2k_n} \tag{5.16}$$

and

$$A_s^{90} = A_L^{90} + (A_L^{90} - A_L^{o})\, e^{-\Delta\varepsilon_p/2k_n}, \tag{5.17}$$

in which k_n is a material constant.

The stabilized ellipse area of an arbitrary loading path, A_s, is obtained by calculating the degree of nonproportionality of the loading path, β, and interpolating the area between A_s^u and A_s^{90}, i.e.

$$A_s = \beta(A_s^{90} - A_s^u) + A_s^u. \tag{5.18}$$

The nonproportionality parameter, β, is zero for the uniaxial case and one for the 90° out-of-phase tension-torsion case. The value between these two limits is obtained by counting the number of directions along which plastic strain occurs. A 180 degree two-dimensional direction range is divided into 20 divisions. For each division, the amount of the accumulated plastic strain of that direction is recorded. A direction division is said activated if the accumulated plastic strain along that direction is larger than 0.2 percent. The nonproportionality parameter, β, is related to the number of the activated divisions through an equation given as

$$\beta = (k_\beta - 2)p^3 + (3 - 2k_\beta)p^2 + k_\beta p \tag{5.19}$$

where p is the number of the activated divisions divided by the number of total divisions and k_β is a material constant. Eq. (5.19) is derived from the assumption that the relation between the nonproportionality of a loading path and the number of the activated divisions can be described by a third order polynomial function. The condition that the nonproportionality parameter is insensitive to the number of activated divisions when the number of the activated directions becomes large, i.e.

$$\frac{d\beta}{dp} = 0 \quad \text{when } p = 1 \qquad (5.20)$$

has also been considered.

The ellipse area always evolves from the initial value, π, into the stabilized value, A_s. It is assumed that the ellipse area is an exponential function of the accumulated plastic strain. Incrementally, this evolution procedure can be described as

$$\Delta A = (A_s - A)\ |\Delta\varepsilon_p|/k_p \qquad (5.21)$$

where $|\Delta\varepsilon_p|$ is the magnitude of the plastic strain increment.

The Major/Minor Axis Ratio and The Major Axis Direction

In order to allow the major/minor axis ratio be changed in the way described in the last chapter, a parameter, q, is calculated for each of the direction division. The initial value of this parameter, q_o, is defined as

$$q_o = \frac{\pi}{40(\rho^u - 1)} \qquad (5.22)$$

where ρ^u is the stabilized major/minor axis ratio under uniaxial cycling. When the direction of the plastic strain increment, ϕ, is in the range of division i, the parameter of that division, q, is increased by

$$\Delta q = [1 - (q - q_o)] \, |\Delta\varepsilon_p|/k_t \qquad (5.23)$$

where k_t is a material constant. To allow the major/minor axis ratio be erasable, the parameter of the division having a direction different from the direction of the plastic strain increment is decreased by

$$\Delta q = (q - q_o) \, |\sin(\phi - \theta)| \, |\Delta\varepsilon_p|/k_t \qquad (5.24)$$

in which θ is the direction of the division being considered.

The major/minor axis ratio is determined by comparing the distribution of these direction parameters. To do this, a ratio defined as

$$\alpha = \frac{\Sigma_{i=0}^{20} \, q_i |\cos(\phi-\theta_i)| \pi/20}{\Sigma_{i=0}^{20} \, q_i |\sin(\phi-\theta_i)| \pi/20} \qquad (5.25)$$

is calculated for each division. In that equation, ϕ is the plastic strain increment direction, α and θ are the ratio and direction for each division. The major/minor axis ratio is the maximum of α among all divisions. The direction at which the maximum value of α is recorded is the major axis direction of the ellipse.

In general, Eqs. (22) to (25) make the major/minor axis ratio equal ρ^u if only one direction division is activated. When a large number of divisions are activated, the value of this ratio reduces to one. Since the parameter q is dynamically changed by Eqs. (23) and (24), the major/minor axis ratio becomes dependent on the loading path of the latest cycles. The evolution behavior described in the last chapter can, therefore, be described.

5.2.2 Results and Discussion

The loading conditions used to examine the capability of the model are the two cyclic biaxial tests on 304 stainless steel conducted by McDowell, as shown in Figs. 44 and 47. A detailed description about the loading path is given in Ref. [61].

To model the transient material behavior, there are generally two sets of material constants required in addition to the constants used in predicting the stabilized behavior. The first set of constants include the initial limit stress, σ_L^i, the stabilized limit stress at zero plastic strain amplitude, σ_L^0, and the stabilized limit stresses under the uniaxial and 90° out-of-phase tension-torsion loading at a large plastic strain amplitude, σ_L^u and σ_L^{90}, the cyclic hardening parameter, k_n, and the constant for the change rate of the nonproportionality parameter, k_β. Another set of constants includes the stabilized cross hardening ratio under the uniaxial loading case, ρ^i, the factor describing the evolution rate of the ellipse area, k_p, and the factor for the evolution rate of the major/minor axis ratio, k_t.

Material constants from first set are important for the quantitative description of the material behavior. Particularly, the stabilized limit stresses are critical for the modeling of the stabilized hysteresis loop. The initial limit stress can be obtained from the uniaxial stress-strain curve at the first cycle. The stabilized limit stresses, σ_L^o, σ_L^u and σ_L^{90}, can be obtained by plotting the stabilized peak stress as a function of the plastic strain amplitude for both the uniaxial and the 90° out-of-phase tension-torsion loading cases. The cyclic hardening parameter, k_n, can be determined by fitting an exponential relation into the cyclic stress-strain curve similar to Fig. 68. Determination of the constant k_β requires a number of tests that activate different number of slip planes. By plotting the cyclic stress as a function of the number of the activated planes, this constant can be determined.

The second set of constants are designed for the description of the transient material behavior. Like the constant k_β, these constants normally require tests of high complexity. For example, the uniaxial cross hardening ratio, ρ^u, can only be determined by a test that changes the loading direction abruptly after the material behavior has been stabilized under a proportional cycling, such as the test in Fig. 44. The evolution rate constants, k_p, k_t and k_β, can only be obtained by fitting the transient material behavior during the change of the loading path. Since the effect of these three constants cannot be uncoupled by any test, they are quite difficult to determine.

Comparing the transient model of this section to the stabilized model suggested in the last section, it is found that the number of material constants increases drastically from six to fourteen. Although these additional eight constants can help the model to describe the transient material behavior under complicated loading paths, it has lost the requirement of simplicity which is usually important for engineering applications. Additionally, in view of the complexity involved in determining the value of those material constants, it is unlikely that the limit stress predicted from this approach can be more accurate than the method suggested in the last section. For these reasons, the values of the constants introduced in this section are estimated through a trial and error process. It is not suggested that this transient model be used for engineering calculation. The purpose of the modeling work here is to show the mechanism presented in the last chapter. A list of the constants for the 304 stainless steel is presented in Table 8.

Figures 66 and 67 show the predicted cyclic stresses as functions of the cycle number for the paths shown in Figs. 44 and 47. From these figures, it can be seen that the predicted results agree with the experimental data qualitatively. Most significantly, the ellipse model is shown to be capable of describing the sudden increase of the cyclic stress that has been discussed earlier, Fig. 66. The tendency of the cyclic softening effect after the change of the loading direction is also predicted.

Although the suggested model seems to work well for many cases, it should be noted that this model is developed from an approach that is not mathematically rigorous. As a result, how the model may behave under a loading condition cannot be easily predicted. A significant problem of this kind is the definition of the plastic compliance given in Eq. (4.9). In that equation, the plastic compliance, C_p, after an increase of the effective stress, $d\sigma_{eff}$, is defined as a summation of two quantities: one is a function related to the second derivative of the stress-strain curve, $g(\sigma_L, \sigma_{eff})d\sigma_{eff}$, and the other is the modified initial plastic compliance, kC_p^o. In general, the slope of the stress-strain curve defined by this method is not a single function of the stress. As the limit stress, σ_L, can be changed in the transient model, the resultant stress-strain relation becomes more unpredictable when the loading path becomes complicated. It is found that Eq. (4.9) may predict incorrect peak stress if the limit stress is changed during the cycling. An example is given in Fig. 69(b), which is the predicted peak stress for a loading path given in Fig. 69(a). Assuming the stabilized limit stress is 430 MPA, the limit stress predicted by the ellipse model increases from the initial value, 260 MPa, to the stabilized value gradually. Regardless of the increase of the limit stress, the peak stress obtained from Eq. (4.9) decreases, Fig. 69(b). This result suggests that Eq. (4.9), although works well for many other cases, is not an appropriate method of defining the slope of the stress-strain curve. How to develop quantitative assumptions so that a plasticity model can have well-defined mathematical properties while still satisfying the requirements from the mechanistic consideration is still a highly challenging issue in the area of plasticity modeling.

6. CONCLUSION

The macroscopic mechanical behavior of metals under nonproportional cyclic loading is an integration of highly complicated deformation mechanisms occurring at the microscopic level. In order to develop a mechanistic model for the metal plasticity, it is necessary to identify the controlling mechanisms which are responsible for the macroscopic material behavior. With the controlling mechanisms being chosen, quantitative assumptions are made for each of those mechanisms. The macroscopic plasticity model is a combination of the quantitative assumptions made for those mechanisms.

The following three conclusions are drawn from the observation of the dislocation substructure.

* The major dislocation substructure formed in simple metals, such as aluminum, copper and stainless steel, under the nonproportional cyclic loading can also be created by the proportional loading. However, all the substructures resulting from the nonproportional cycling belong to the category of substructures that involve multi-slip mechanisms.

* The slip mode dominates the substructure formed in the material. Materials which can cross slip easily form multi-slip structures under both proportional and nonproportional loadings. Materials which cannot cross slip easily form single-slip structures under proportional loadings and multi-slip structures under nonproportional loadings.

* The additional cyclic hardening observed for materials such as copper and stainless steel results from the change of the dislocation substructure from a single-slip structure to a multi-slip structure when the loading changes from proportional to nonproportional. The material which has the same substructure under both loadings does not increase the hardening level for the nonproportional cycling case.

A cyclic plasticity model developed from the deformation mechanism of metals should consider the following mechanisms.

* The dislocation substructure represents the arrangement of the inactive dislocation in the material. Since active dislocations slip in the area which is confined by the inactive dislocation, the level of the cyclic hardening of a material is related to the dimension and configuration of the dislocation substructure.

* The strain of a deformed metal results from two mechanisms: the adjustment of the space between atoms and the slip of the active dislocation. Under small deformation, the macroscopically measured strain can be assumed as resulting from these two deformation mechanisms additively.

* The strain resulting from the change of atomic spacing, the elastic strain, is linear and elastic. This mechanism dominates the total strain only if the total strain is within a small range that can be specified in the strain space.

* The strain resulting from the slip of active dislocations, the plastic strain, depends on the dislocation substructure and stress. This mechanism is the major mechanism for the deformation of materials when the stress is high. The dimension of the dislocation substructure determines the amount of strain hardening of the material. The amount of strain hardening increases as the size of the dislocation-free zone decreases.

In this study, a number of quantitative assumptions have been made to describe the three major deformation mechanisms of metals: the dislocation substructure, the elastic range and the plastic flow. By combining these assumptions, it is found the stress-strain response of the material under a highly complicated loading condition can be successfully modeled. In general, a model developed from this approach is capable of predicting more sophisticated material behavior than those based on the classical plasticity theory. The number of material constants is also reduced. As the plasticity model is supported by the microscopic deformation mechanism, estimation of the material constant for a new material without testing becomes feasible.

Table 1 Test Results of 1100 Aluminum

(T: Torsion, 0: 90° Out-of-Phase Tension-Torsion)

SPEC. I.D.	PATH	$\Delta\varepsilon/2$ (%)	$\Delta\gamma/2$ (%)	$\Delta\sigma/2$ (MPa)	$\Delta\tau/2$ (MPa)	$\Delta\varepsilon_p/2$ (%)	$\Delta\gamma_p/2$ (%)	N_f (Cycles)
A104	0	0.15	0.25	60.0	31.5	0.071	0.127	1969
A108	0	0.15	0.25	63.3	28.7	0.061	0.139	2849
A103	0	0.11	0.18	60.3	30.9	0.027	0.052	12938
A107	0	0.11	0.18	62.5	29.9	0.023	0.061	19402
A110	0	0.09	0.15	57.6	29.0	0.014	0.036	109781
A106	0	0.07	0.13	51.9	28.1	0.006	0.019	268168
A112	0	0.07	0.12	51.0	28.3	0.003	0.012	145380
A101	T		0.25		30.4		0.132	7644
A109	T		0.17		30.9		0.051	9543
A102	T		0.13		30.4		0.013	25914
A111	T		0.11		26.9		0.005	>700000
A105	T		0.09		21.4		0.004	>512000

Table 2 Test Results of OFHC Copper
(T: Torsion, O: 90° Out-of-Phase Tension-Torsion)

SPEC. I.D.	PATH	$\Delta\varepsilon/2$ (%)	$\Delta\gamma/2$ (%)	$\Delta\sigma/2$ (MPa)	$\Delta\tau/2$ (MPa)	$\Delta\varepsilon_p/2$ (%)	$\Delta\gamma_p/2$ (%)	N_f (Cycles)
C002	O	0.18	0.32	159.9	83.2	0.087	0.154	6051
C003	O	0.12	0.20	125.4	66.6	0.030	0.054	34582
C005	O	0.09	0.15	105.5	60.2	0.008	0.007	115587
C001	T		0.32		64.1		0.178	61670
C004	T		0.20		57.0		0.080	340315

Table 3 Test Results of 310 Stainless Steel
(T: Torsion, O: 90° Out-of-Phase Tension-Torsion)

SPEC. I.D.	PATH	$\Delta\varepsilon/2$ (%)	$\Delta\gamma/2$ (%)	$\Delta\sigma/2$ (MPa)	$\Delta\tau/2$ (MPa)	$\Delta\varepsilon_p/2$ (%)	$\Delta\gamma_p/2$ (%)	N_f (Cycles)
S102	O	0.35	0.61	438.5	245.6	0.133	0.275	1838
S101	O	0.20	0.35	310.5	177.5	0.046	0.122	38879
S106	O	0.15	0.25	236.2	137.2	0.028	0.068	383011
S104	T		0.61		170.2		0.390	50980
S107	T		0.45		143.2		0.264	368523
S105	T		0.35		142.6		0.189	835713

Table 4 Test Results of the 304 Stainless Steel Specimens Chosen for Microscopical Examination
(I: In-Phase Tension-Torsion, O: 90° Out-of-Phase Tension-Torsion)

SPEC. I.D.	PATH	$\Delta\varepsilon/2$ (%)	$\Delta\gamma/2$ (%)	$\Delta\sigma/2$ (MPa)	$\Delta\tau/2$ (MPa)	$\Delta\varepsilon_p/2$ (%)	$\Delta\gamma_p/2$ (%)	N_f (Cycles)
SS10	O	0.35	0.61	477	267	0.235	0.206	3560
SS28	O	0.20	0.35	300	168	0.041	0.152	50000
SS12	I	0.25	0.43	176	101	0.156	0.297	52900

Table 5 Test Results of the 7075 Aluminum Alloy Specimens Chosen for Microscopical Examination
(T: Torsion, O: 90° Out-of-Phase Tension-Torsion)

SPEC. I.D.	PATH	$\Delta\varepsilon/2$ (%)	$\Delta\gamma/2$ (%)	$\Delta\sigma/2$ (MPa)	$\Delta\tau/2$ (MPa)	$\Delta\varepsilon_p/2$ (%)	$\Delta\gamma_p/2$ (%)	N_f (Cycles)
A710	O	0.41	0.70	286	185	0.006	0.003	4953
A709	O	0.20	0.34	140	91	0.000	0.000	243211
A702	T		0.69		184		0.000	18760

Table 6 Summary of the Dislocation Substructures in 1100 Aluminum, OFHC Copper, 304 and 310 Stainless Steels

MATERIAL	SPEC. I.D.	PATH	MATRIX & VEIN	PLANAR DISLO.	LADDER	DISLO. TANGLE	UNCON-DENCED CELL	WALL	CELL	LABY-RINTH
1100	A109	T							X	
Al	A106	0							X	
	A104	0							X	
OFHC	C001	T	X		X			X	X	
Cu	C005	0					X	X		
	C002	0						X	X	X
304	SS12	I		X				X		
Stainless	SS28	0				X		X		
Steel	SS10	0						X	X	X
310	S105	T		X				X		
Stainless	S101	0				X		X		
Steel	S102	0						X	X	X

Table 7 Material Constants of 1100 Aluminum

Shear Modulus, G (MPA)	25928
Poisson Ratio, ν	0.33
Uniaxial Yield Stress, σ_y (MPA)	32
Strain Hardening Constant, c	0.012
Flow Direction Parameter, ζ	0.7

Table 8 Material Constants of Stainless Steel

Shear Modulus, G (MPA)	77418
Poisson Ratio, ν	0.33
Uniaxial Yield Stress, σ_y (MPA)	160
Strain Hardening Constant, c	0.001
Flow Direction Parameter, ζ	0.5
Cyclic Hardening Constant, k_n	0.0007
Nonproportionality Change Factor, k_β	1.5
Ellipse Area Change Factor, k_p	0.15
Ellipse Ratio Change Factor, k_t	0.35
Stabilized Uniaxial Ratio, ρ^u	1.2
Initial Limit Stress, σ_L^i (MPA)	260
Zero Plastic Strain Limit Stress, σ_L^o (MPA)	220
Infinite Plastic Strain Limit Stress, σ_L^u (MPA) (Uniaxial cycling)	280
Infinite Plastic Strain Limit Stress, σ_L^{90} (MPA) (90° Out-Of-Phase Tension-Torsion)	560

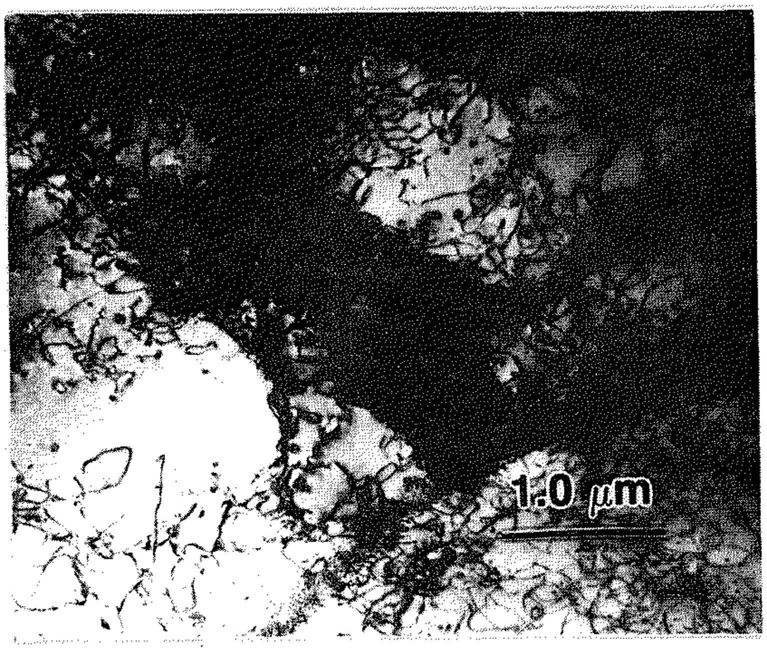

Figure 1. Dislocation Substructures of 1100 Aluminum Before Testing.

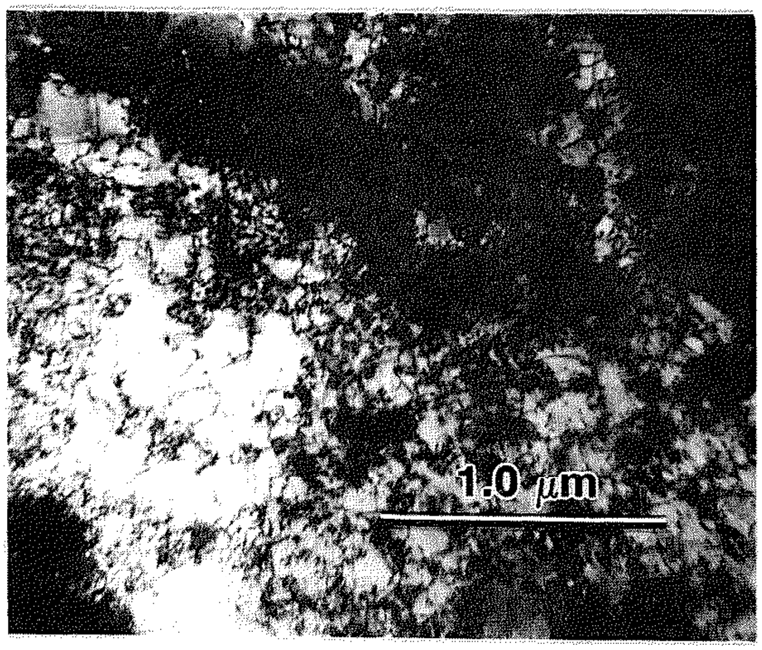

Figure 2. Dislocation Substructures of OFHC Copper Before Testing.

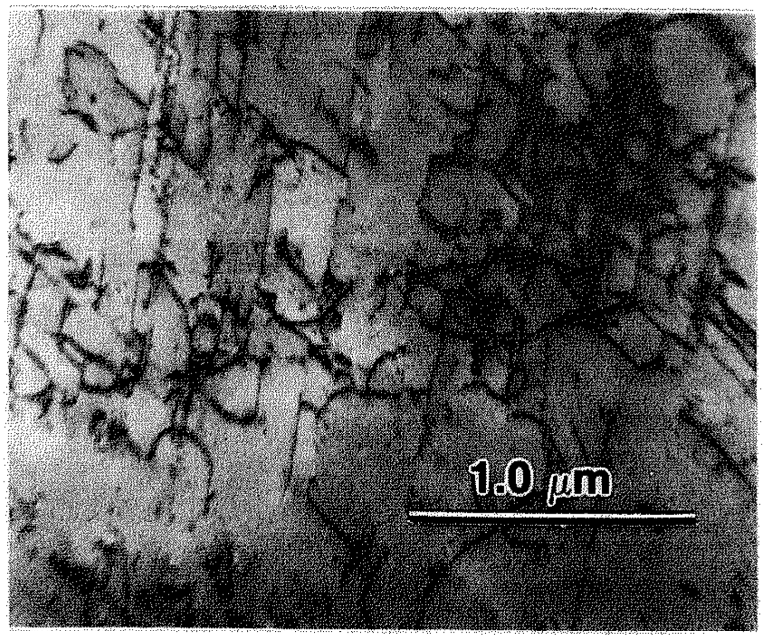

Figure 3. Dislocation Substructures of 310 Stainless Steel Before Testing.

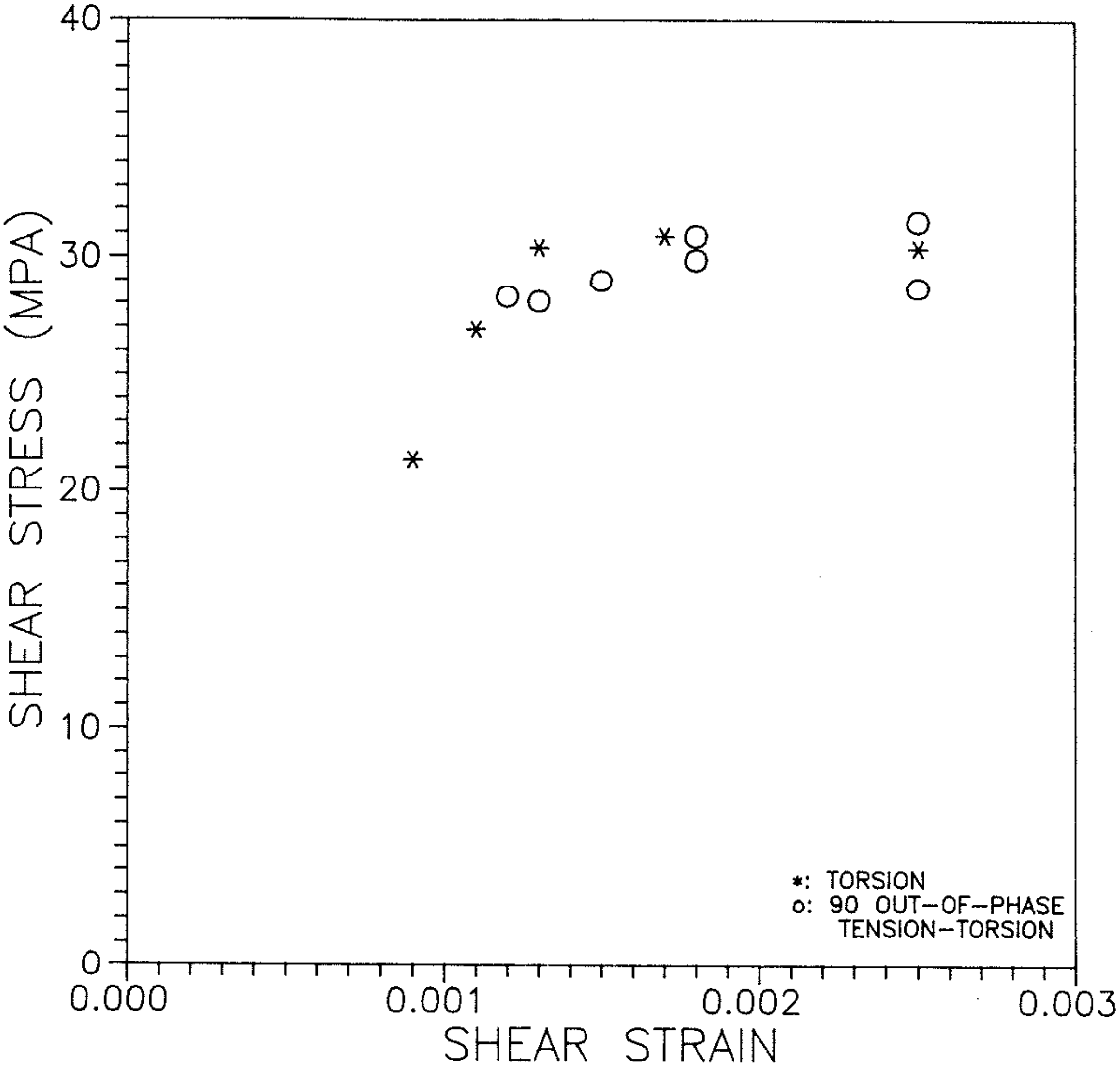

Figure 4. The Stabilized Shear Stress as a Function of Shear Strain for 1100 Aluminum.

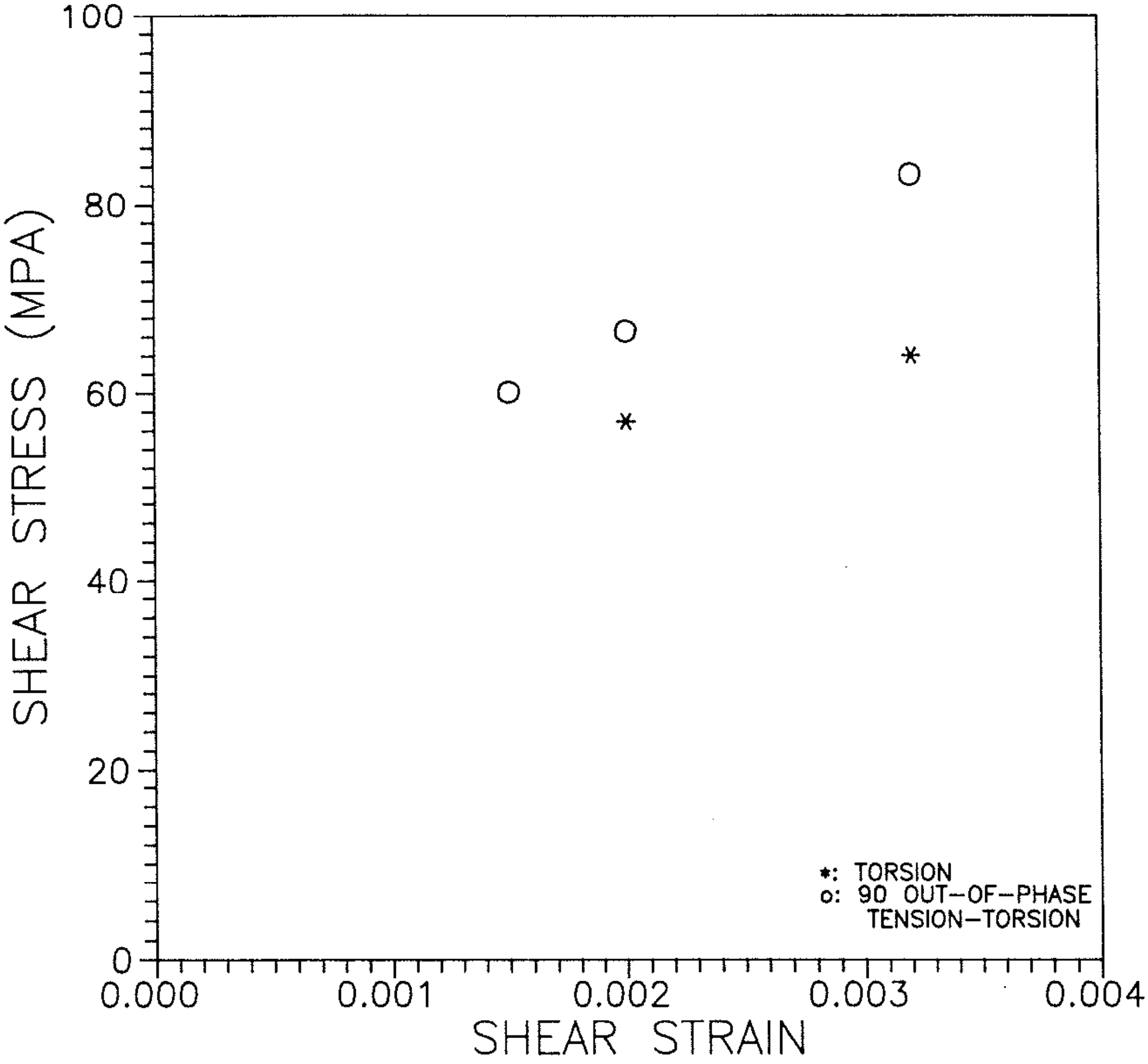

Figure 5. The Stabilized Shear Stress as a Function of Shear Strain for OFHC Copper.

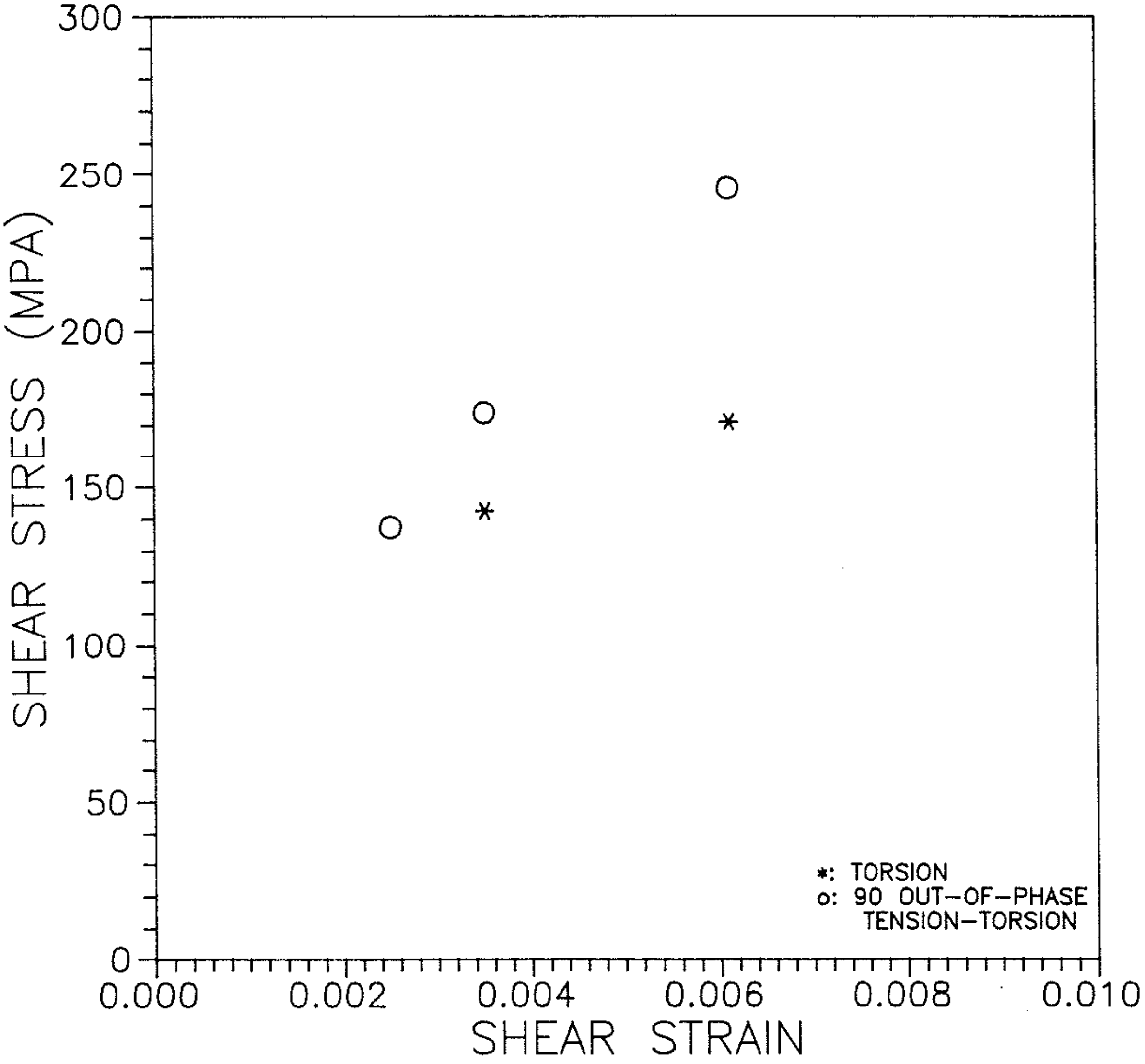

Figure 6. The Stabilized Shear Stress as a Function of Shear Strain for 310 Stainless Steel.

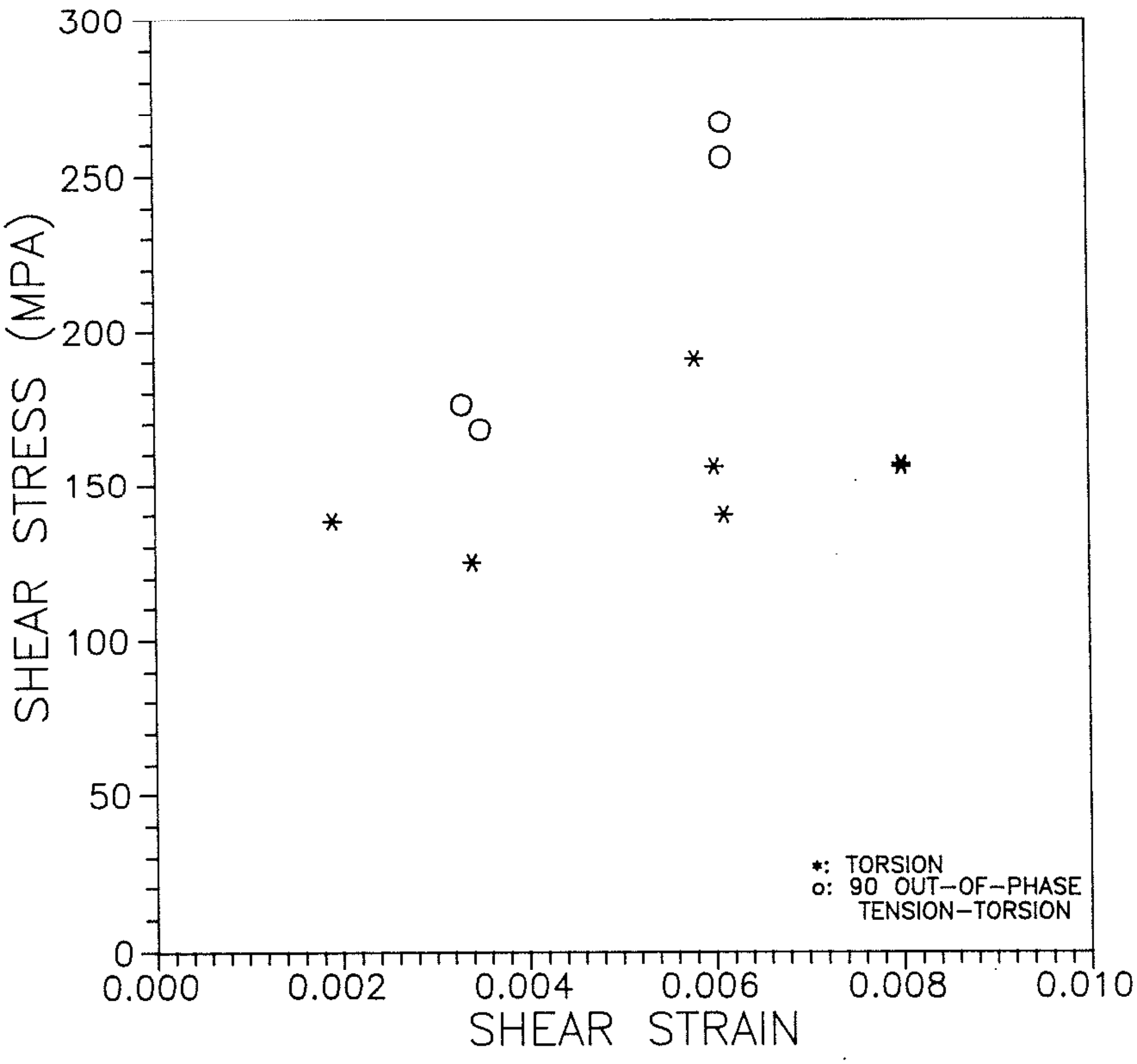

Figure 7. The Stabilized Shear Stress as a Function of Shear Strain for 304 Stainless Steel.

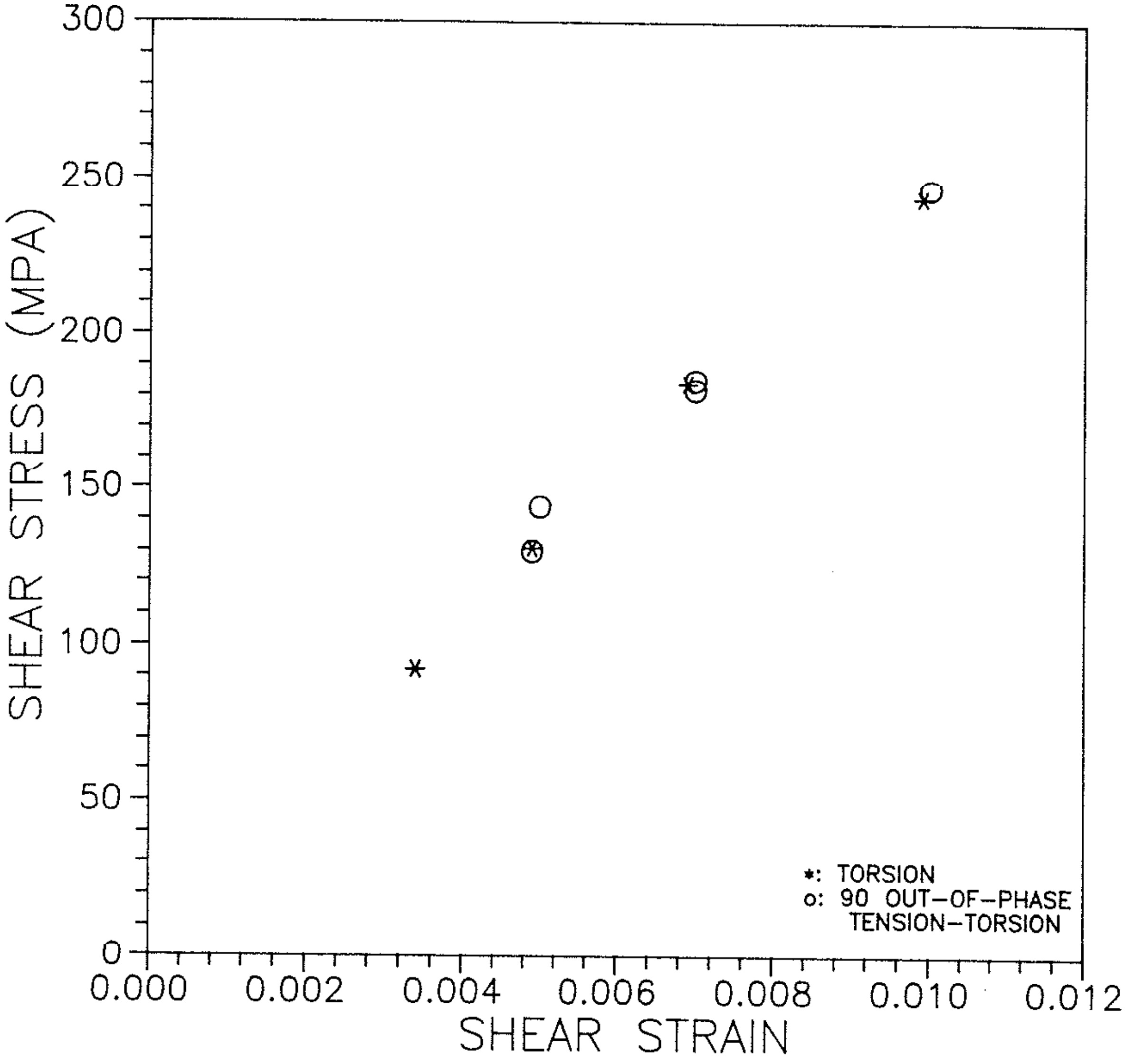

Figure 8. The Stabilized Shear Stress as a Function of Shear Strain for 7075 Aluminum Alloy.

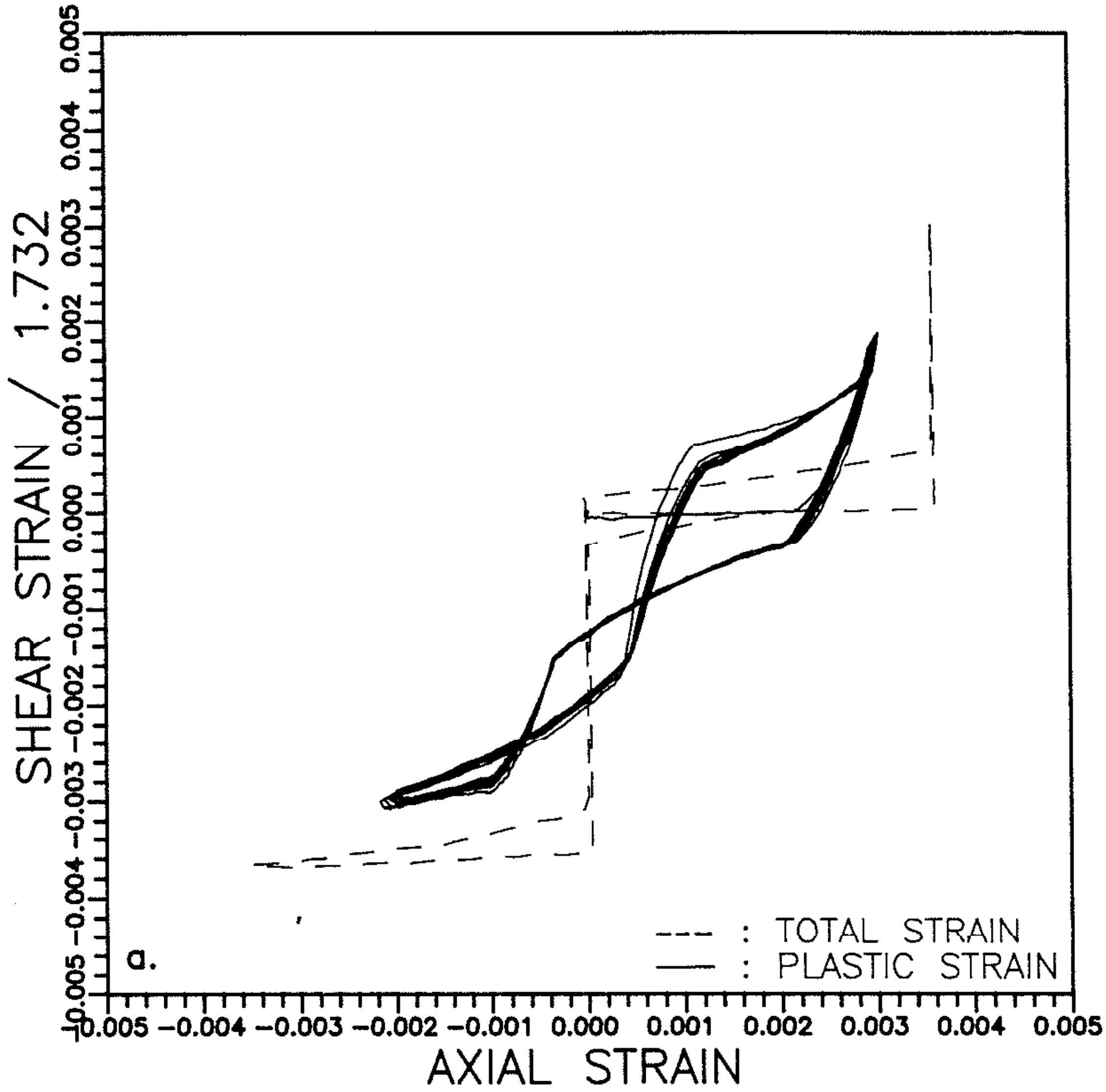

Figure 9. (a) - (d) The Stress-Strain History of 310 Stainless Steel under a Two-Stair Tension-Torsion Strain Controlled Cycling (Specimen S113).

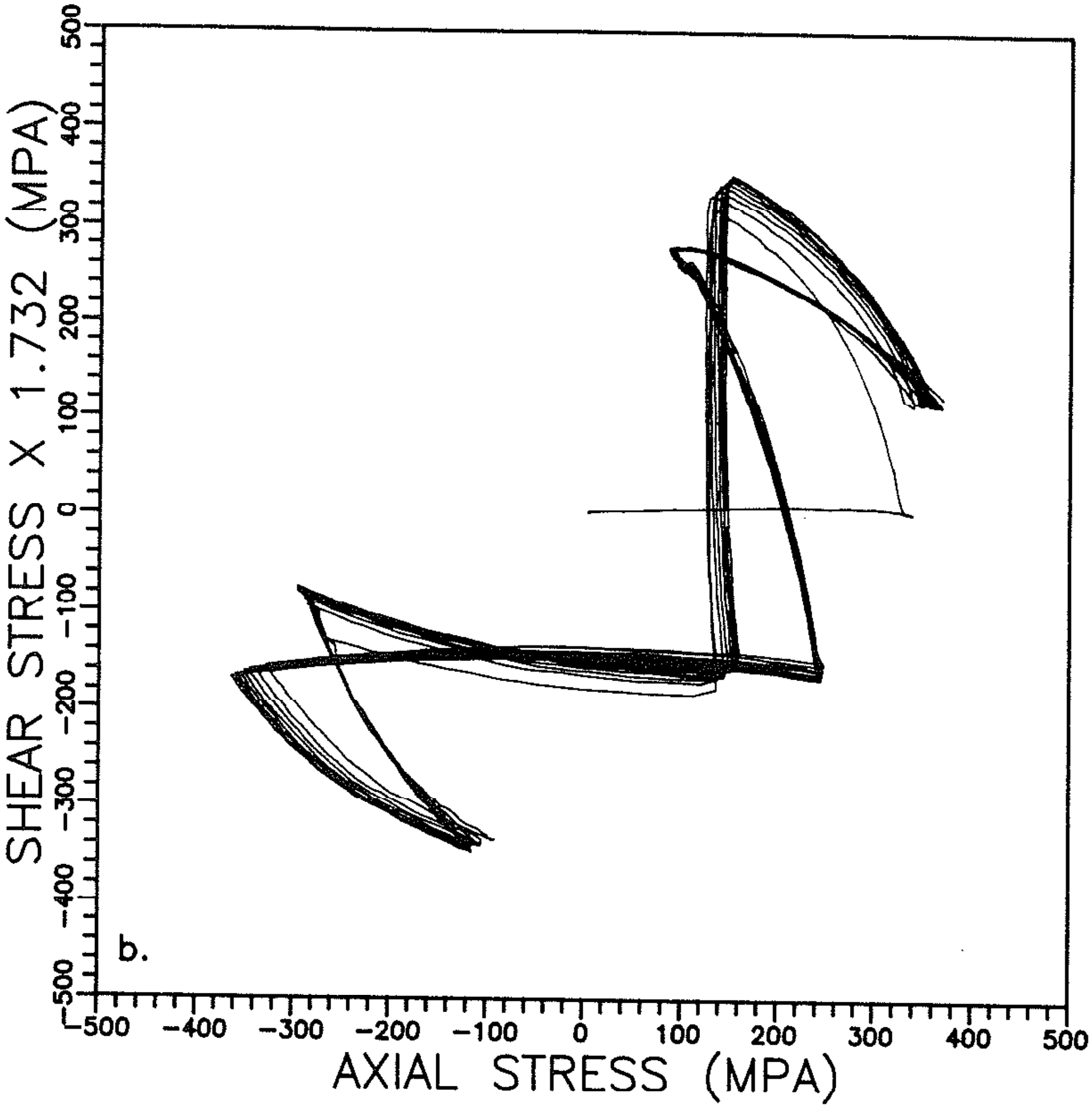
SHEAR STRESS X 1.732 (MPA)
AXIAL STRESS (MPA)
500
400
300
200
100
0
-100
-200
-300
-400
-500
-500
-400
-300
-200
-100
0
100
200
300
400
500
b.

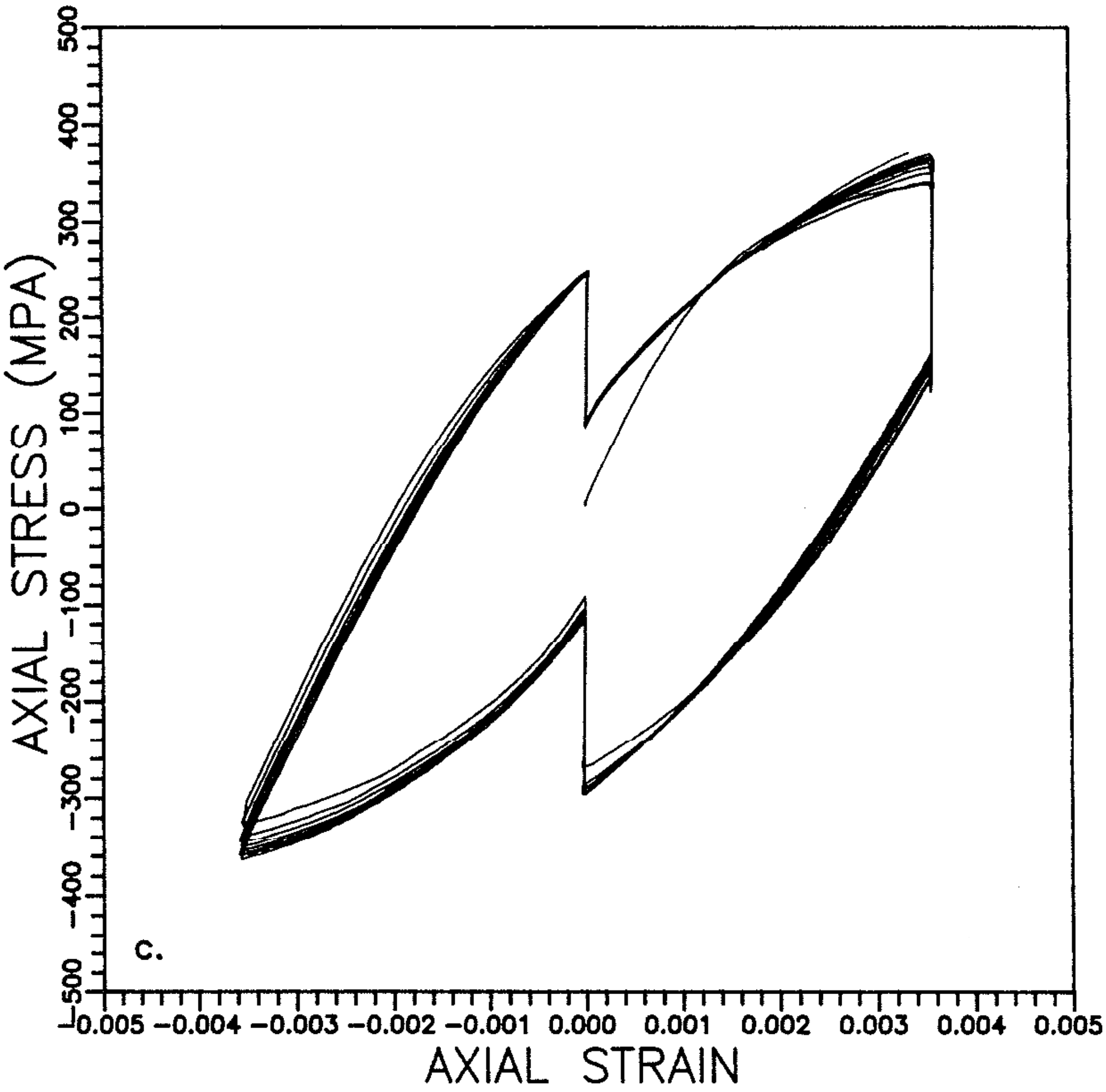
AXIAL STRESS (MPA)
500
400
300
200
100
0
-100
-200
-300
-400
-500
-0.005
-0.004
-0.003
-0.002
-0.001
0.000
0.001
0.002
0.003
0.004
0.005
AXIAL STRAIN
c.

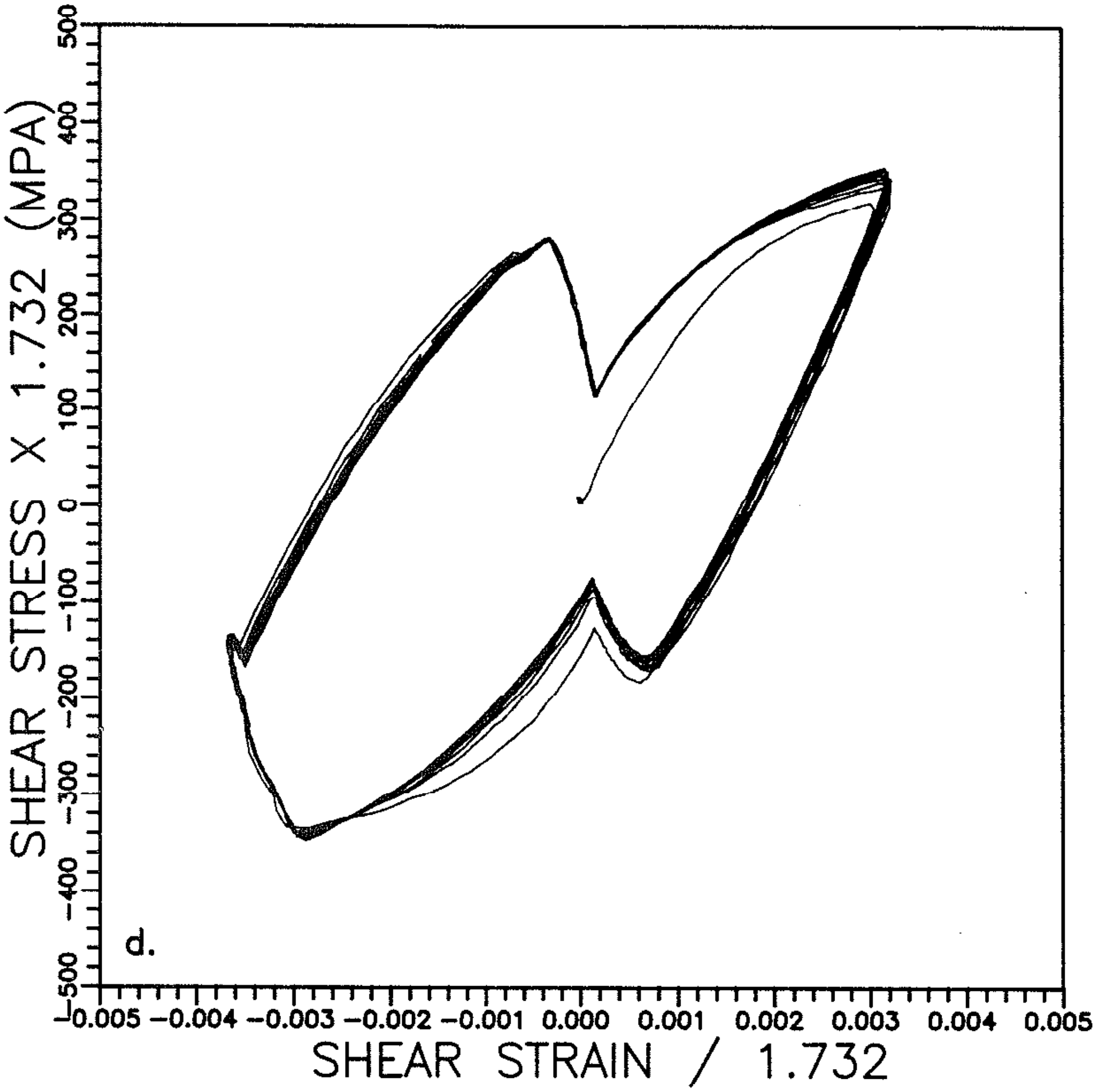
SHEAR STRESS X 1.732 (MPA)
500
400
300
200
100
0
-100
-200
-300
-400
-500
-0.005
-0.004
-0.003
-0.002
-0.001
0.000
0.001
0.002
0.003
0.004
0.005
SHEAR STRAIN / 1.732
d.

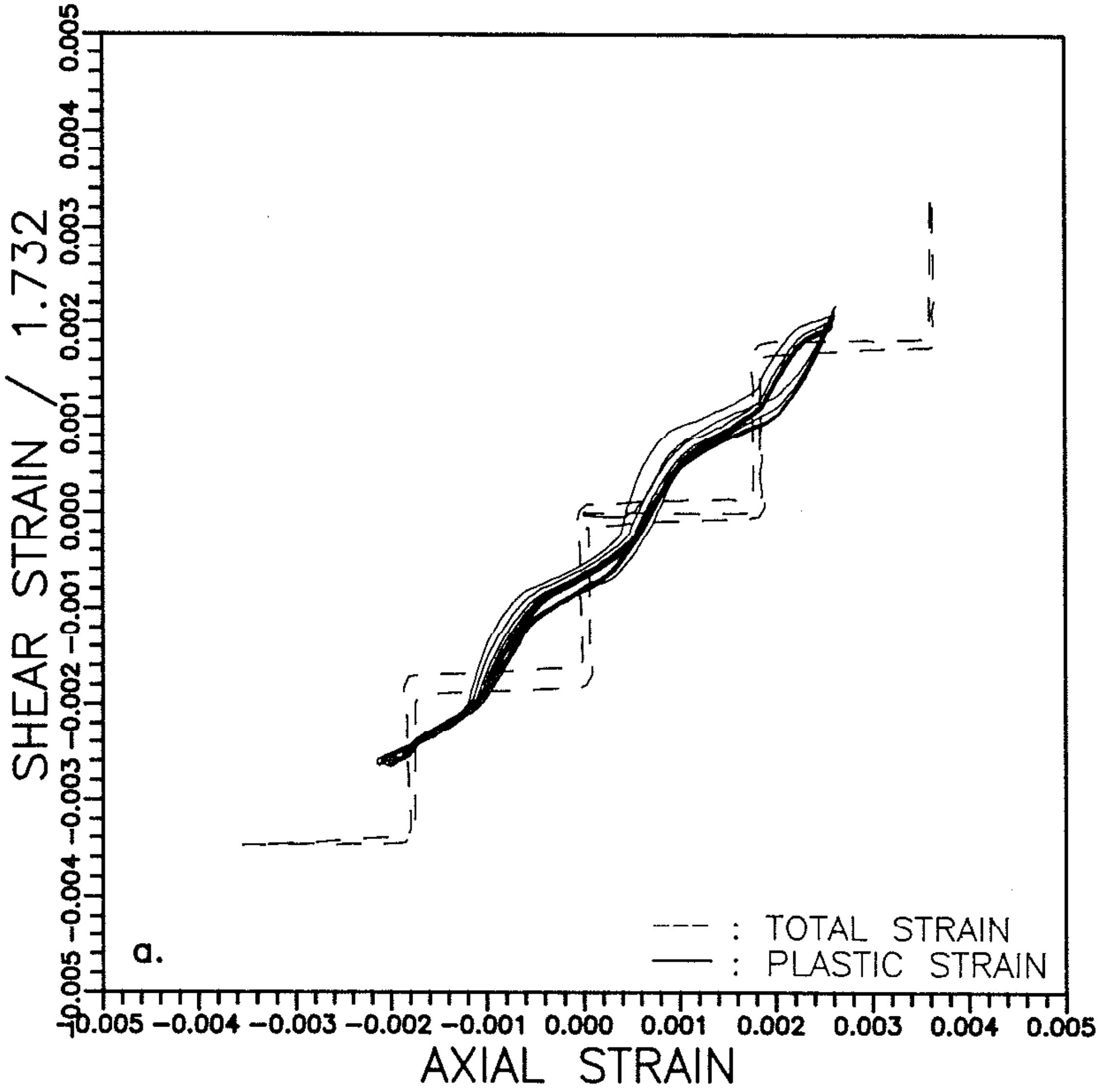

Figure 10. (a) - (d) The Stress-Strain History of 310 Stainless Steel under a Four-Stair Tension-Torsion Strain Controlled Cycling (Specimen S111).

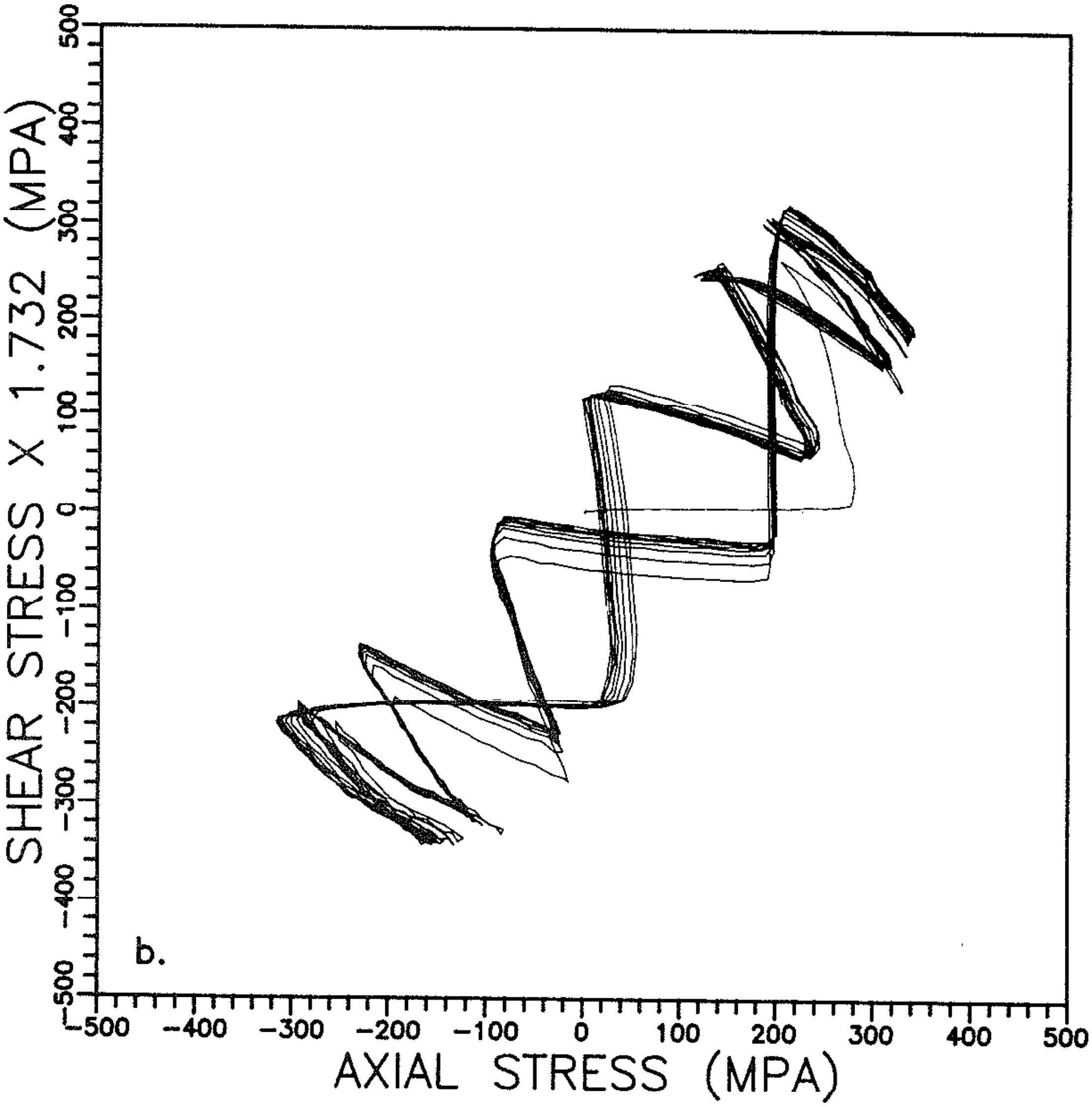
SHEAR STRESS X 1.732 (MPA)
AXIAL STRESS (MPA)
500
400
300
200
100
0
−100
−200
−300
−400
−500
−500
−400
−300
−200
−100
0
100
200
300
400
500
b.

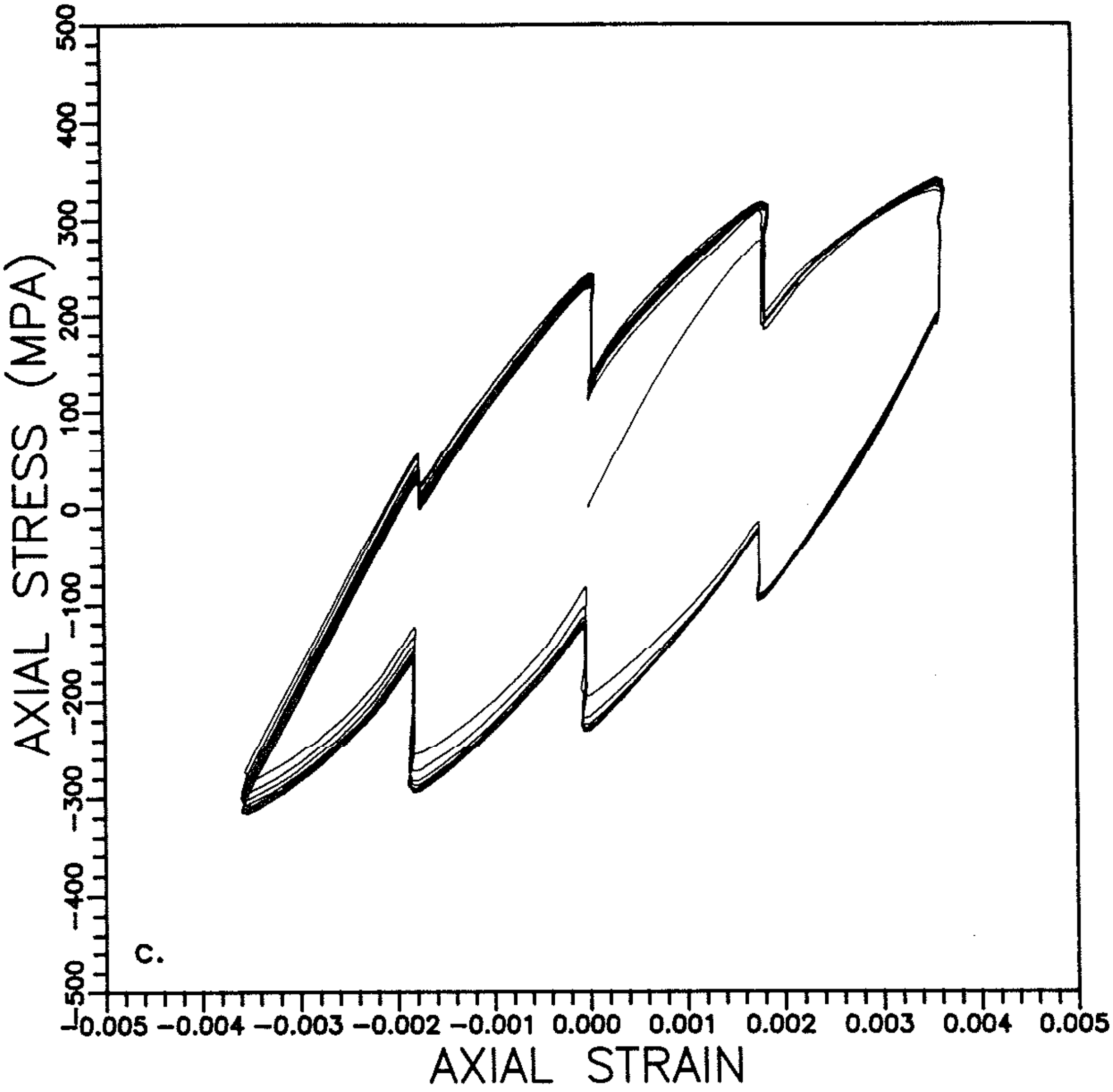
AXIAL STRESS (MPA)
500
400
300
200
100
0
-100
-200
-300
-400
-500
c.
-0.005
-0.004
-0.003
-0.002
-0.001
0.000
0.001
0.002
0.003
0.004
0.005
AXIAL STRAIN

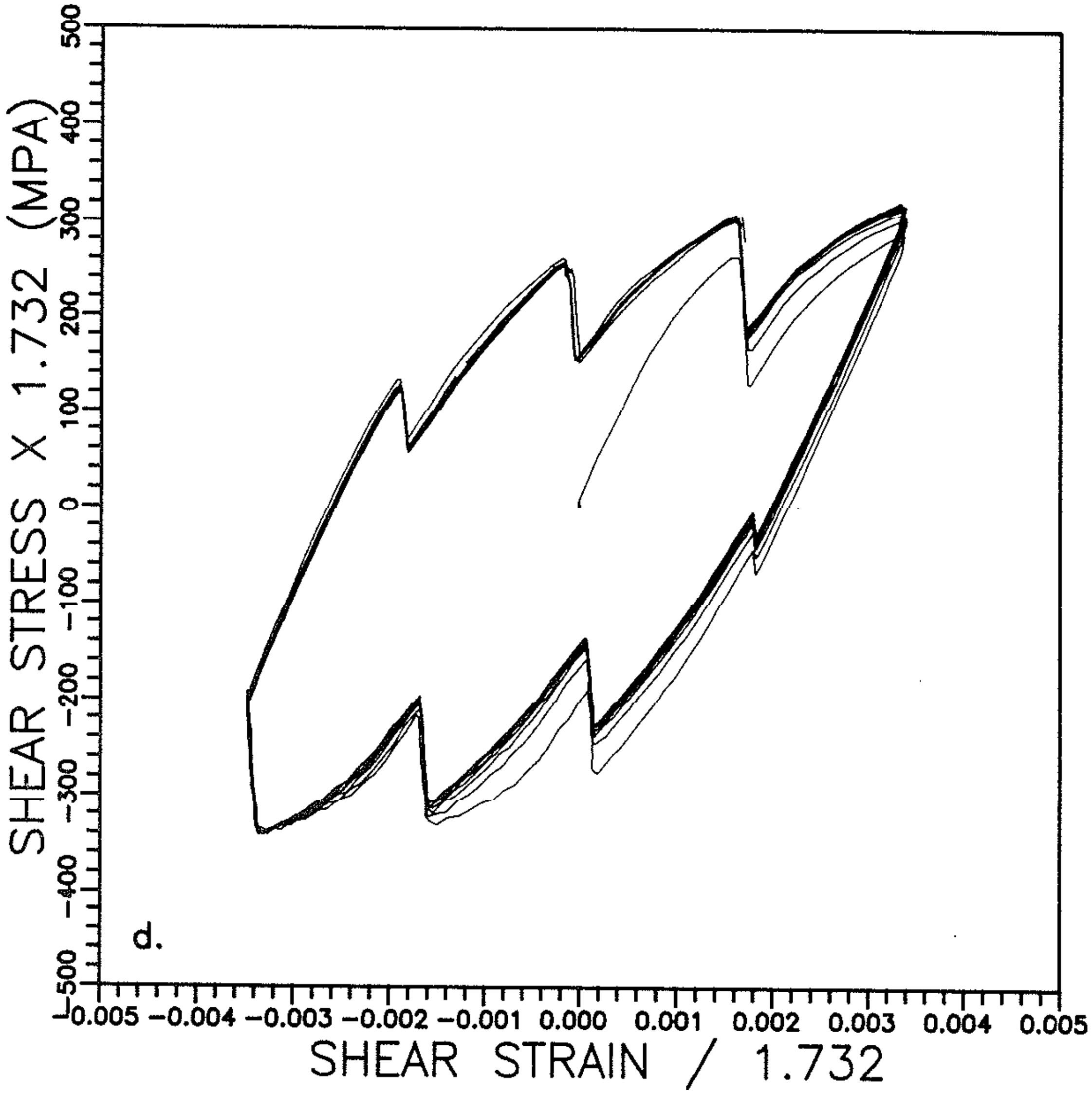
SHEAR STRESS X 1.732 (MPA)
500
400
300
200
100
0
-100
-200
-300
-400
-500
d.
-0.005
-0.004
-0.003
-0.002
-0.001
0.000
0.001
0.002
0.003
0.004
0.005
SHEAR STRAIN / 1.732

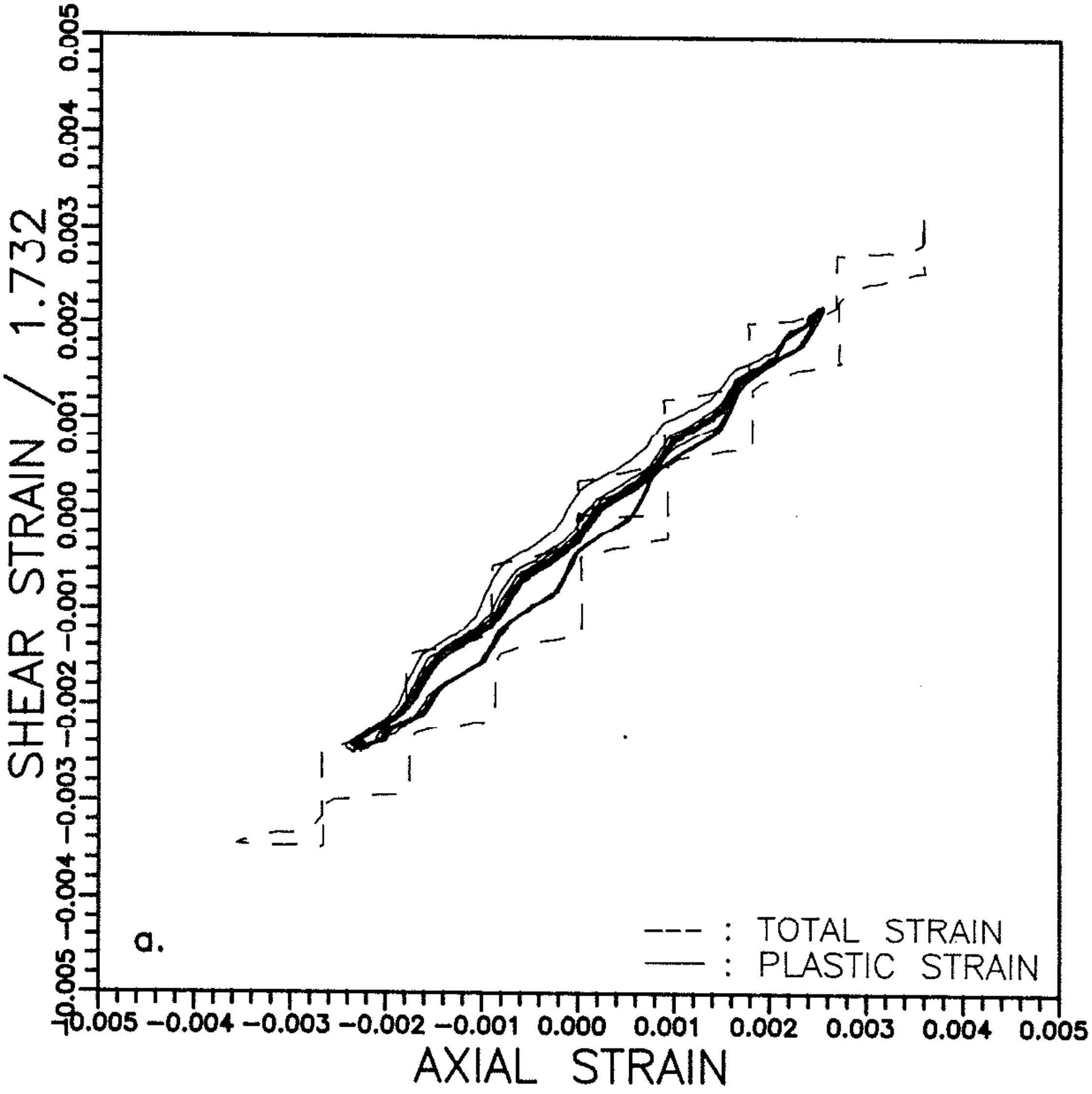

Figure 11. (a) - (d) The Stress-Strain History of 310 Stainless Steel under a Eight-Stair Tension-Torsion Strain Controlled Cycling (Specimen S112).

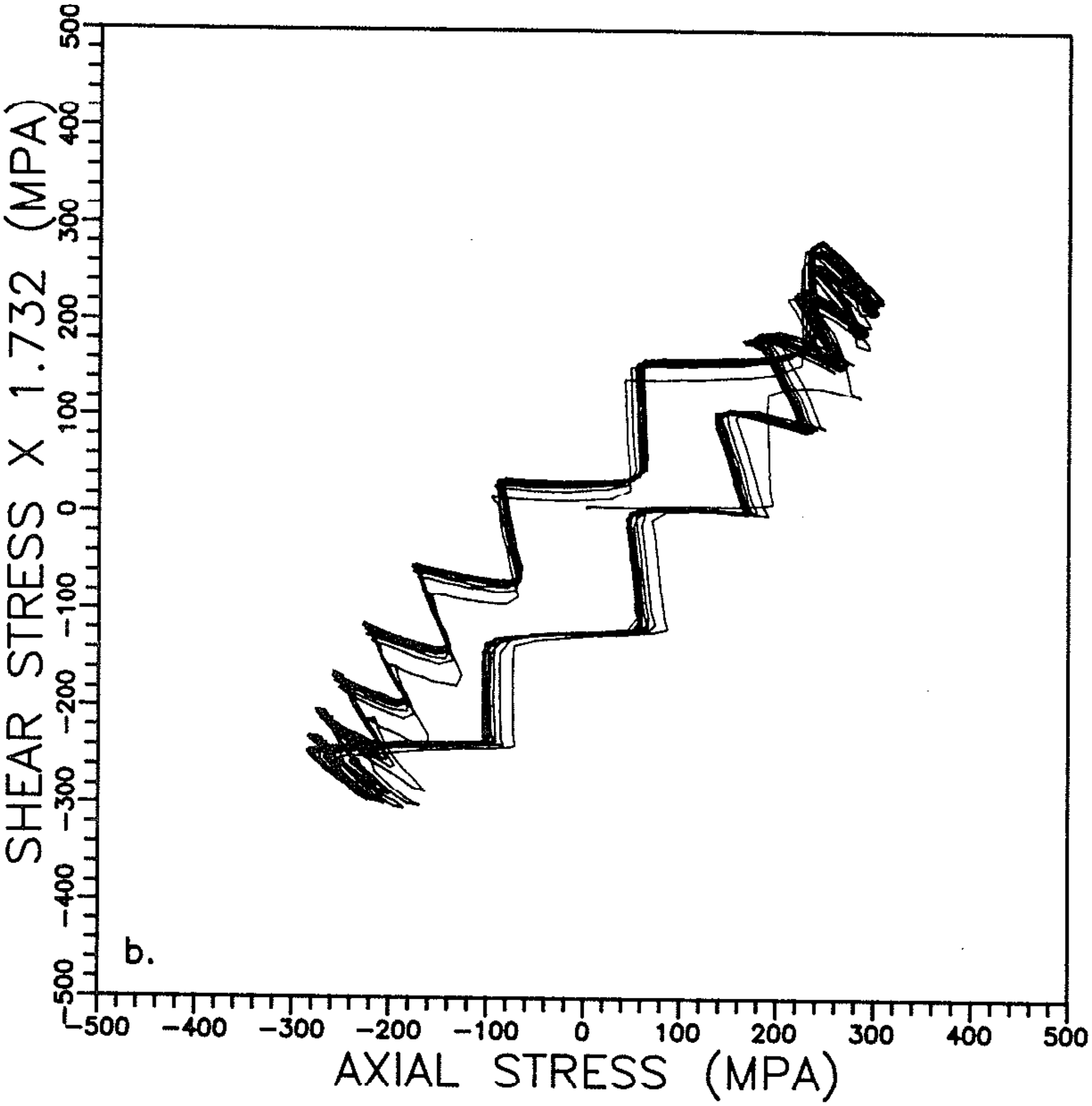
SHEAR STRESS X 1.732 (MPA)
AXIAL STRESS (MPA)
-500
-400
-300
-200
-100
0
100
200
300
400
500
b.

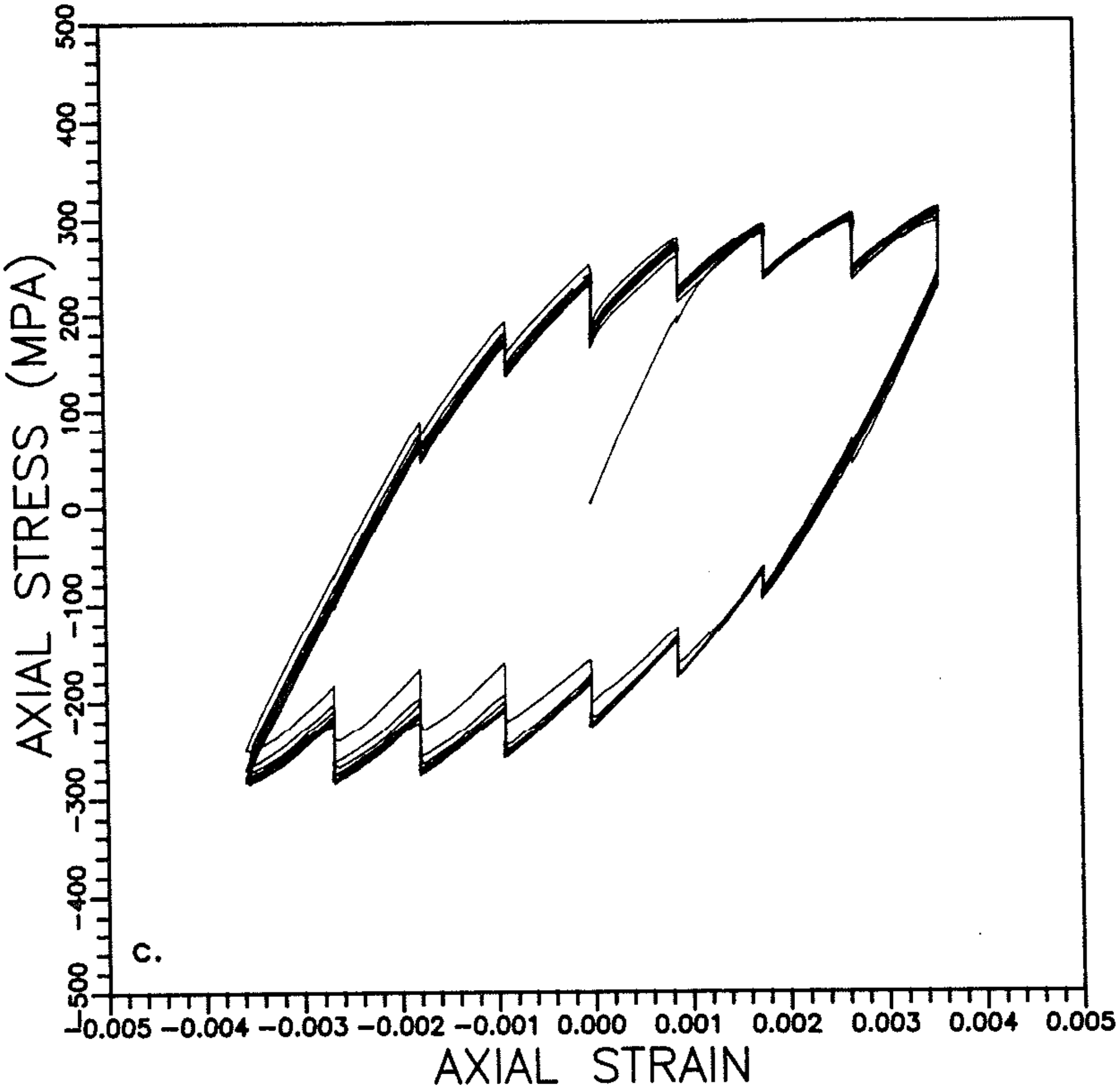
AXIAL STRESS (MPA)
500
400
300
200
100
0
-100
-200
-300
-400
-500
-0.005
-0.004
-0.003
-0.002
-0.001
0.000
0.001
0.002
0.003
0.004
0.005
AXIAL STRAIN
c.

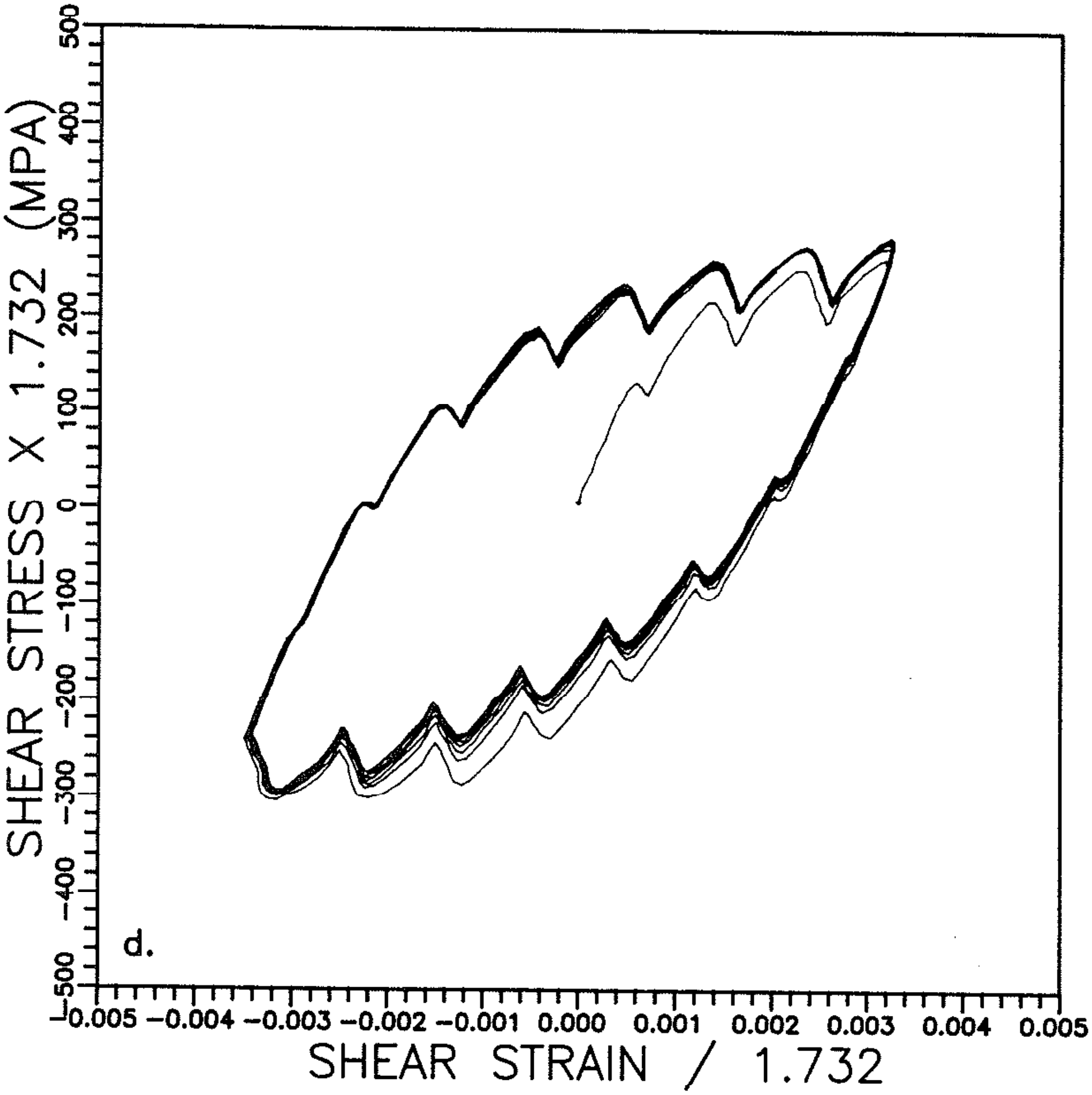
SHEAR STRESS X 1.732 (MPA)
500
400
300
200
100
0
−100
−200
−300
−400
−500
d.
−0.005
−0.004
−0.003
−0.002
−0.001
0.000
0.001
0.002
0.003
0.004
0.005
SHEAR STRAIN / 1.732

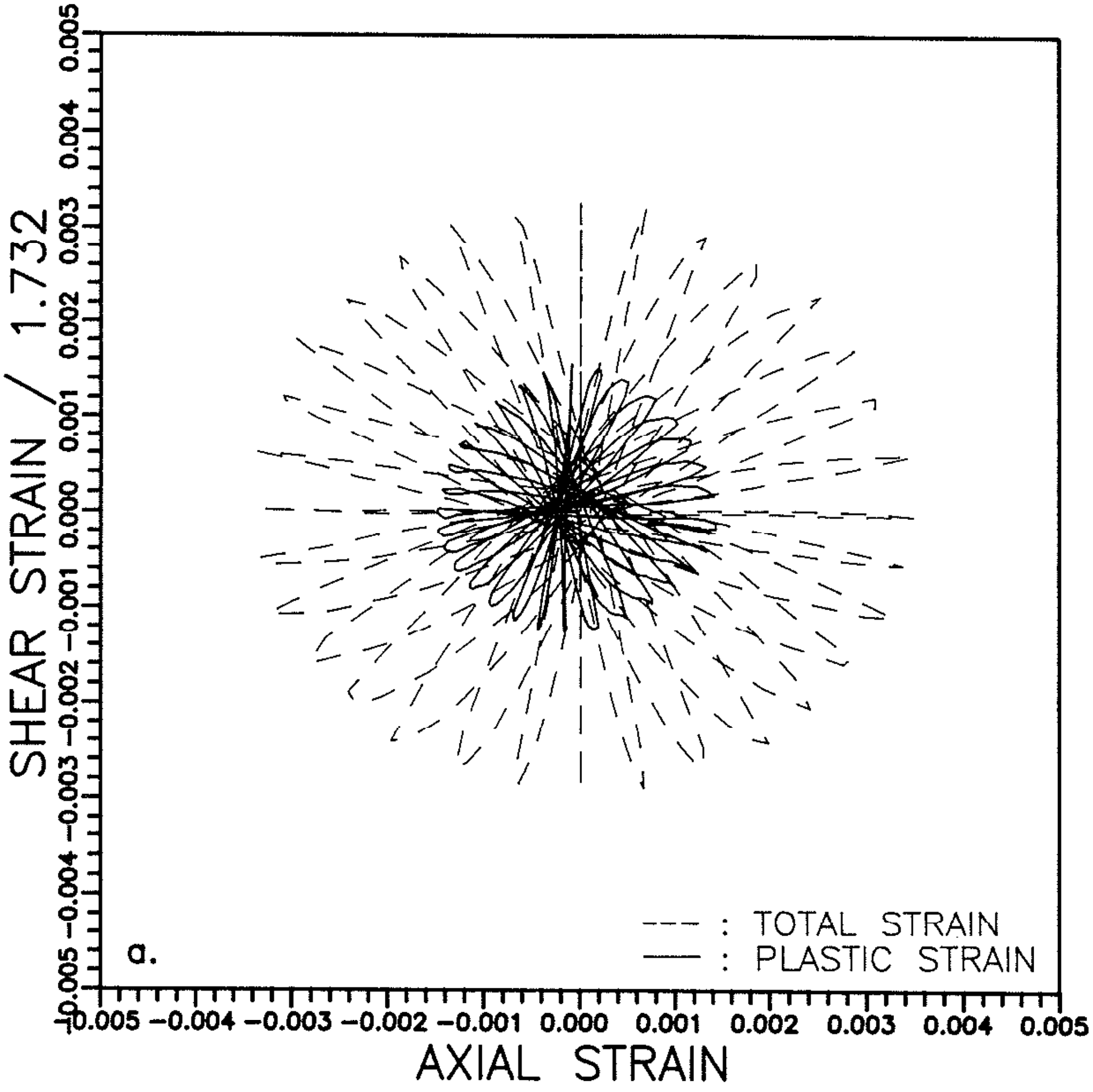

Figure 12. (a) - (d) The Stress-Strain History of 310 Stainless Steel under a Strain Path of Slowly Changed Loading Direction (Specimen S114).

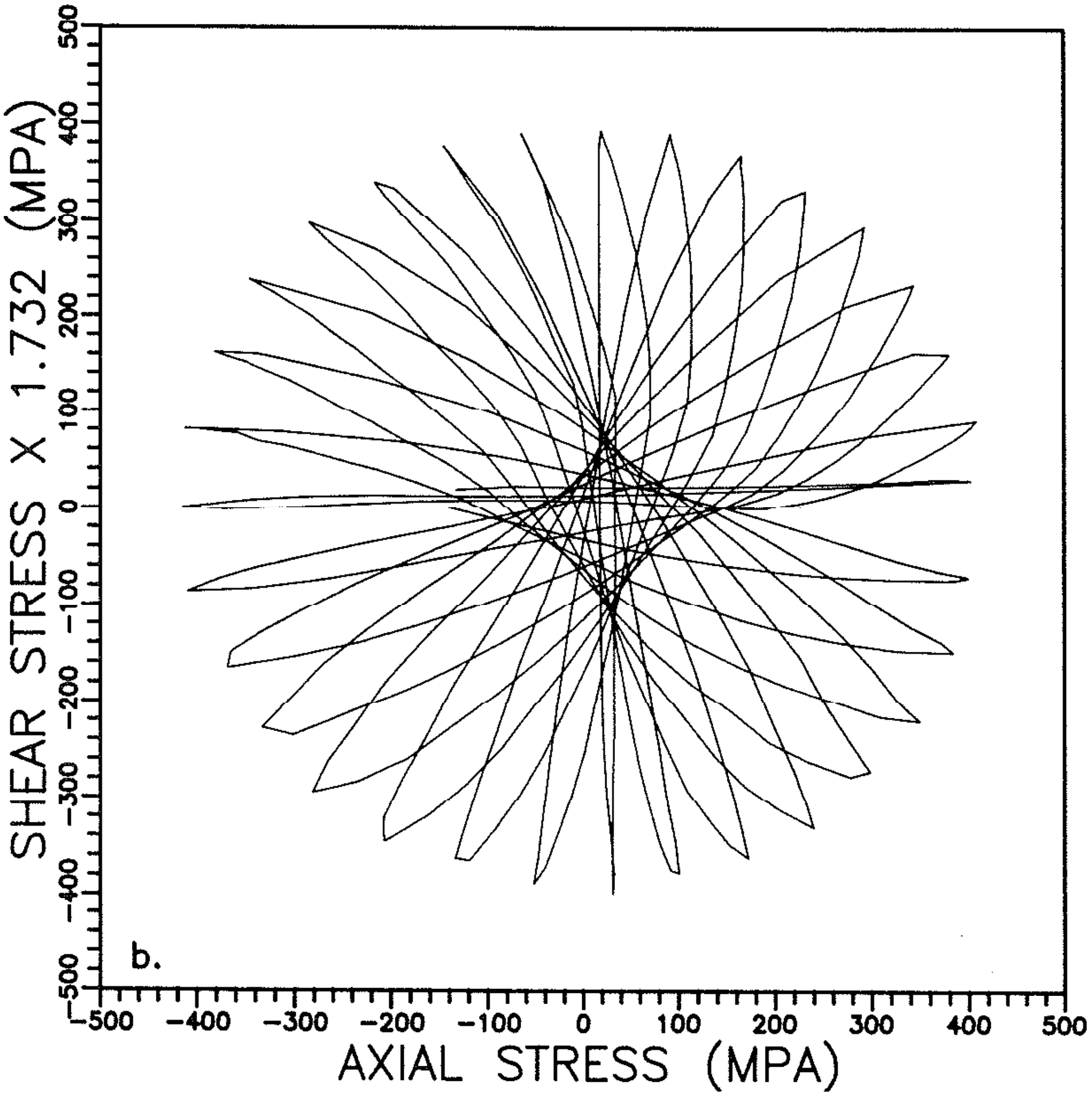
b.
SHEAR STRESS X 1.732 (MPA)
500
400
300
200
100
0
−100
−200
−300
−400
−500
AXIAL STRESS (MPA)
−500
−400
−300
−200
−100
0
100
200
300
400
500

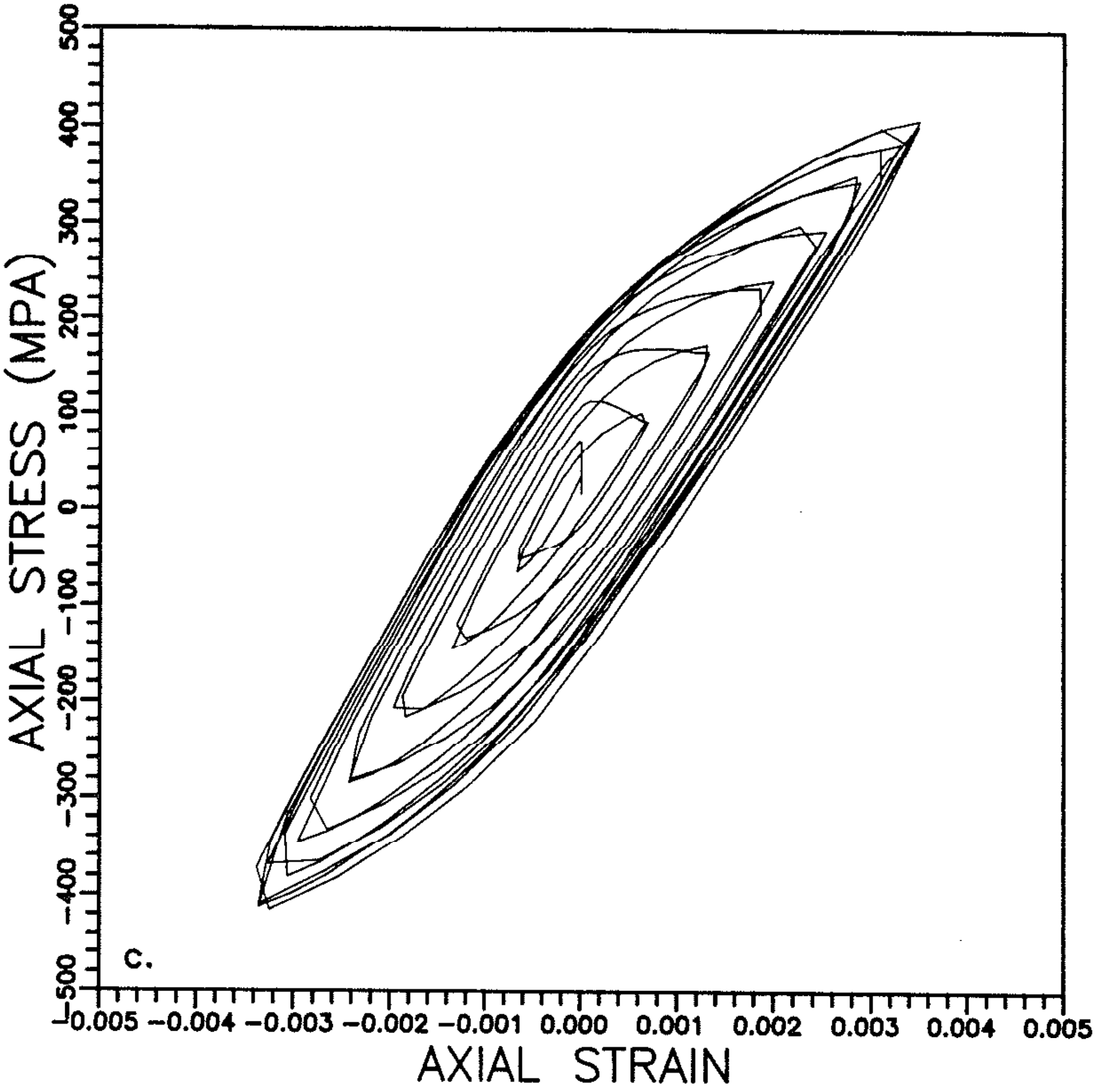
c.
AXIAL STRESS (MPA)
500
400
300
200
100
0
-100
-200
-300
-400
-500
-0.005
-0.004
-0.003
-0.002
-0.001
0.000
0.001
0.002
0.003
0.004
0.005
AXIAL STRAIN

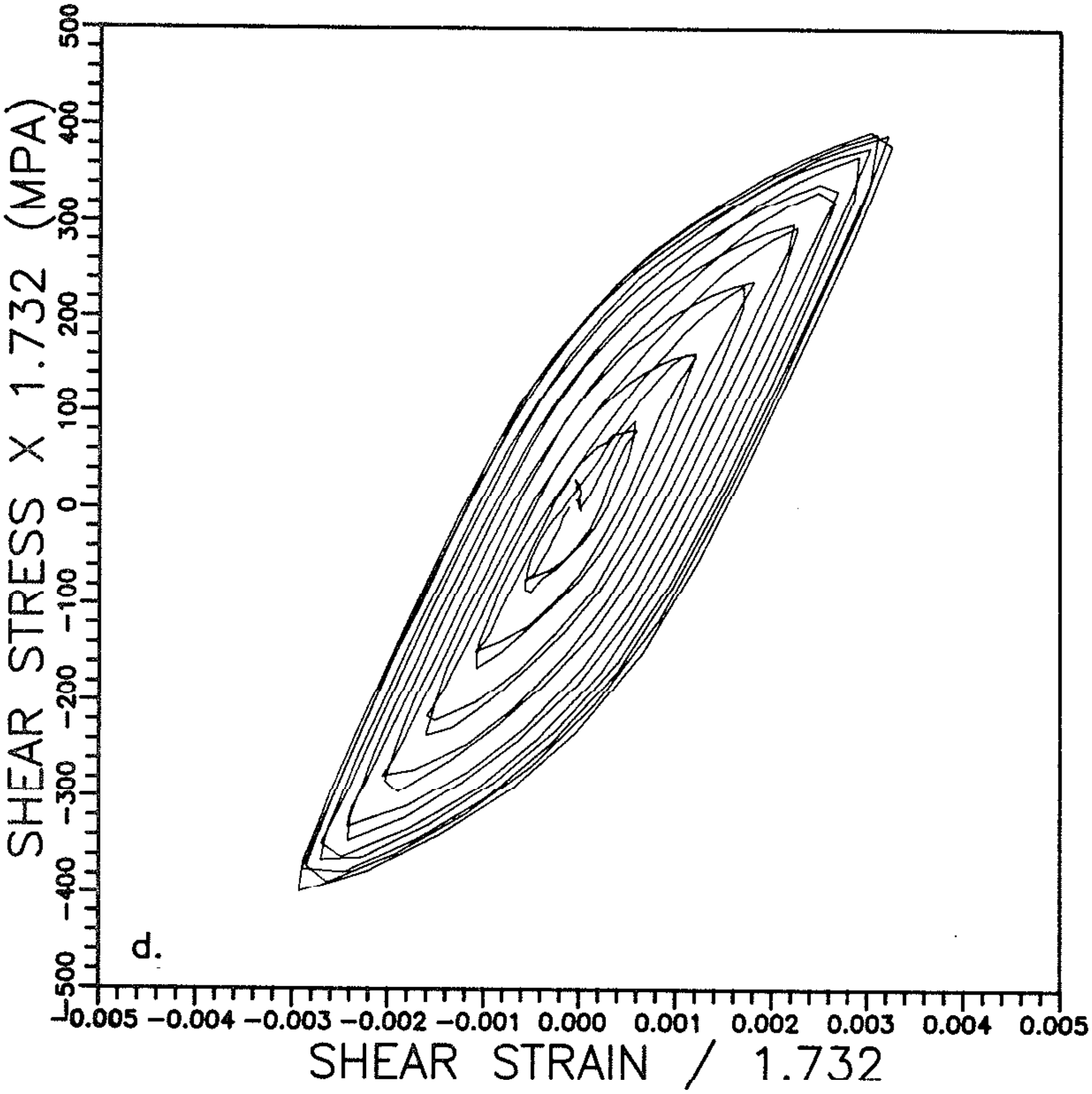
SHEAR STRESS X 1.732 (MPA)
500
400
300
200
100
0
-100
-200
-300
-400
-500
-0.005
-0.004
-0.003
-0.002
-0.001
0.000
0.001
0.002
0.003
0.004
0.005
SHEAR STRAIN / 1.732
d.

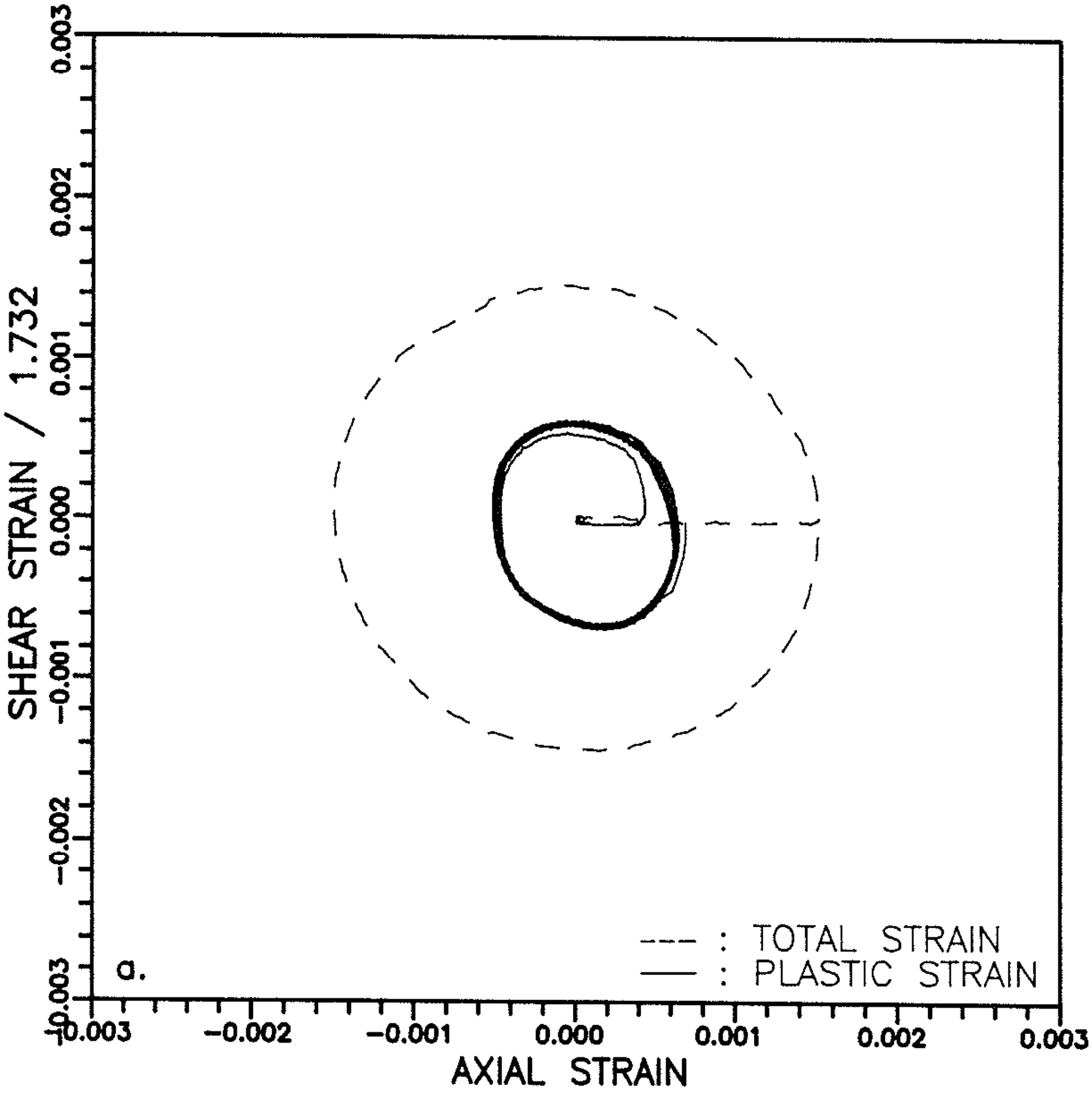

Figure 13. (a) - (d) The Stress-Strain History of 1100 Aluminum under a 90° Out-Of-Phase Tension-Torsion Strained-Controlled Cycling (Specimen A104).

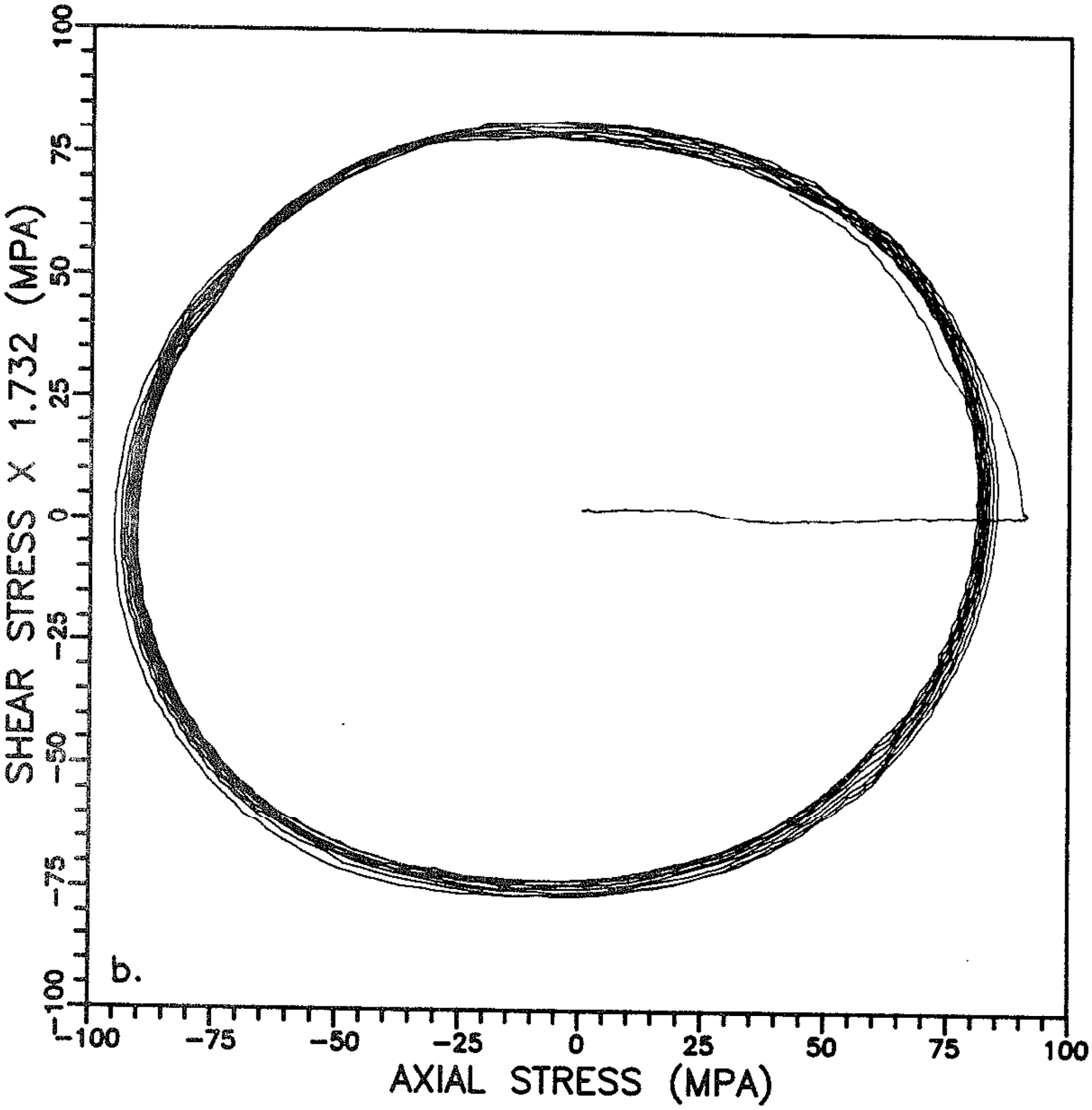
SHEAR STRESS X 1.732 (MPA)
AXIAL STRESS (MPA)
b.
100
75
50
25
0
−25
−50
−75
−100
−100
−75
−50
−25
0
25
50
75
100

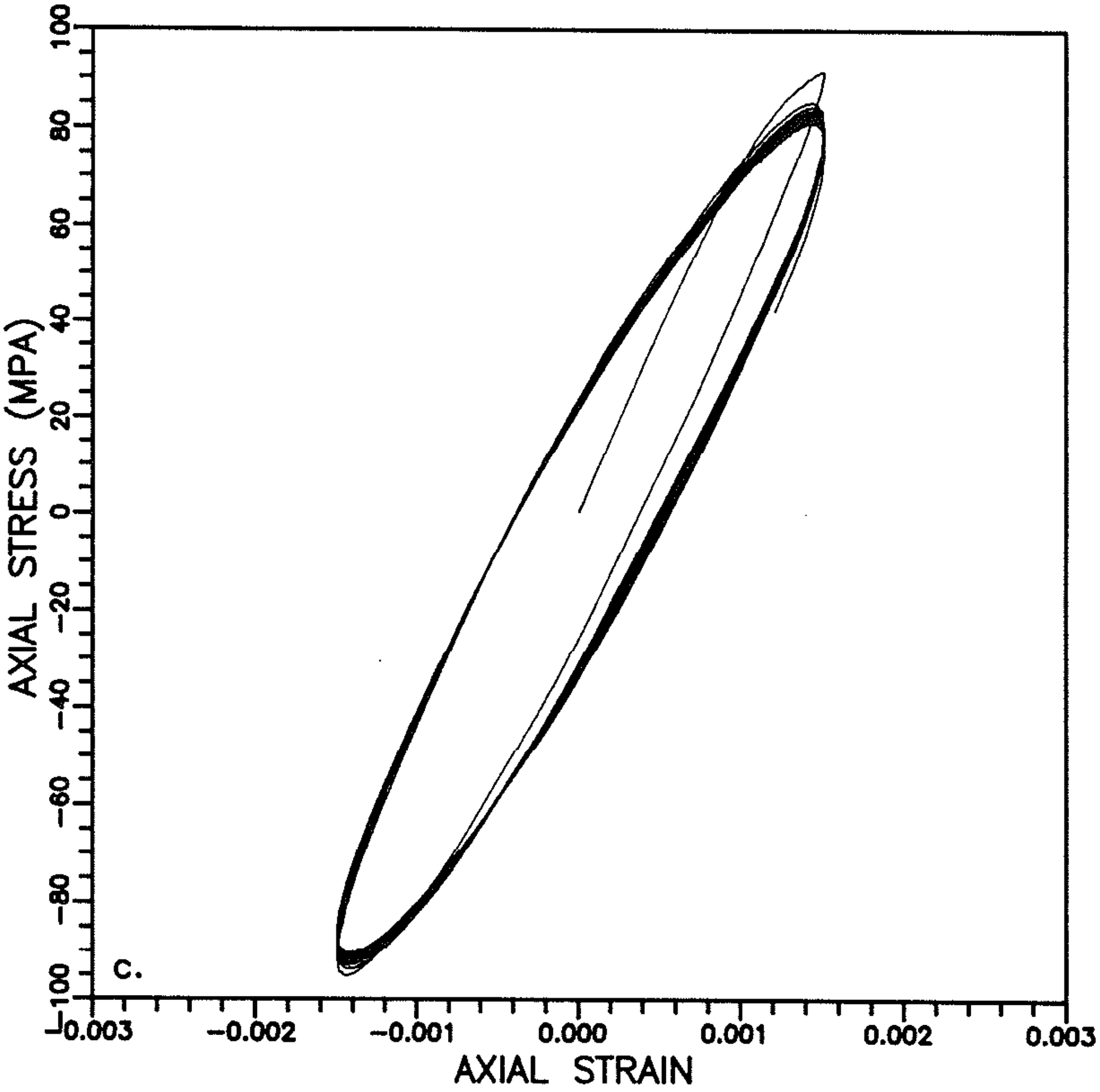
AXIAL STRESS (MPA)
100
80
60
40
20
0
−20
−40
−60
−80
−100
c.
−0.003
−0.002
−0.001
0.000
0.001
0.002
0.003
AXIAL STRAIN

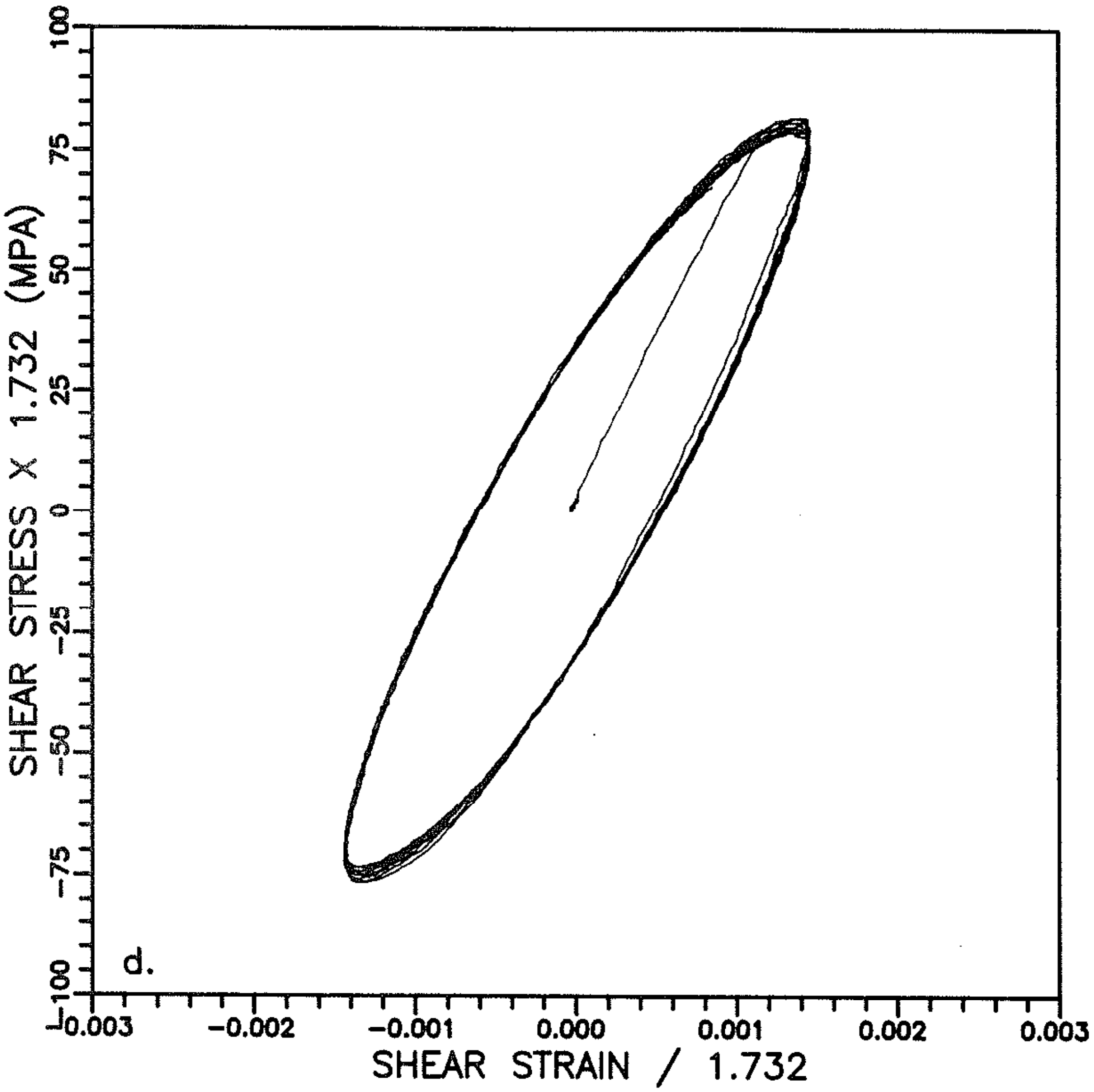
SHEAR STRESS X 1.732 (MPA)
100
75
50
25
0
-25
-50
-75
-100
-0.003
-0.002
-0.001
0.000
0.001
0.002
0.003
SHEAR STRAIN / 1.732
d.

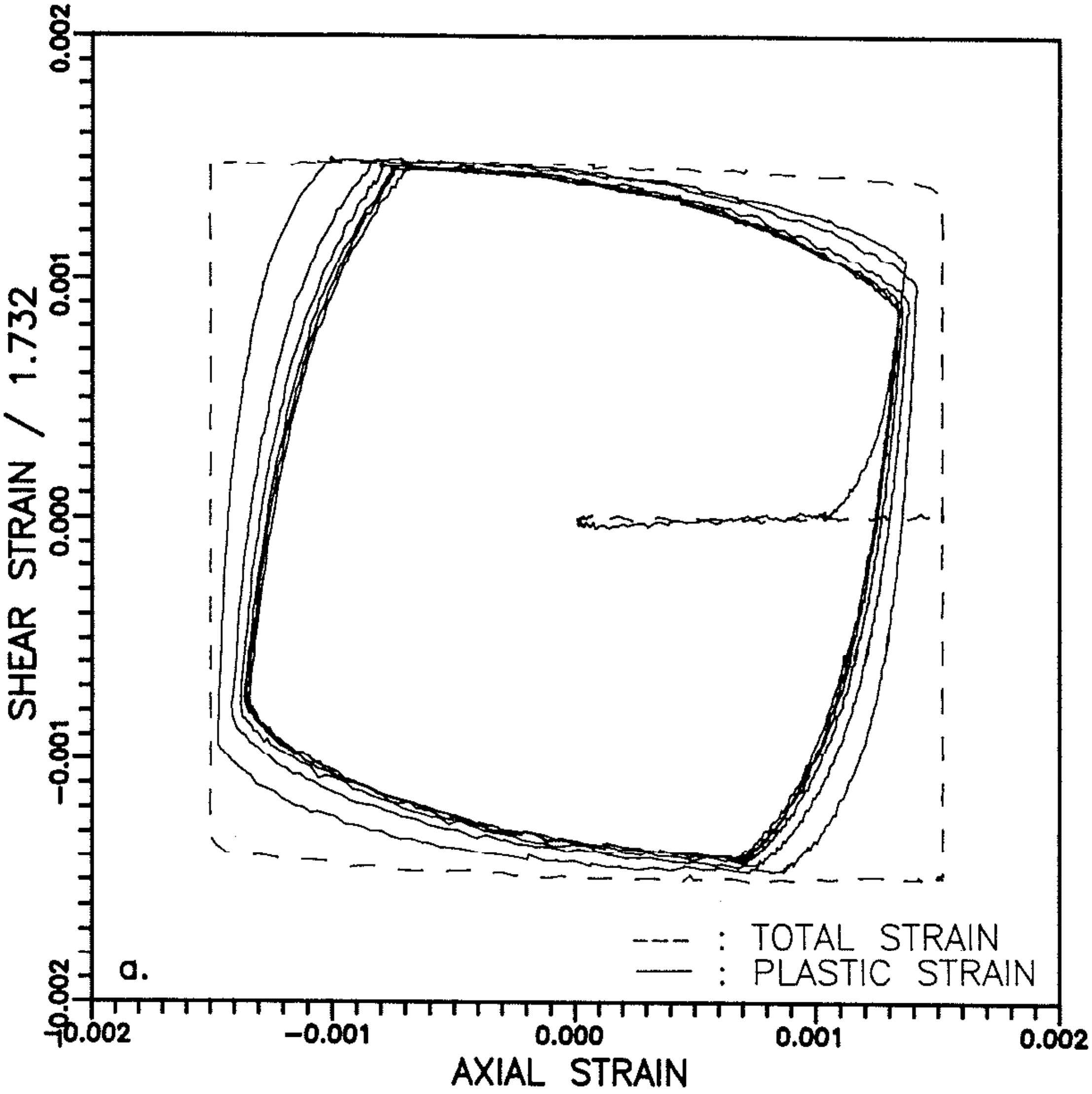

Figure 14. (a) - (d) The Stress-Strain History of 1100 Aluminum under a One-Square Path of Strain-Controlled Cycling (Specimen A113).

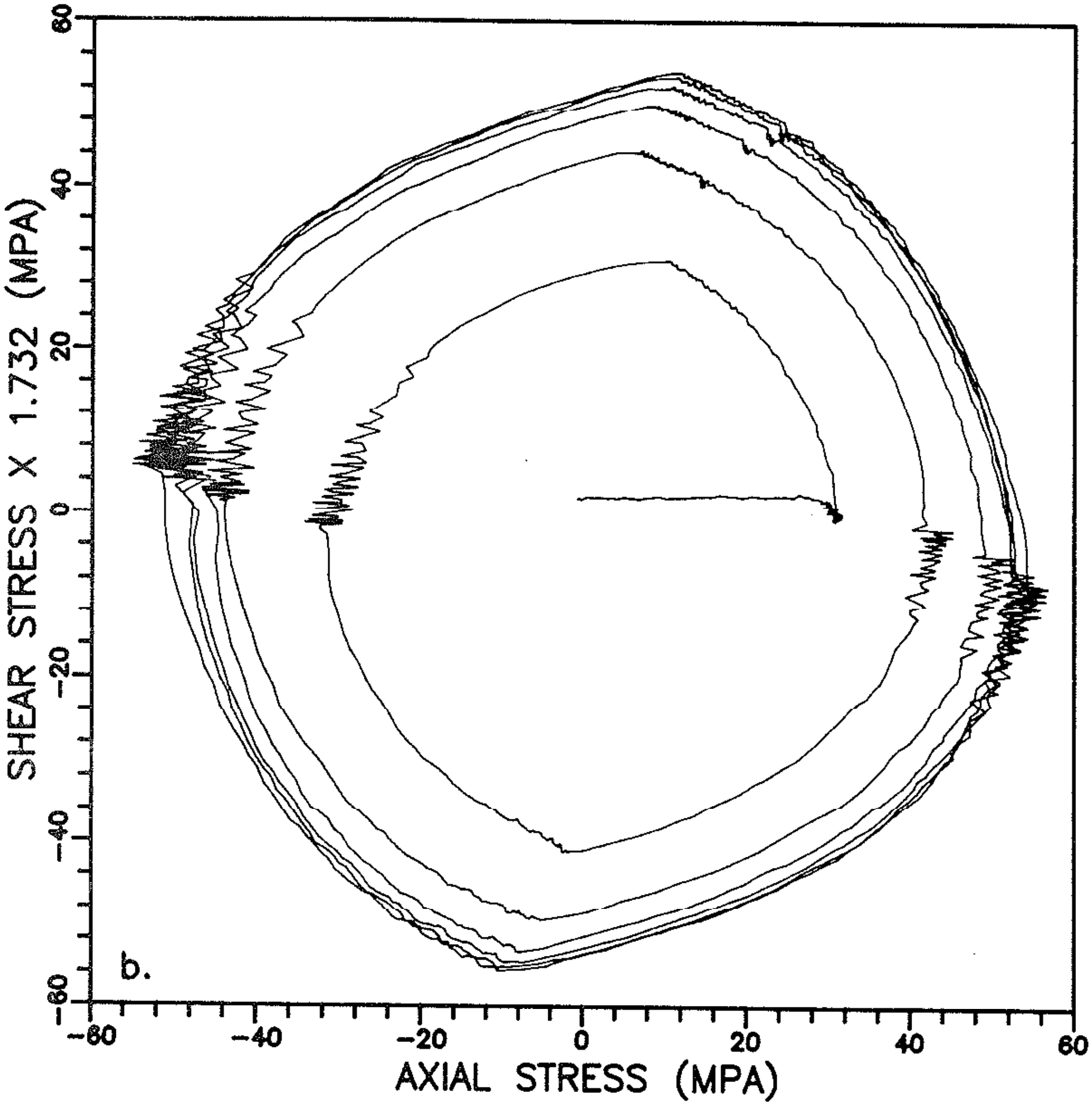
b.
SHEAR STRESS X 1.732 (MPA)
AXIAL STRESS (MPA)
-60
-40
-20
0
20
40
60
-60
-40
-20
0
20
40
60

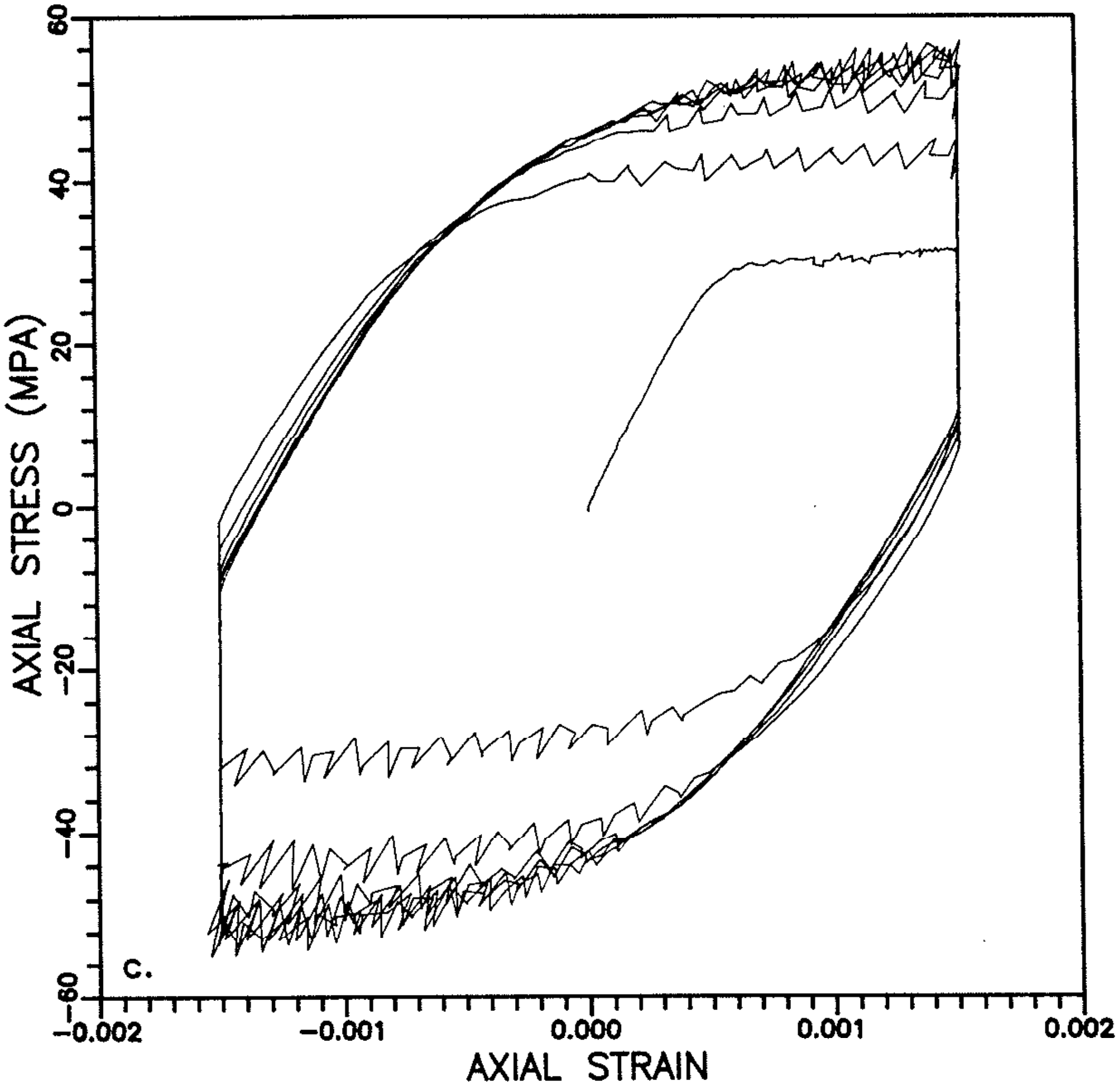
AXIAL STRESS (MPA)
60
40
20
0
−20
−40
−60
−0.002
−0.001
0.000
0.001
0.002
AXIAL STRAIN
c.

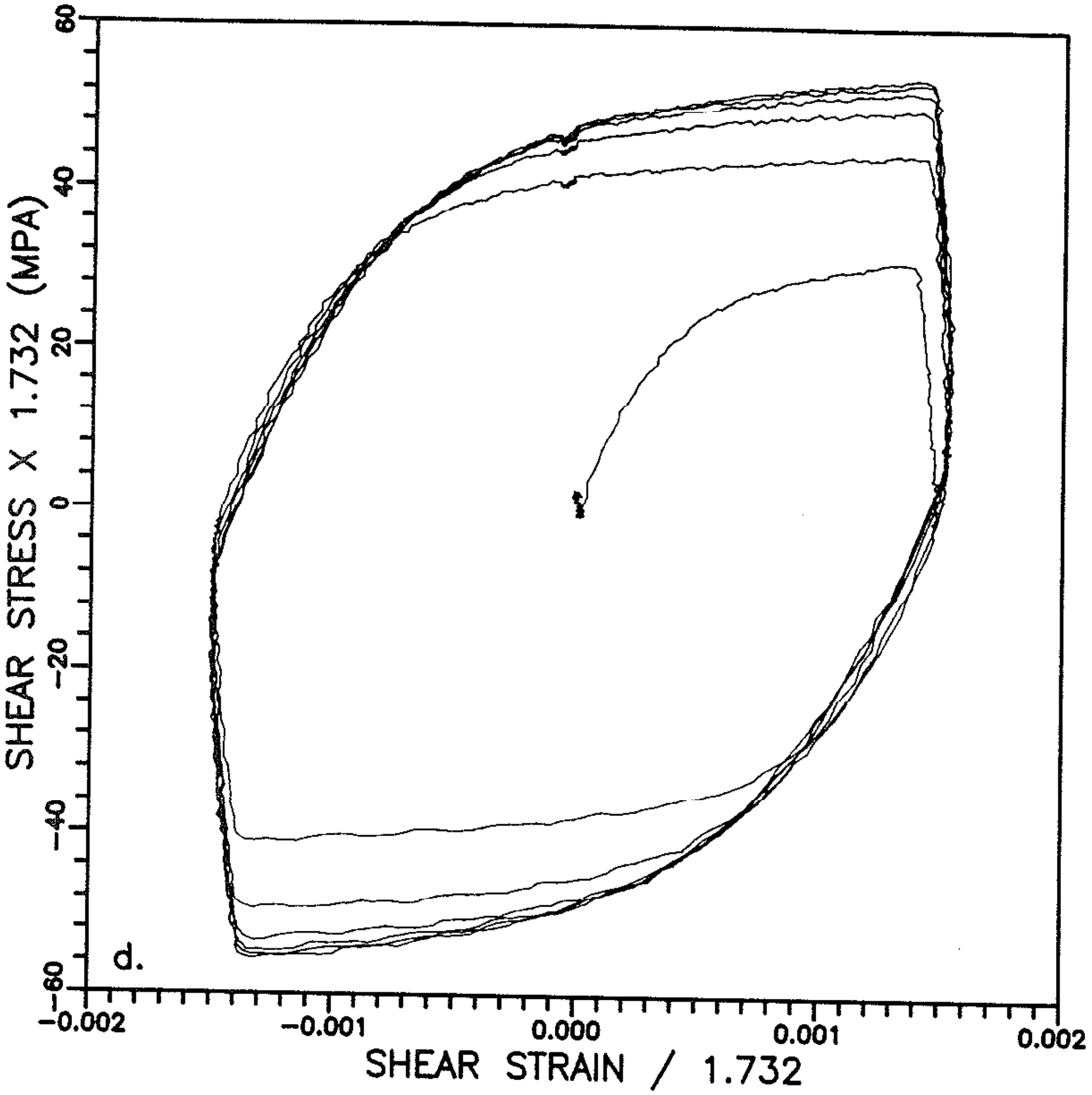
SHEAR STRESS X 1.732 (MPA)
60
40
20
0
-20
-40
-60
SHEAR STRAIN / 1.732
-0.002
-0.001
0.000
0.001
0.002
d.

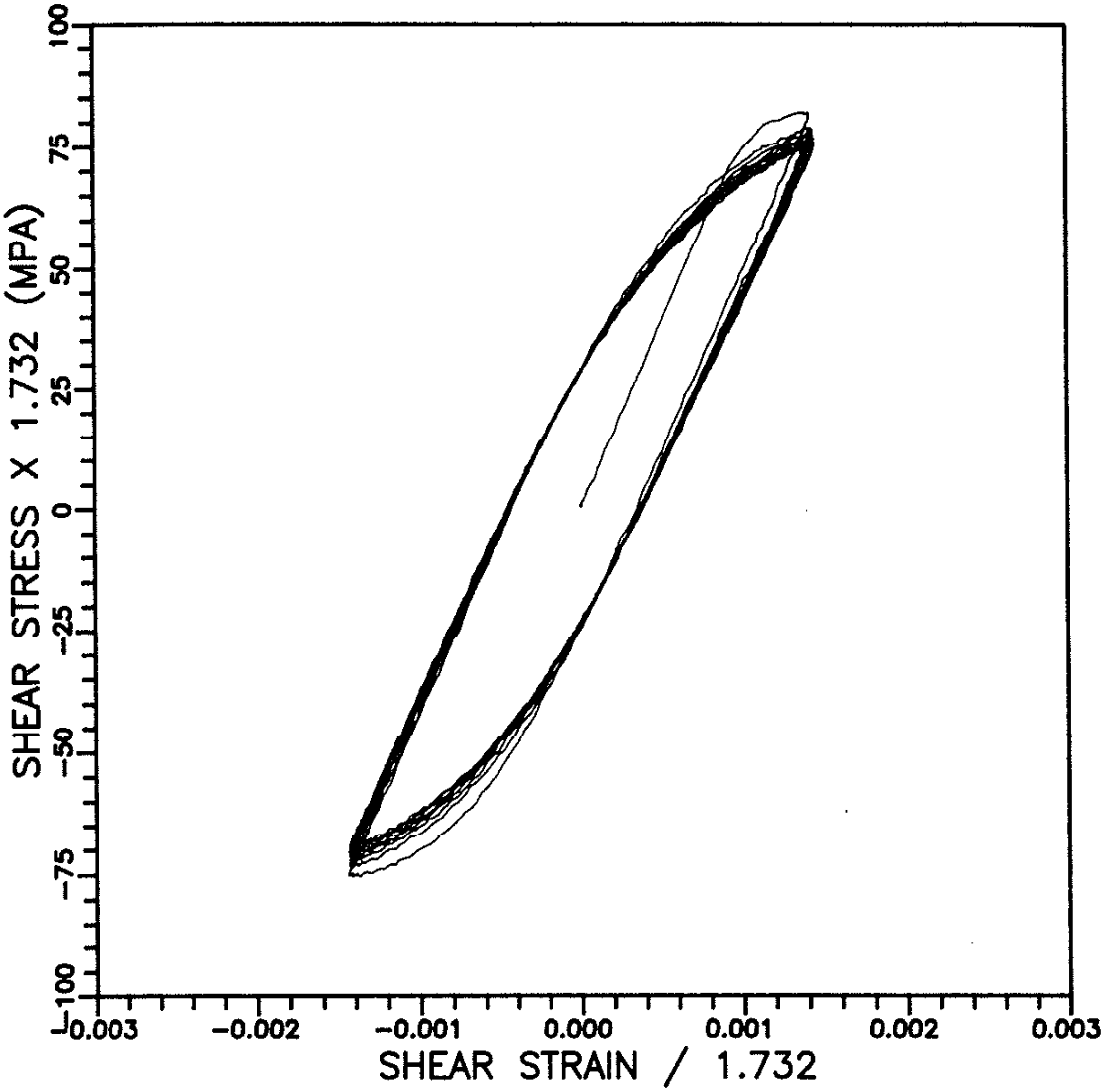

Figure 15. The Stress-Strain History of 1100 Aluminum under Cyclic Torsion (Specimen A 109).

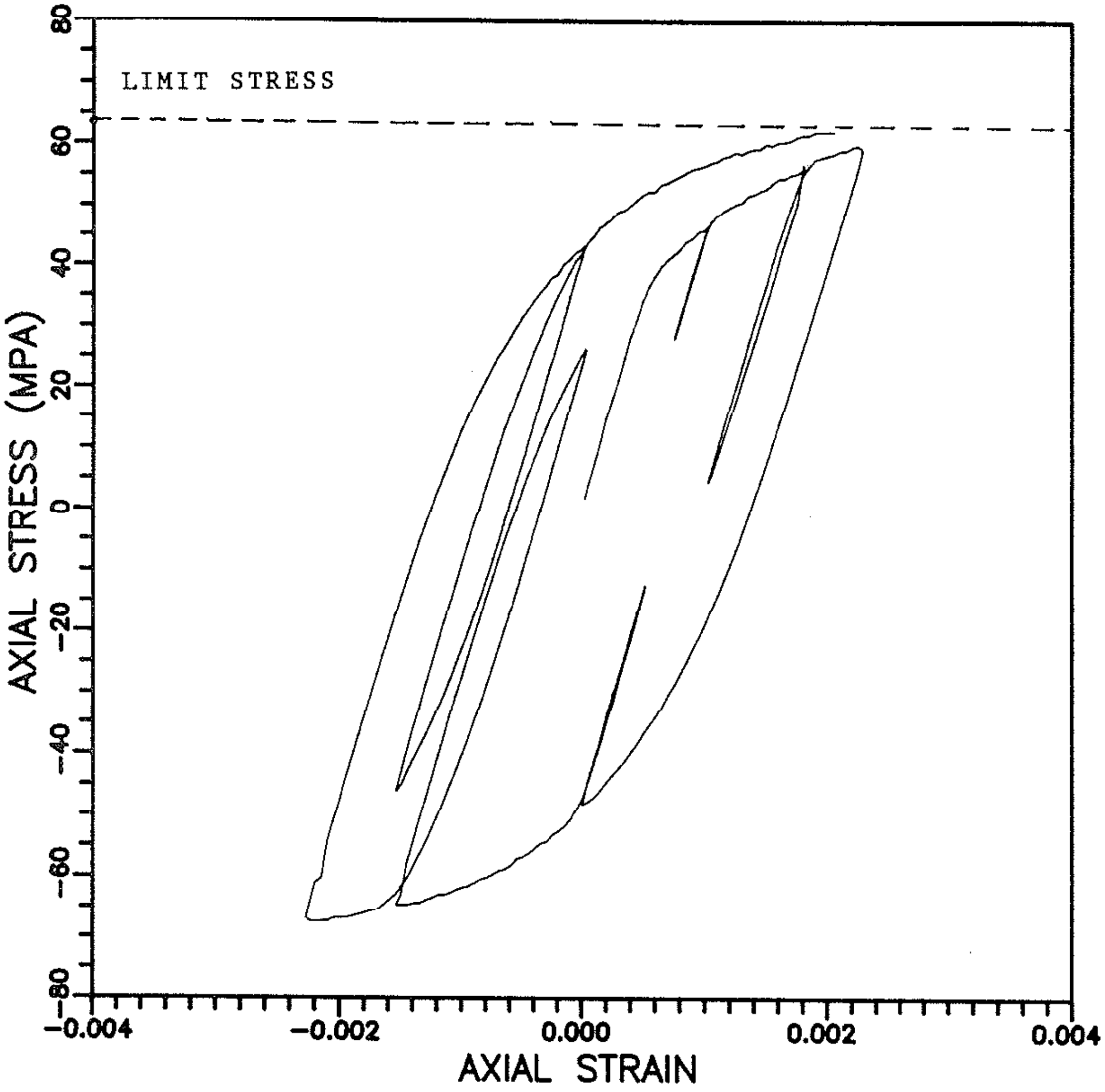

Figure 16. The Stress-Strain Response of 1100 Aluminum under a Random Uniaxial Loading (Specimen A114).

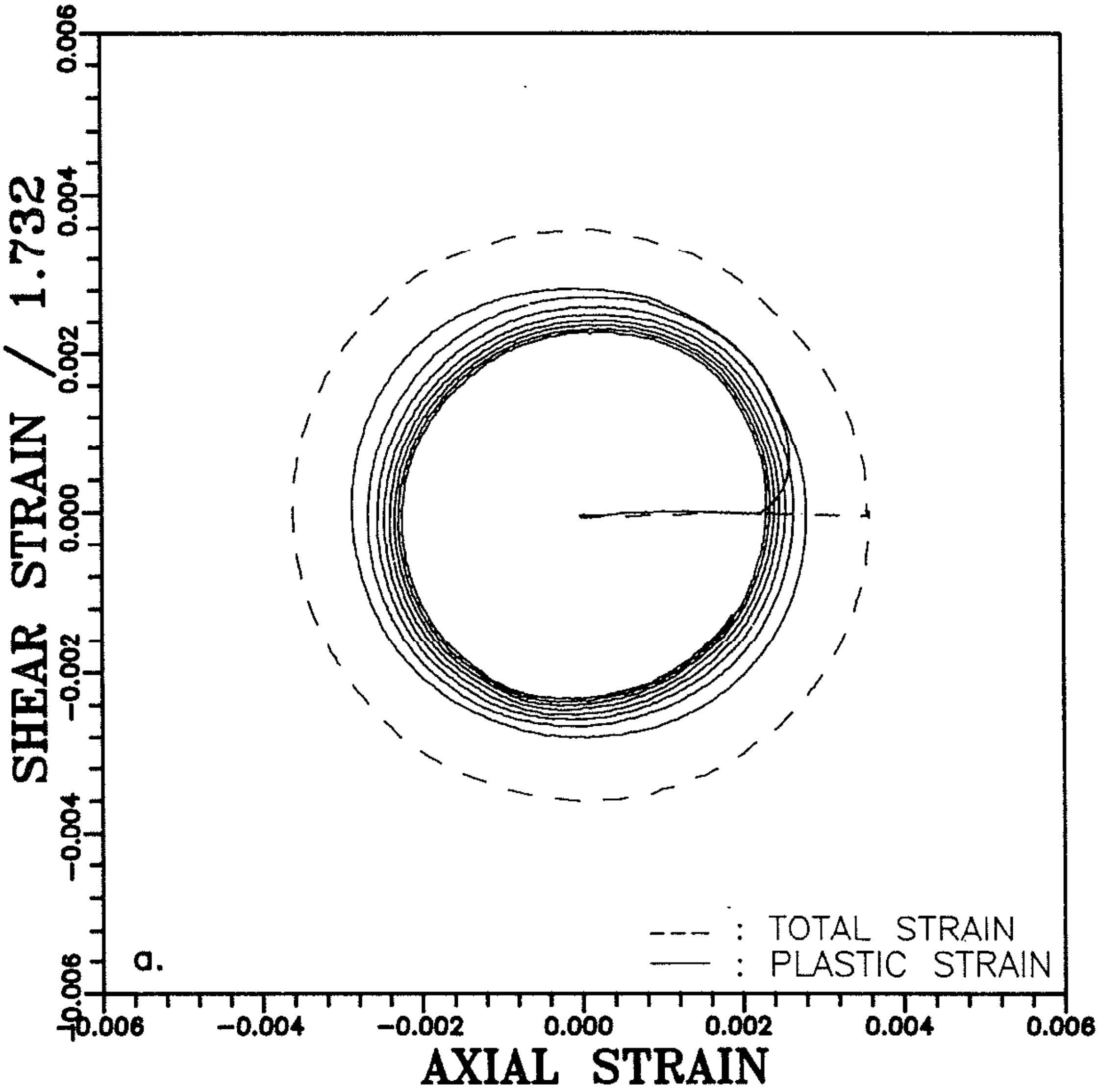

Figure 17. (a) - (d) The Stress-Strain History of 304 Stainless Steel under 90° Out-Of-Phase Tension-Torsion Strain-Controlled Cycling (Specimen SS13) [36].

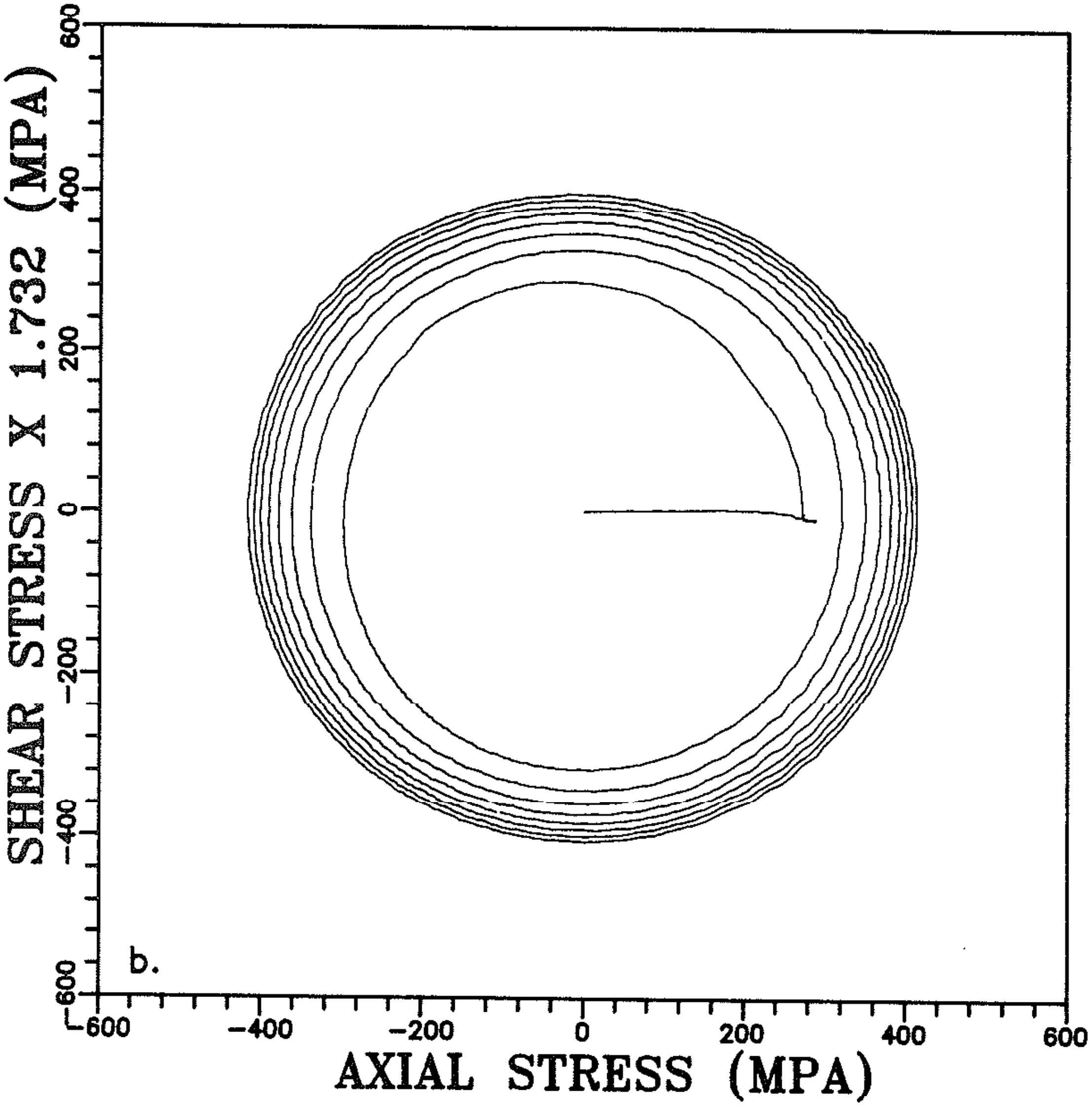
SHEAR STRESS X 1.732 (MPA)
AXIAL STRESS (MPA)
600
400
200
0
-200
-400
-600
-600
-400
-200
0
200
400
600
b.

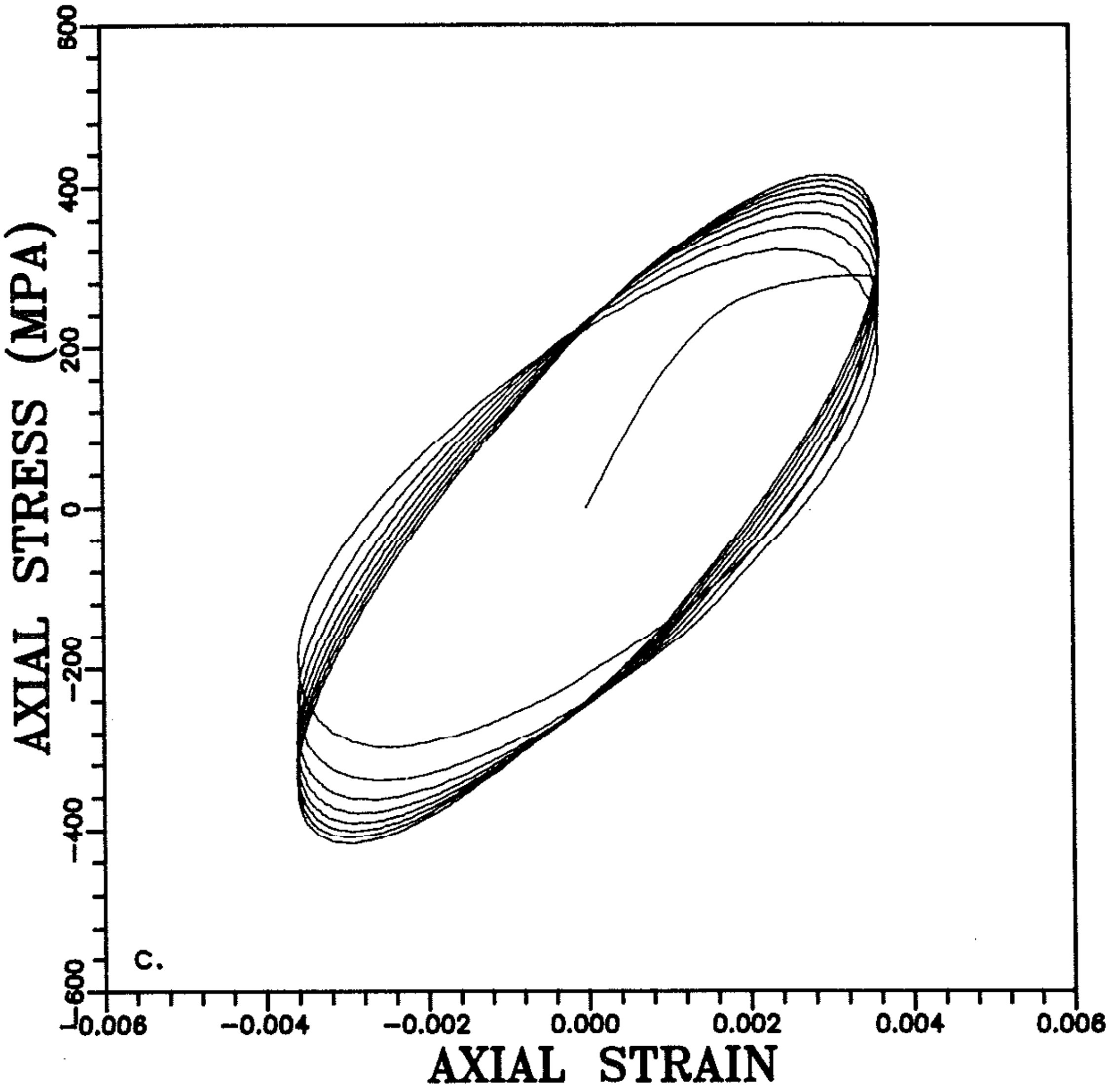
AXIAL STRESS (MPA)
AXIAL STRAIN
600
400
200
0
−200
−400
−600
−0.006
−0.004
−0.002
0.000
0.002
0.004
0.006
c.

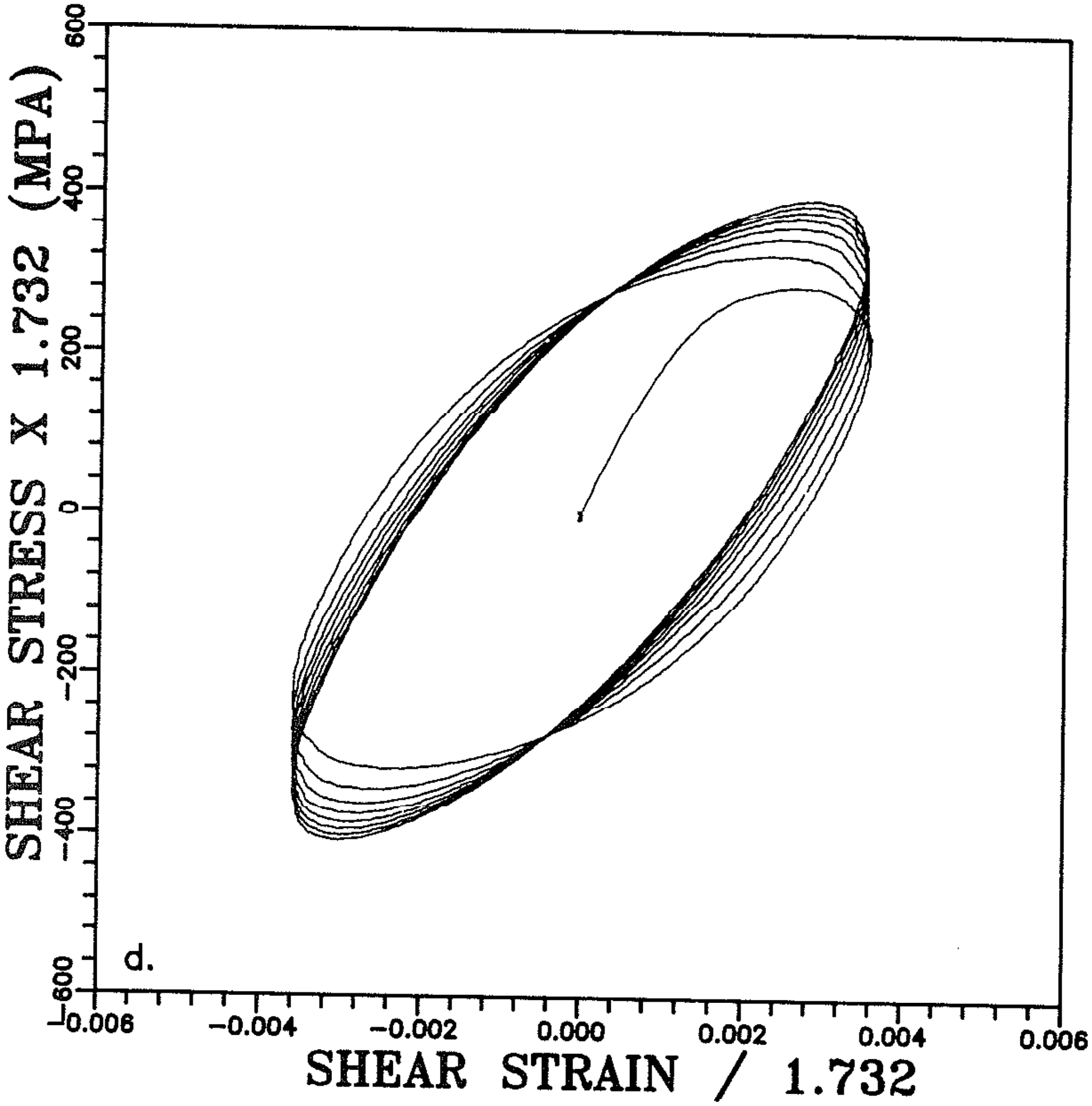
SHEAR STRESS X 1.732 (MPA)
600
400
200
0
−200
−400
−600
d.
−0.006
−0.004
−0.002
0.000
0.002
0.004
0.006
SHEAR STRAIN / 1.732

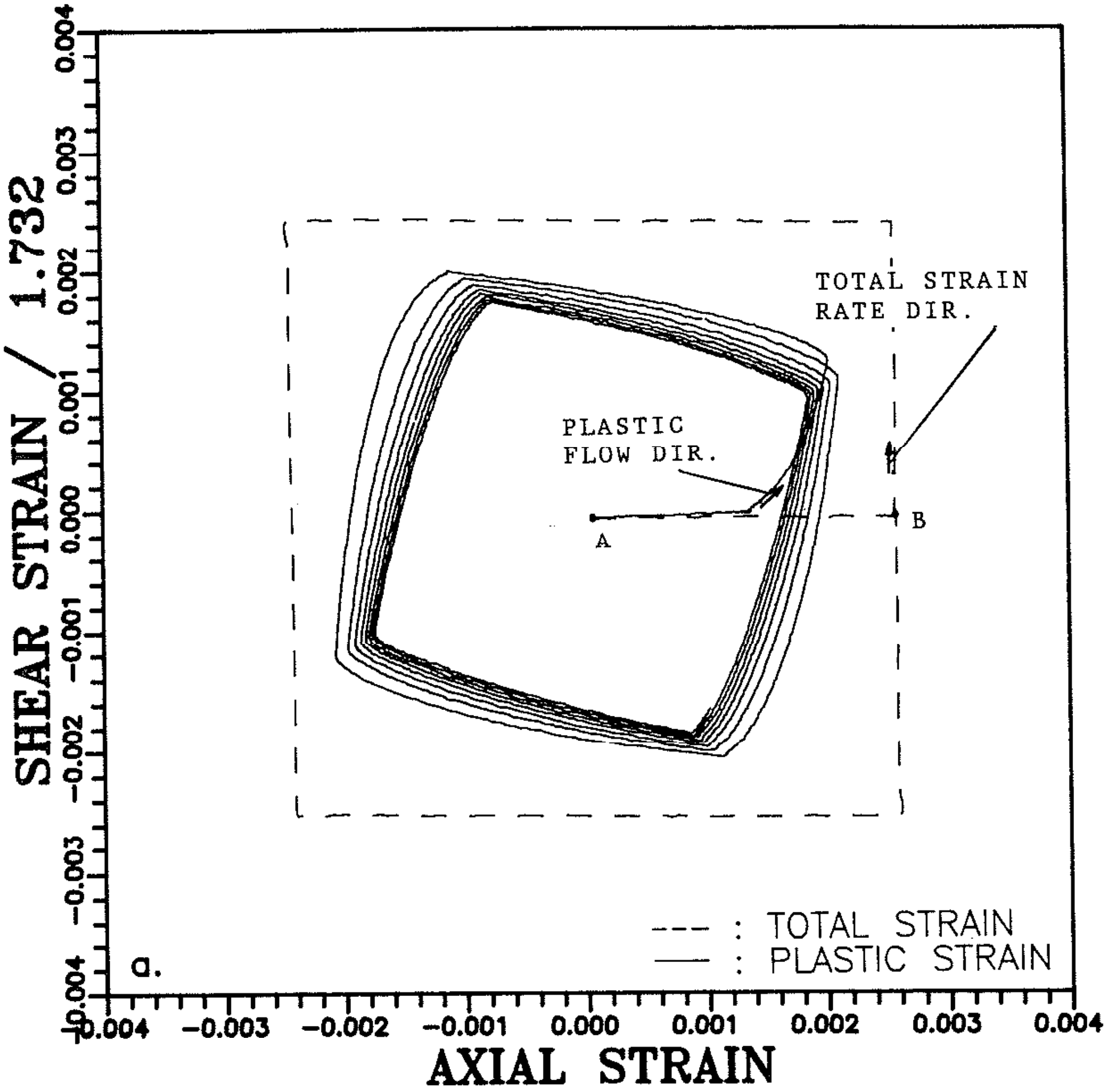

Figure 18. (a) - (d) The Stress-Strain History of 304 Stainless Steel under a One-Square Path of Strain-Controlled Cycling (Specimen SS03) [36].

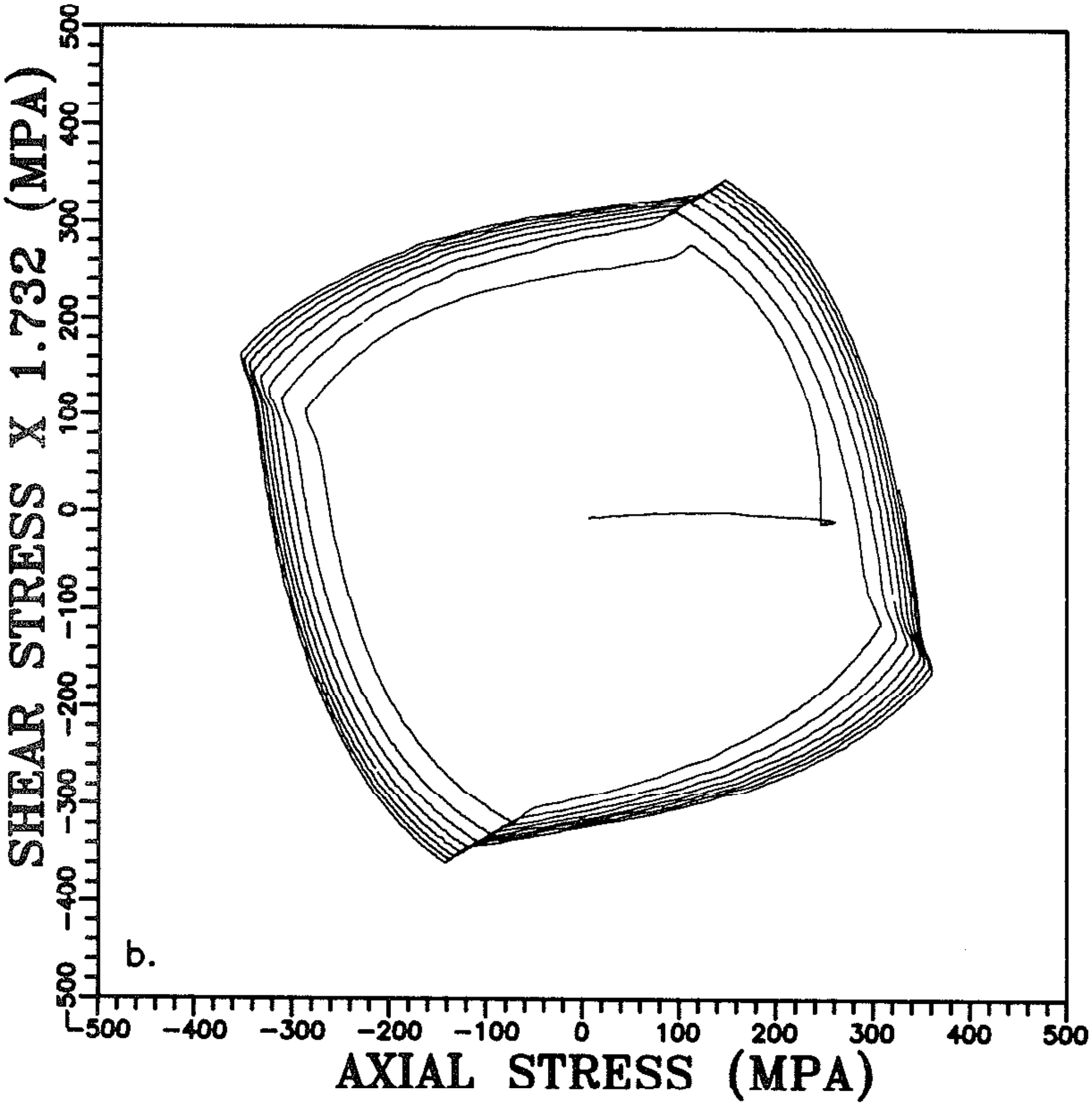
SHEAR STRESS X 1.732 (MPA)
500
400
300
200
100
0
−100
−200
−300
−400
−500
AXIAL STRESS (MPA)
−500
−400
−300
−200
−100
0
100
200
300
400
500
b.

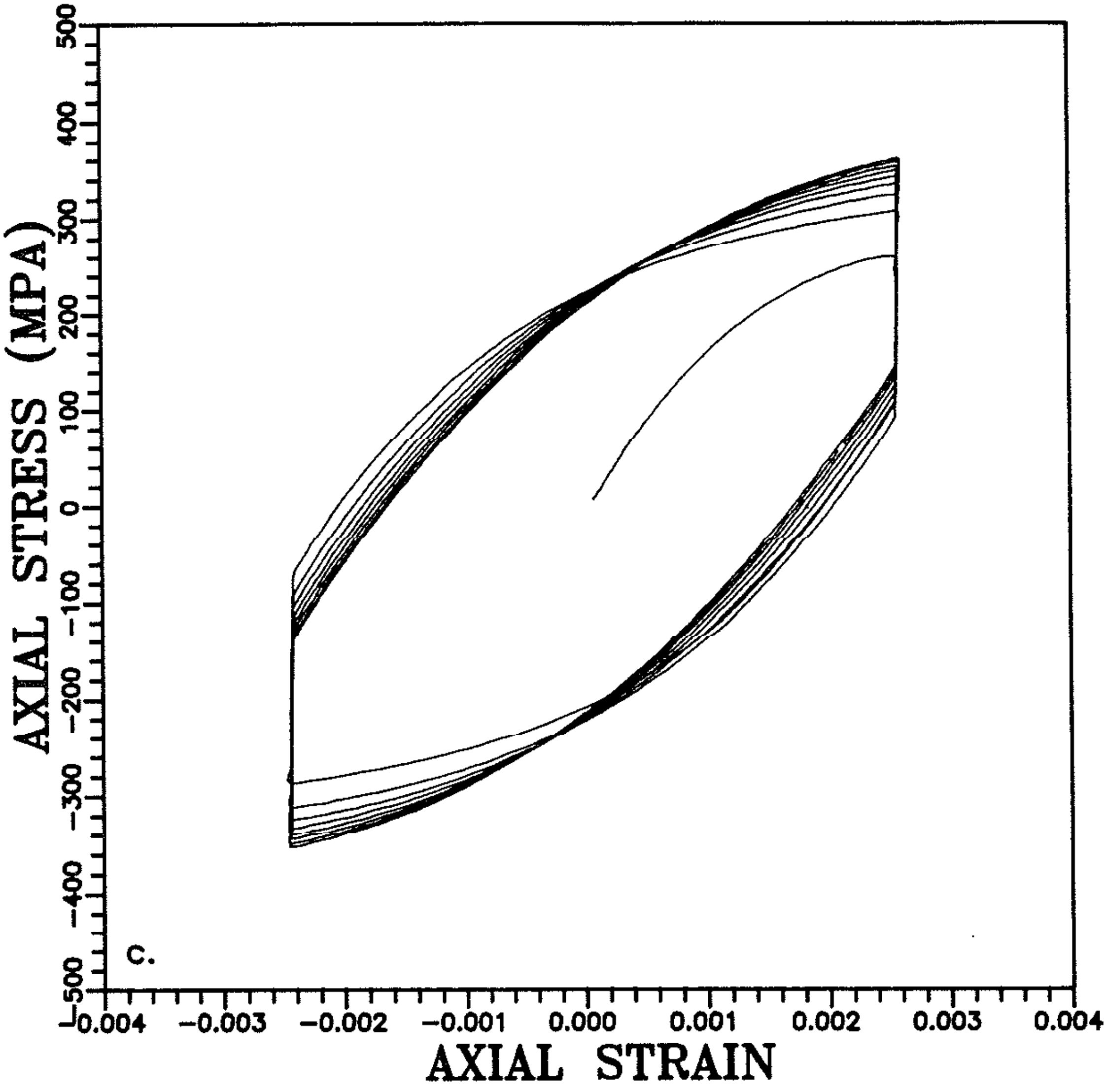
AXIAL STRESS (MPA)
500
400
300
200
100
0
−100
−200
−300
−400
−500
−0.004
−0.003
−0.002
−0.001
0.000
0.001
0.002
0.003
0.004
AXIAL STRAIN
c.

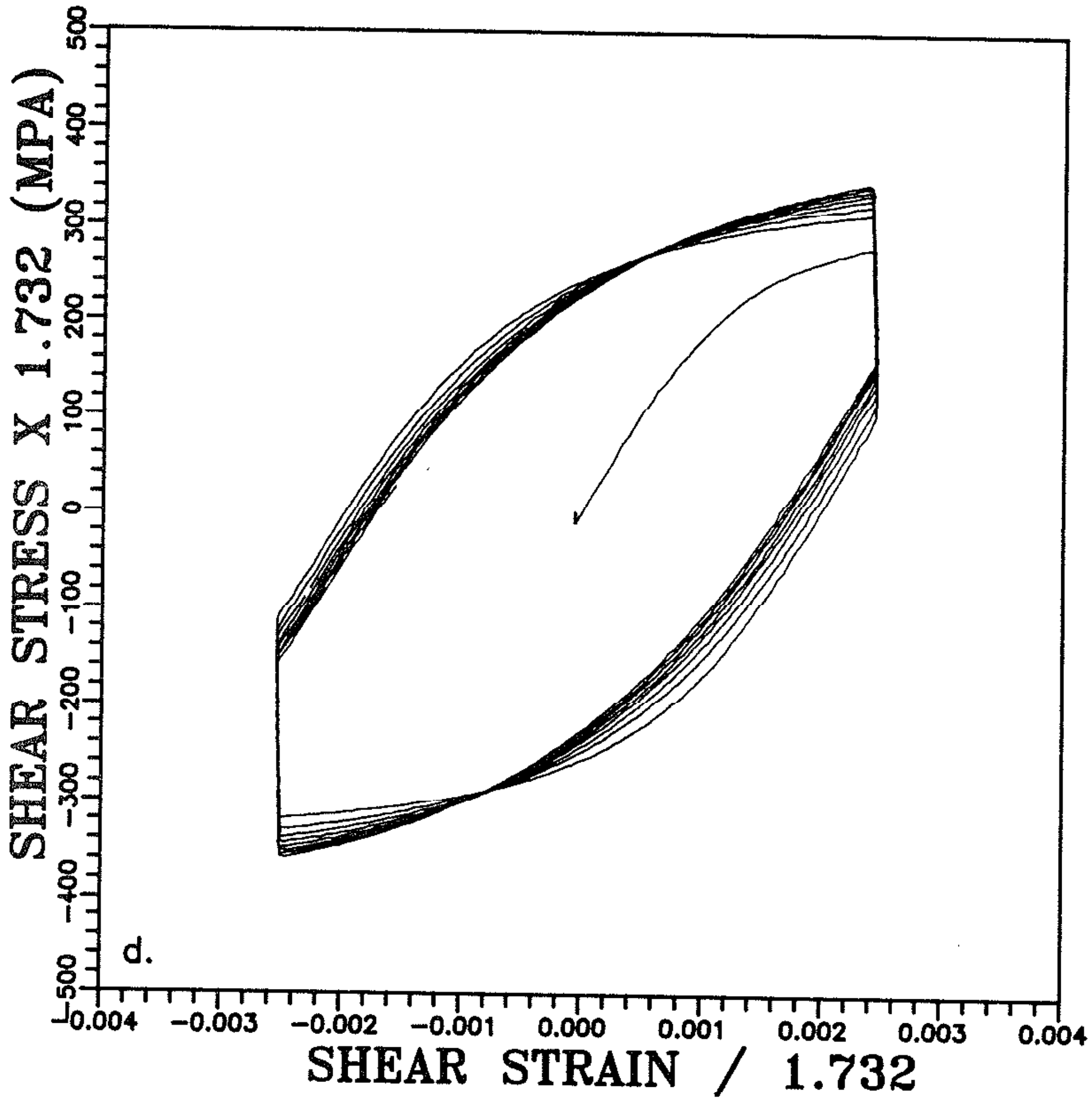
d.
SHEAR STRESS X 1.732 (MPA)
500
400
300
200
100
0
−100
−200
−300
−400
−500
SHEAR STRAIN / 1.732
−0.004
−0.003
−0.002
−0.001
0.000
0.001
0.002
0.003
0.004

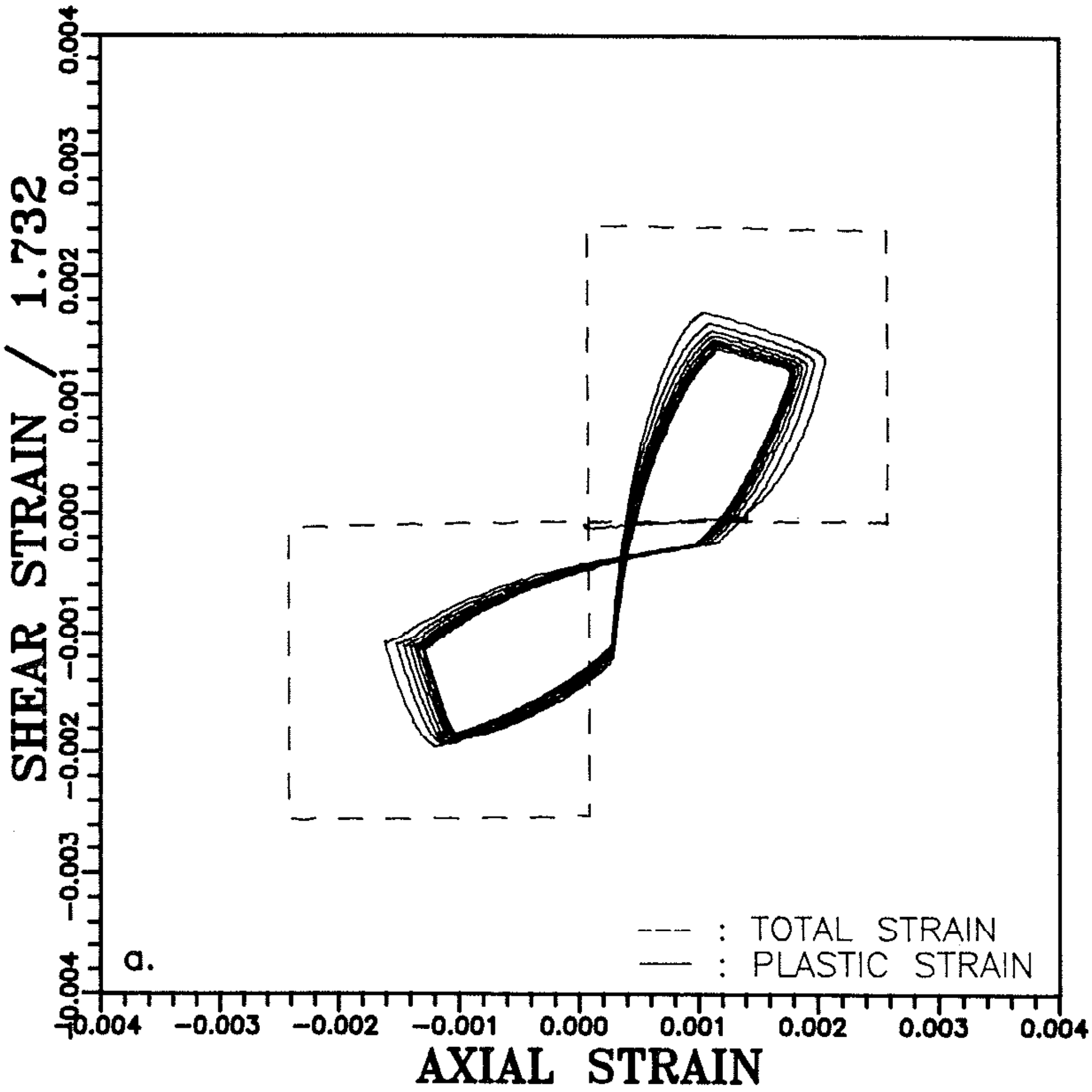

Figure 19. (a) - (d) The Stress-Strain History of 304 Stainless Steel under a Two-Square Path of Strain-Controlled Cycling (Specimen SS04) [36].

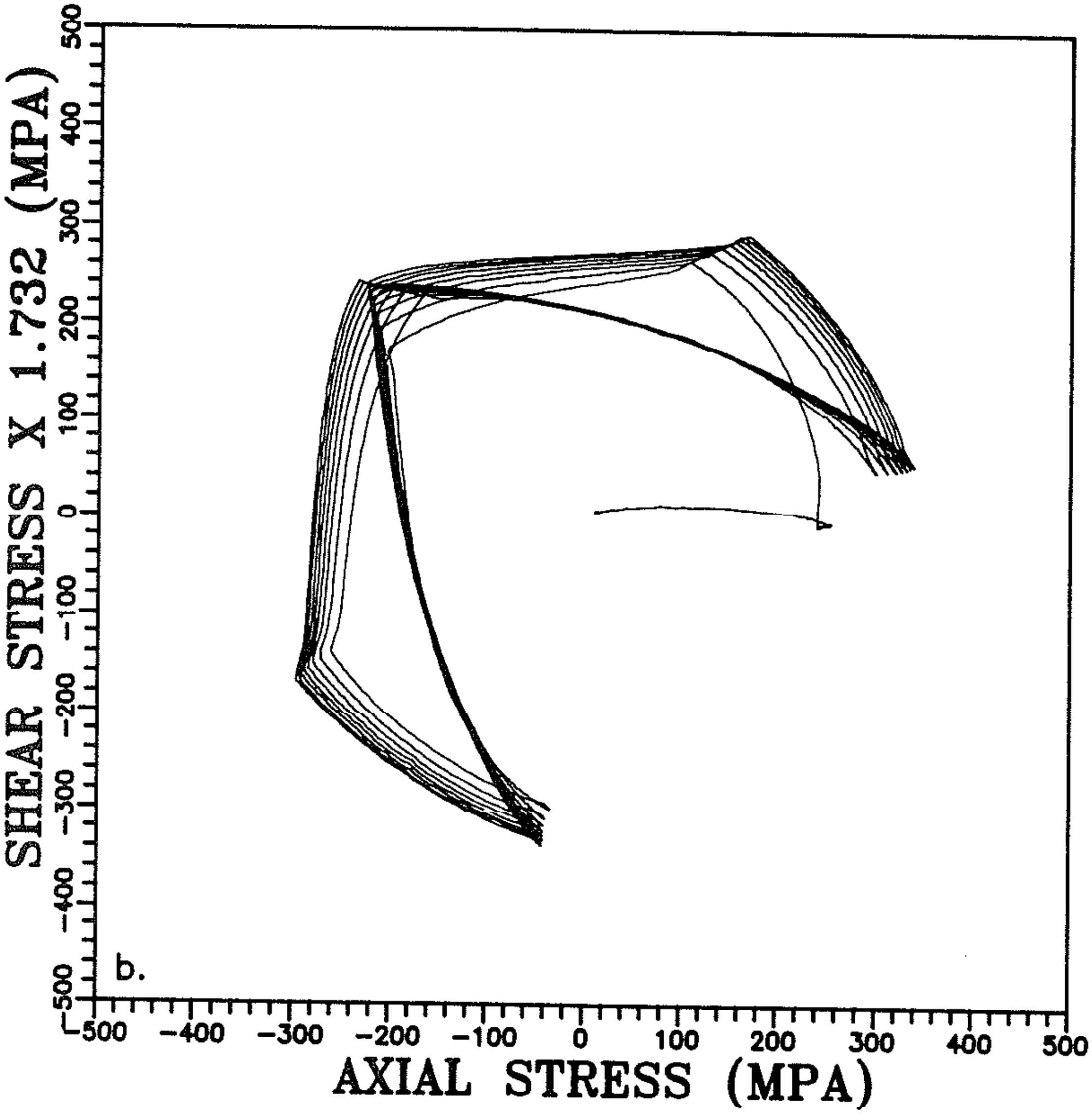
b.
SHEAR STRESS X 1.732 (MPA)
500
400
300
200
100
0
−100
−200
−300
−400
−500
AXIAL STRESS (MPA)
−500
−400
−300
−200
−100
0
100
200
300
400
500

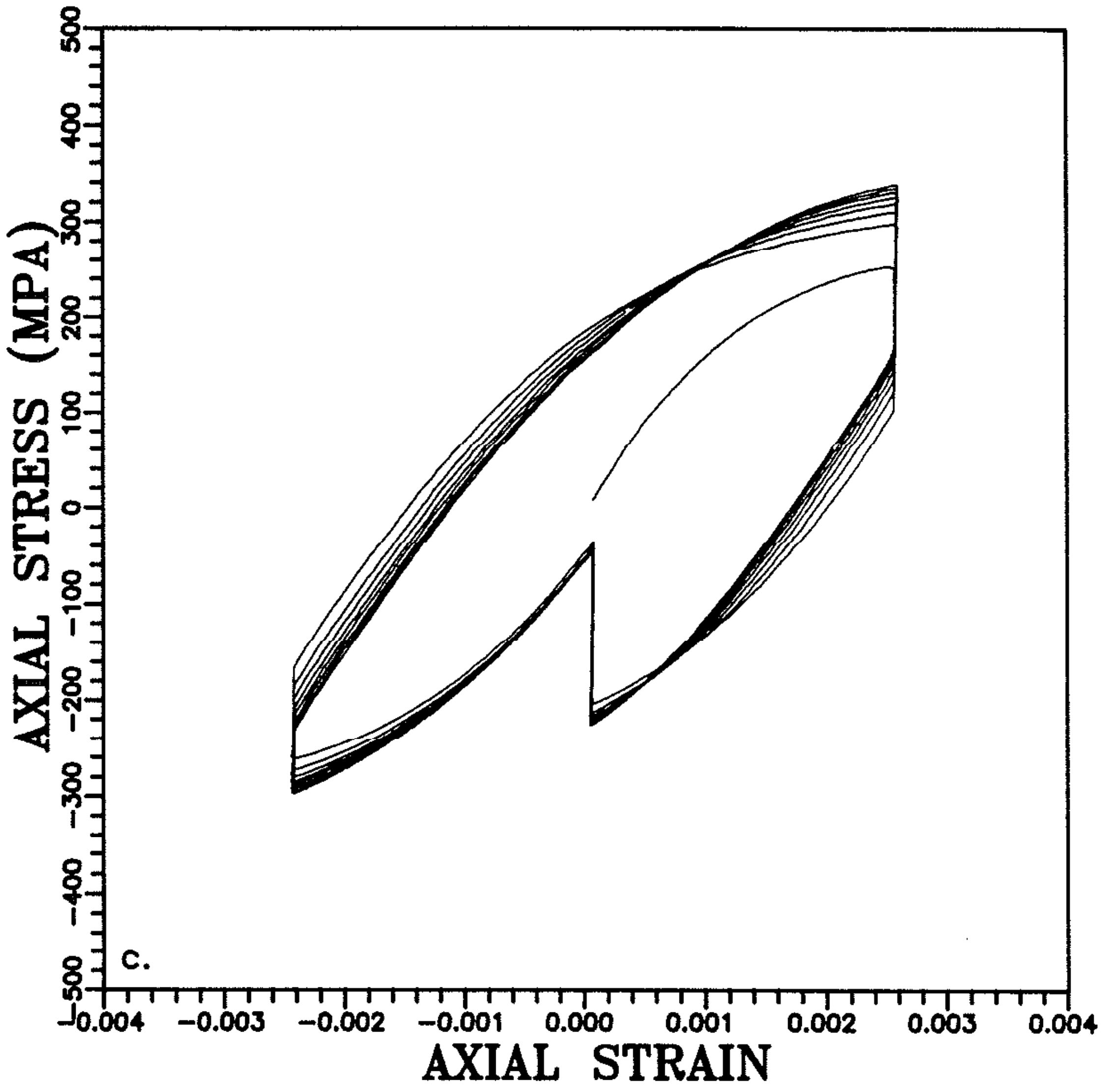
AXIAL STRESS (MPA)
500
400
300
200
100
0
-100
-200
-300
-400
-500
AXIAL STRAIN
-0.004
-0.003
-0.002
-0.001
0.000
0.001
0.002
0.003
0.004
C.

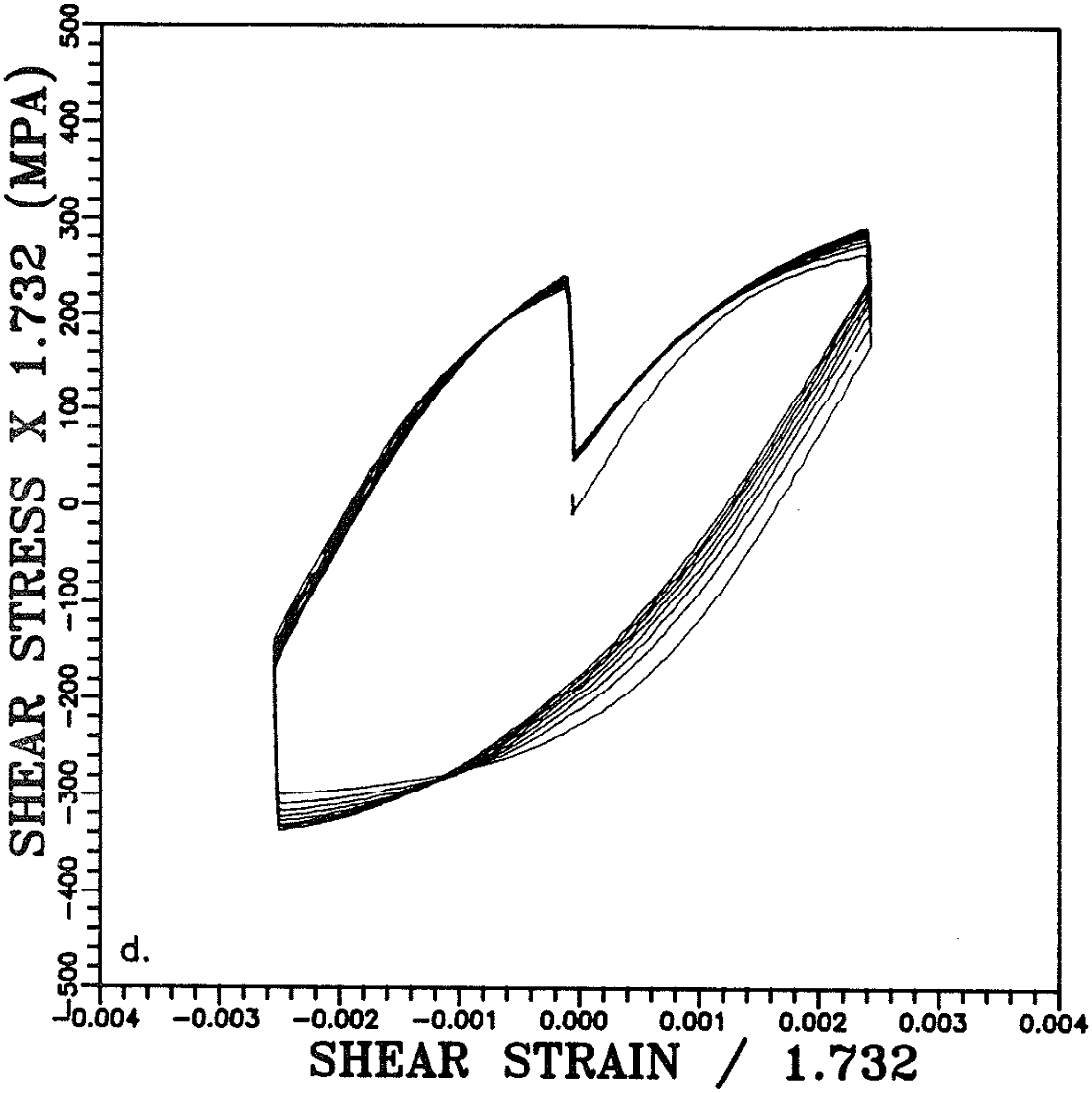
SHEAR STRESS X 1.732 (MPA)
500
400
300
200
100
0
-100
-200
-300
-400
-500
d.
-0.004
-0.003
-0.002
-0.001
0.000
0.001
0.002
0.003
0.004
SHEAR STRAIN / 1.732

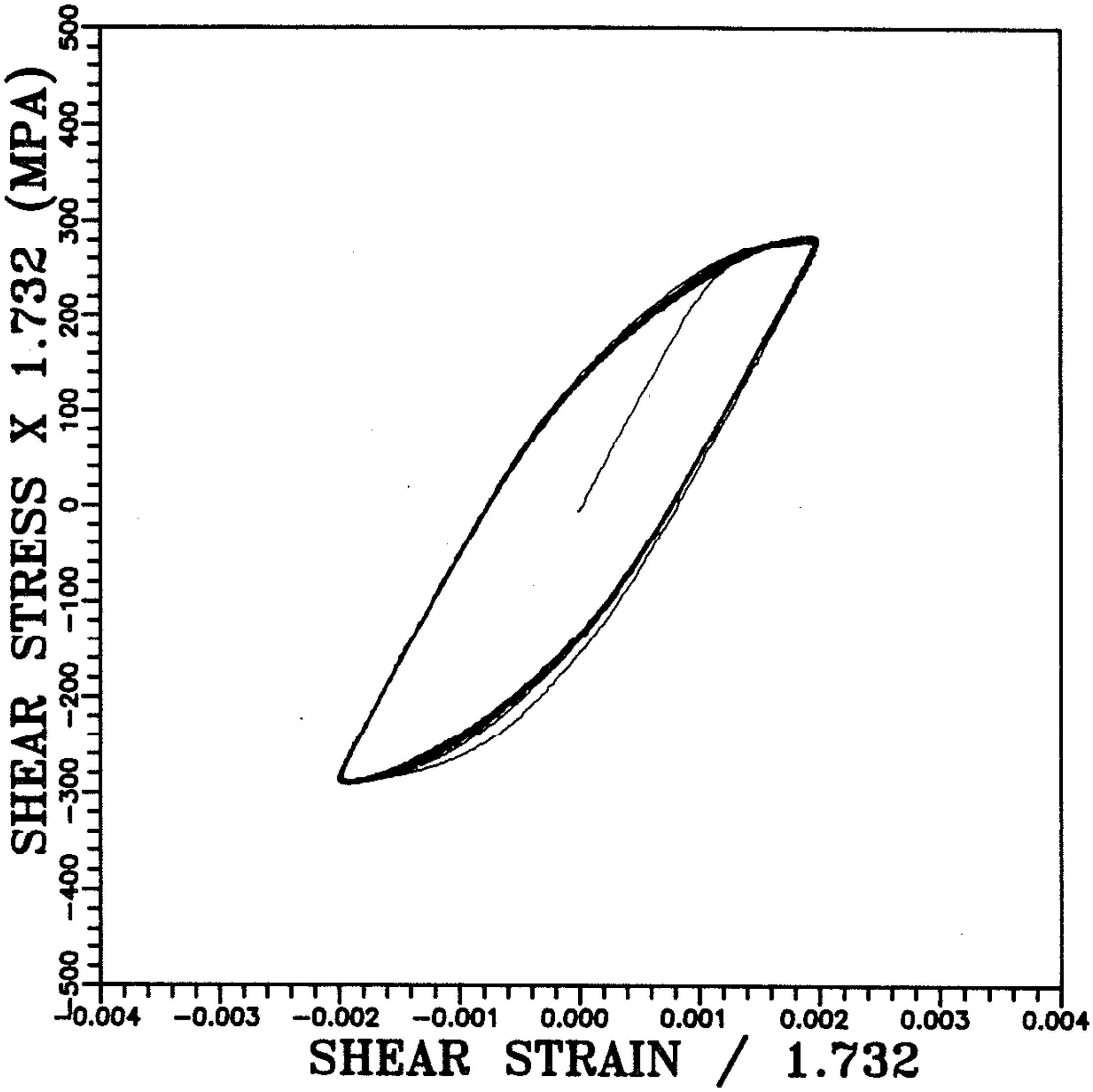

Figure 20. The Stress-Strain History of 304 Stainless Steel under Cyclic Torsion (Specimen SS20) [36].

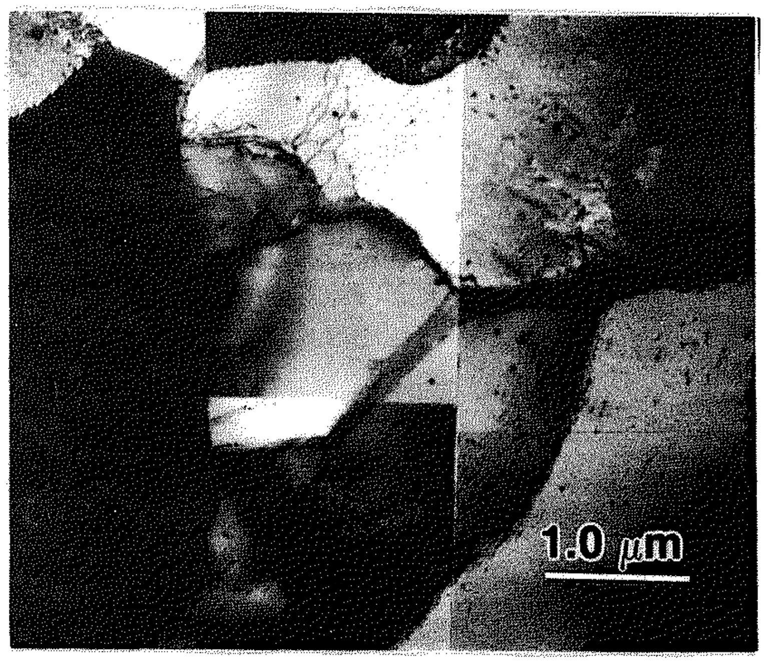

Figure 21. Cells Formed in 1100 Aluminum (Specimen A109).

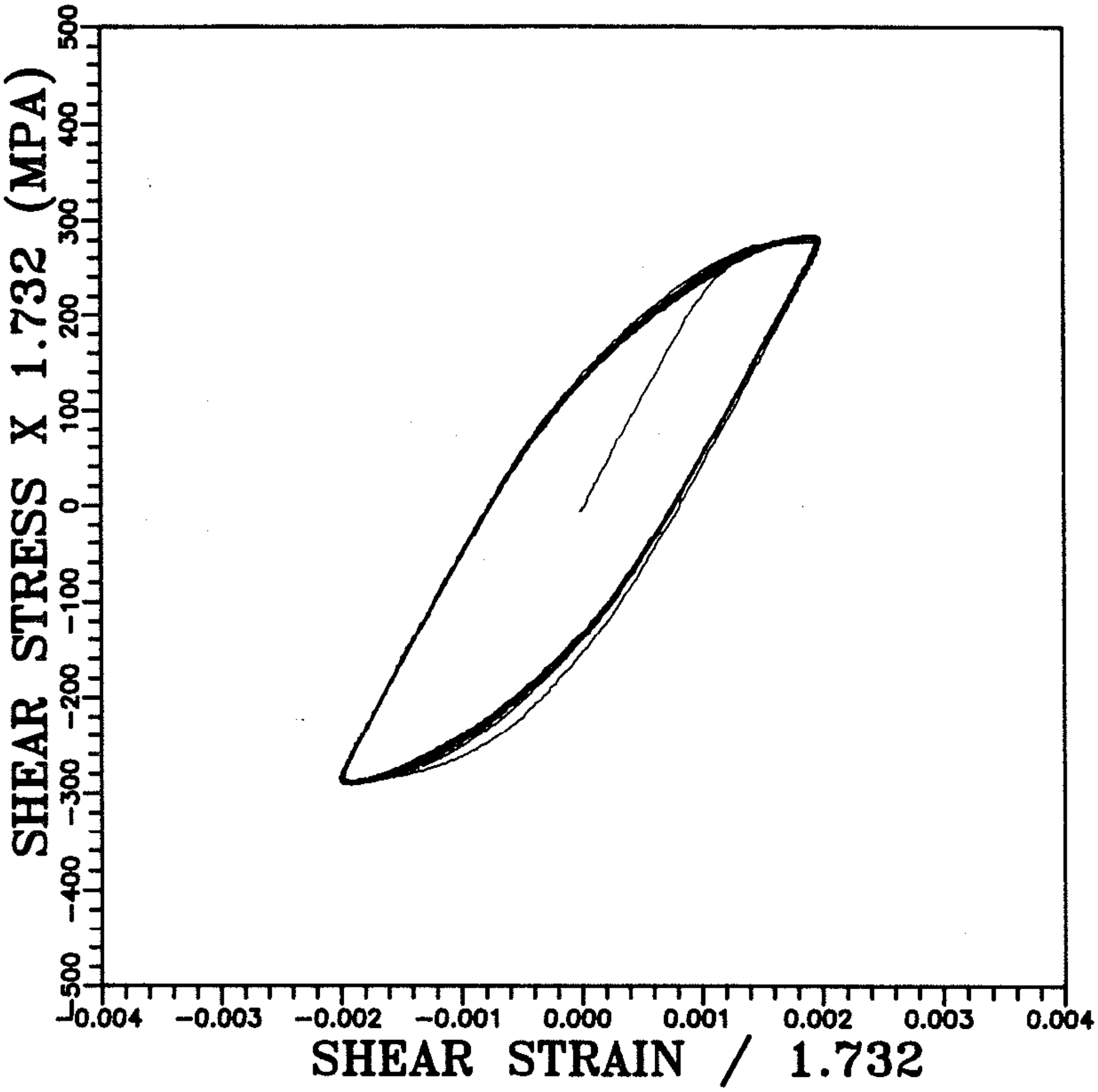

Figure 20. The Stress-Strain History of 304 Stainless Steel under Cyclic Torsion (Specimen SS20) [36].

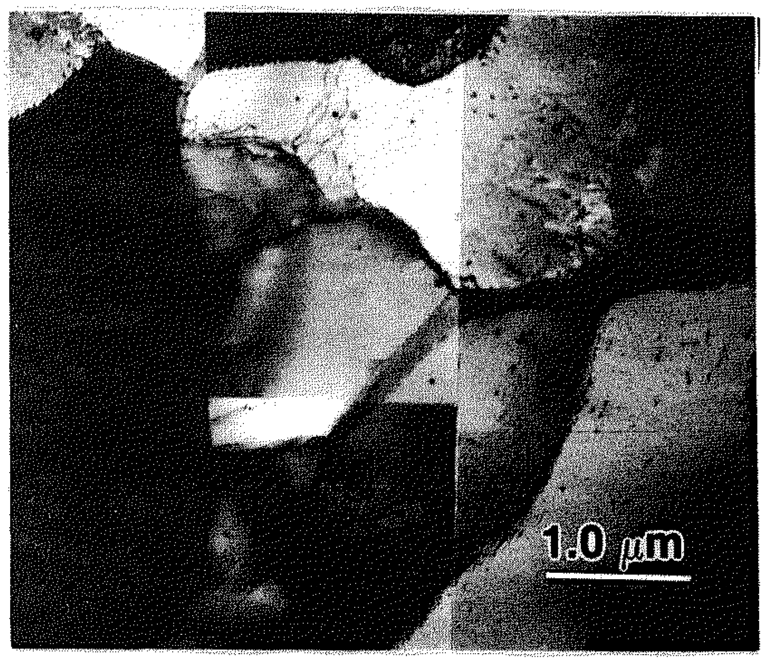

Figure 21. Cells Formed in 1100 Aluminum (Specimen A109).

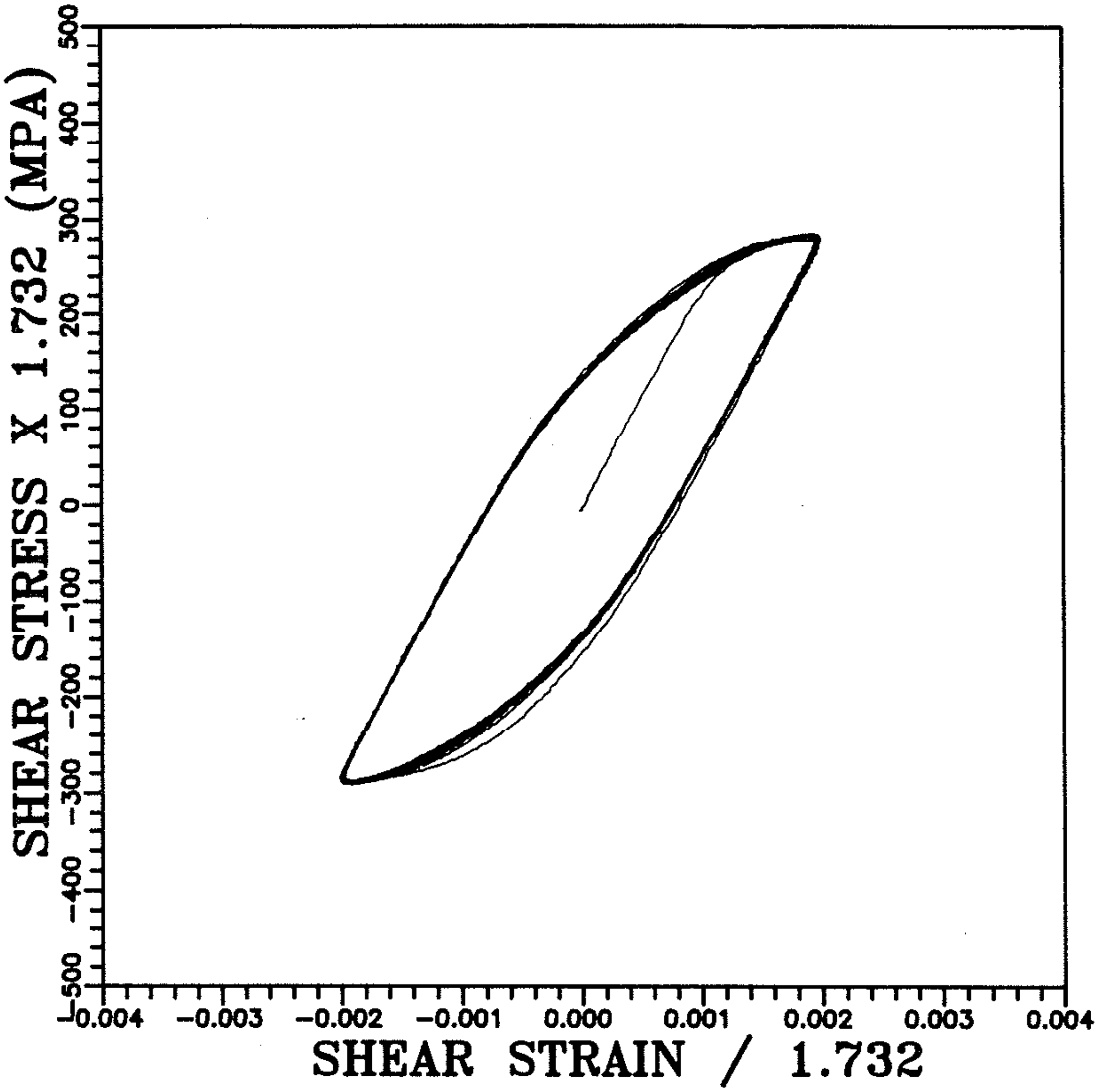

Figure 20. The Stress-Strain History of 304 Stainless Steel under Cyclic Torsion (Specimen SS20) [36].

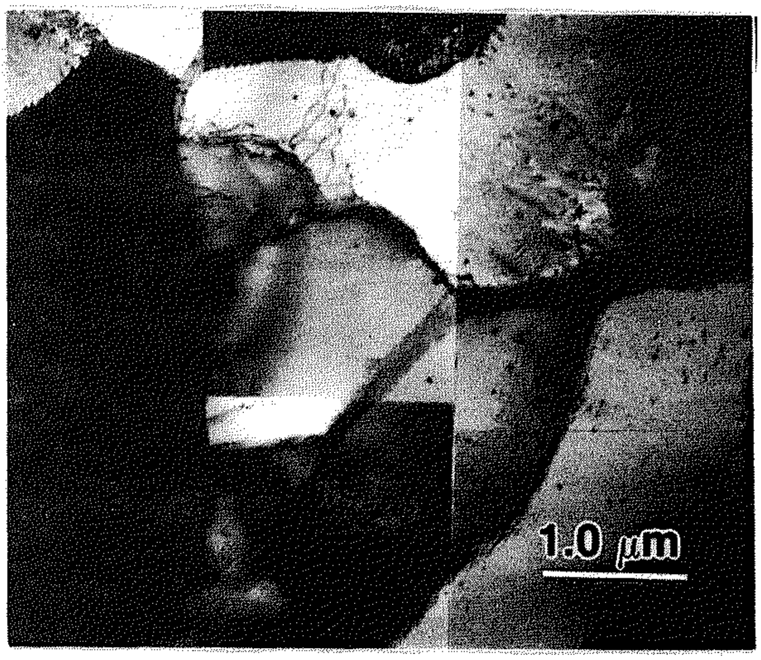

Figure 21. Cells Formed in 1100 Aluminum (Specimen A109).

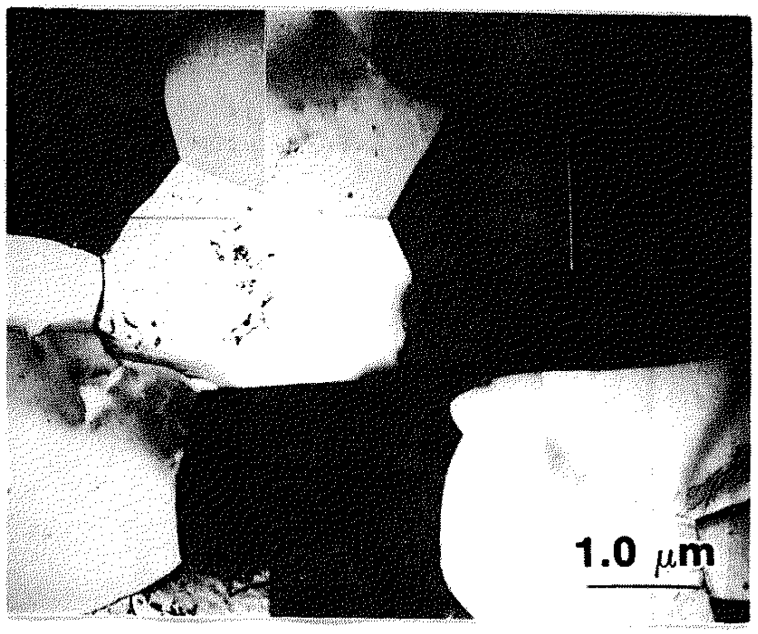

Figure 22. Cells Formed in 1100 Aluminum (Specimen A104).

Figure 23. Ladders Formed in Copper (Specimen C001).

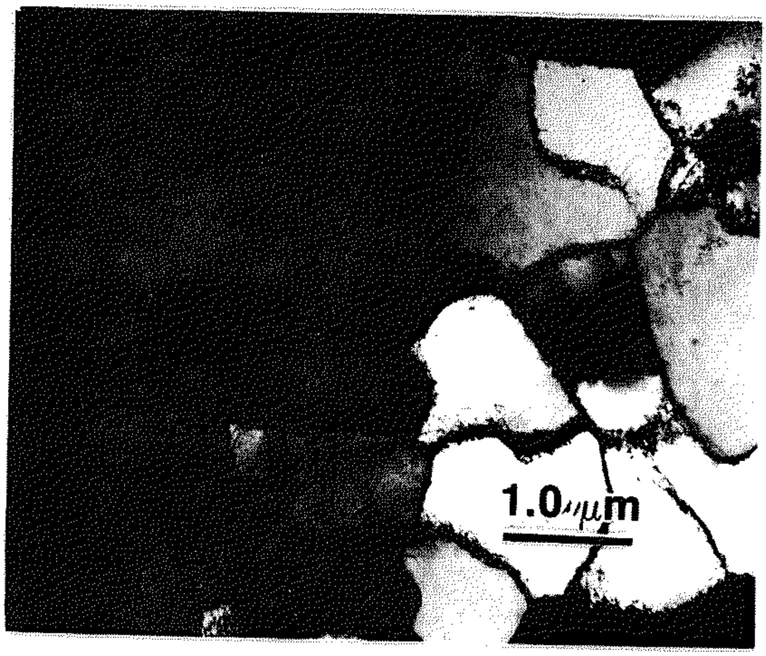

Figure 24. Cells Formed in Copper (Specimen C001). (Average Cell Size = 1.32 μm^2)

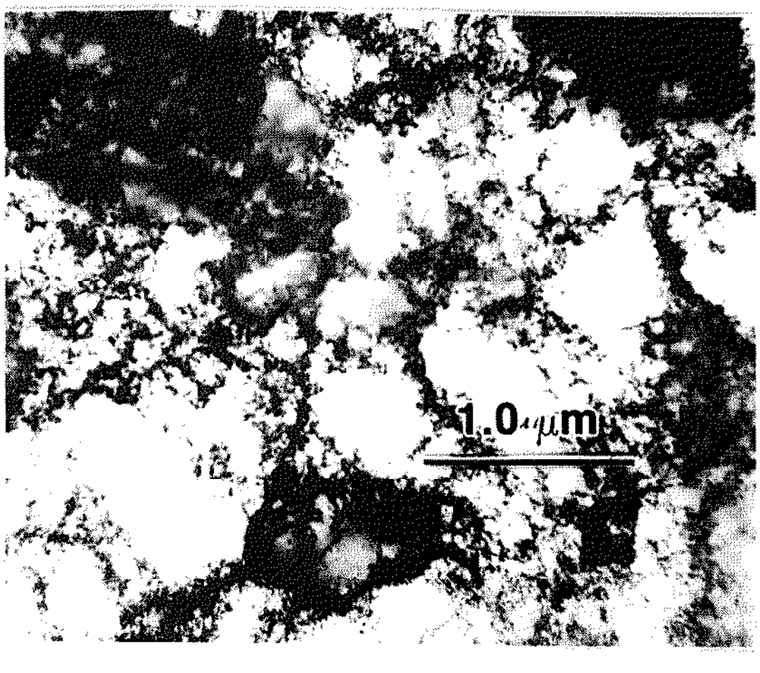

Figure 25. Uncondensed Cells Formed in Copper (Specimen C005).

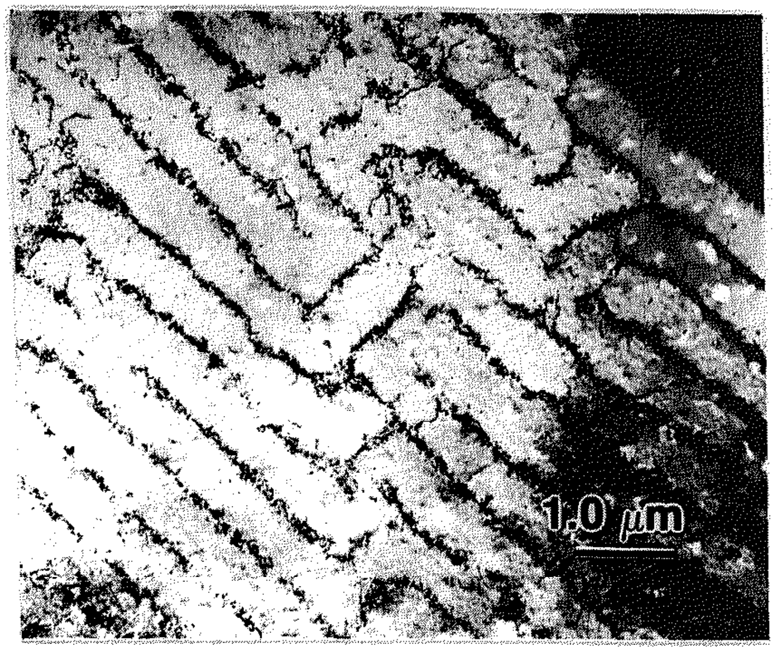

Figure 26. Labyrinths Formed in Copper (Specimen C003).

Figure 27. Walls Formed in Copper (Specimen C002).

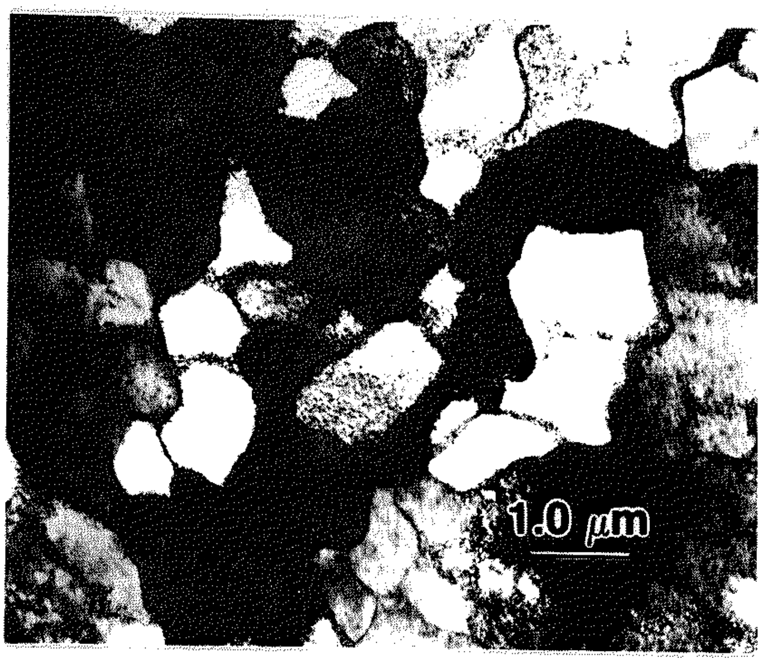

Figure 28. Cells Formed in Copper (Specimen C002). (Average Cell Size = 0.93 μm^2)

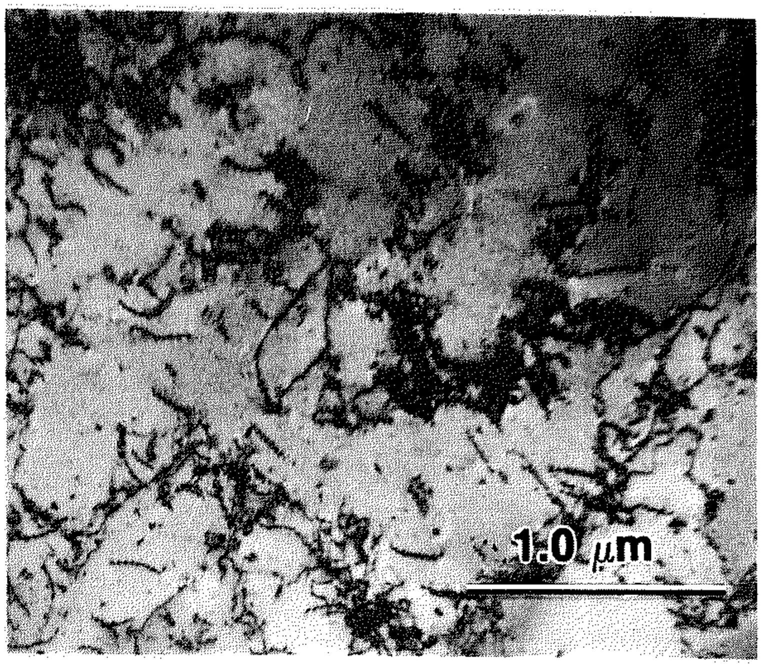

Figure 29. Planar Dislocations Formed in 304 Stainless Steel (Specimen SS12).

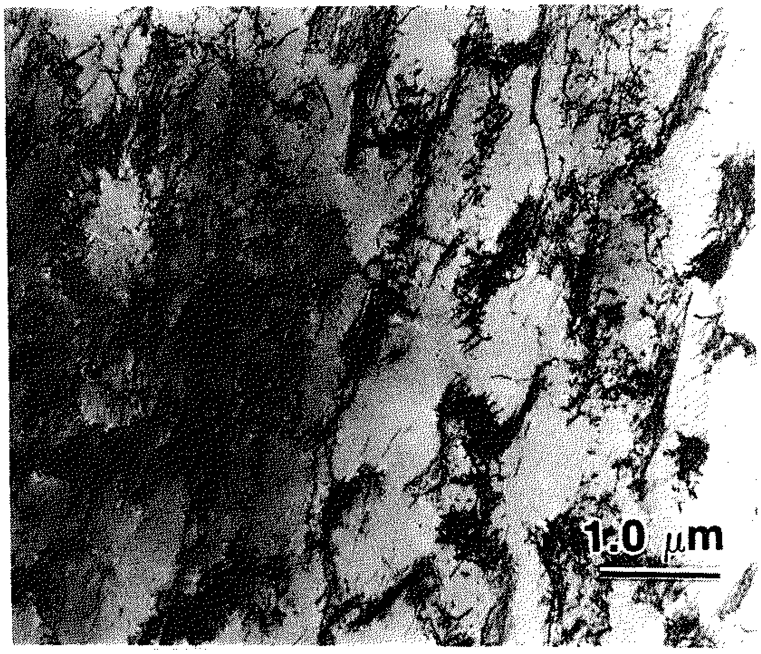

Figure 30. Tangles of Dislocations Formed in 310 Stainless Steel (Specimen S101).

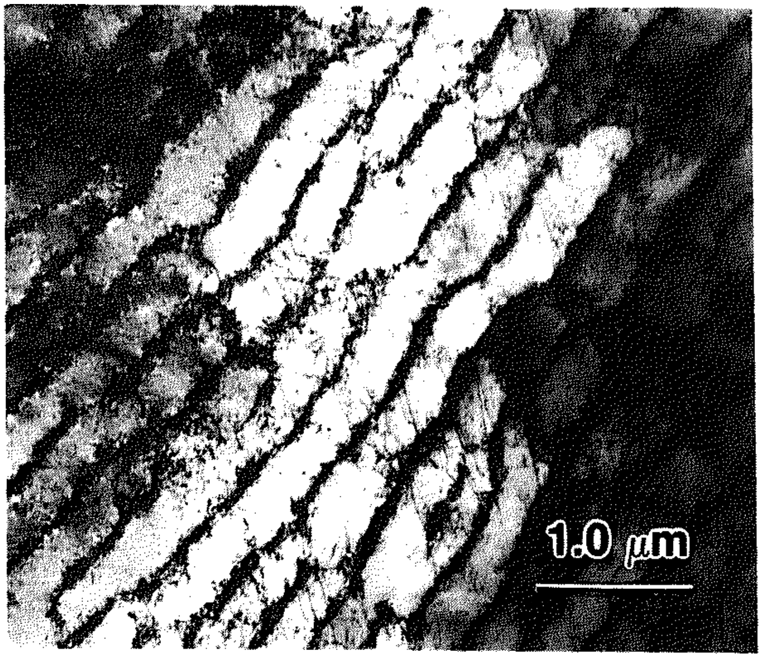

Figure 31. Walls Formed in 304 Stainless Steel (Specimen SS10).

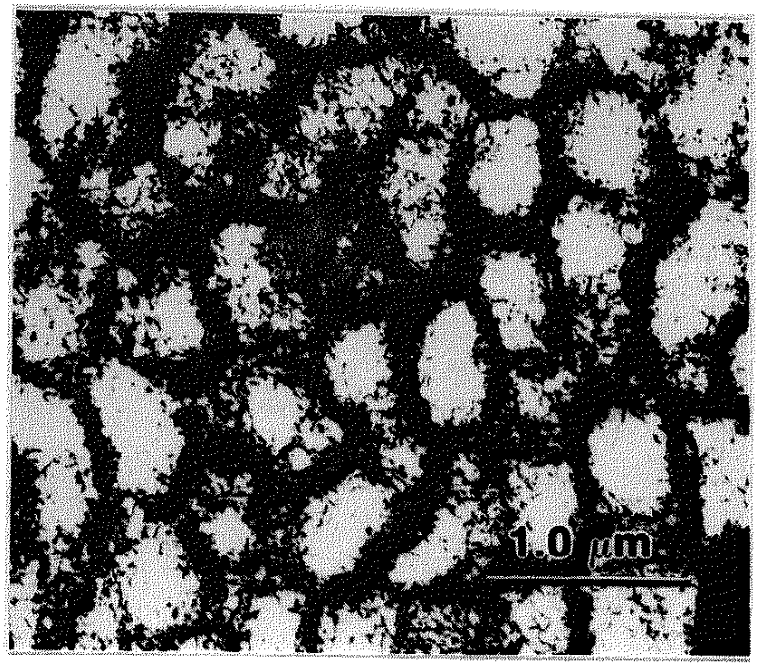

Figure 32. Cells Formed in 310 Stainless Steel (Specimen S102).

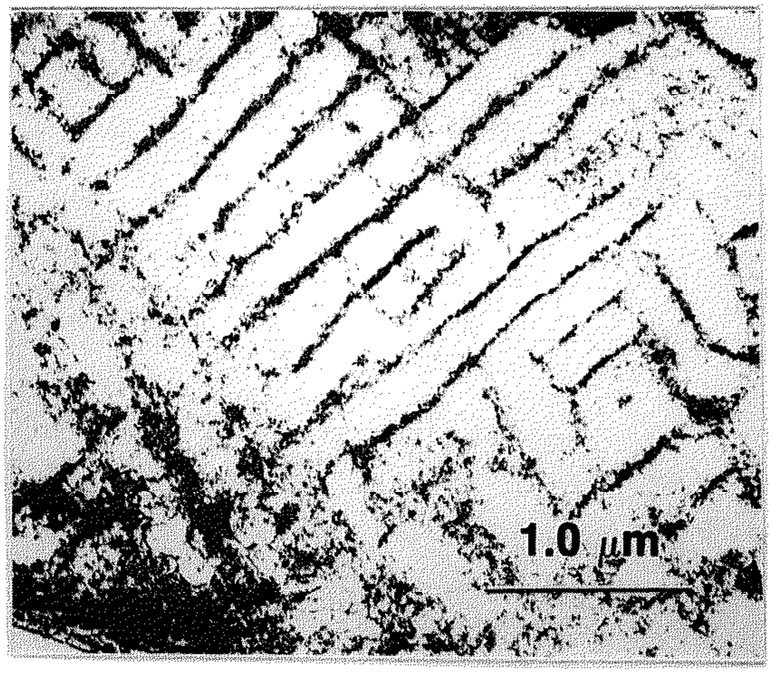

Figure 33. Labyrinths Formed in 310 Stainless Steel (Specimen S102).

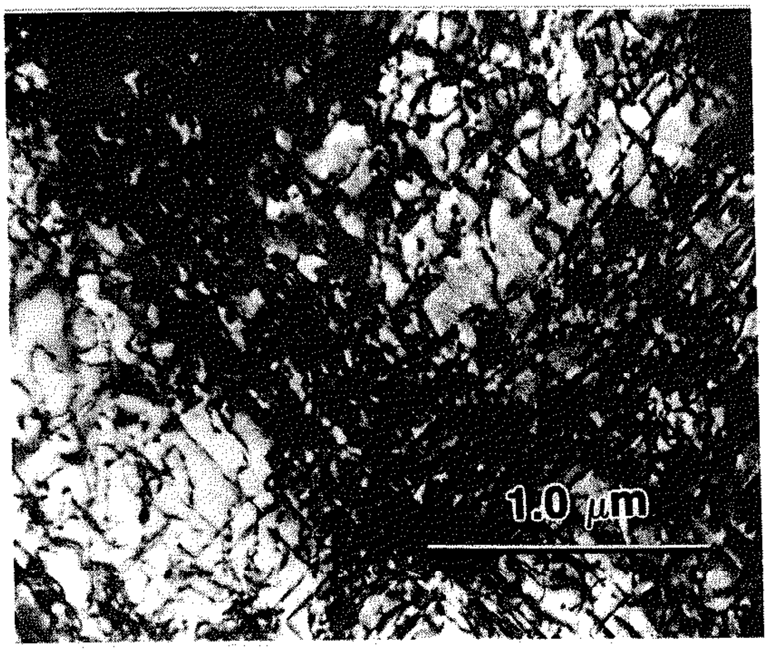

Figure 34. Dislocation Loops Formed in 7075 Aluminum Alloy (Specimen A710).

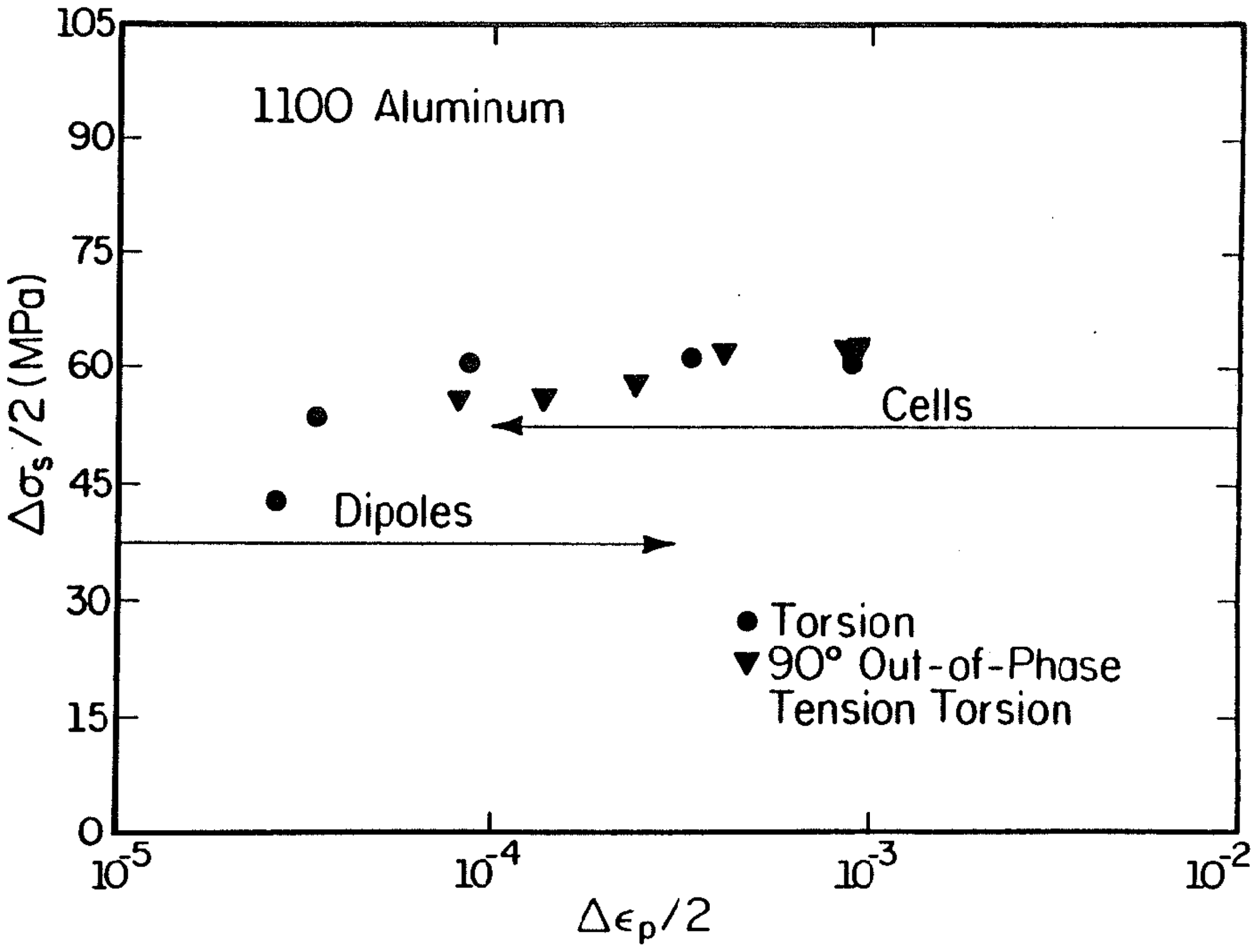

Figure 35. The Stabilized Stress as a Function of Cyclic Plastic Strain for 1100 Aluminum.

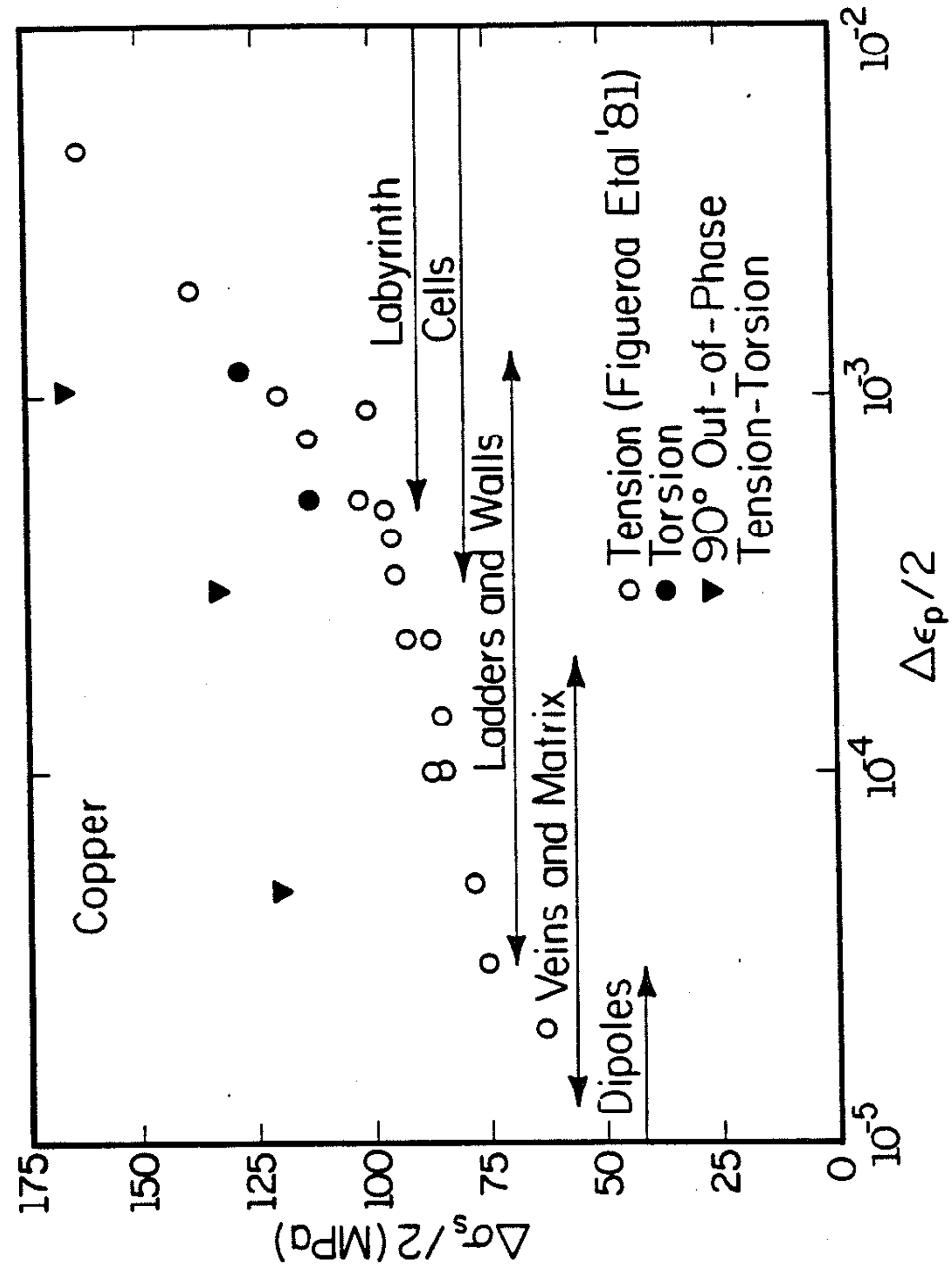

Figure 36. The Stabilized Stress as a Function of Cyclic Plastic Strain for OFHC Copper.

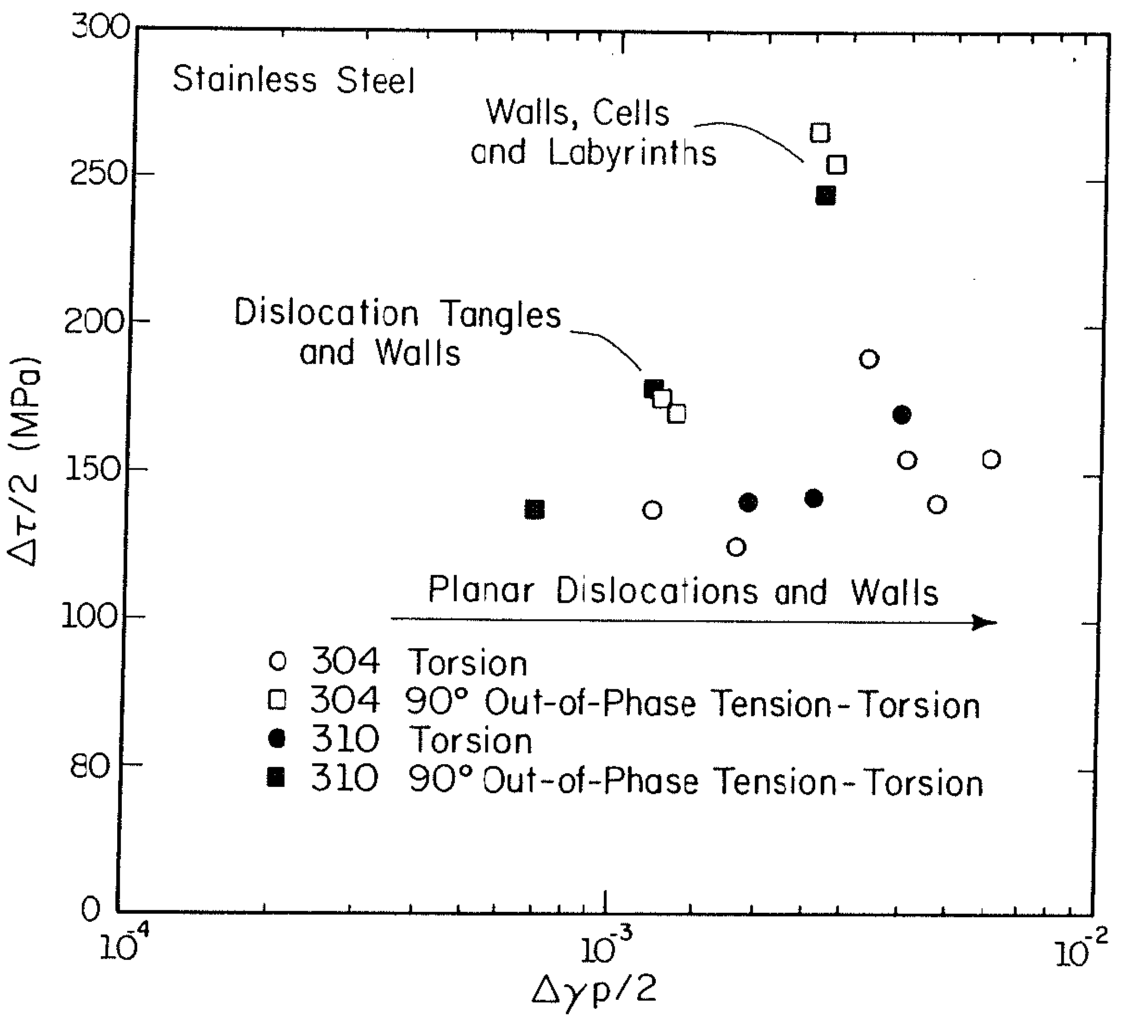

Figure 37. A Comparison of the Stabilized Stress Between 304 and 310 Stainless Steel.

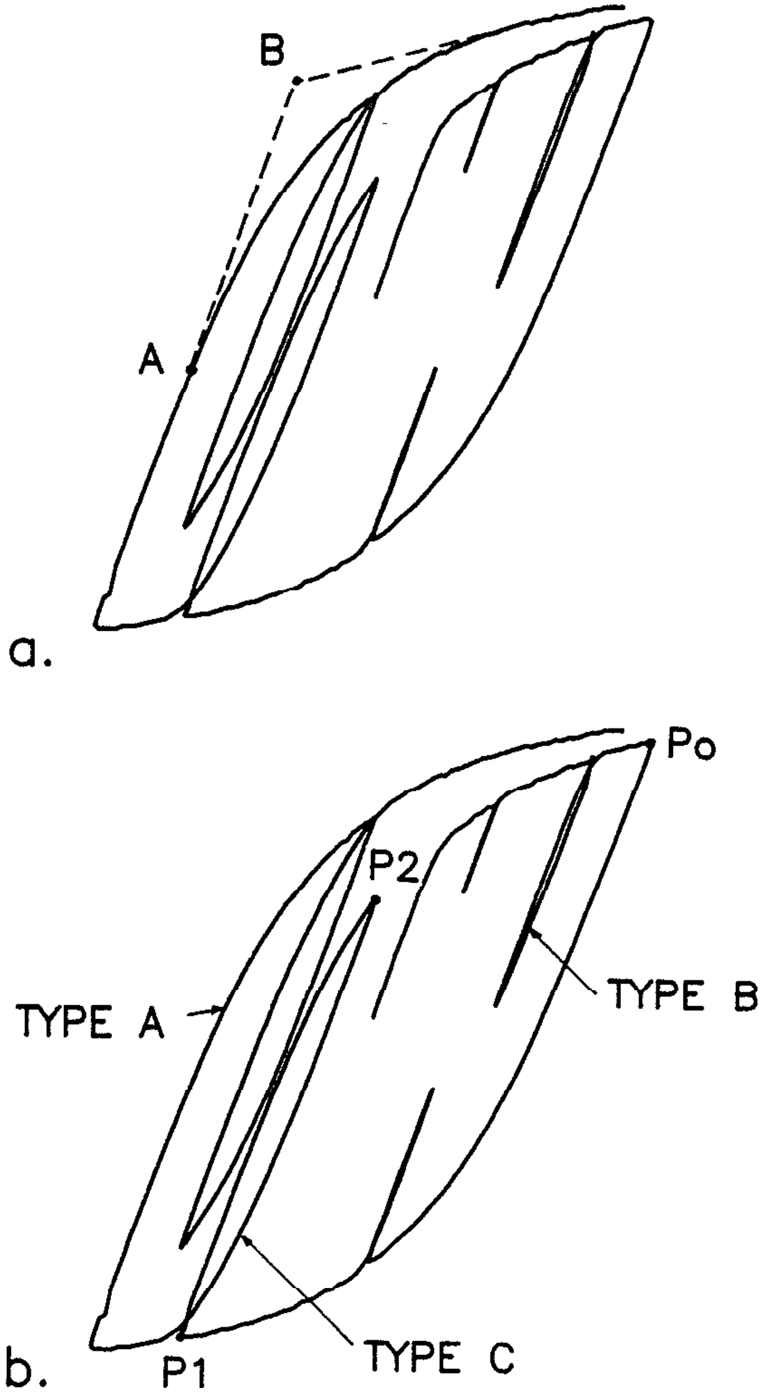

Figure 38. (a) Two Possible Ways of Defining the Yield Point.
(b) Three Types of Unloading and Reloading Paths.
(Specimen A114).

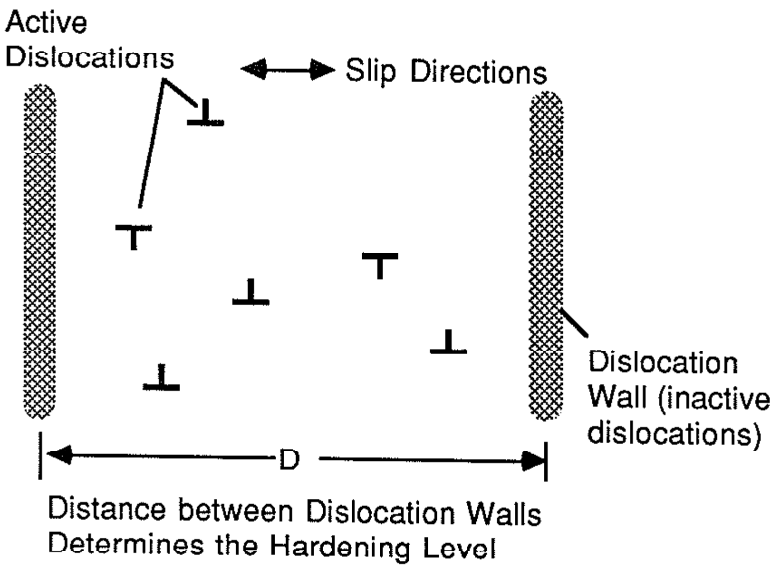

Figure 39. The Deformation Mechanism of Metals under the Cyclic Loading.

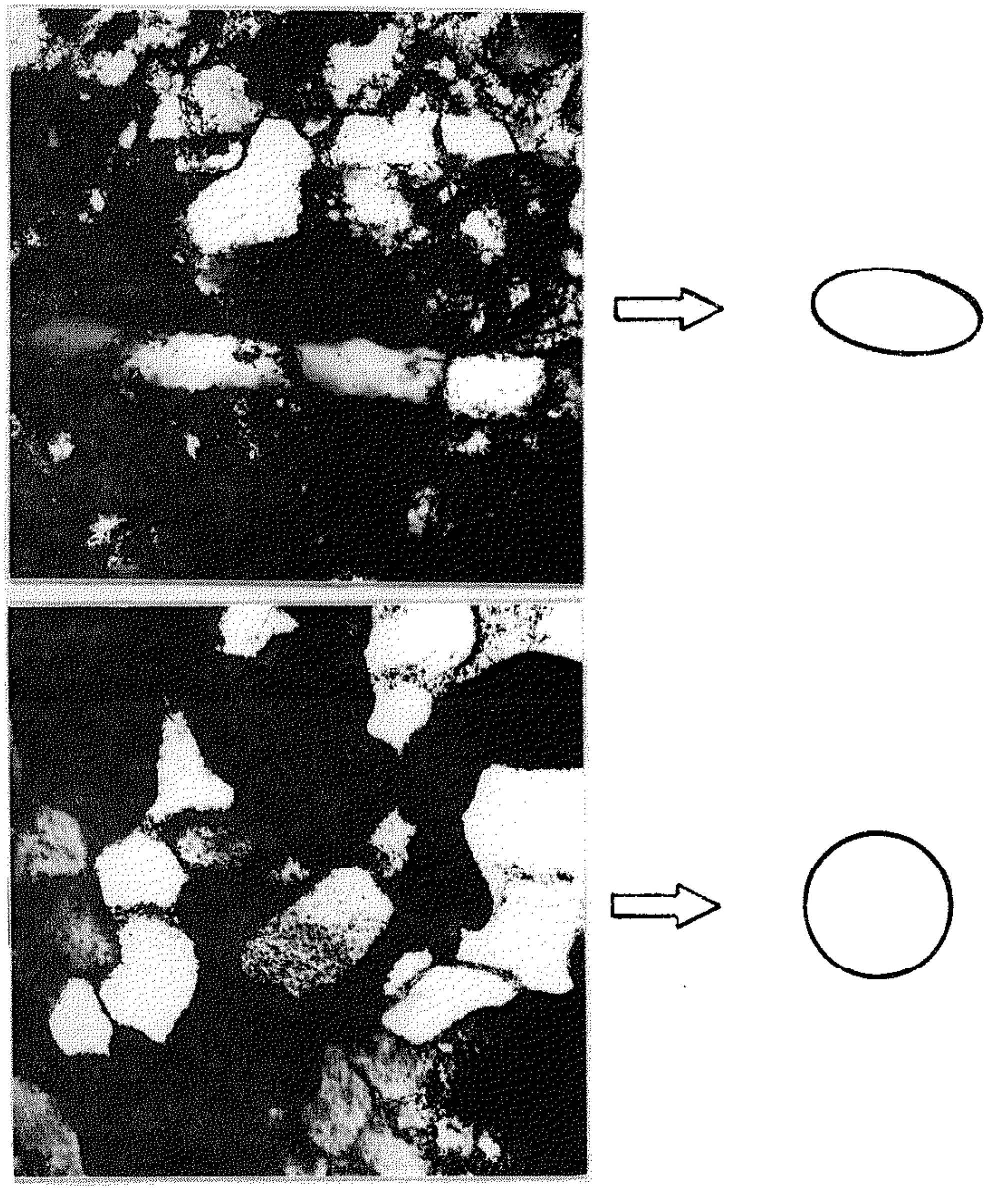

Figure 40. A Comparison Between the Dislocation Substructure and the Ellipse Model.

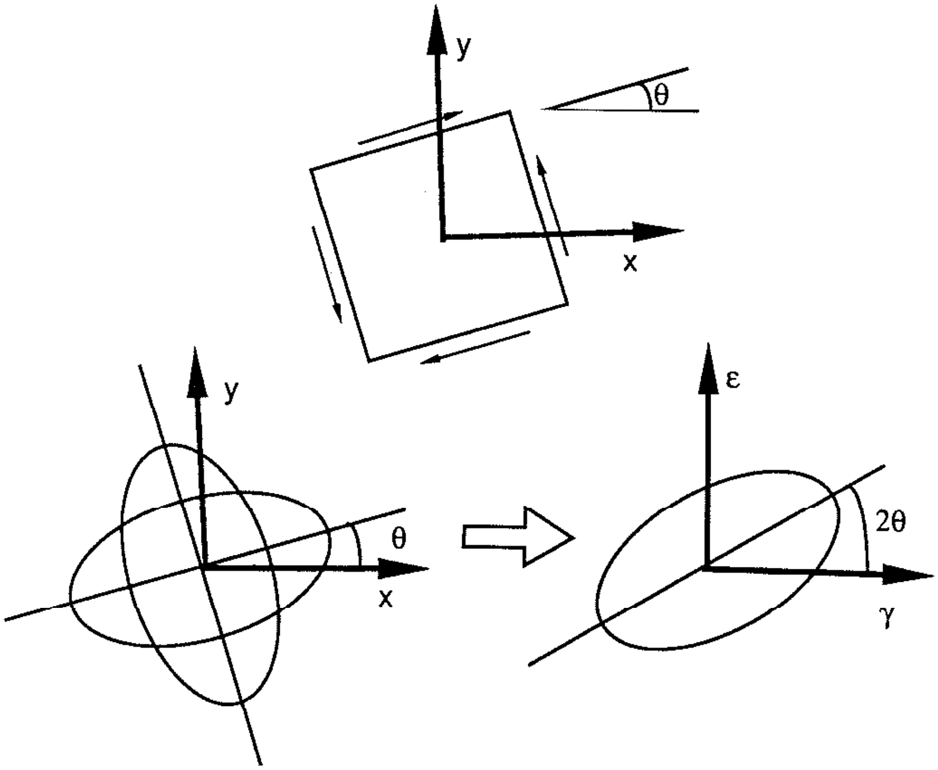

Figure 41. A Comparison Between the Two-Dimensional Maximum Shear Planes and the Strain-Plane Defined Ellipse Model.

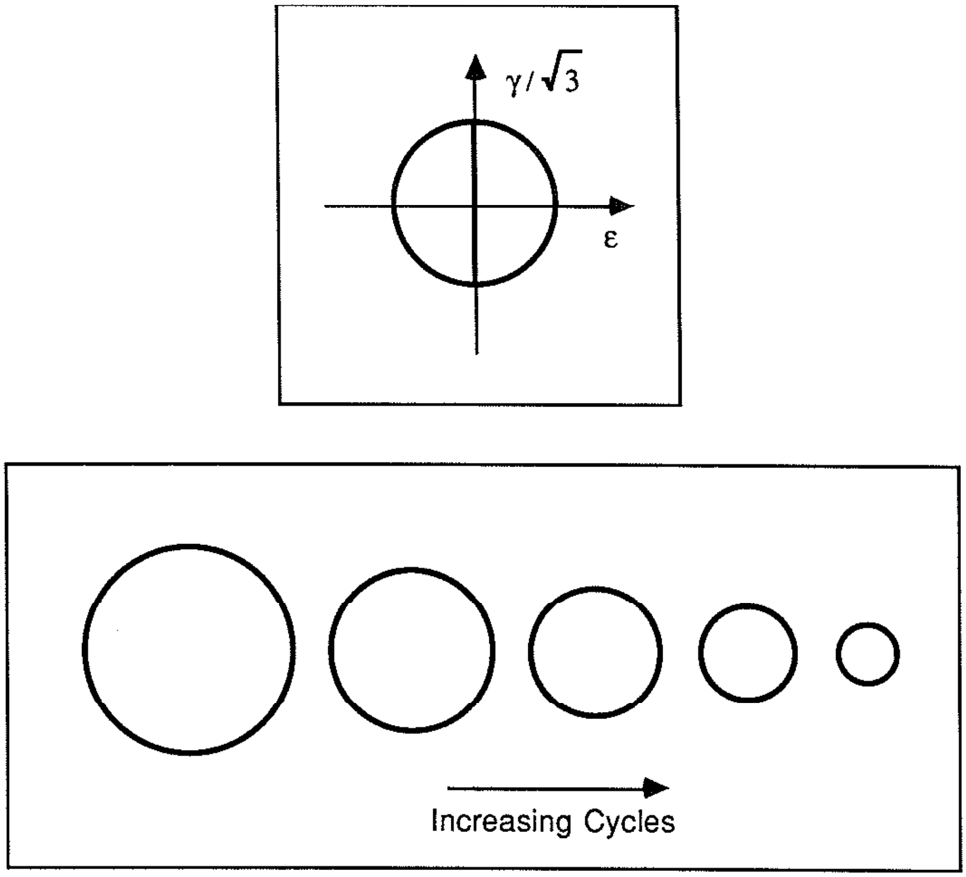

Figure 42. The Deformation State of 1100 Aluminum Under either Torsion or 90° Out-Of-Phase Tension-Torsion Cycling.

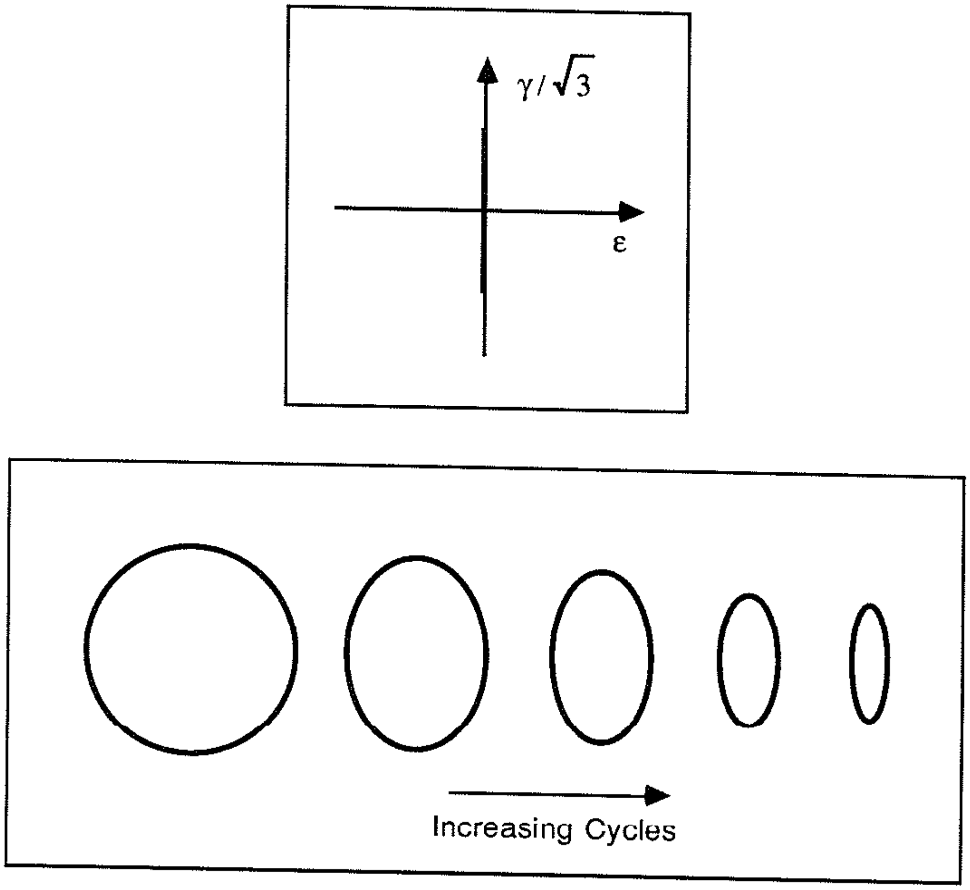

Figure 43. The Deformation State of Stainless Steel under Cyclic Torsion.

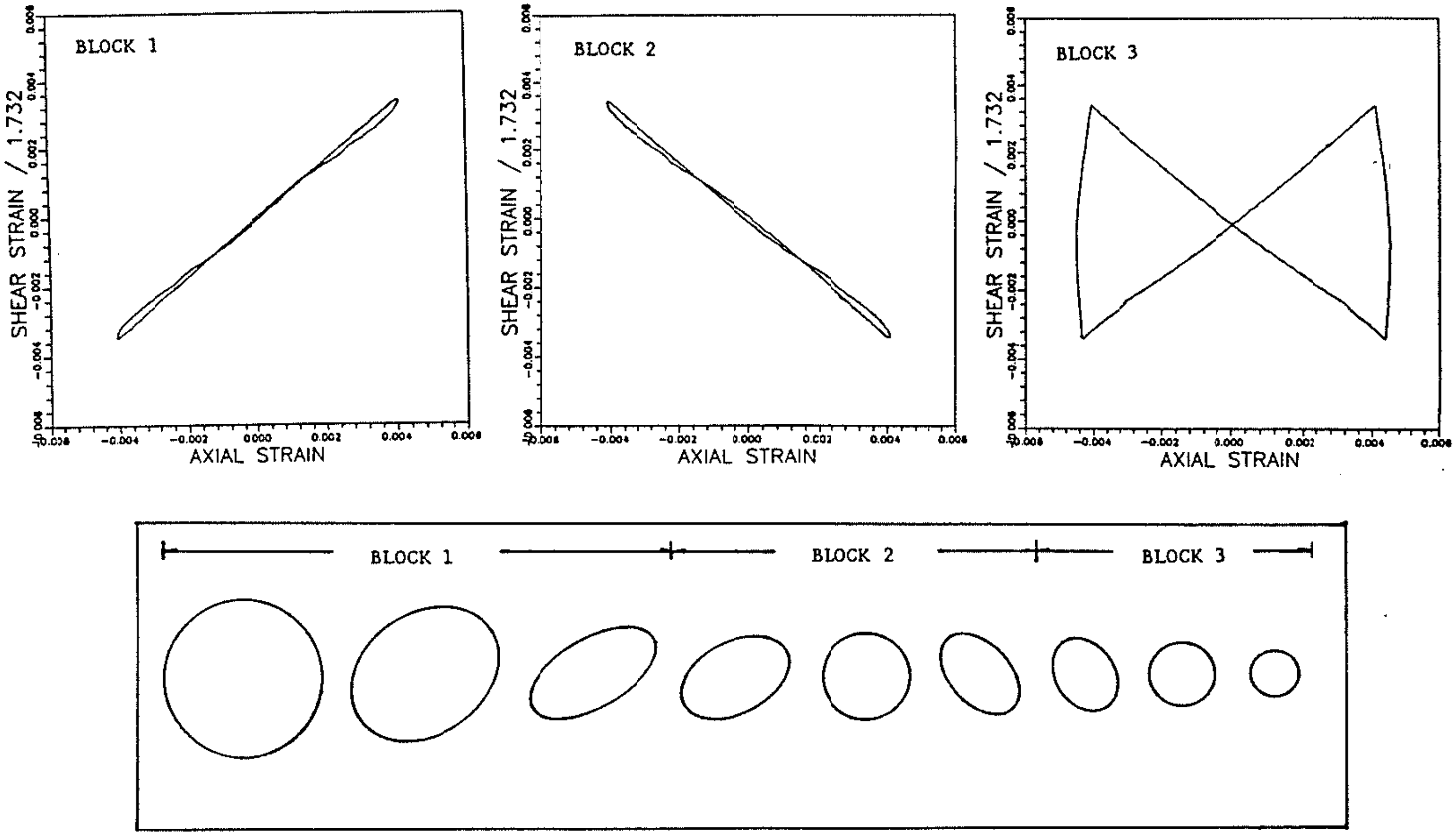

Figure 44. The Deformation State of Stainless Steel under the Loading with a Sudden Change in Loading Direction [61].

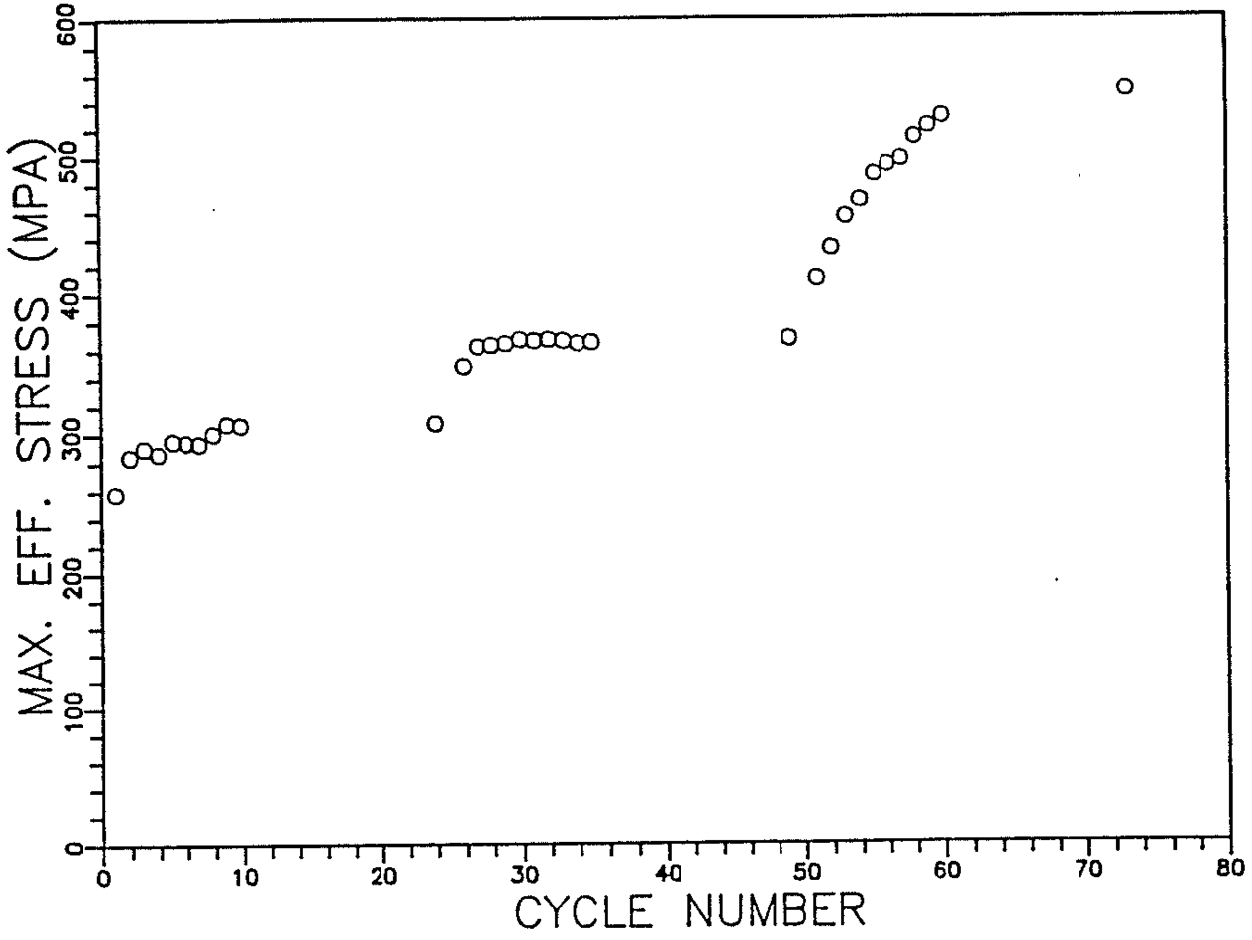

Figure 45. The Cyclic Hardening Behavior of Stainless Steel under the Cyclic Loading of Fig. 44 [61].

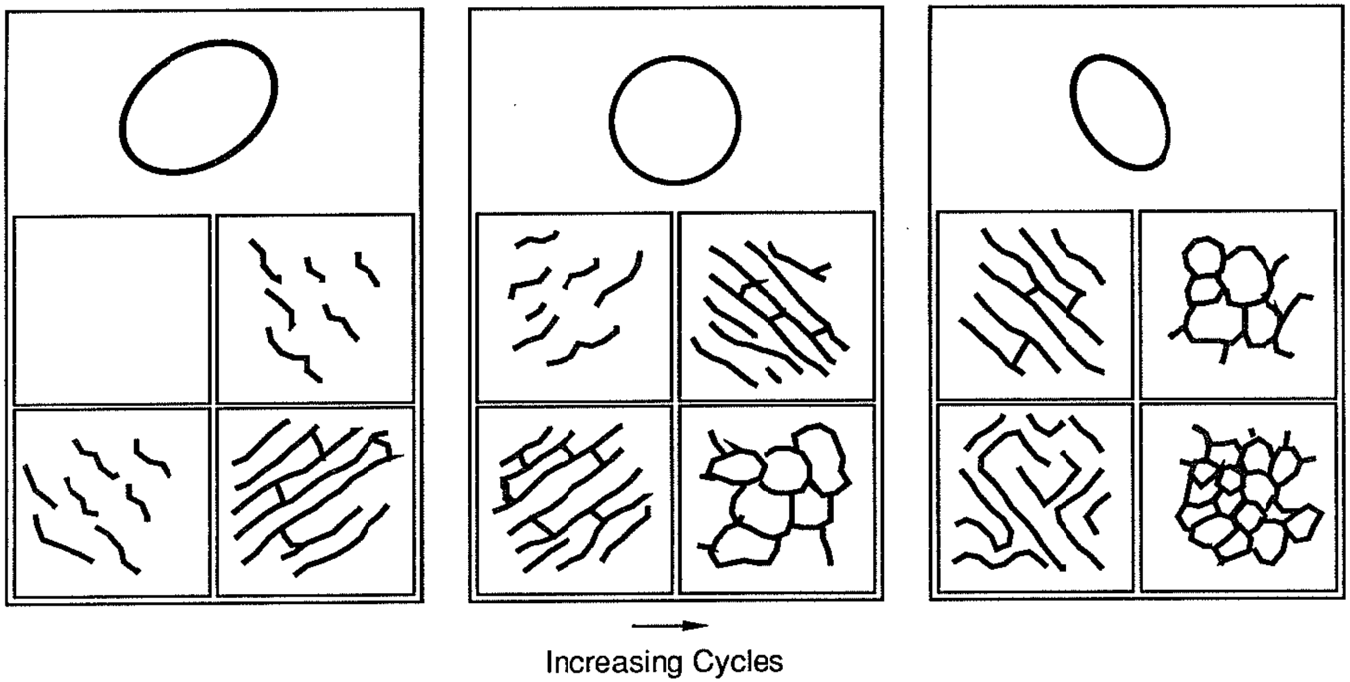

Figure 46. The Possible Dislocation Substructure Formed in the Stainless Steel under the Loading of Fig. 44.

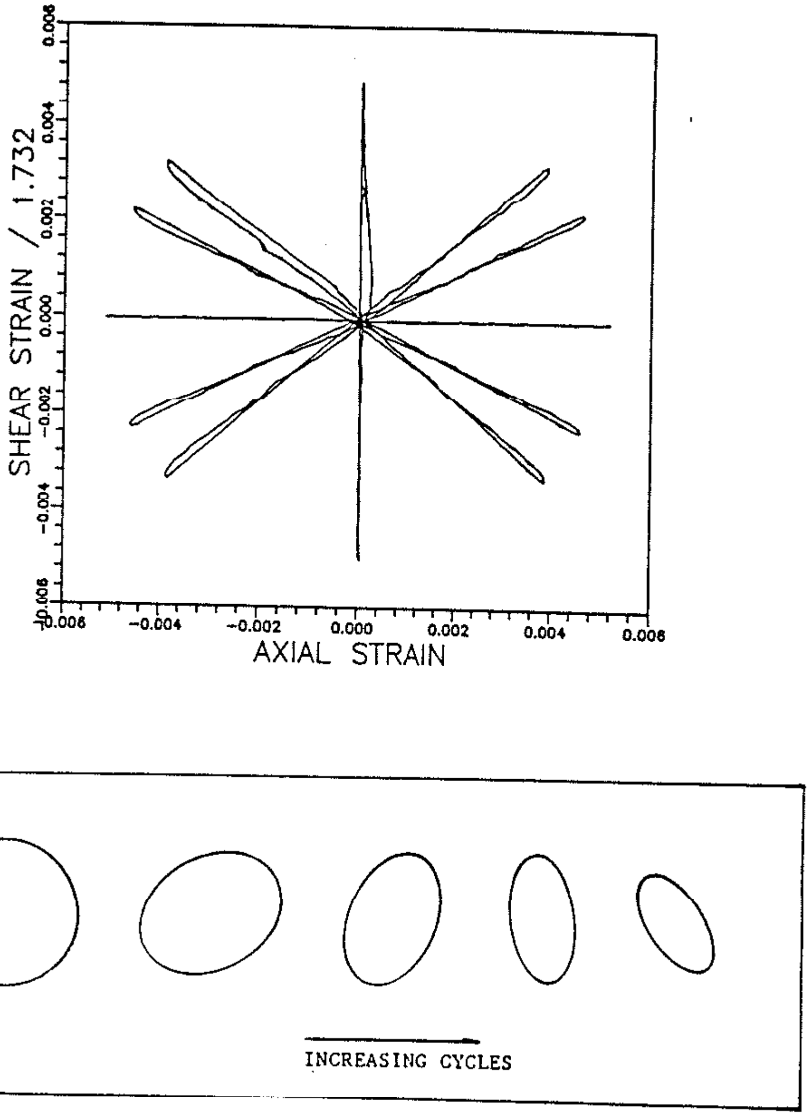

Figure 47. The Deformation State of Stainless Steel under the Loading with a Slow Change in Loading Direction [61].

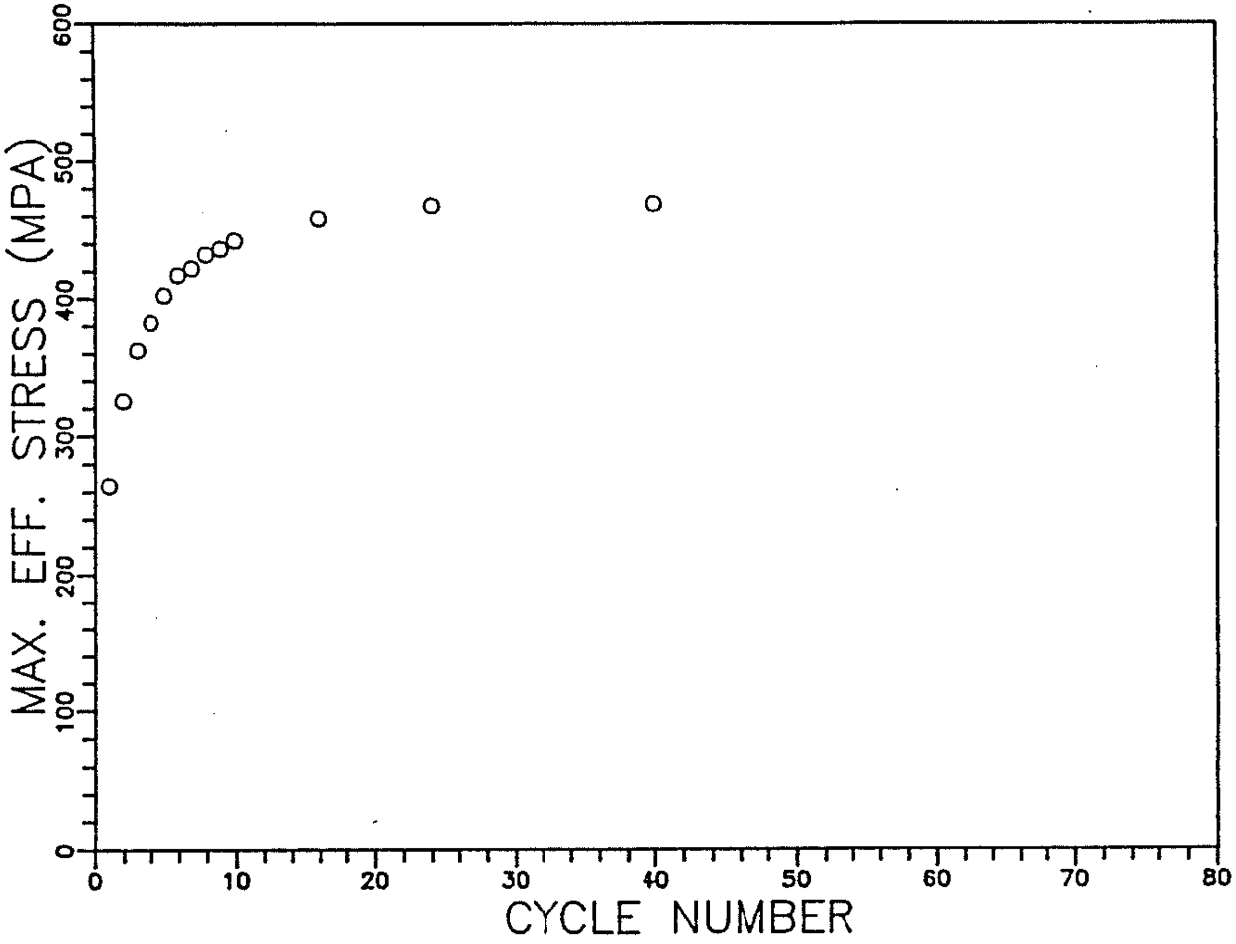

Figure 48. The Cyclic Hardening Behavior of Stainless Steel under the Cyclic Loading of Fig. 47 [61].

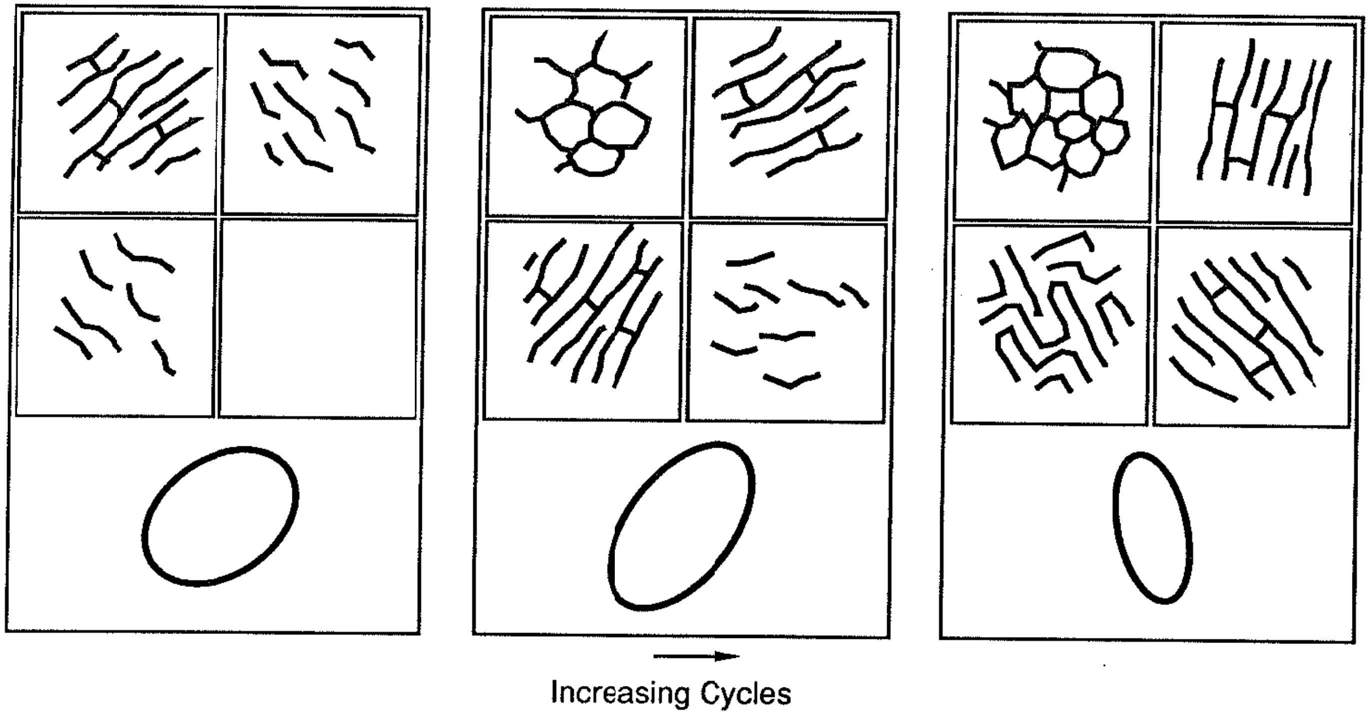

Figure 49. The Possible Dislocation Substructure Formed in the Stainless Steel under the Loading of Fig. 47.

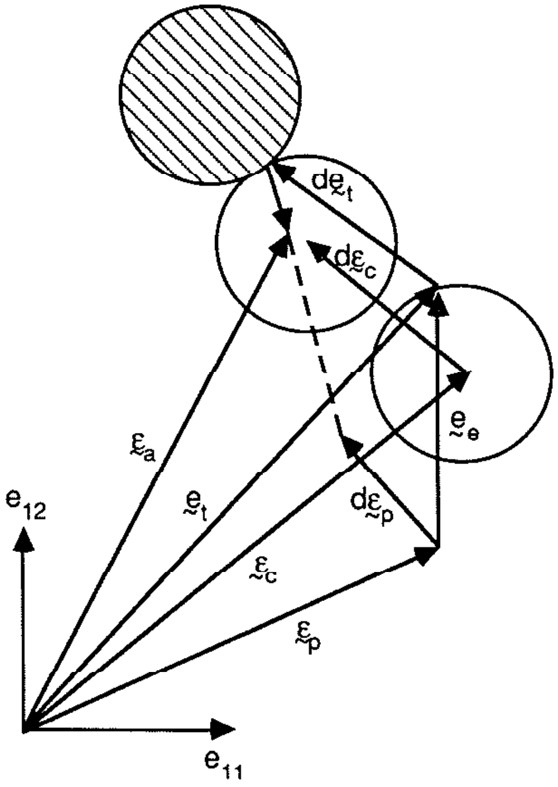

Figure 50. The Relation Between the Total Strain, the Plastic Strain and the Elastic Range in the Biaxial Deviatoric Strain Plane.

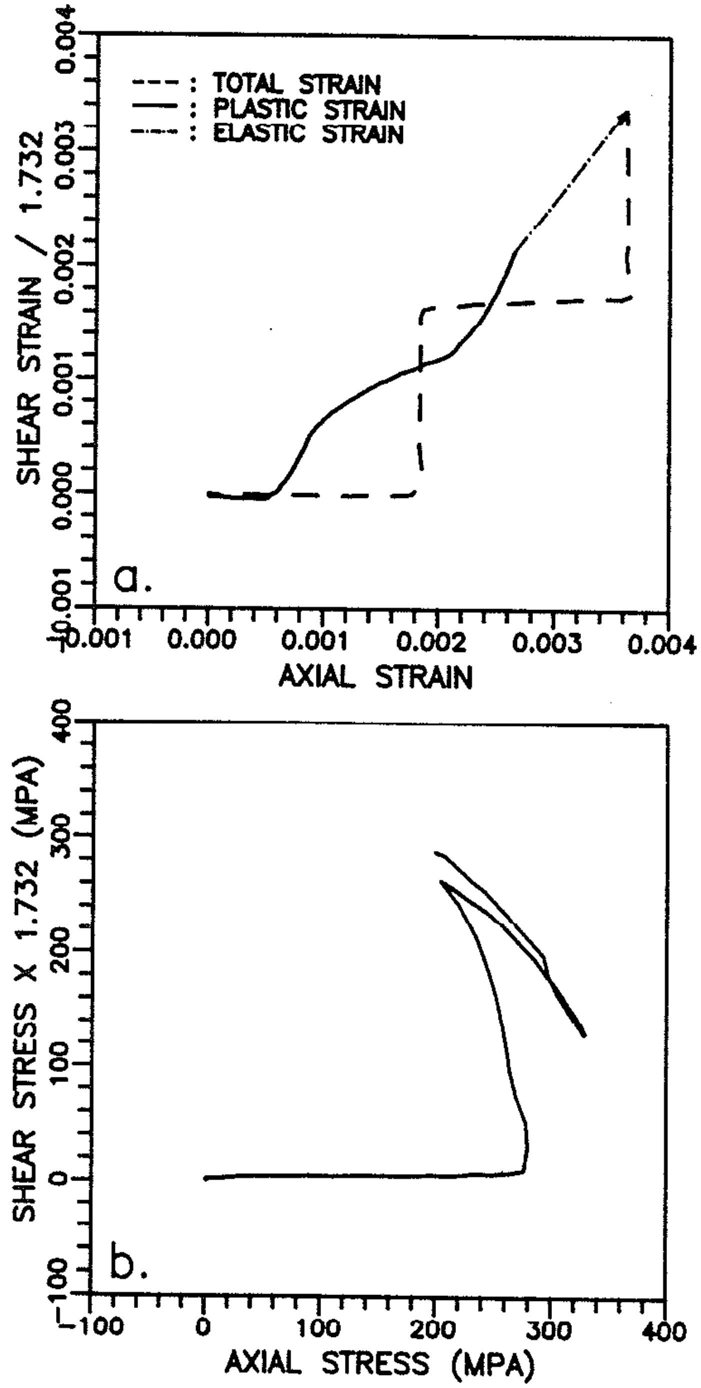

Figure 51. A Comparison Between the Stress and Strain Plane Formulation

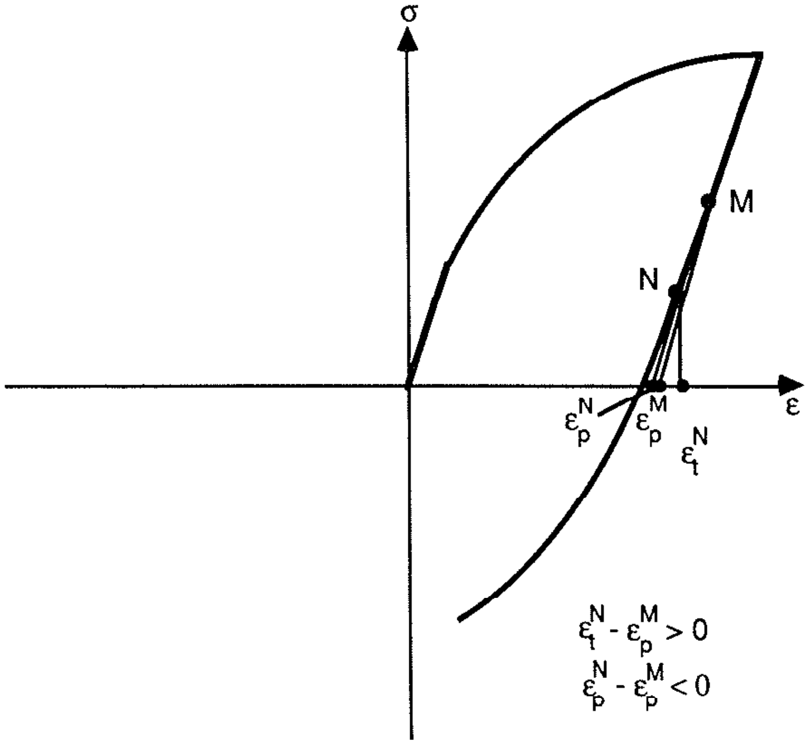

Figure 52. A Schematic Stress-Strain Curve for a Material with Strong Bauchinger Effect.

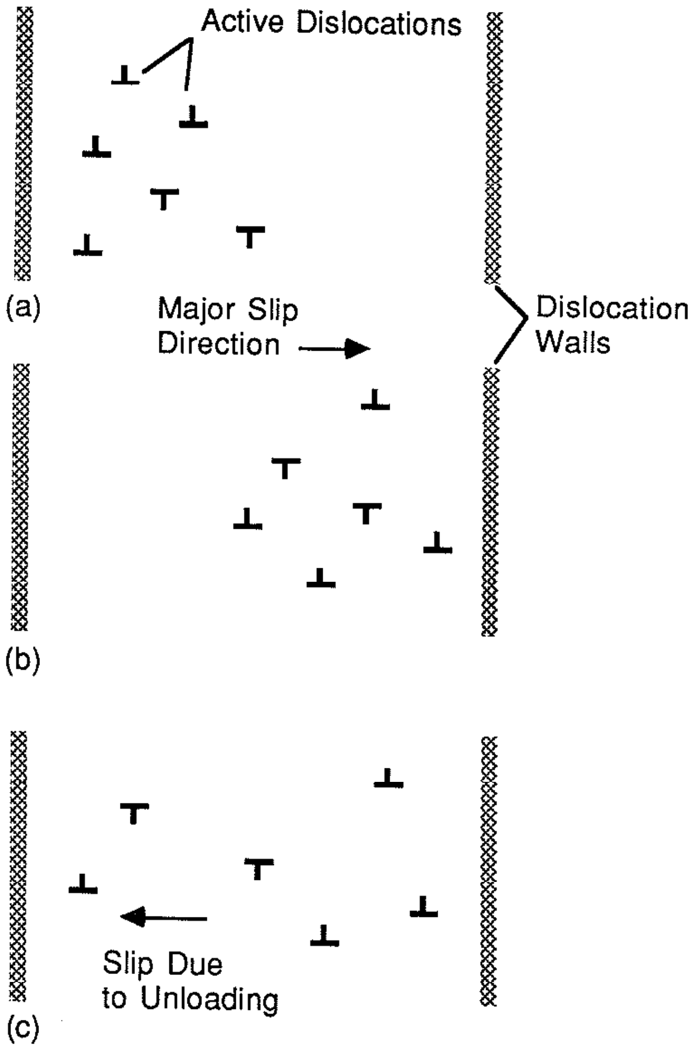

Figure 53. (a) - (c) The Behavior of Active Dislocations During the Unloading and Reloading Procedure.

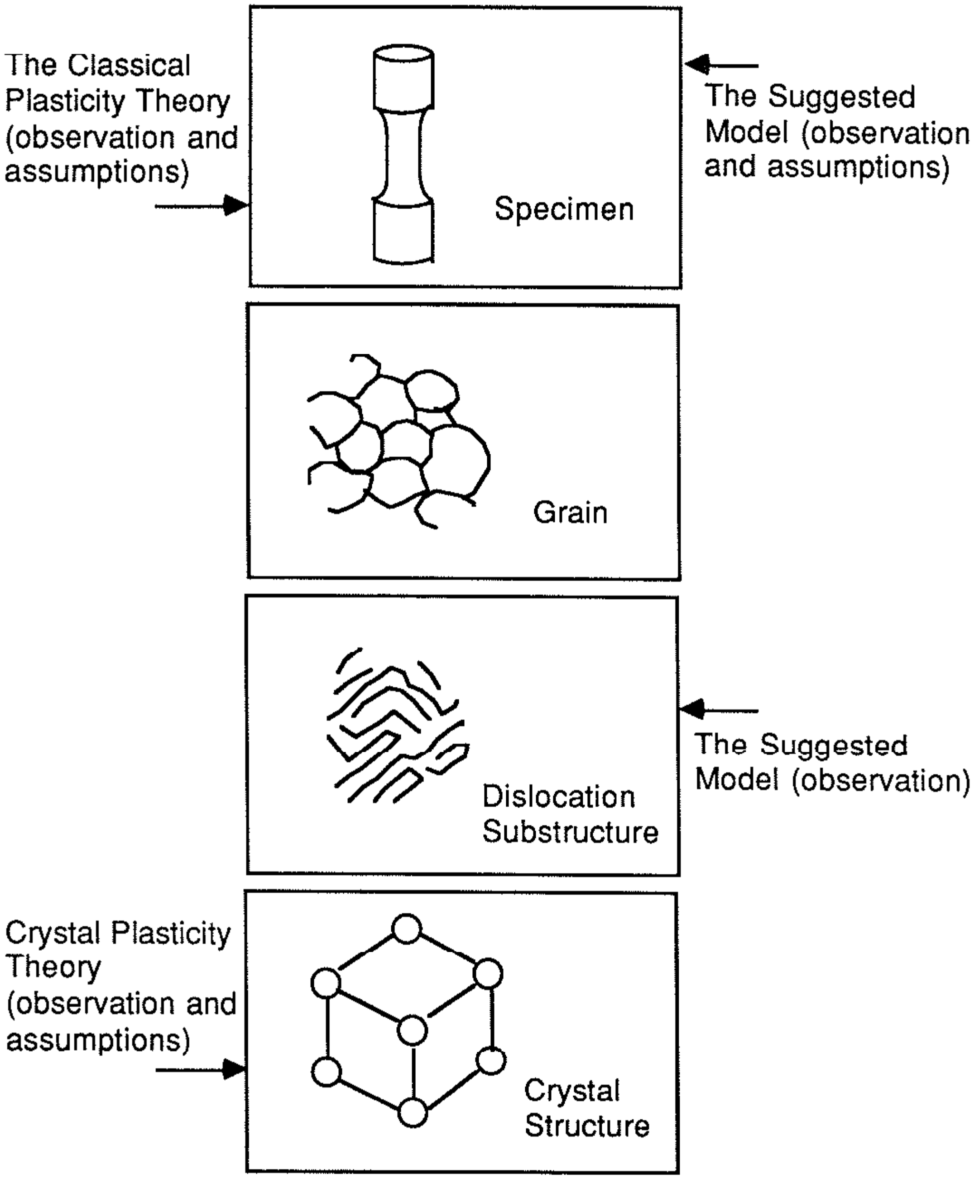

Figure 54. A Comparison Between the Suggested Model, the Classical Plasticity Theory and the Crystal Plasticity Theory.

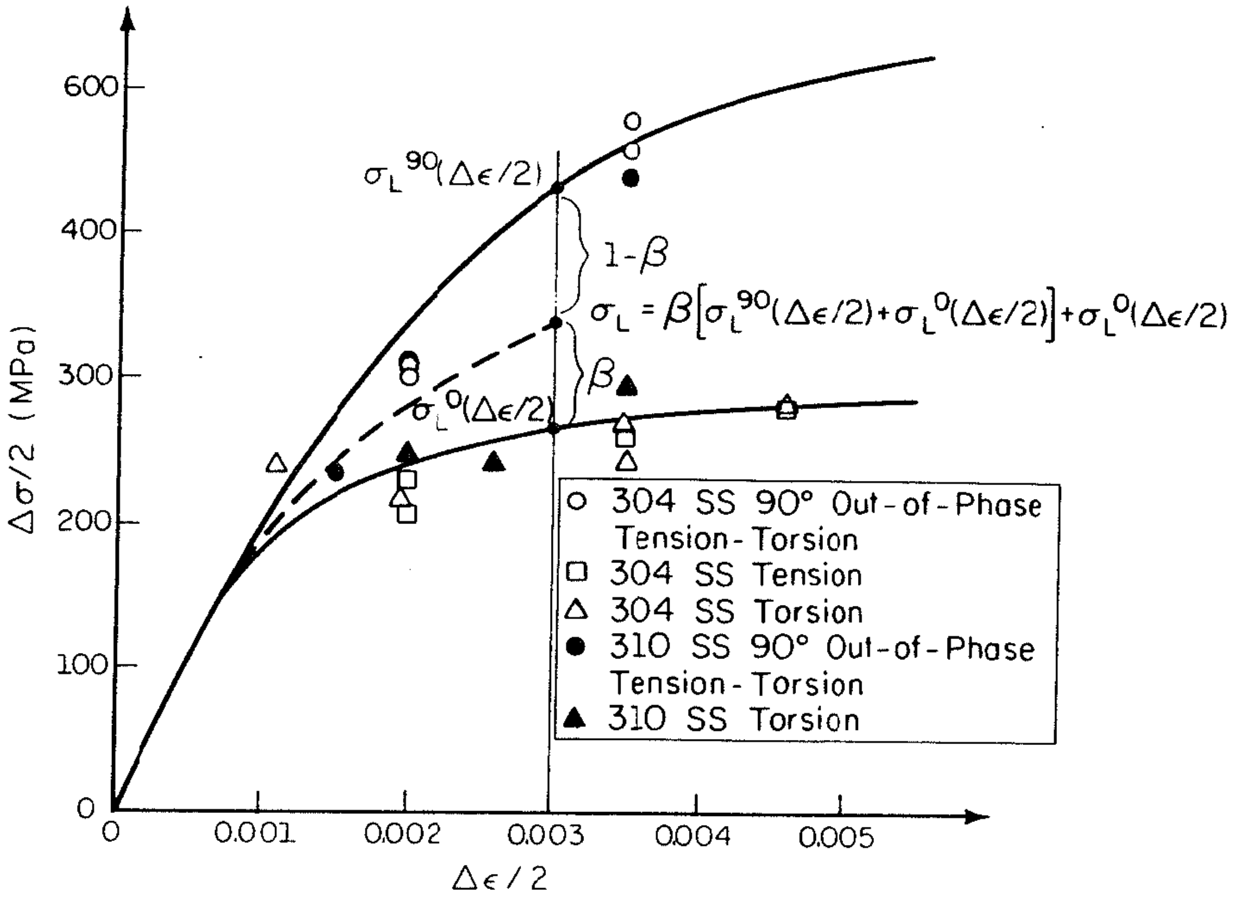

Figure 55. A Simplified Method of Estimating the Limit Stress from the Cyclic Stress-Strain Curve.

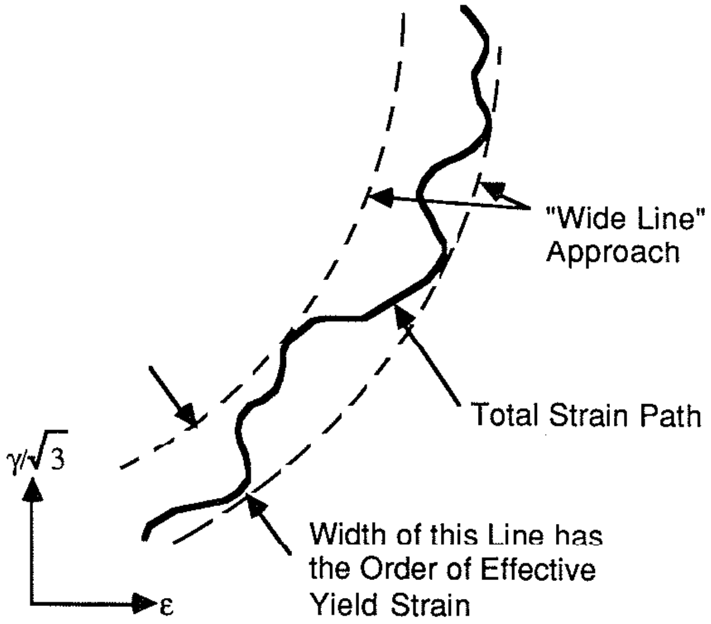

Figure 56. A Simplified Method of Estimating the Degree of Nonproportionality from the Total Strain History.

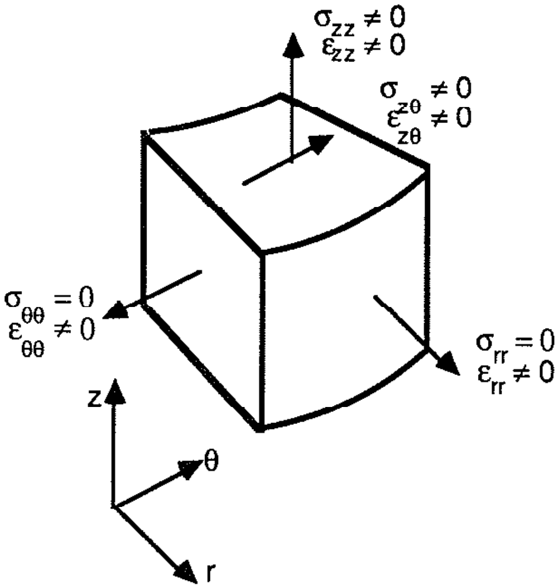

Figure 57. The Approximated Stress and Strain State of the Tube Specimen.

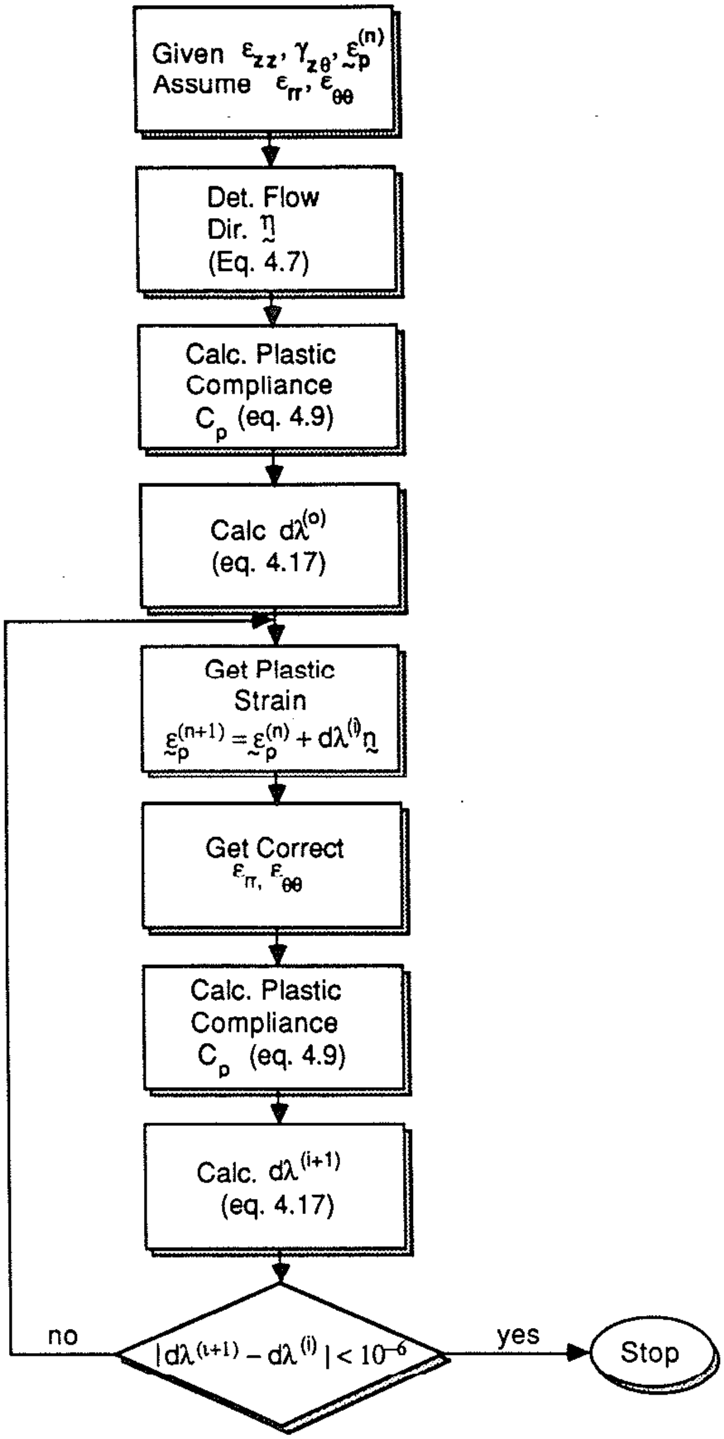

Figure 58. The Flow Chart of Calculating the Correct value of ε_{rr} and $\varepsilon_{\theta\theta}$

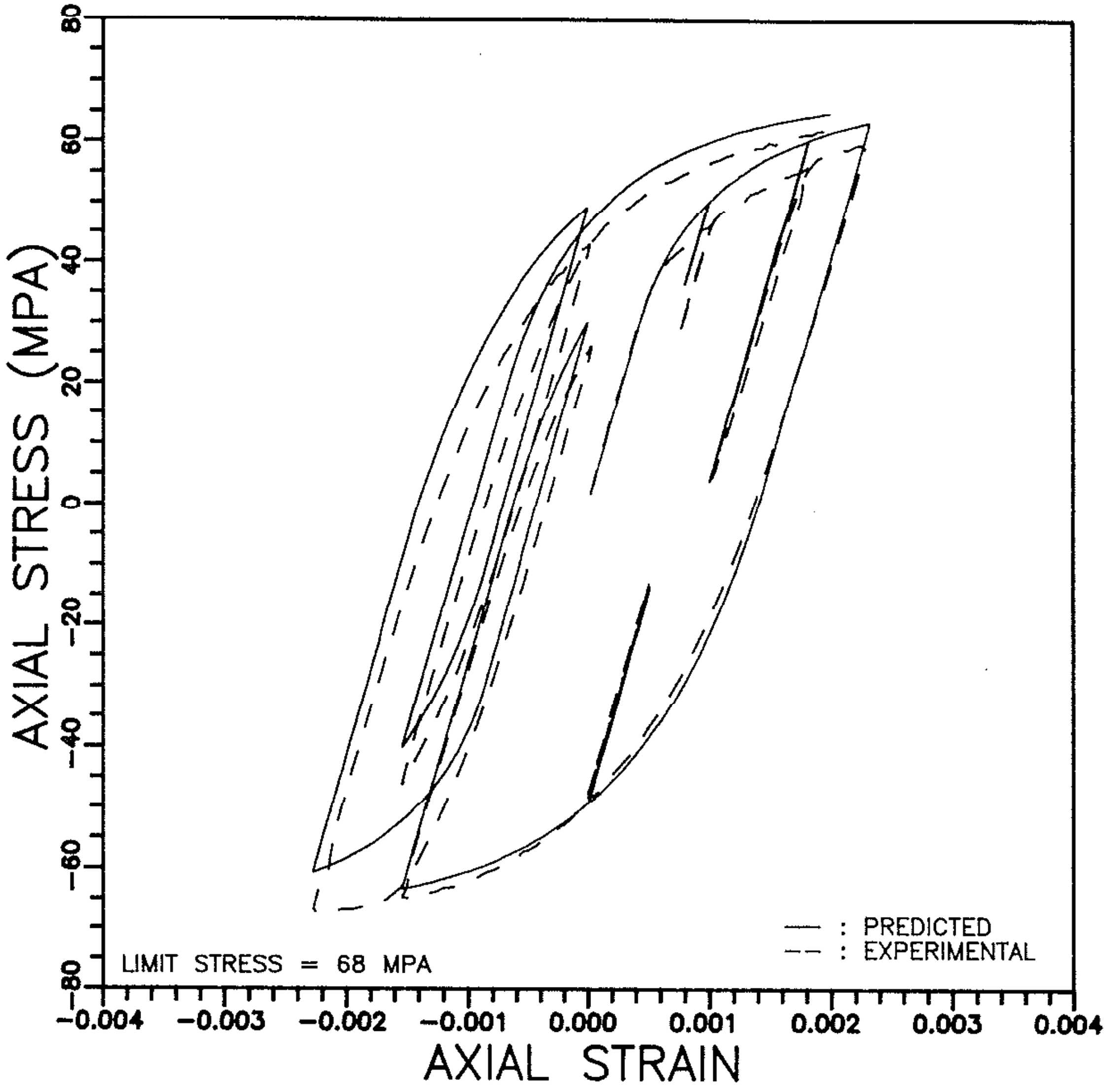

Figure 59. A Comparison Between the Predicted and the Experimental Results for the 1100 Aluminum under a Random Uniaxial Loading (Specimen A114).

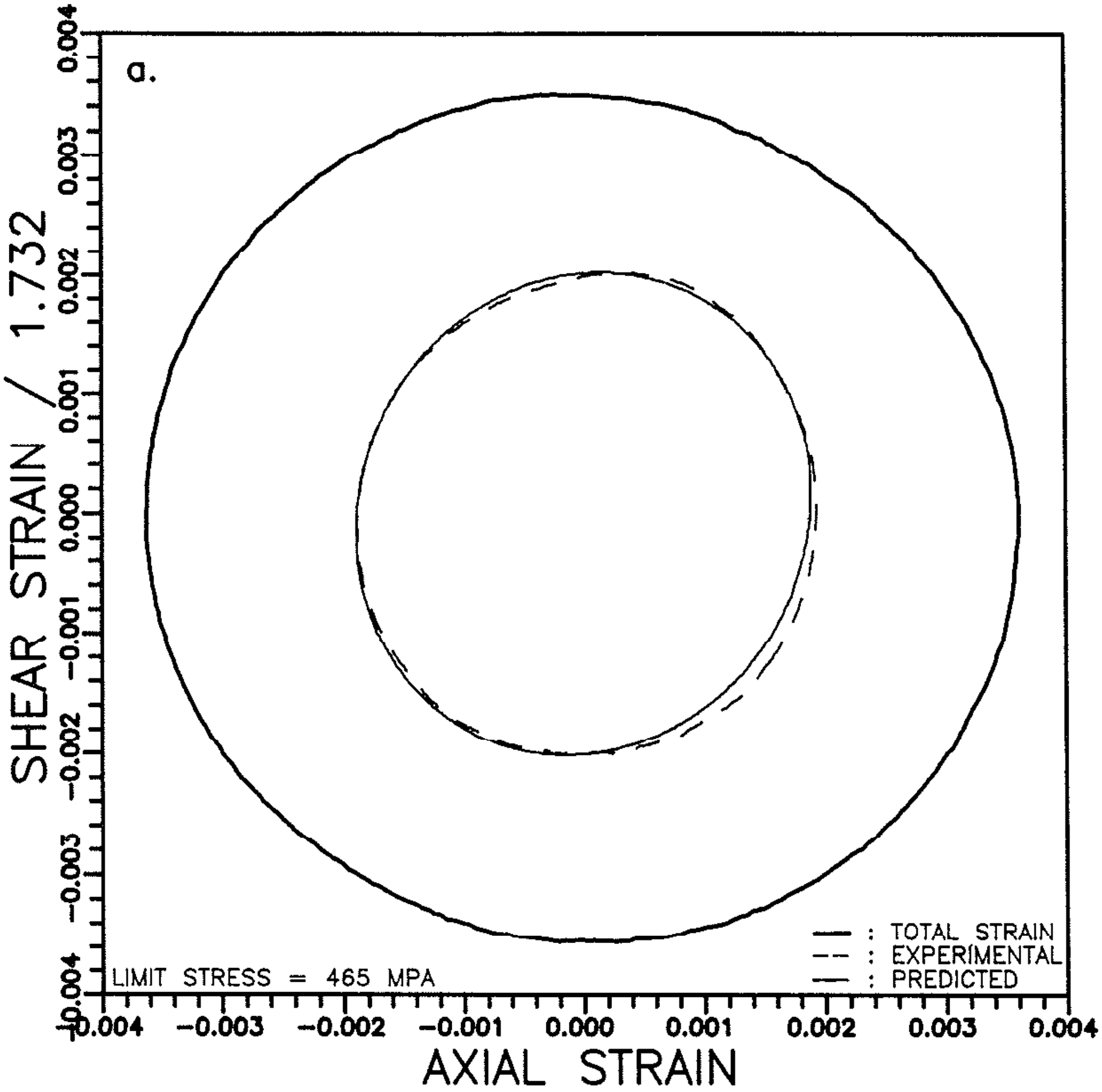

Figure 60. (a) - (d) A Comparison Between the Predicted and the Stabilized Stress-Strain History of 304 Stainless Steel under the 90° Out-Of-Phase Tension-Torsion Cycling (Specimen SS13) [36].

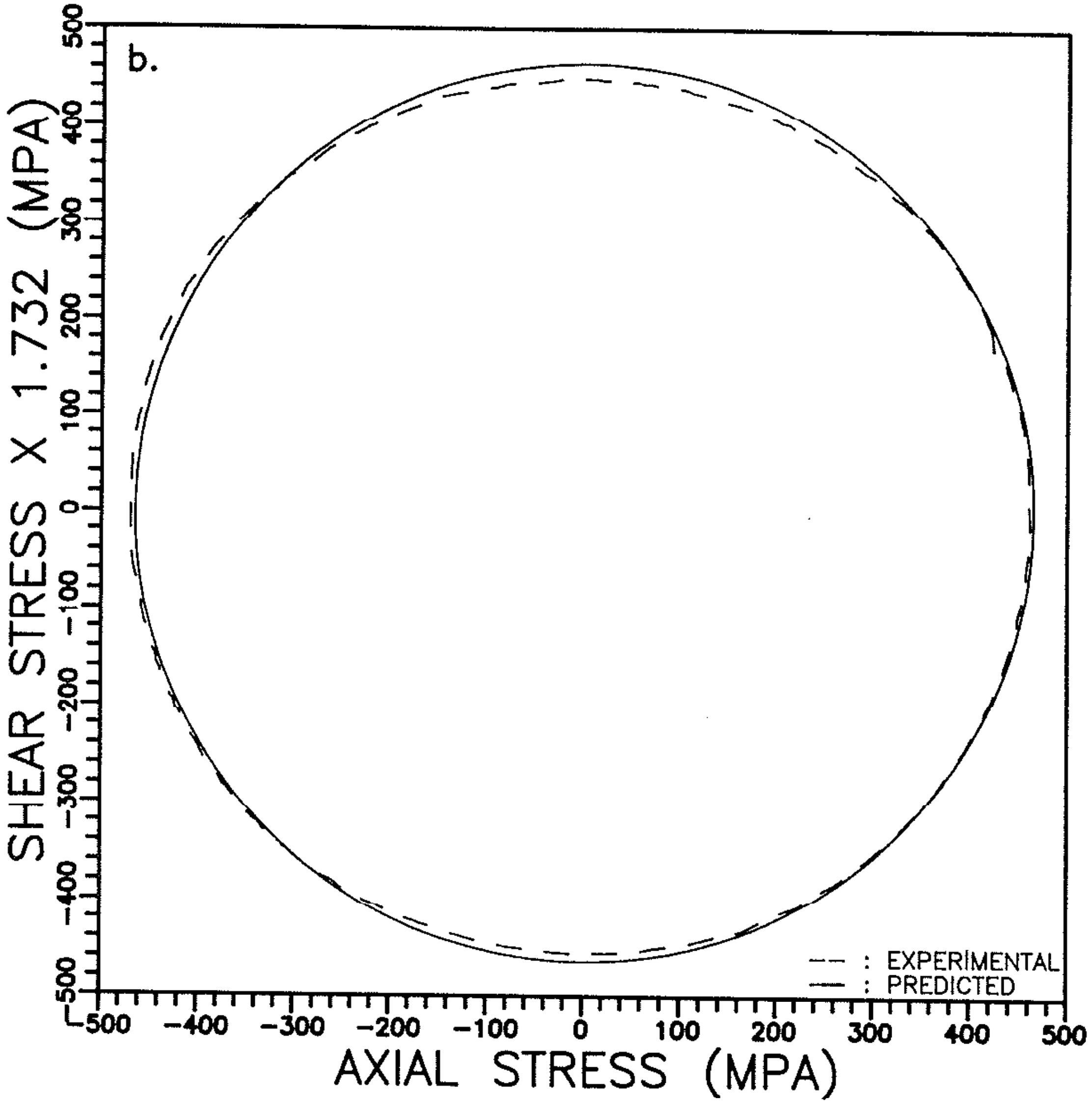
b.
SHEAR STRESS X 1.732 (MPA)
500
400
300
200
100
0
−100
−200
−300
−400
−500
−500
−400
−300
−200
−100
0
100
200
300
400
500
AXIAL STRESS (MPA)
— — : EXPERIMENTAL
—— : PREDICTED

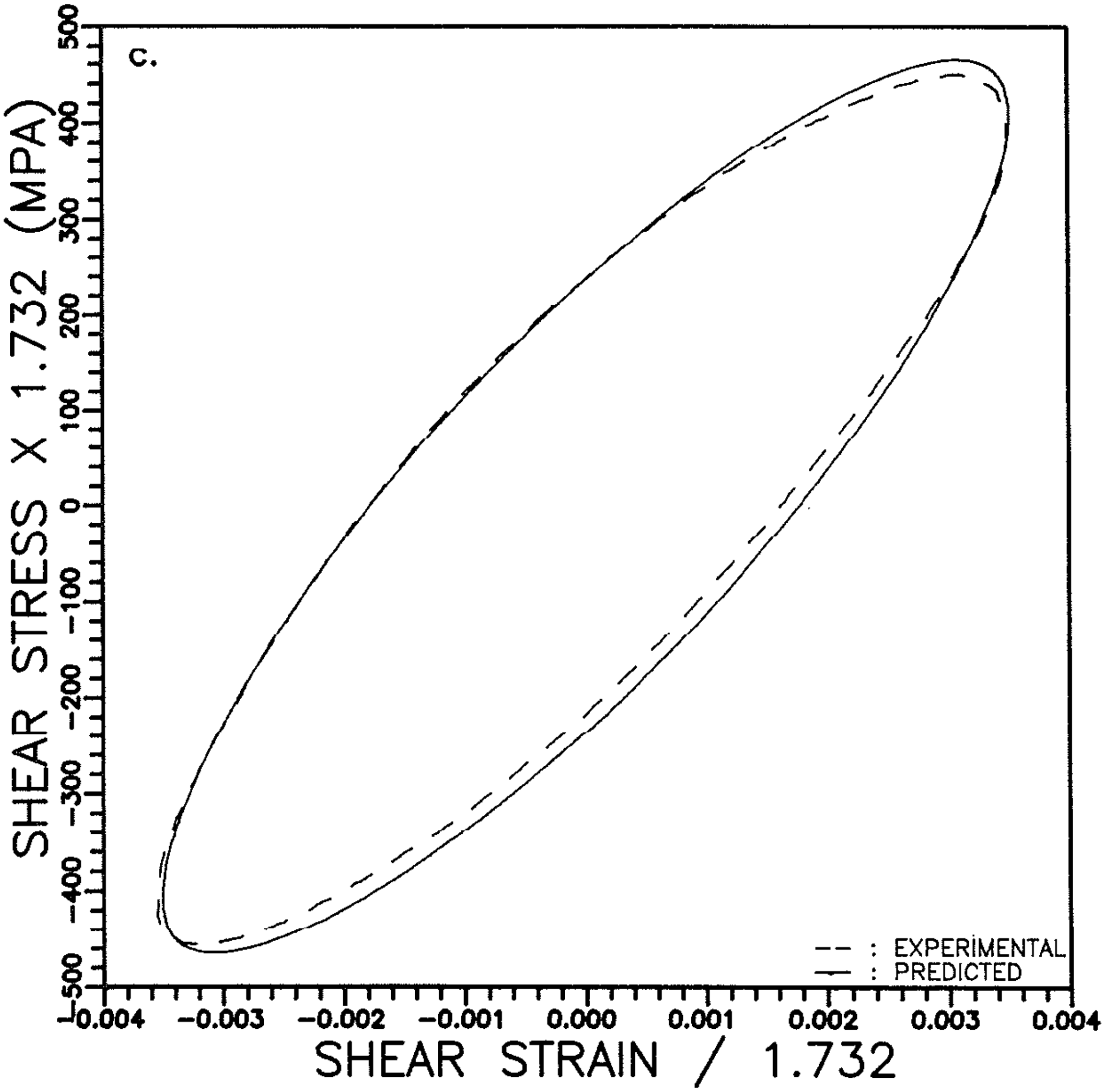
c.
SHEAR STRESS X 1.732 (MPA)
500
400
300
200
100
0
-100
-200
-300
-400
-500
-0.004
-0.003
-0.002
-0.001
0.000
0.001
0.002
0.003
0.004
SHEAR STRAIN / 1.732
— — : EXPERIMENTAL
—— : PREDICTED

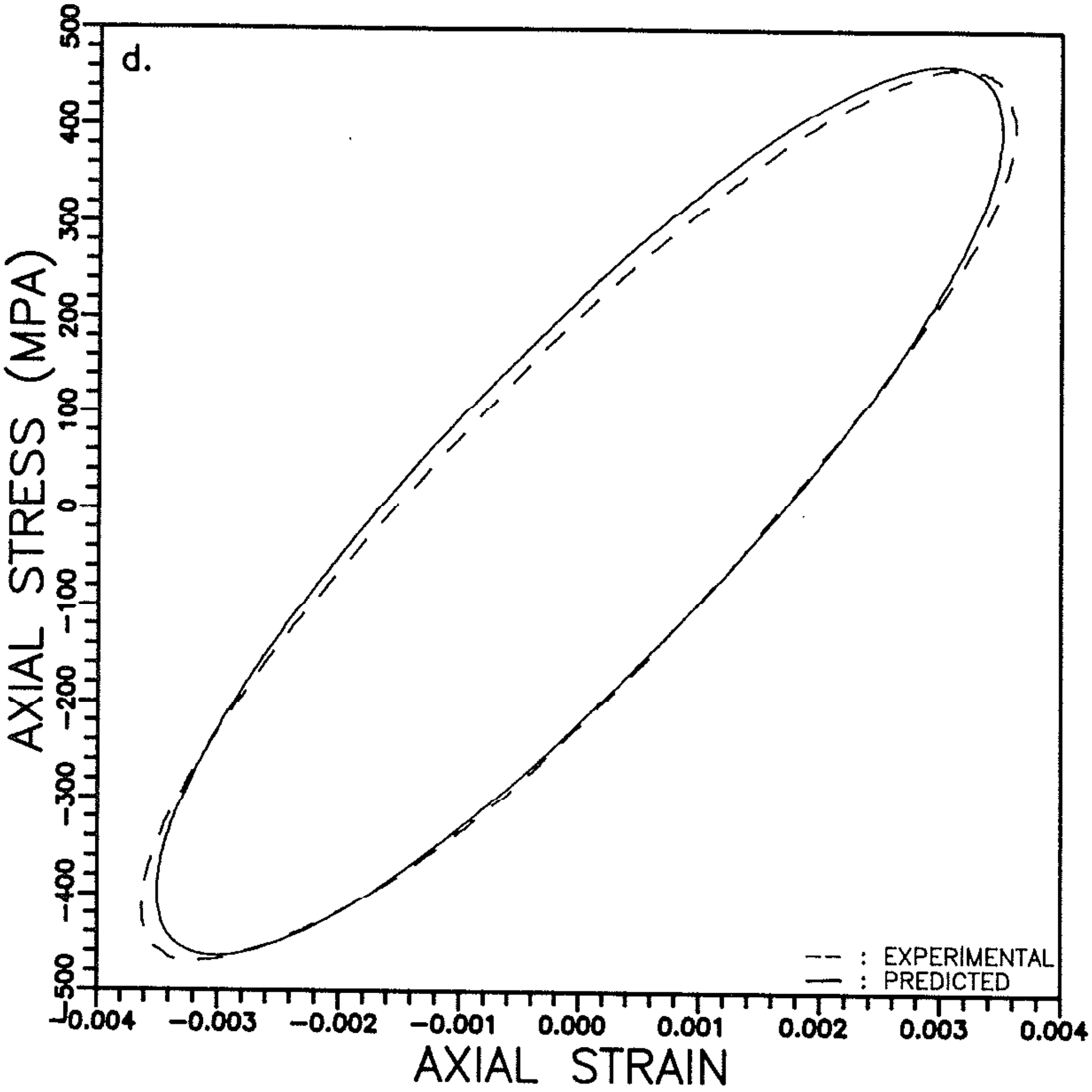
d.
AXIAL STRESS (MPA)
500
400
300
200
100
0
−100
−200
−300
−400
−500
AXIAL STRAIN
−0.004
−0.003
−0.002
−0.001
0.000
0.001
0.002
0.003
0.004
– – : EXPERIMENTAL
—— : PREDICTED

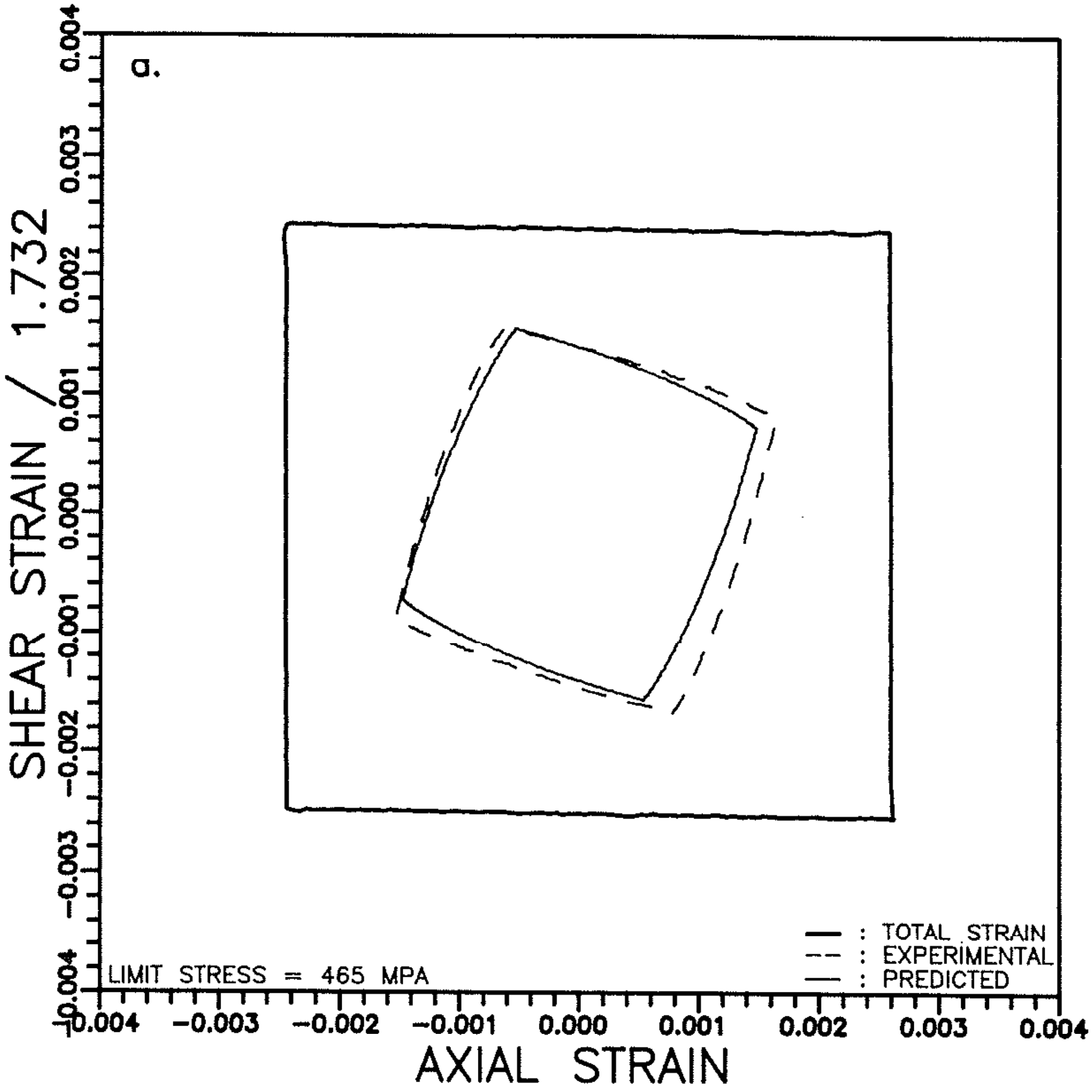

Figure 61. (a) - (d) A Comparison Between the Predicted and the Stabilized Stress-Strain History of 304 Stainless Steel under the One-Square Tension-Torsion Cycling (Specimen SS03) [36].

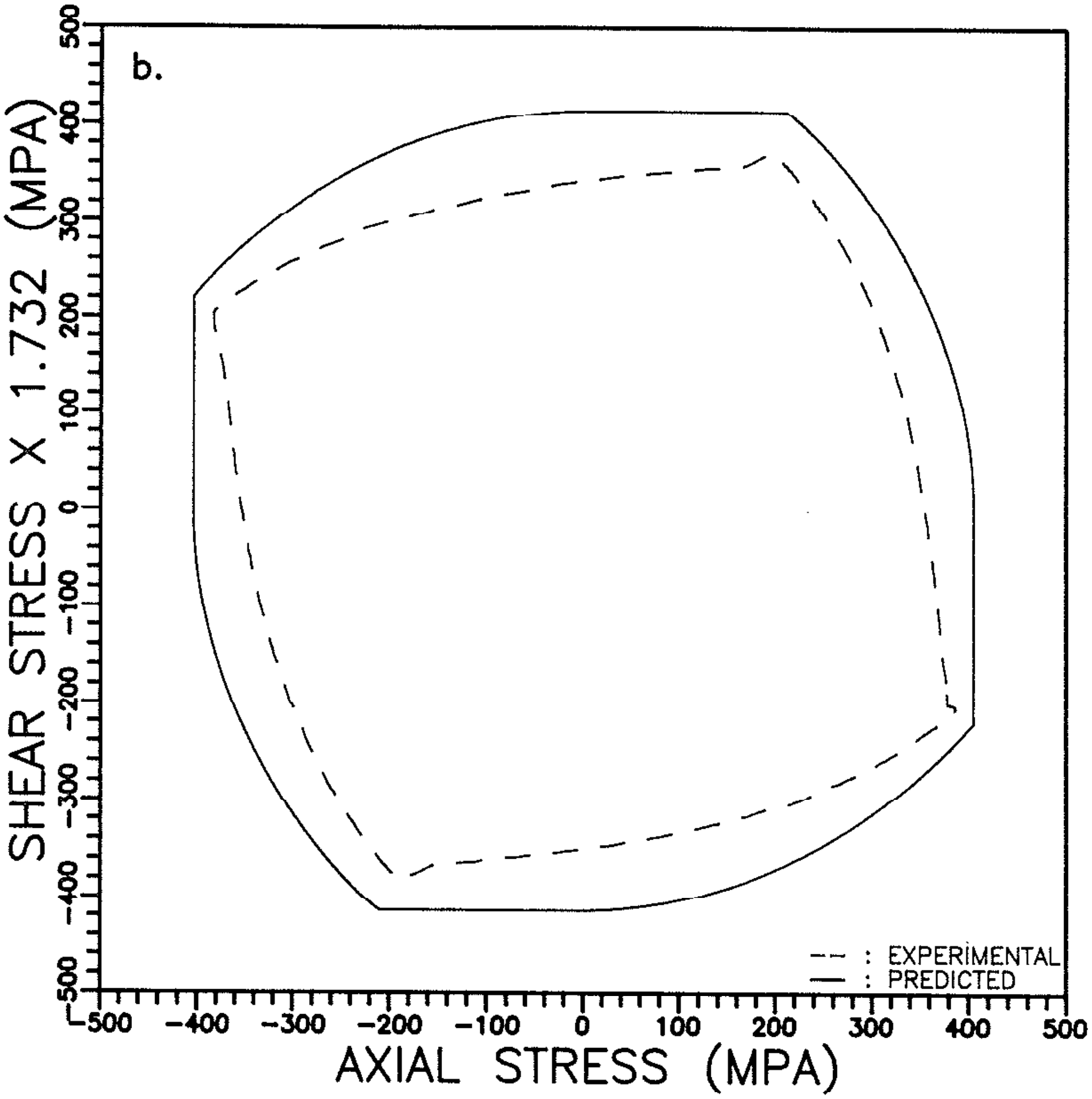
b.
SHEAR STRESS X 1.732 (MPA)
500
400
300
200
100
0
−100
−200
−300
−400
−500
AXIAL STRESS (MPA)
−500
−400
−300
−200
−100
0
100
200
300
400
500
– – : EXPERIMENTAL
—— : PREDICTED

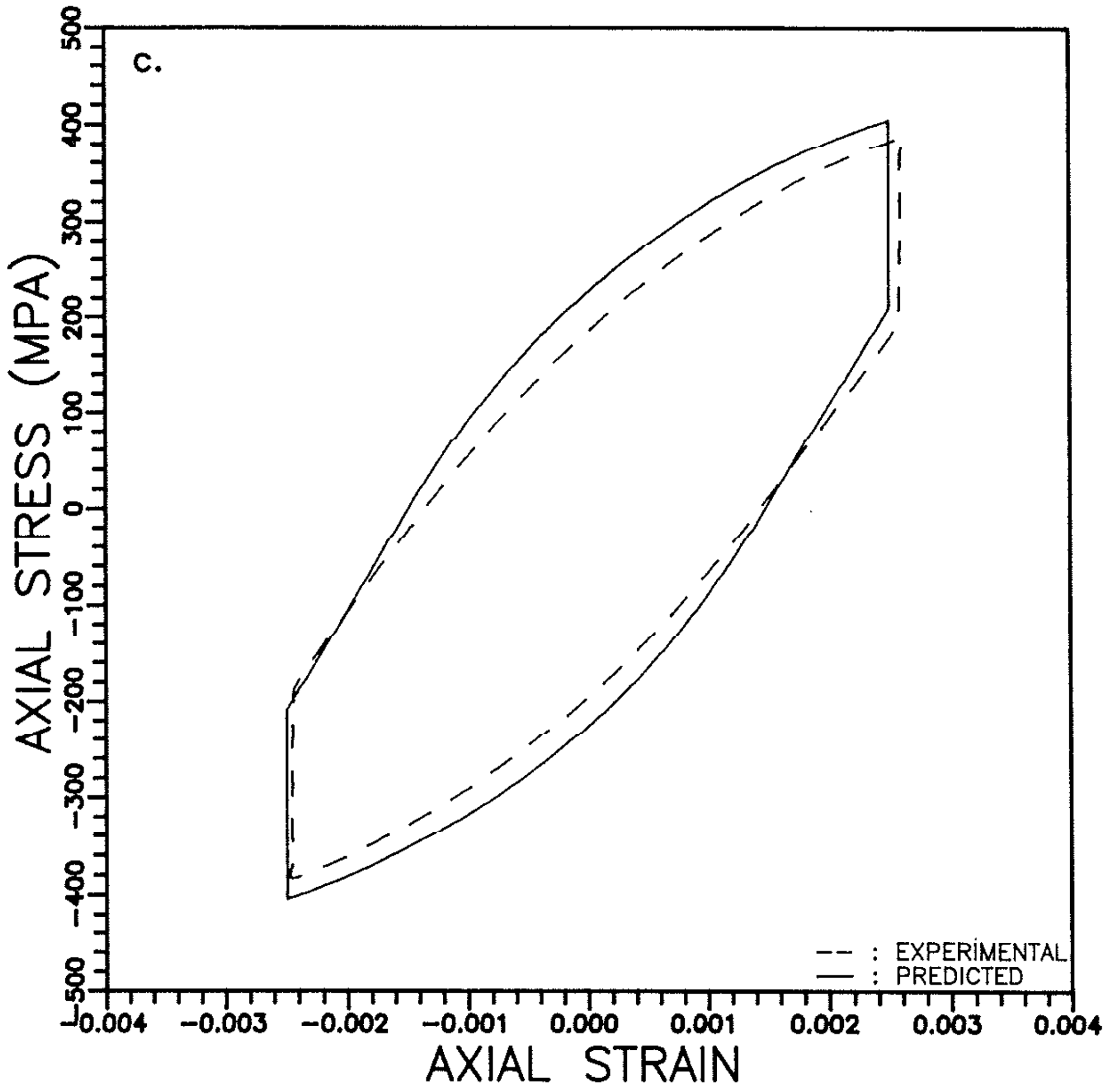
c.
AXIAL STRESS (MPA)
500
400
300
200
100
0
-100
-200
-300
-400
-500
-0.004
-0.003
-0.002
-0.001
0.000
0.001
0.002
0.003
0.004
AXIAL STRAIN
-- : EXPERIMENTAL
— : PREDICTED

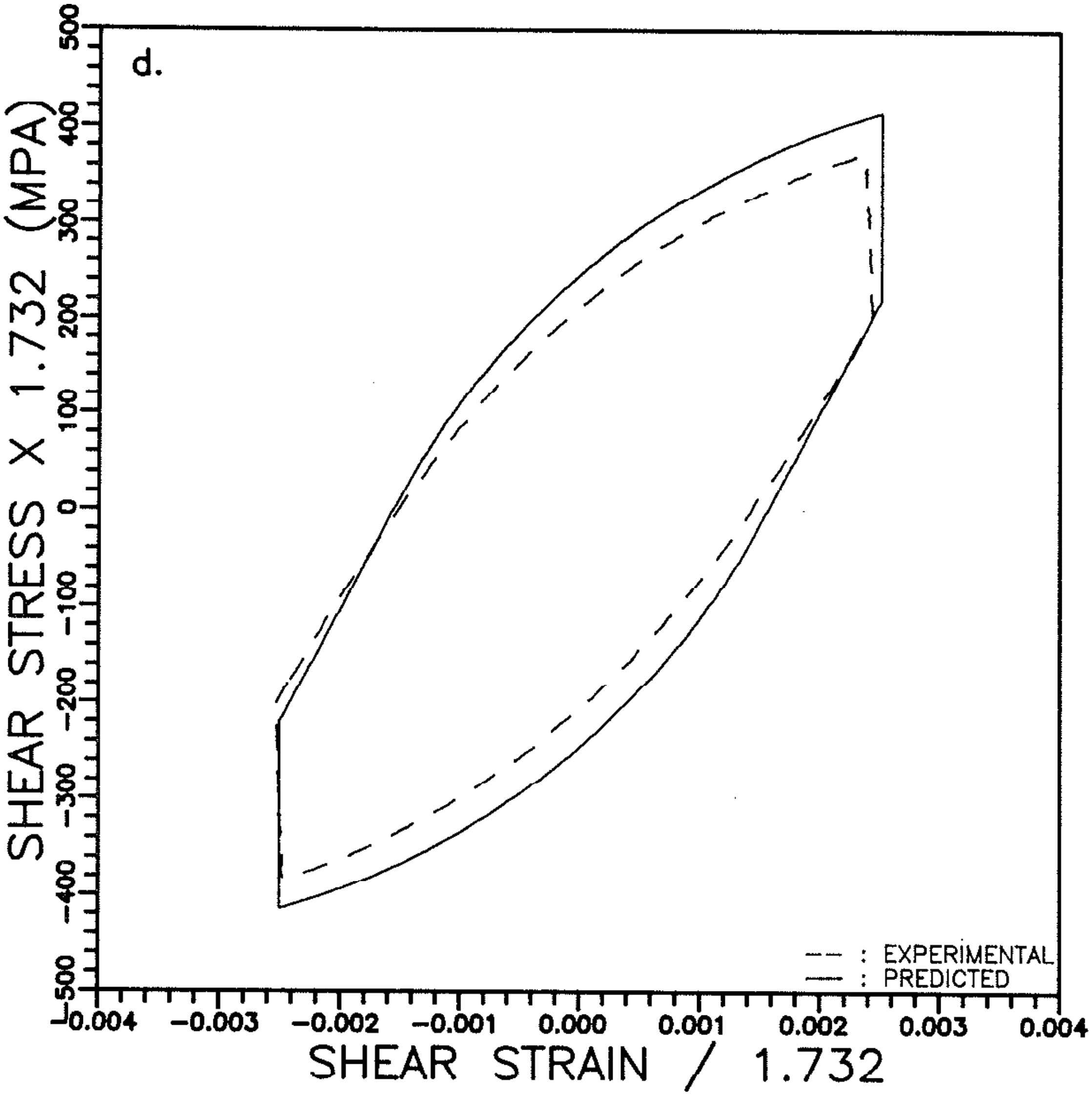
d.
SHEAR STRESS X 1.732 (MPA)
500
400
300
200
100
0
-100
-200
-300
-400
-500
SHEAR STRAIN / 1.732
-0.004
-0.003
-0.002
-0.001
0.000
0.001
0.002
0.003
0.004
— — : EXPERIMENTAL
—— : PREDICTED

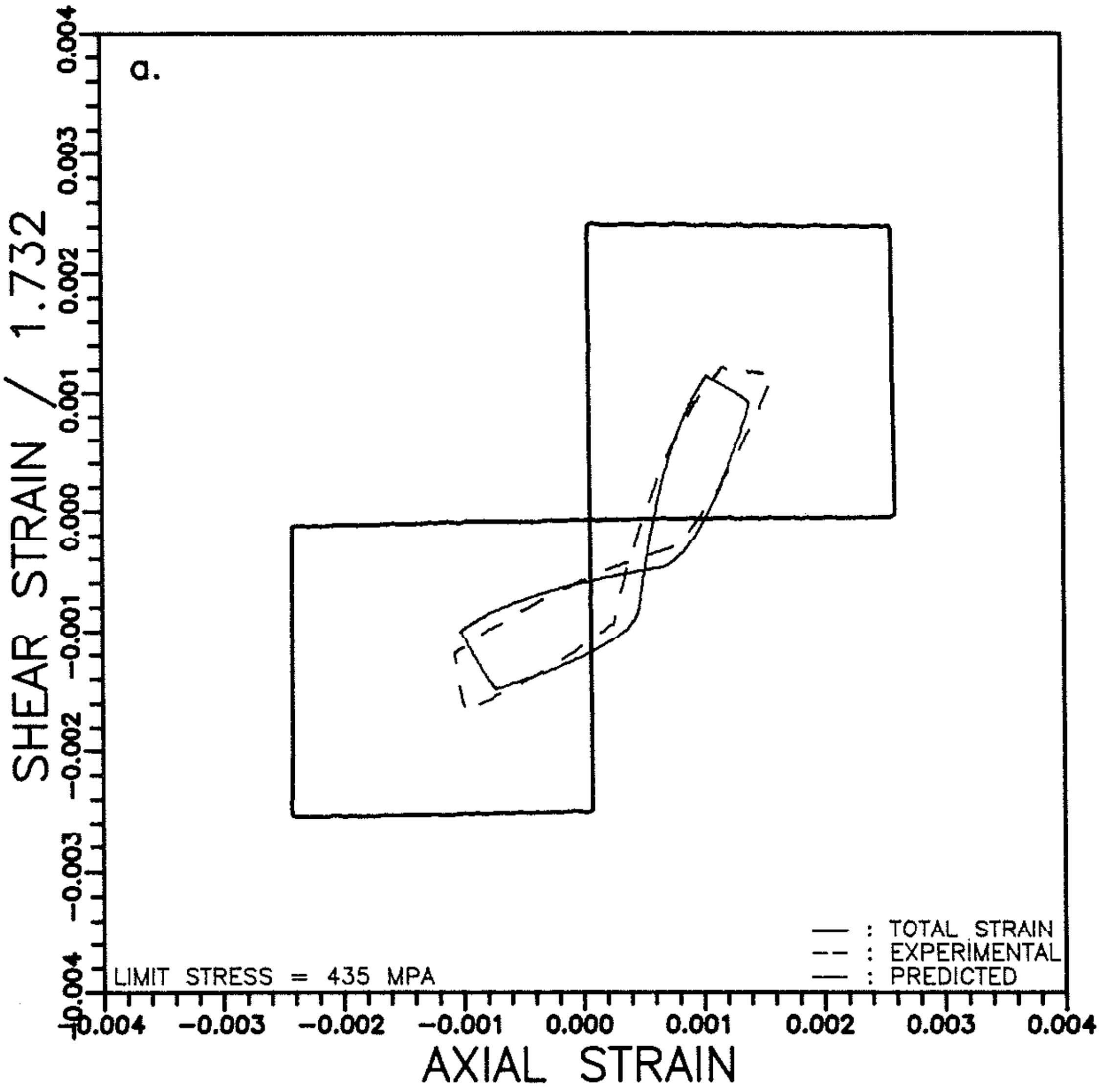

Figure 62. (a) - (d) A Comparison Between the Predicted and the Stabilized Stress-Strain History of 304 Stainless Steel under the Two-Square Tension-Torsion Cycling (Specimen SS04) [36].

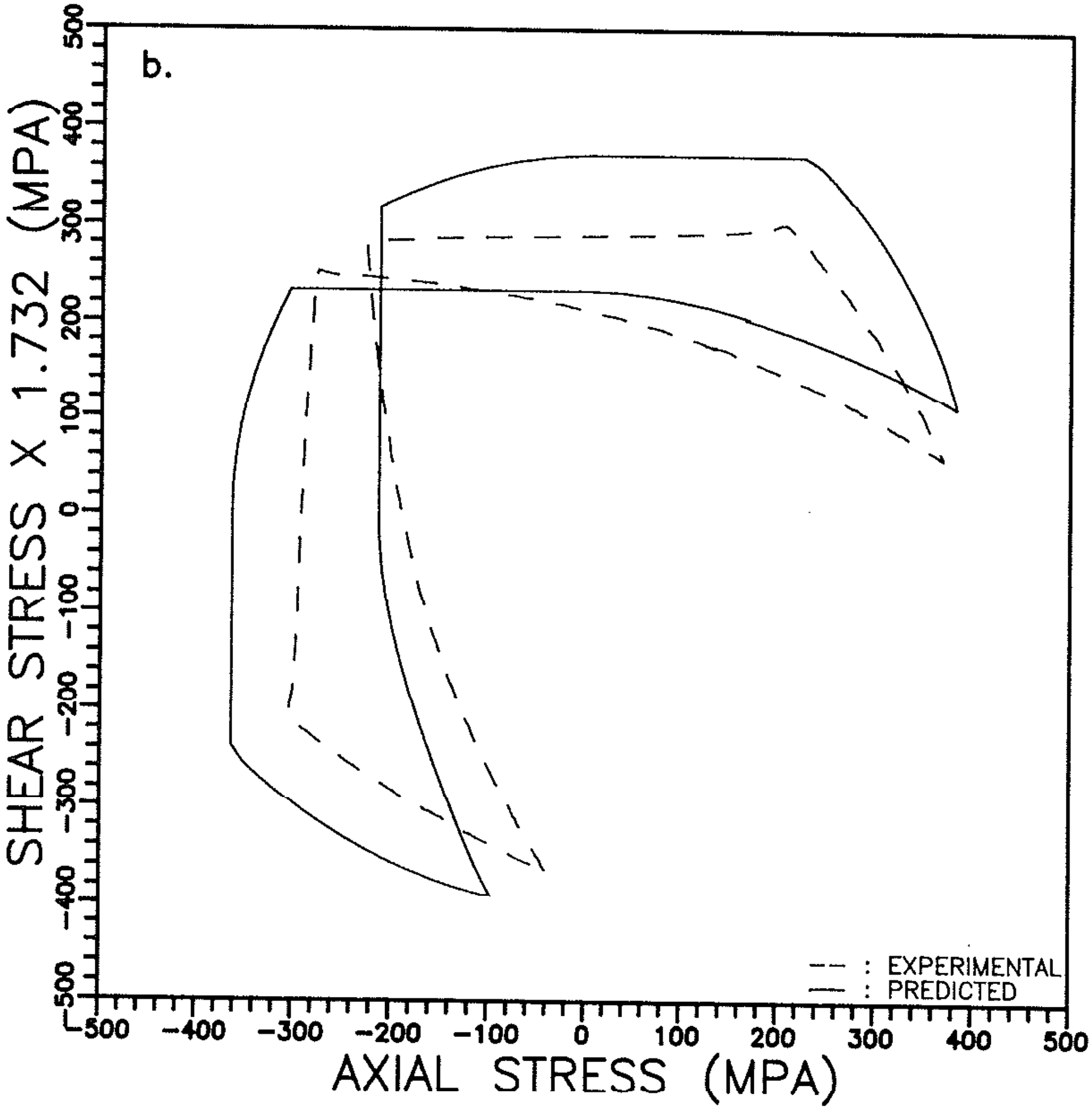
b.
SHEAR STRESS X 1.732 (MPA)
500
400
300
200
100
0
−100
−200
−300
−400
−500
AXIAL STRESS (MPA)
−500
−400
−300
−200
−100
0
100
200
300
400
500
-- : EXPERIMENTAL
— : PREDICTED

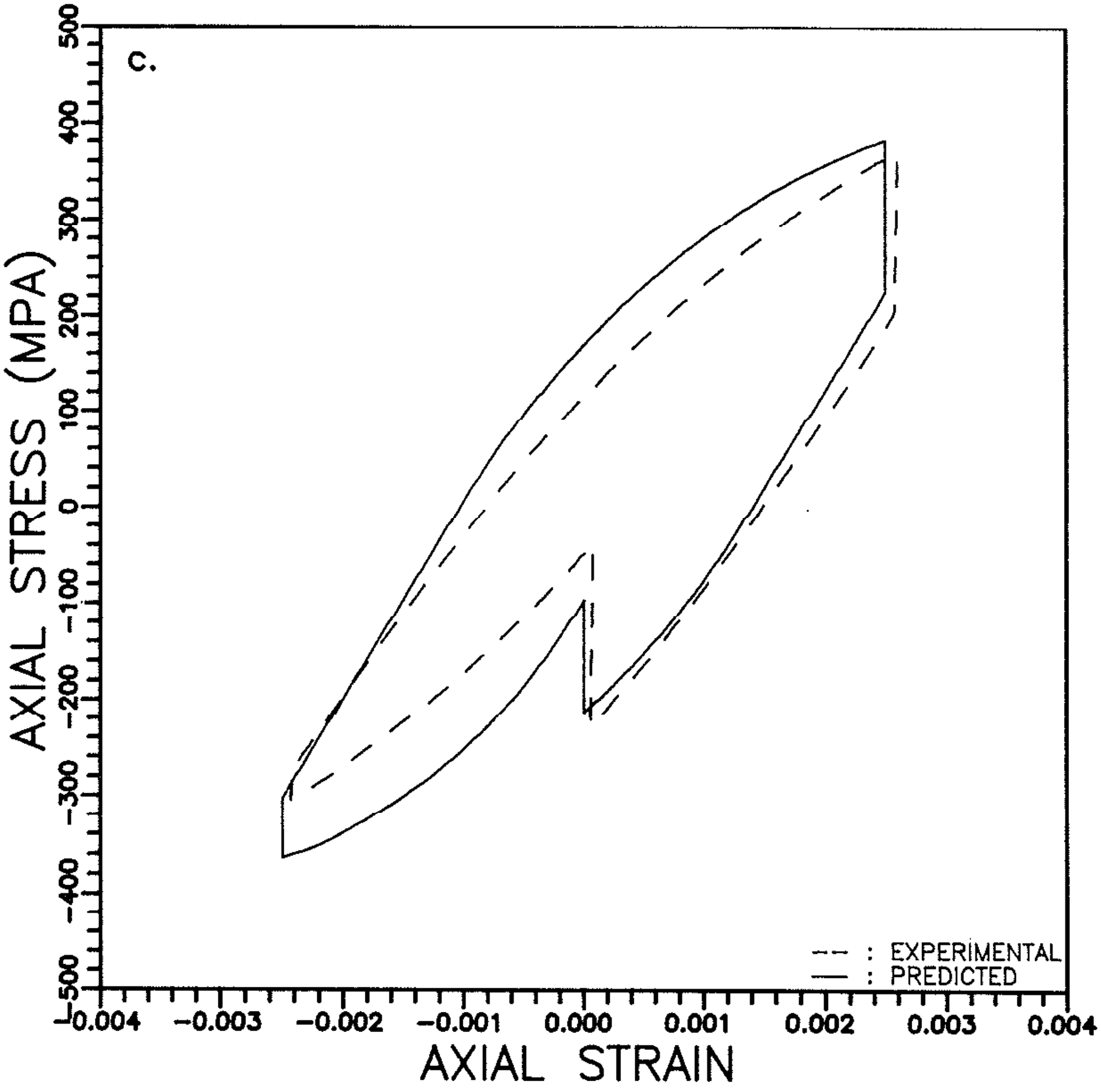
c.
AXIAL STRESS (MPA)
500
400
300
200
100
0
−100
−200
−300
−400
−500
AXIAL STRAIN
−0.004
−0.003
−0.002
−0.001
0.000
0.001
0.002
0.003
0.004
-- : EXPERIMENTAL
— : PREDICTED

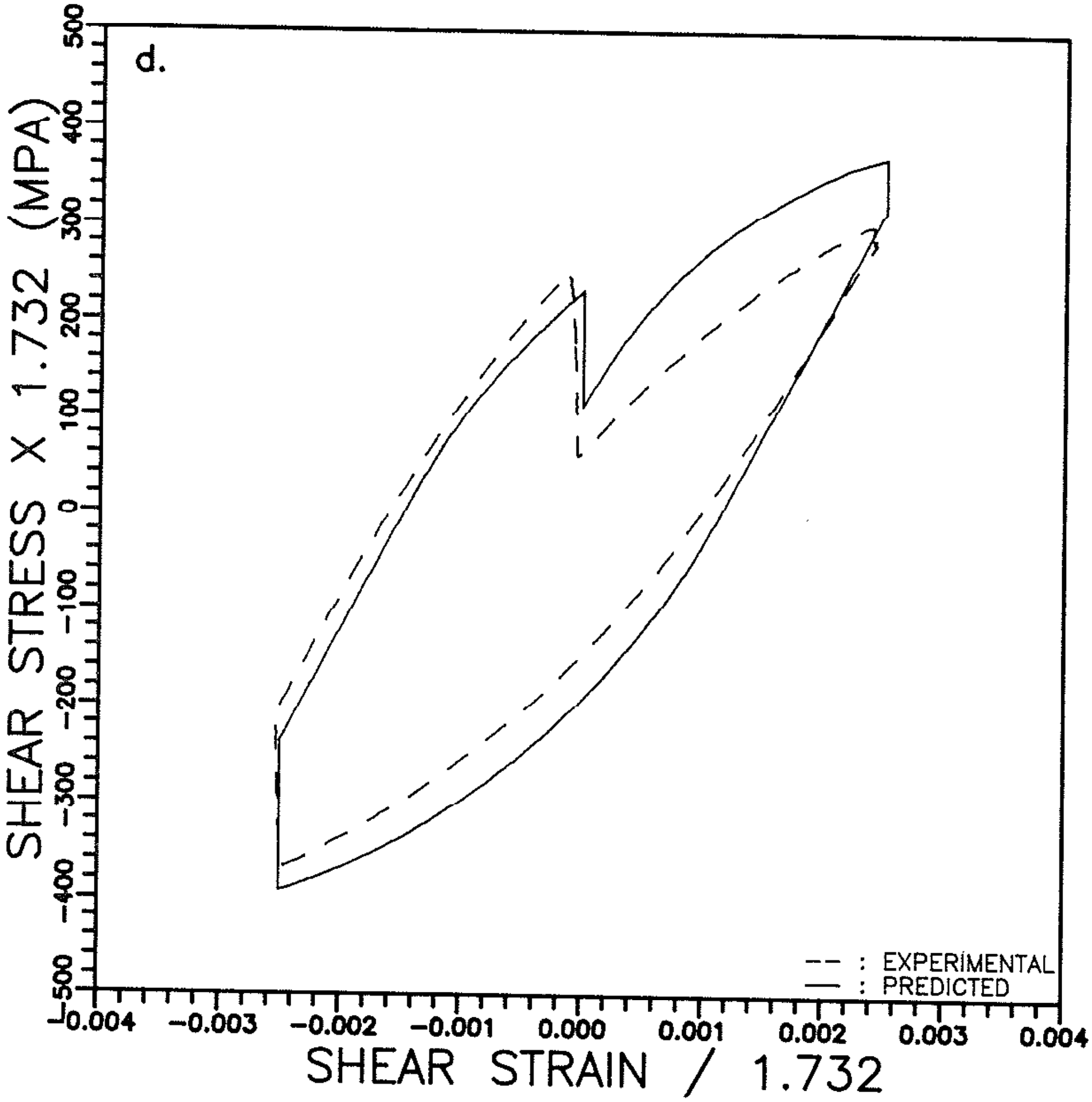
d.
SHEAR STRESS X 1.732 (MPA)
500
400
300
200
100
0
-100
-200
-300
-400
-500
SHEAR STRAIN / 1.732
-0.004
-0.003
-0.002
-0.001
0.000
0.001
0.002
0.003
0.004
-- : EXPERIMENTAL
— : PREDICTED

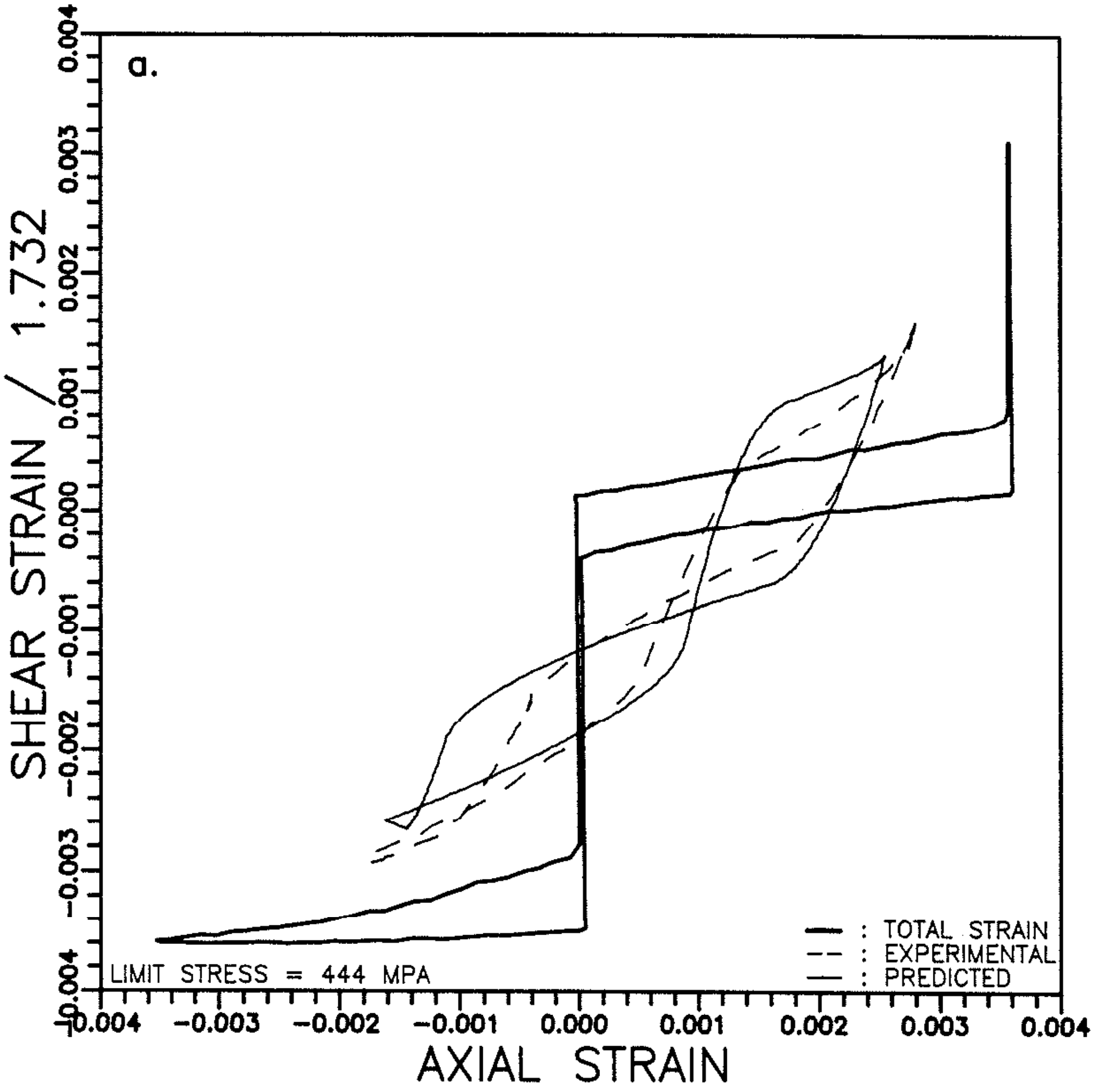

Figure 63. (a) - (d) A Comparison Between the Predicted and the Stabilized Stress-Strain History of 310 Stainless Steel under the Two-Stair Tension-Torsion Cycling (Specimen S112).

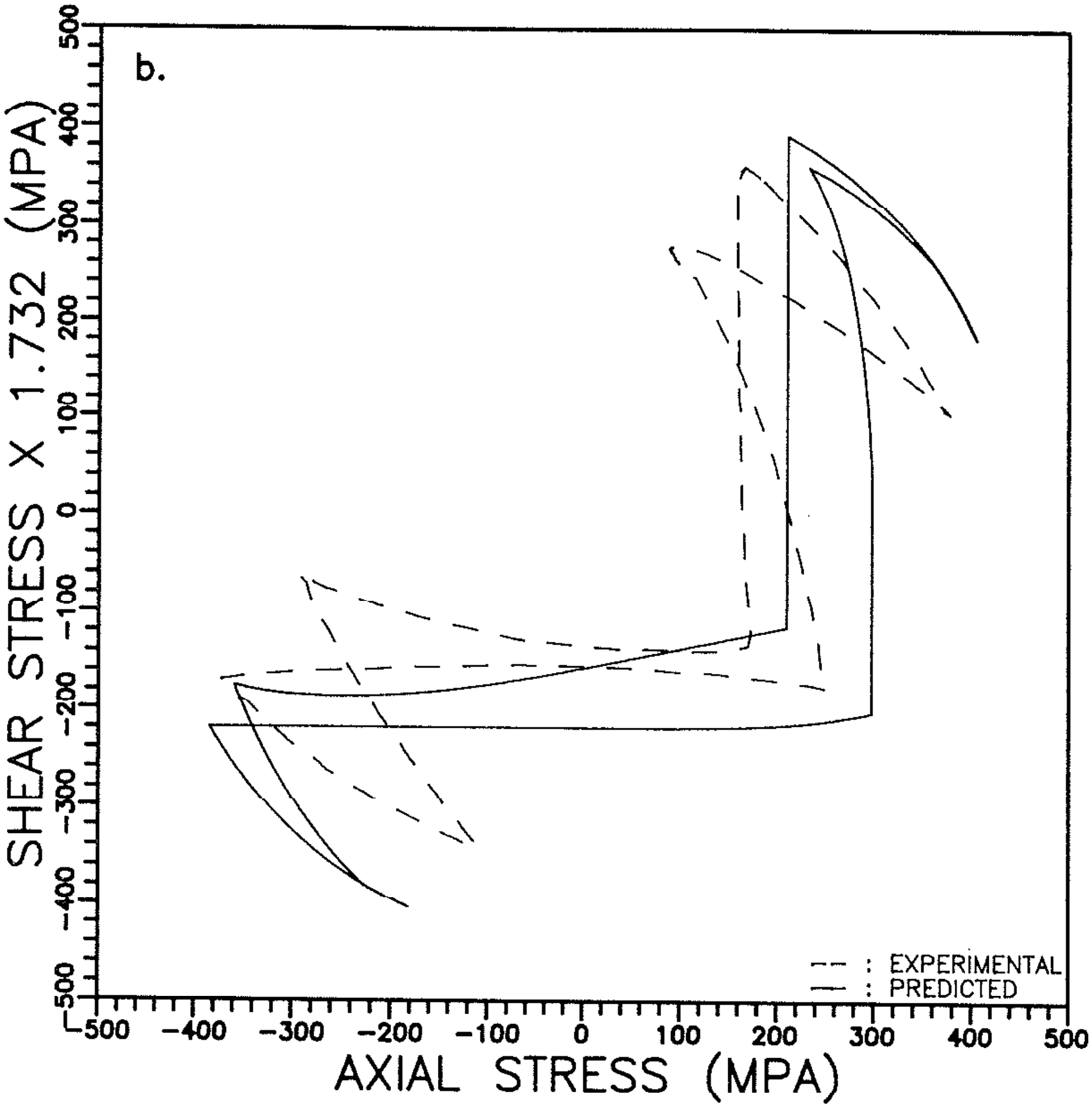
b.
SHEAR STRESS X 1.732 (MPA)
AXIAL STRESS (MPA)
500
400
300
200
100
0
−100
−200
−300
−400
−500
−500
−400
−300
−200
−100
0
100
200
300
400
500
-- : EXPERIMENTAL
— : PREDICTED

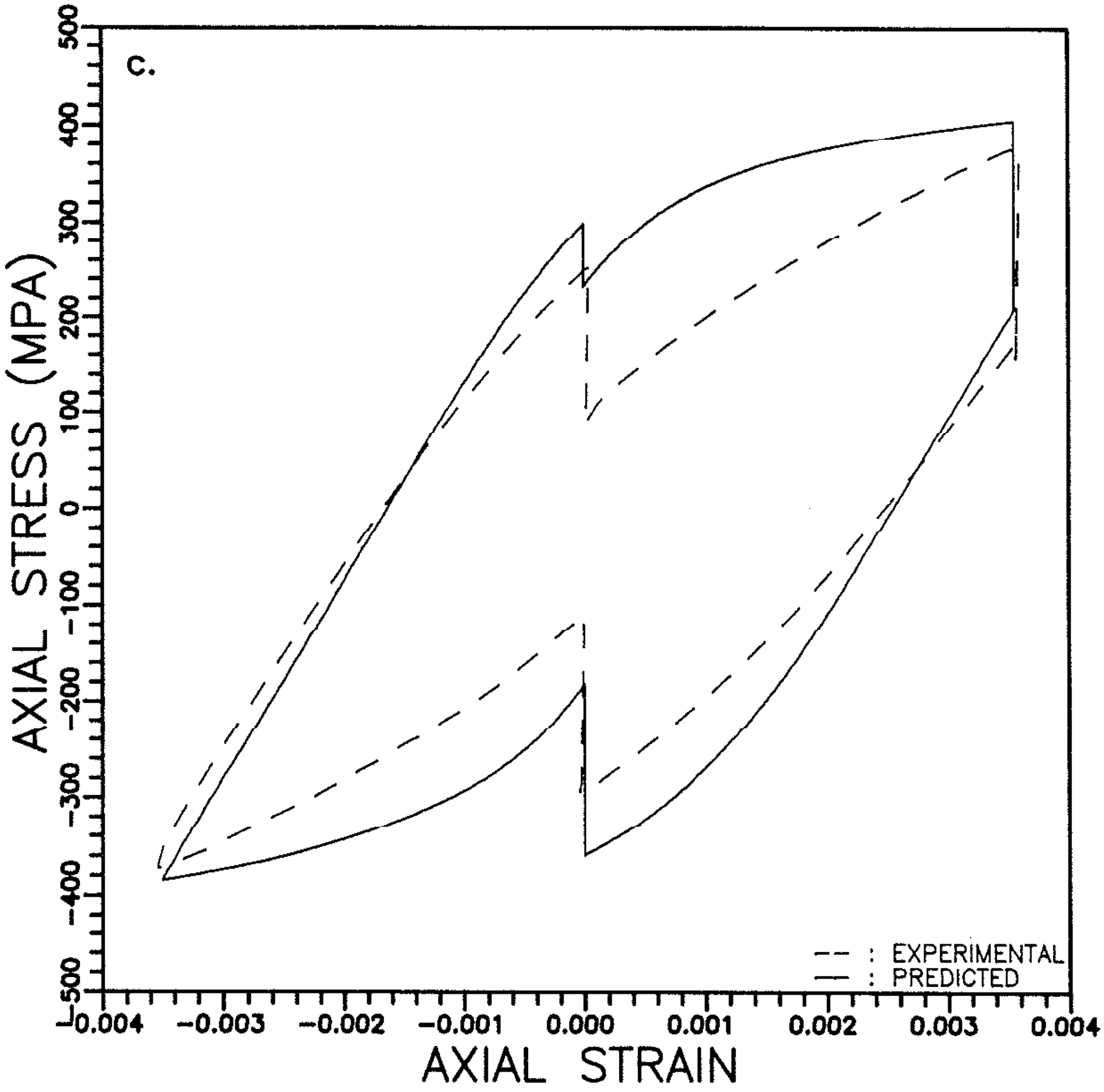
c.
AXIAL STRESS (MPA)
500
400
300
200
100
0
-100
-200
-300
-400
-500
-0.004
-0.003
-0.002
-0.001
0.000
0.001
0.002
0.003
0.004
AXIAL STRAIN
– – : EXPERIMENTAL
—— : PREDICTED

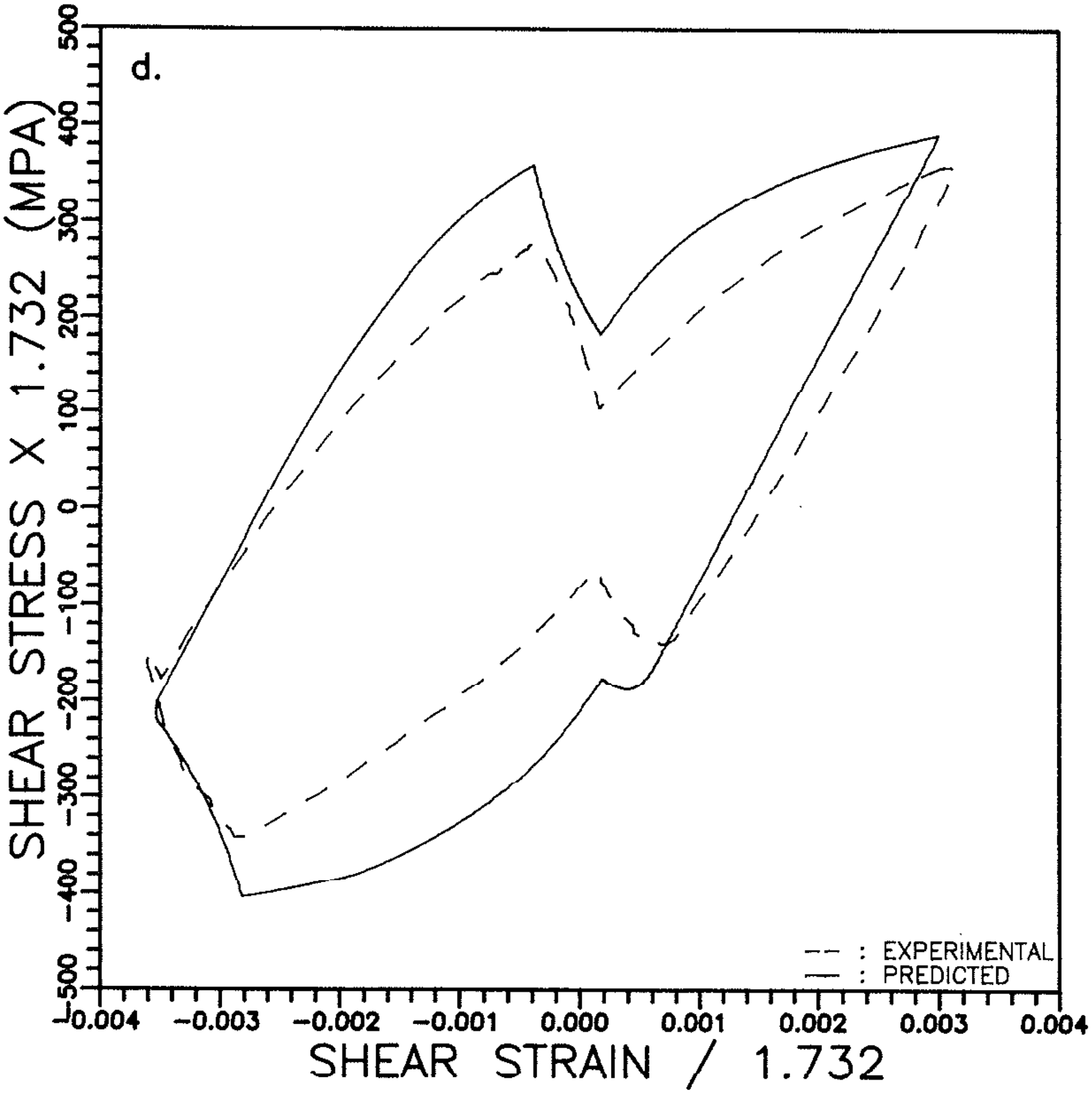
d.
SHEAR STRESS X 1.732 (MPA)
500
400
300
200
100
0
−100
−200
−300
−400
−500
SHEAR STRAIN / 1.732
−0.004
−0.003
−0.002
−0.001
0.000
0.001
0.002
0.003
0.004
– – : EXPERIMENTAL
— : PREDICTED

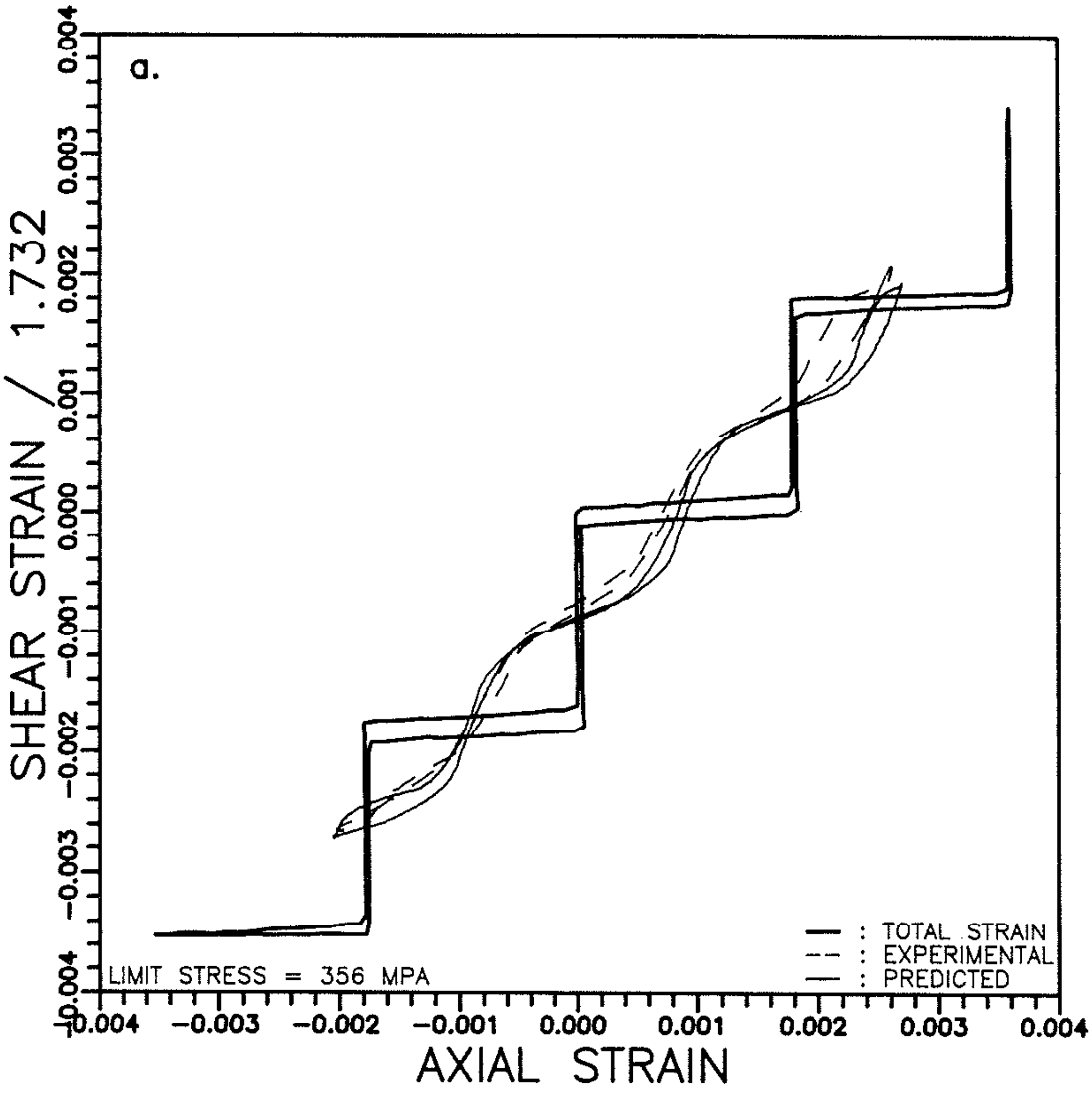

Figure 64. (a) - (d) A Comparison Between the Predicted and the Stabilized Stress-Strain History of 310 Stainless Steel under the Four-Stair Tension-Torsion Cycling (Specimen S111).

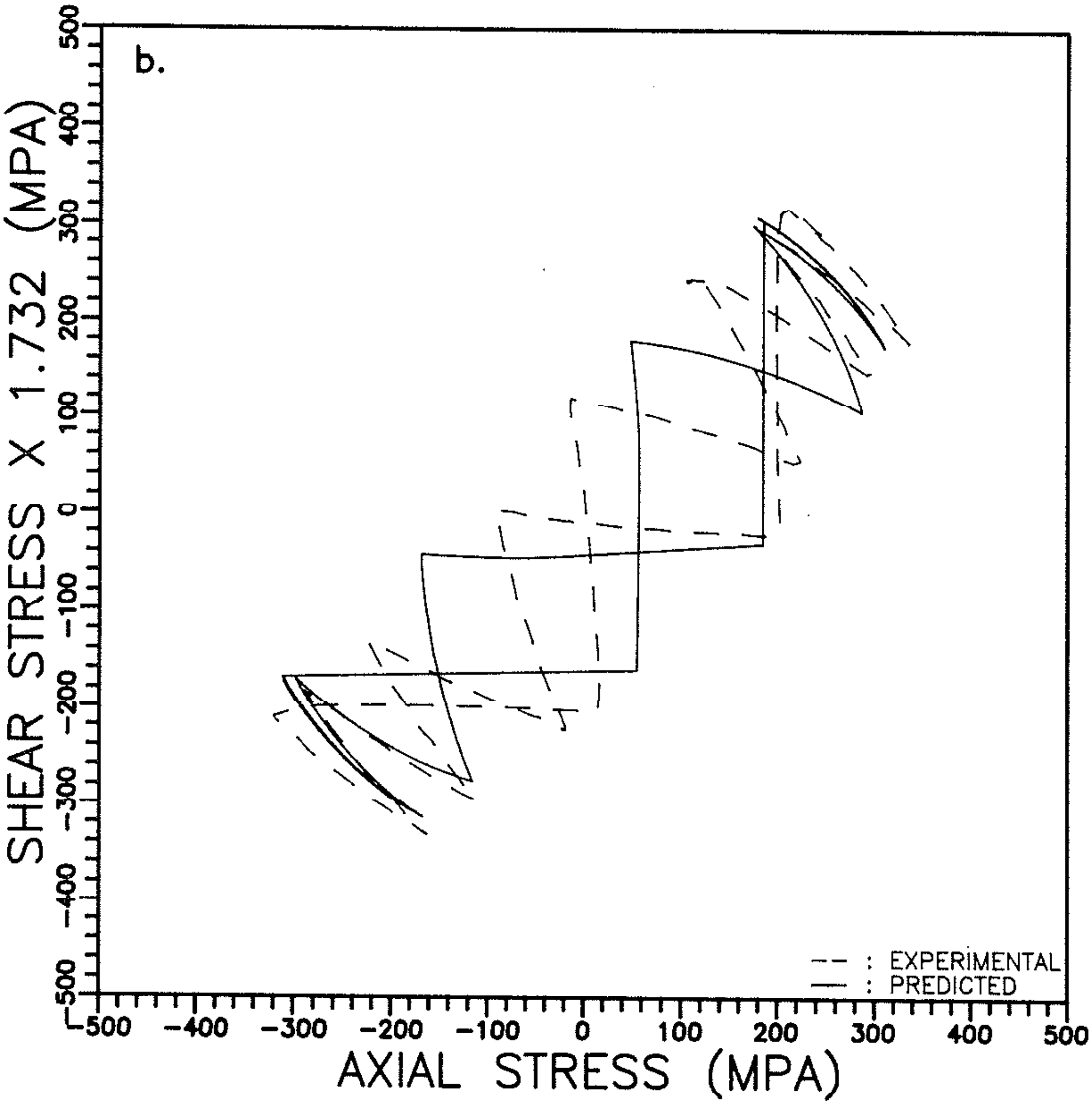
b.
SHEAR STRESS X 1.732 (MPA)
500
400
300
200
100
0
−100
−200
−300
−400
−500
AXIAL STRESS (MPA)
−500
−400
−300
−200
−100
0
100
200
300
400
500
– – : EXPERIMENTAL
—— : PREDICTED

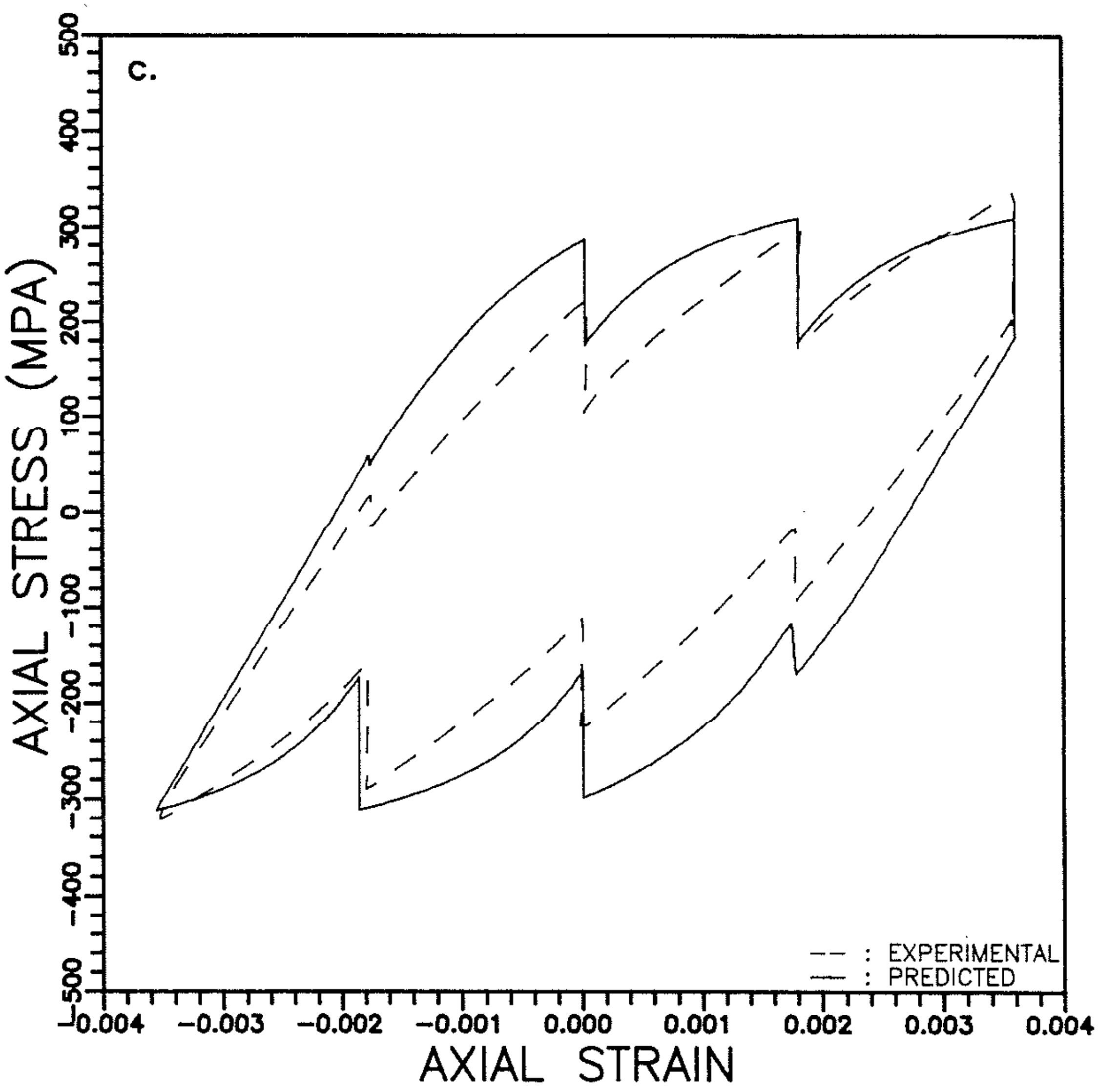
c.
AXIAL STRESS (MPA)
500
400
300
200
100
0
-100
-200
-300
-400
-500
AXIAL STRAIN
-0.004
-0.003
-0.002
-0.001
0.000
0.001
0.002
0.003
0.004
— — : EXPERIMENTAL
—— : PREDICTED

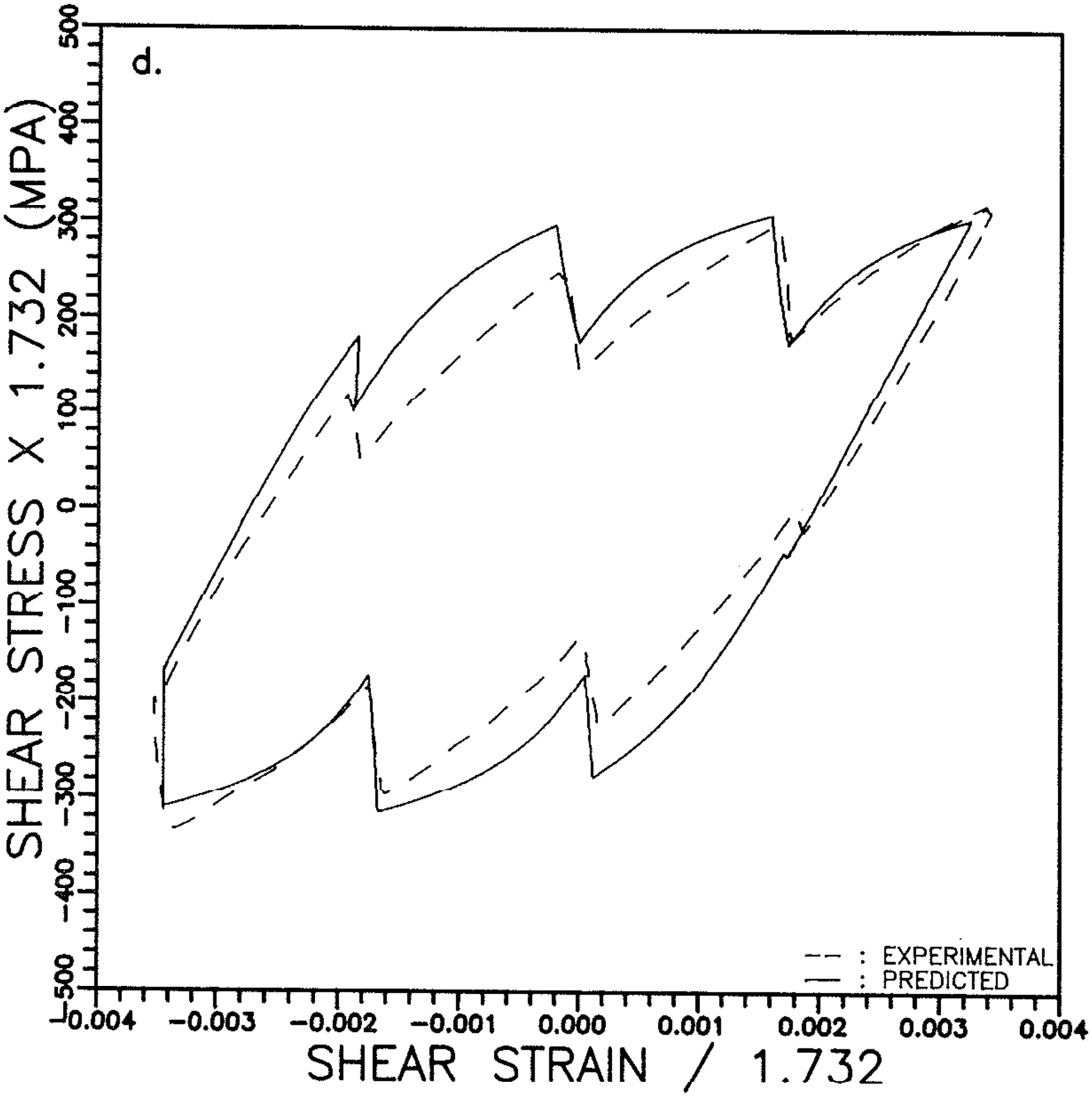
d.
SHEAR STRESS X 1.732 (MPA)
500
400
300
200
100
0
-100
-200
-300
-400
-500
-0.004
-0.003
-0.002
-0.001
0.000
0.001
0.002
0.003
0.004
SHEAR STRAIN / 1.732
-- : EXPERIMENTAL
— : PREDICTED

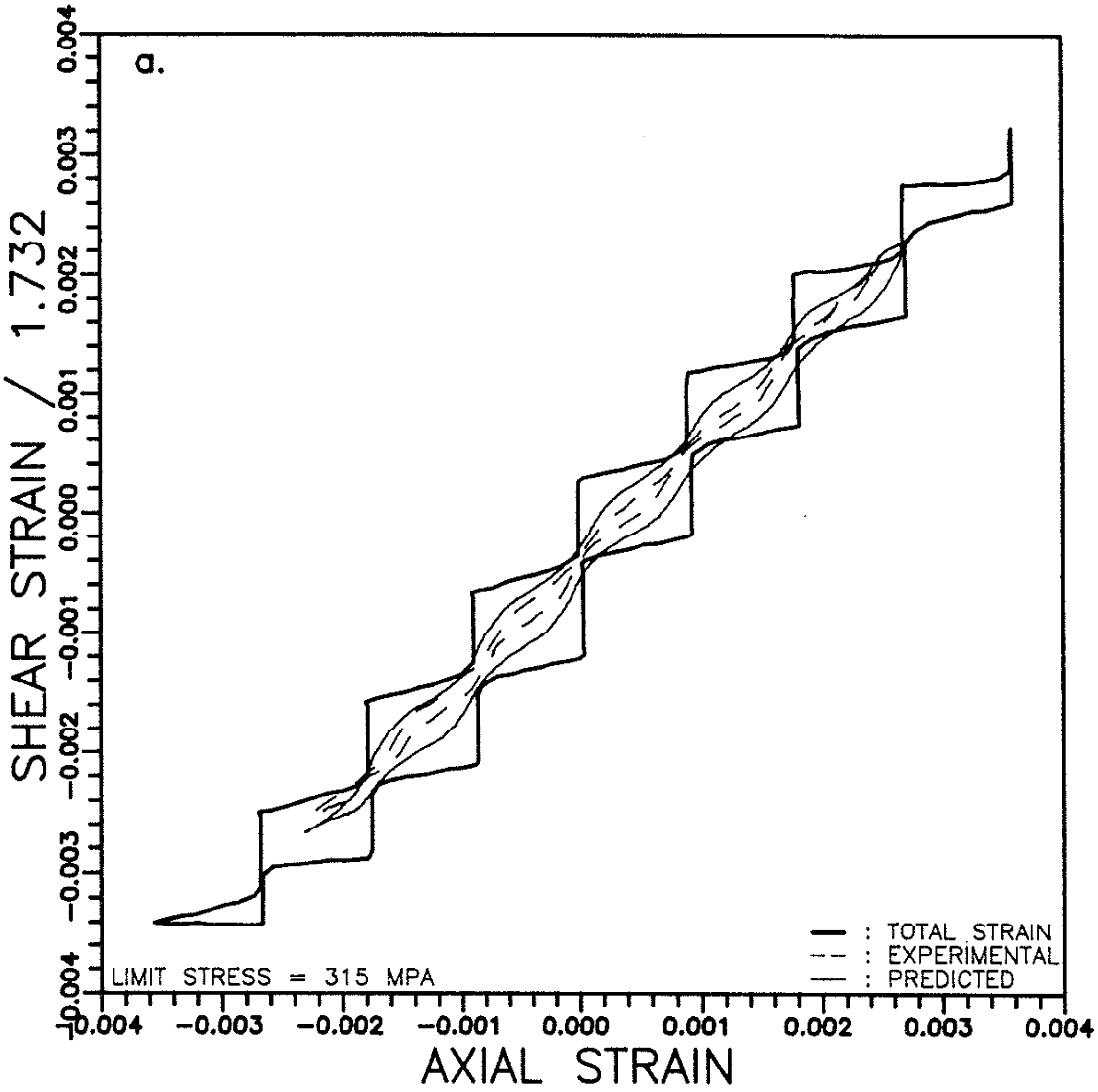

Figure 65. (a) - (d) A Comparison Between the Predicted and the Stabilized Stress-Strain History of 310 Stainless Steel under the Eight-Stair Tension-Torsion Cycling (Specimen S113).

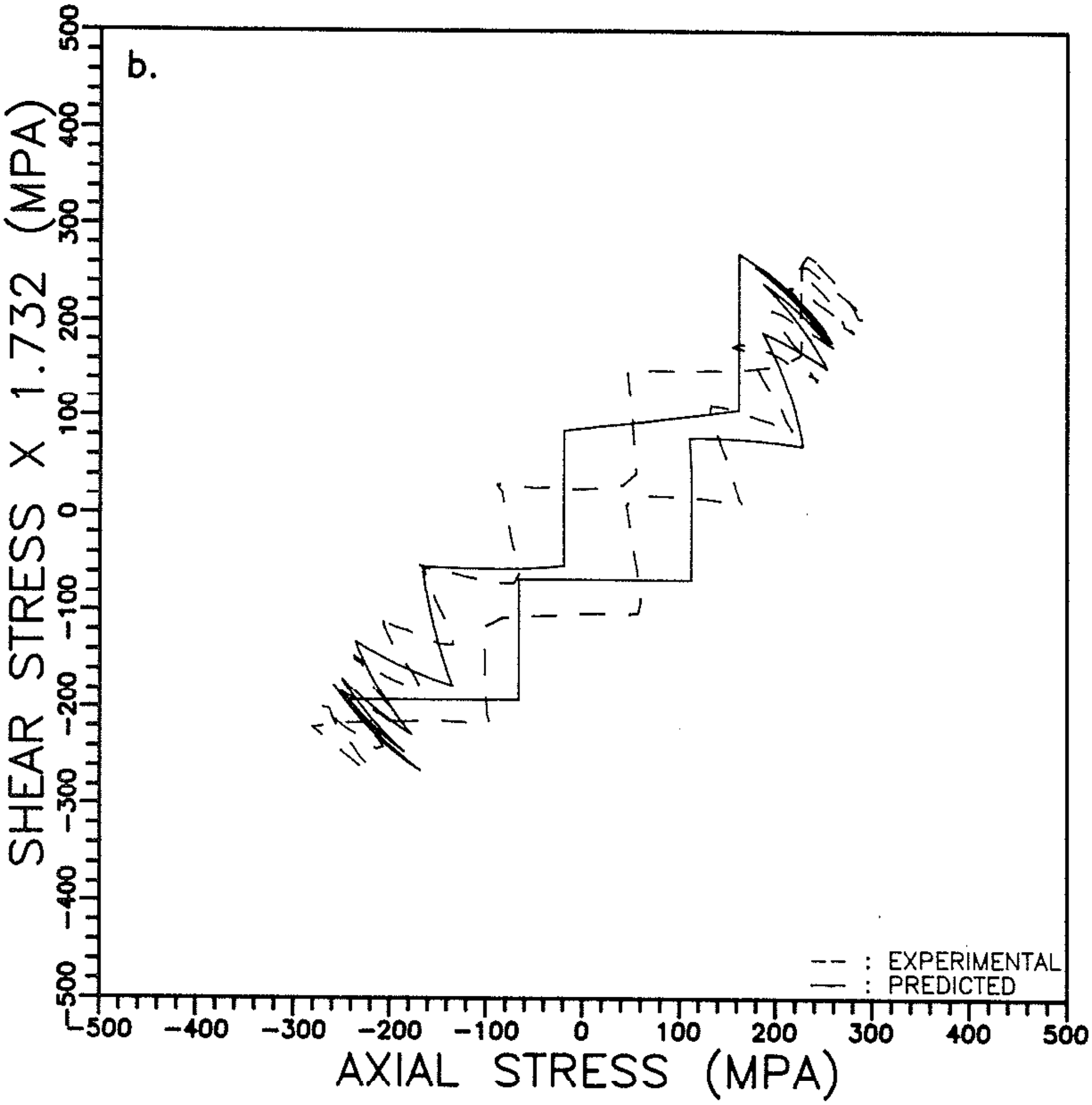
b.
SHEAR STRESS X 1.732 (MPA)
500
400
300
200
100
0
-100
-200
-300
-400
-500
AXIAL STRESS (MPA)
-500
-400
-300
-200
-100
0
100
200
300
400
500
-- : EXPERIMENTAL
— : PREDICTED

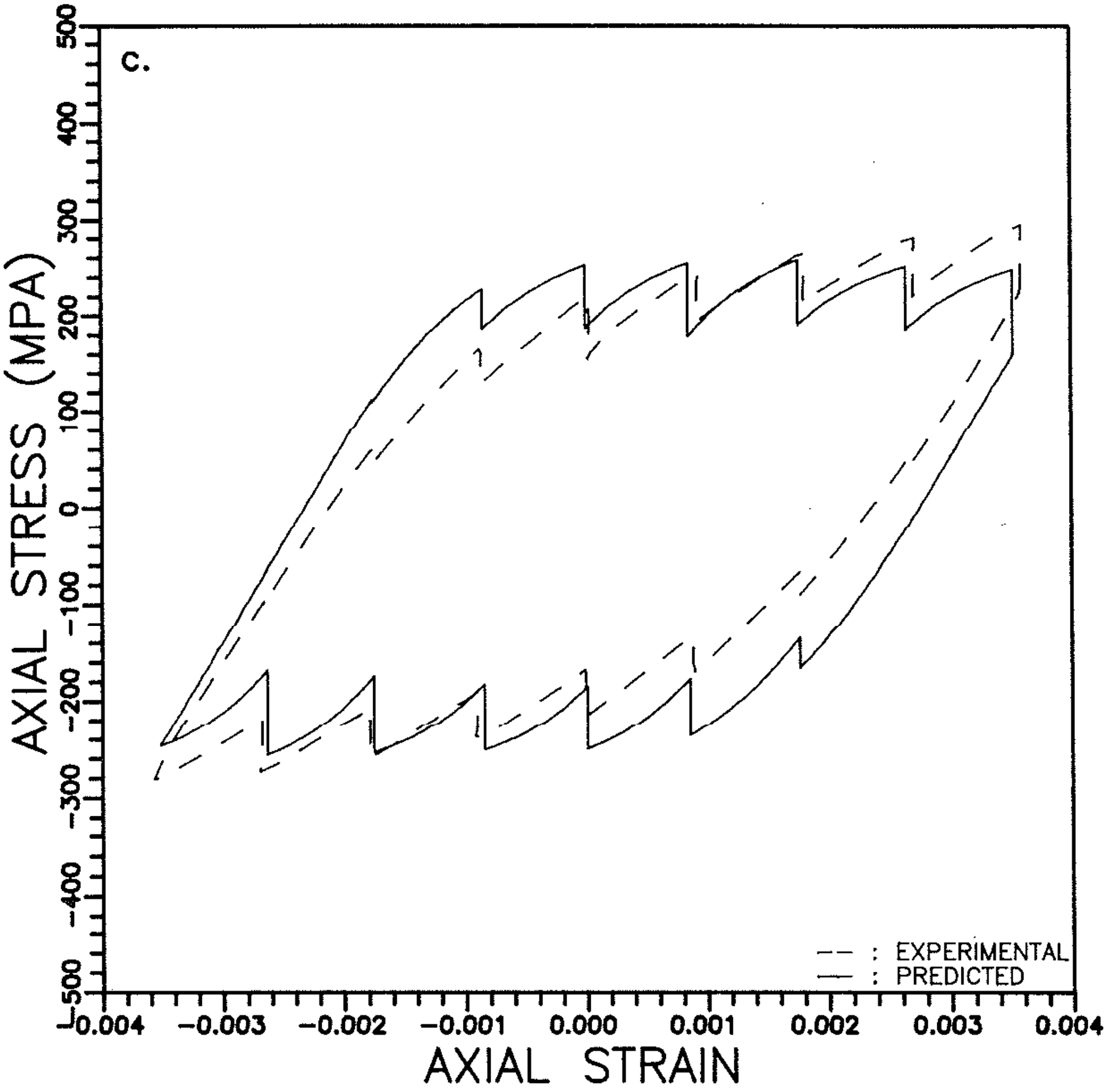
c.
AXIAL STRESS (MPA)
500
400
300
200
100
0
-100
-200
-300
-400
-500
-0.004
-0.003
-0.002
-0.001
0.000
0.001
0.002
0.003
0.004
AXIAL STRAIN
— — : EXPERIMENTAL
—— : PREDICTED

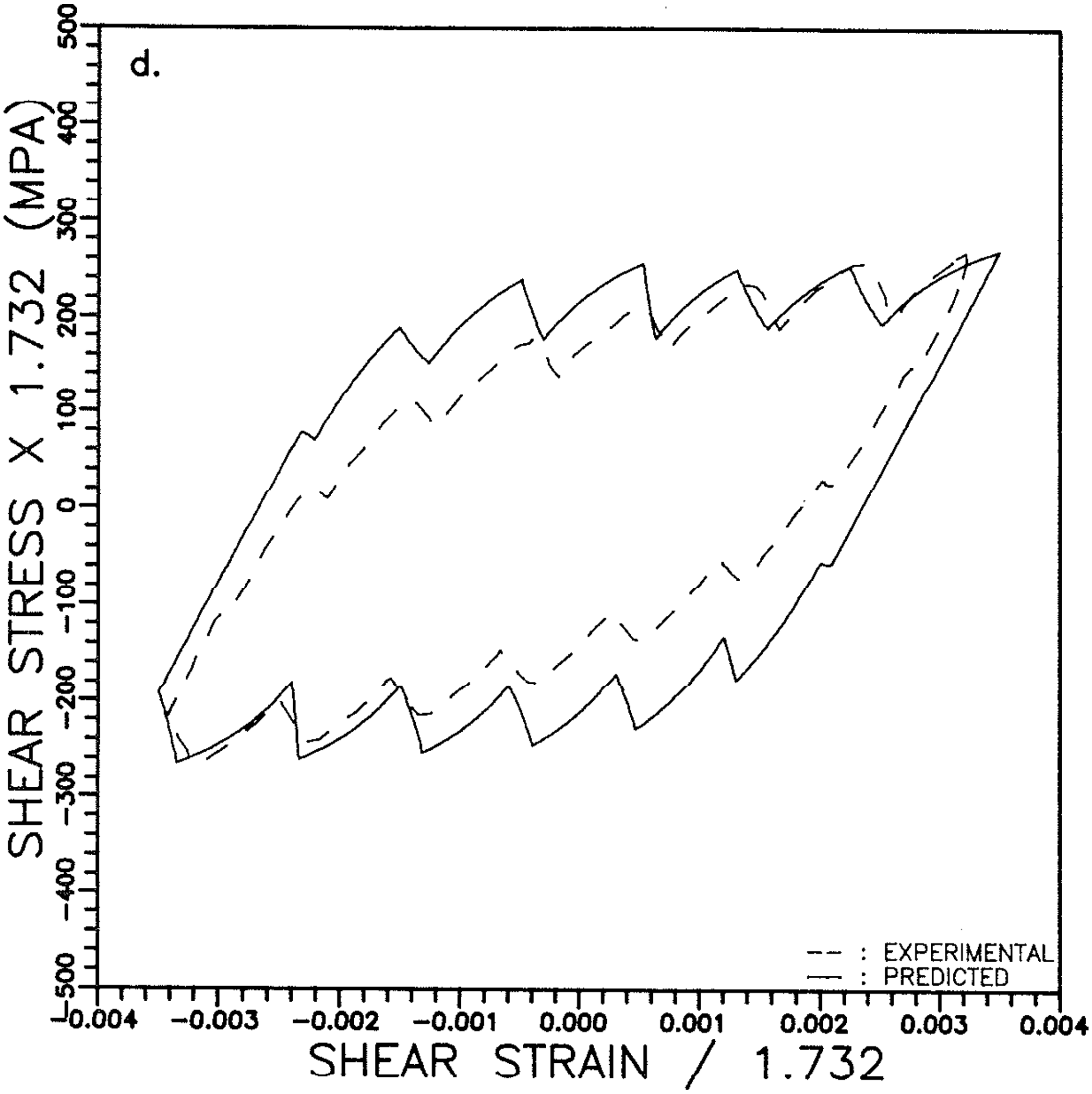
d.
SHEAR STRESS X 1.732 (MPA)
500
400
300
200
100
0
-100
-200
-300
-400
-500
-0.004
-0.003
-0.002
-0.001
0.000
0.001
0.002
0.003
0.004
SHEAR STRAIN / 1.732
-- : EXPERIMENTAL
— : PREDICTED

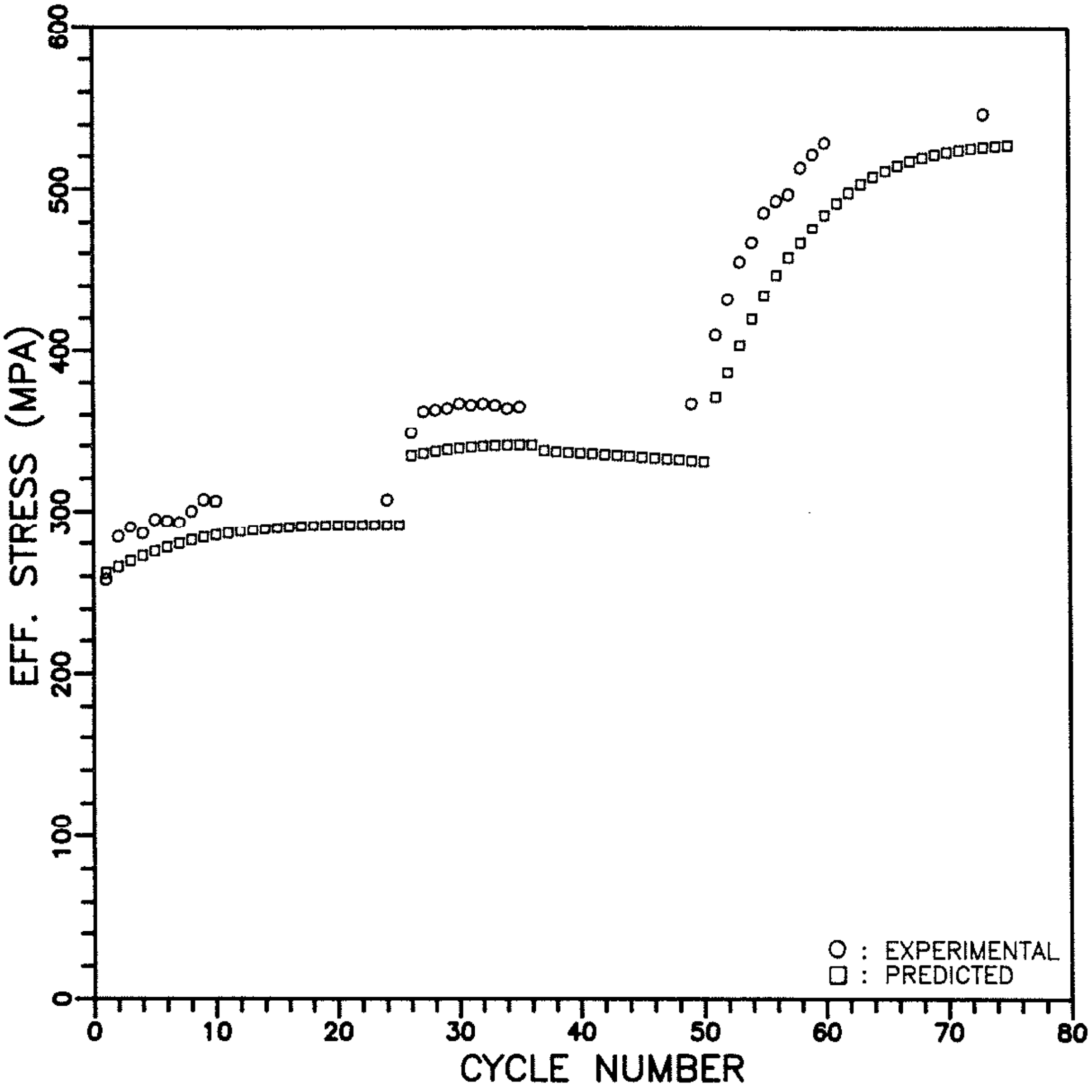

Figure 66. A Comparison Between the Predicted and the Experimental Peak Stress for the Loading of Fig. 44 [61].

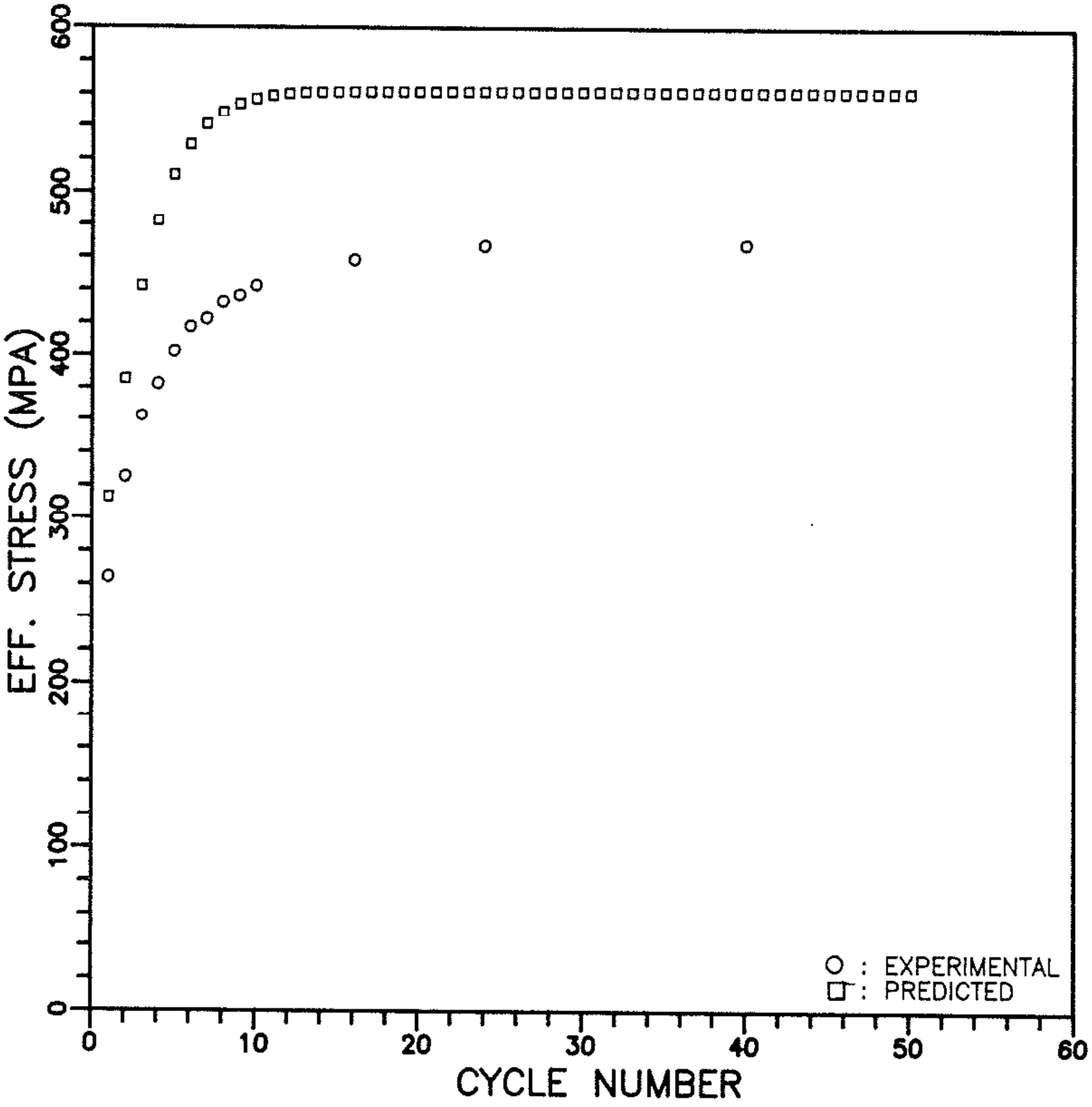

Figure 67. A Comparison Between the Predicted and the Experimental Peak Stress for the Loading of Fig. 47 [61].

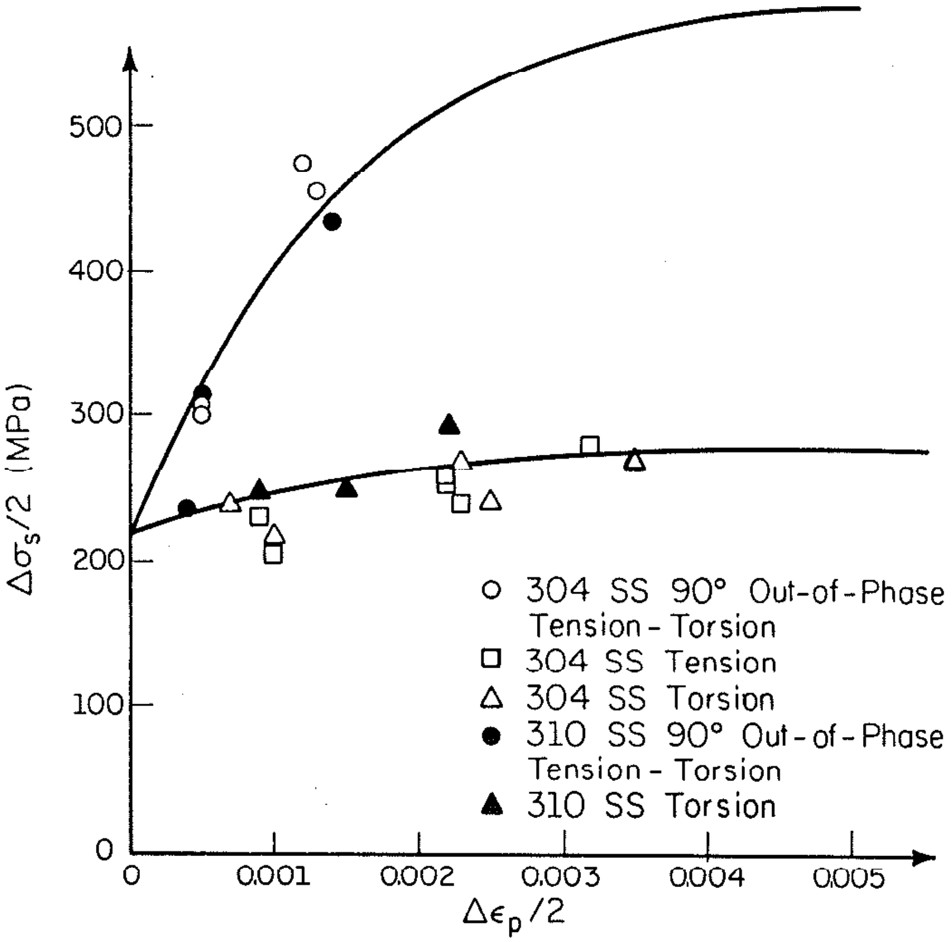

Figure 68. The Experimental and the Assumed Stabilized Cyclic Stress as a Function of the Plastic Strain Amplitude.

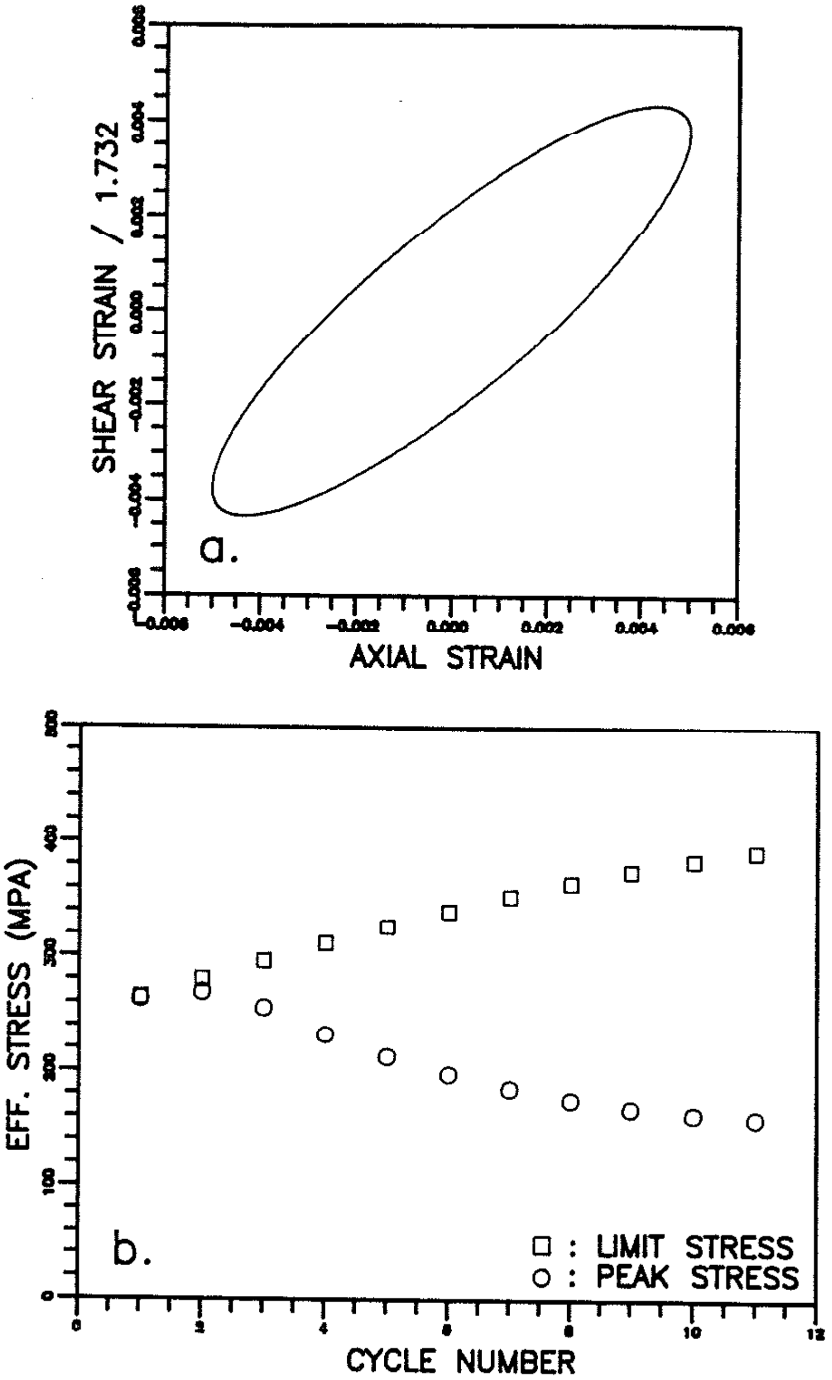

Figure 69. The Evolution of the Predicted Limit Stress and the Peak Stress (b) under a 30° Out-Of-Phase Tension-Torsion Path Shown in (a).

REFERENCE

1. Drucker, D. C., "Some Implications of Work Hardening and Ideal Plasticity," Quarterly of Applied Mathematic, Vol. 7, 1949-50, pp. 411-418.

2. Pragner, W., "The Theory of Plasticity: A Survey of Recent Achievements", Proceedings of Institute of Mechanical Engineers, Vol. 169, 1955, pp. 41-55.

3. Pragner, W, "A New Method of Analyzing Stresses and Strains in Work-Hardening Plastic Solids", ASME Journal of Applied Mechanics, Vol. 23, 1956, pp. 493-496.

4. Hodge, P. G. Jr., "A General Theory of Piecewise Linear Plasticity Based on Maximum Shear", Journal of the Mechanics of Physics and Solids, Vol. 5, pp. 242-260.

5. Ziegler, H., "A Modification of Pragner's Hardening Rule", Quarterly of Applied Mathematics, Vol. XVII, No. 1, 1959.

6. Mroz, Z., Shrivastava, H. P. and Dubey, R. N., "A Nonlinear Hardening Model and Its Application To Cyclic Loading", Acta Mechanica, Vol. 25, 1976, pp. 51-61.

7. Kricg, R. D., "A Practical Two Surface Plasticity Theory," Journal of Applied Mechanics, Vol. 42, 1975, pp. 641-646.

8. Dafalias, Y. F. and Popov, E. P., "Plastic Internal Variables Formalism of Cyclic Plasticity," Journal of Applied Mechanics, Vol. 98, No. 4, 1976, pp. 645-650.

9. Drucker, D. C. and Palgen, L., "On Stress-strain Relation Suitable for Cyclic and Other Loadings", ASME Journal of Applied Mechanics, Vol. 48, 1981, pp. 479-485.

10. McDowell, D. L., "A Two Surface Model for Transient Nonproportional Cyclic Plasticity: Part I and II", ASME Journal of Applied Mechanics, Vol. 52, 1985, pp. 298-308.

11. Naghdi, P. M. and Nikkel, D. J. Jr., "Two Dimensional Strain Cycling in Plasticity", ASME Journal of Applied Mechanics, Vol. 53, 1986, pp. 821-830.

12. Benallel, A. and Marquis, D., "Constitutive Equations Describing Nonproportional Effects In Cyclic Plasticity", Proceedings of 7th International Conference on Constitutive Laws: Applications and Short Course, Tucson, Arizona, 1987.

13. Dafalias, Y. F., "Modeling Cyclic Plasticity: Simplicity Versus Sophistication", Mechanics of Engineering Materials, Desai, C. S. and Gallagher, R. H. ed., 1984, John Wiley & Sons Ltd.

14. Feltner, C. E. and Laird, C., "Cyclic Stress-Strain Response of FCC Metals and Alloys - I and II", Acta Metallurgica, 1967, Vol. 15, pp. 1621-1653.

15. Kayali, E. S. and Plumtree, A., "Stress-SubStructure Relationships in Cyclically and Monotonically Deformed Wavy Slip Mode Metals", Metallurgical Transactions A, Vol. 13A, 1982, pp. 1033-1040.

16. Turner, A. P. L. and Hasegawa, T., "Deformation Microstructures and Mechanical Equations of State", Mechanical Testing for Deformation Model Development, ASTM, STP 765, R. W. Rohde and J. C. Swearengen, Eds., 1982, pp. 322-341.

17. Hill, R. and Rice, J. R., "Constitutive Analysis of Elastic-Plastic Analysis at Arbitrary Strain", Journal of the Mechanics of Physics and Solids, Vol. 20, 1972, pp. 401-413.

18. Asaro, R. J. and Rice, J. R., "Strain Localization in Ductile Single Crystals", Journal of Mechanical Physics and Solids, Vol. 25, 1977, pp. 309-338.

19. Asaro, R. J., "Micro and Macromechanics of Crystalline Plasticity", Plasticity of Metals at Finite Strain: Theory, Computation and Experiment, E. H. Lee and R. L. Mallett, Eds., 1981.

20. Lamba, H. S. and Sidebottom, O. M., "Cyclic Plasticity for Nonproportional Pathes: Part I - Cyclic Hardening, Erasure of Memory and Subsequent Strain Hardening Experiments", ASME Journal of Engineering Materials and Technology, Vol. 100, 1978, pp. 96-103.

21. Kanazawa, K, Miller, K. J. and Brown, M. W., "Cyclic Deformation of 1% Cr- Mo-V Steel Under Out-Of-Phase Loads", Fatigue of Engineering Materials and Structures, Vol. 2, 1979, pp. 217-228.

22. Krempl, E. and Lu, H., "The Hardening and Rate Dependent Behavior of Fully Annealed AISI Type 304 Stainless Steel Under Biaxial In-Phase and Out-Of-Phase Strain Cycling At Room Temperature", ASME Journal of Engineering Materials and Technology", Vol.106, 1984, pp. 376-382.

23. Ohashi, Y., Tanaka, E. and Ooka, M., "Plastic Deformation Behavior of Type 316 Stainless Steel Subject to Out-Of-Phase Strain Cycles", ASME Journal of Engineering Materials and Technology, Vol.107, 1985, pp. 286-292.

24. Woods, P. J., "Low-Amplitude Fatigue of Copper and Copper - 5 at.% Aluminum Single Crystals," Pyilosophical Magazine, Vol. 28, 1973, pp. 155-191.

25. Ackermann, E., Kubin, L. P., Lepinoux, J., and Mughrabi, H., "The Dependence of Dislocation Microstructure on Plastic Strain Amplitude in Cyclically Strained Copper Single Crystals," Acta Metallurgica, Vol. 32, No. 5, 1984, pp. 715-725.

26. Winter, A. T., Pederson, O. B., and Rasmussen, K. V., "Dislocation Microstructures in Fatigued Copper Polycrystals," Acta Metallurgica, Vol. 29, 1981, pp. 735-748.

27. Figueroa, J. C., Bhat, S. P., Dela Veaux, R. , Murzenski, S., and Laird, C., "The Cyclic Stress-Strain Response of Copper at Low Strains - I. Constant Amplitude Testing," Acta Metallurgica, Vol. 29, 1981, pp. 1667-1678.

28. Wilsdorf, D. K., and Laird, C., "Dislocation Behavior in Fatigue V: Breakdown of Loop Patches and Formation of Persistent Slip Bands and Dislocation Cells," Material Science and Engineering, Vol. 46, 1980, pp. 209-219.

29. Jin, N. Y., and Winter, A. T., "Dislocation Substructures in Cyclically Deformed [001] Copper Crystals," Acta Metallurgica, Vol. 32, No. 8, 1984, pp. 1173-1176.

30. Dickson, J. I., Boutin, J. and Lesperance, G., "An Explanation of Labyrinth Walls In Fatigued FCC Metals", Acta Metallurgica, Vol. 34, No. 8, pp. 1505-1514.

31. Krempl, E. and Lu, H, "Comparison of the stress responses of an aluminum alloy tube to proportional and Alternate Axial and Shear Strain Paths at Room Temperature", Mechanics of Materials, Vol. 2, 1983, pp. 183-192.

32. Socie, D. F., "Multiaxial Fatigue Damage Models", Journal of Engineering Materials and Technology, private communication.

33. Hua, C. T., "Fatigue Damage and Small Crack Growth During Biaxial Loading," Design and Material Division, Report No. 109, University of Illinois at Urbana-Champaign, 1984.

34. Kurah, P., Private Communication.

35. Bannantine, J. A., "Observations of Tension and Torsion Fatigue Cracking Behavior and the Effect on Multiaxial Damage Correlations", MS Thesis, University of Illinois at Urbana-Champaign, 1986.

36. Jones, D., "Extension of Simple Cyclic Fatigue Damage Characteristics to Multiaxial Life Prediction Methods", 23rd Student Symposium of Engineering Mechanics, TAM Report No. 482, University of Illinois at Urbana-Champaign, 1986.

37. Lukas, P., and Klensil, M., "Cyclic Stress Strain Response and Fatigue Life of Metals in Low Amplitude Region," Material Science and Engineering, Vol. 11, 1973, pp. 345-356.

38. Saxena, A., and Antolovich, S. D., "Low Cycle Fatigue, Fatigue Crack Propagation and Substructures in a Series of Polycrystalline Cu-Al Alloys," Metallurgical Transactions A, Vol. 6A, 1975, pp. 1809-1828.

39. Figueroa, J. C., and Laird, C., "The Cyclic Stress-Strain Response of Copper at Low Strains - II. Variable Amplitude testing," Acta Metallurgica. Vol. 29, 1981, pp. 1679-1684.

40. Grosskreutz, J. C., and Waldow, P., "Substructure and Fatigue Fracture in Aluminum," Acta Metallurgica, 1963, Vol. 11, pp. 717-724.

41. Laird, C., "Mechanism and Theories of Fatigue," Fatigue and Microstructure, ASM Material Science Semina, St. Louis, MO., 1978, pp. 149-203.

42. Abdel-Raouf, H., Plumtree, A., and Topper T. H., "Temperature and Strain Rate Dependence of Cyclic Deformation Response and Damage Accumulation in OFHC Copper and 304 Stainless Steel," Metallurgical Transactions, Vol. 5, 1974, pp. 267-277.

43. Challenger, K. D., and Moteff, J., "Correlation of Substructure with the Elevated Temperature Low Cycle Fatigue of AISI 304 and 316 Stainless Steels," Fatigue at Elevated Temperatures, ASTM STP520, 1973, pp. 68-79.

44. Ermi, A. M., and Moteff, J., "Microstructural Development and Cracking Behavior of AISI 304 Stainless Steel Tested in Time Dependent Fatigue Modes," Journal of Engineering Materials and Technology, 1983, Vol. 105, pp. 21-30.

45. Duquette, D. J., and Swann, P. R., "An Electron Microscopic Examination of Pre-crack Fatigue Damage in Aged Hardened Al 5.0wt.% Zn 2.5wt.% Mg," Acta Metallurgica, 1976, Vol. 24, pp. 241-248.

46. Vogel, W., Wilhelm, M., and Gerold, V., "Persistent Slip Bands in Fatigued Peak Aged Al-Zn-Mg Single Crystals - I. Development of Dislocation Microstructure and Change of Precipitation Distribution," Acta Metallurgica, 1982, Vol. 30, pp. 21-30.

47. McDowell, D. L., Stock, S. R., Stahl, D., and Antolovich, S. D., "Biaxial Path Dependence of Deformation Substructure of Type 304 Stainless Steel," Metallurgical Transactions A, 1988, Vol. 19A, pp. 1277-1293.

48. Drucker, D. C., "A More Fundamental Approach to Plastic Stress-Strain Relation,", 1st U.S. Congress of Applied Mechanics, ASME, 1952, pp. 487-491.

49. Fung, Y. C., Foundations of Solid Mechanics, Prentice-Hall, Inc., Englewood Cliffs, NJ, 1965.

50. Michno, M. J. Jr., and Findley, W. N., An Historical Perspective of Yield Surface Investigations for Metals, 1972.

51. Shiratori, E., and Ikegami, K., "Experimental Study of the Subsequent Yield Surface by Using Cross-Shaped Specimens," Journal of Mechanical Physics and Solids, Vol. 16, 1968, pp. 373-394.

52. Naghdi, P. M., Essenburg, F., and Koff, W., "An Experimental Study of Initial and Subsequent Yield Surfaces in Plasticity," Journal of Applied Mechanics, Vol. 25, No. 2, 1958, pp. 201-209.

53. Baltov, A., and Sawezuk, A., "A Rule of Anisotropic Hardening", Acta Mechanica, 1965, Vol. 1, pp. 81-92.

54. Eisenberg, M. A., and Phillips, A., "On Nonlinear Kinematic Hardening," Acta Mechanica, Vol. 5, 1968, pp. 1-13.

55. McDowell, D. L., "An Experimental Study of the Structure of Constitutive Equations for Nonproportional Cyclic Plasticity," Journal of Engineering Materials and Technology, Vol. 107, 1985, pp. 307-315.

56. Lamba, H. S., Nonproportional Cyclic Plasticity, Ph.D. Thesis, Department of Theoretical and Applied Mechanics, University of Illinois at Urbana-Champaign, 1974.

57. Dafalias, Y. F. and Popov, E. P., "Cyclic Loading for Materials with a Vanishing Elastic Region," Nuclear Engineering and Design, Vol. 41, 1977, pp 293-302.

58. Stouffer, D. C., and Bodner, S. R., "A Relationship Between Theory and Experimental for a State Variable Constitutive Equation," Mechanical Testing for Deformation Model Development, ASTM STP765, R. W. Rohde and J. C. Swearengen, Eds., ASTM, 1982, pp. 239-250.

59. Chaboche, J. L., and Rousselier, G., "On the Plastic and Viscoplastic Constitutive Equations, Part I and II.," Journal of Pressure Vessel Technology, Vol. 105, 1983, pp. 153-164

60. Mughrabi, H., Ackermann, F., and Herz, K., "Persistent Slipbands in Fatigued Face-Centered and Body-Centered Cubic Metals," Fatigue Mechanisms ASTM STP 675, edited by J. T. Fong, ASTM, Philadelphia, 1979, pp. 69-97.

61. McDowell, D. L., Transient Nonproportional Cyclic Plasticity, Ph.D. Thesis, Design and Material Division, Report No. 107, Department of Mechanical and Industrial Engineering, University of Illinois at Urbana-Champaign, 1983.

APPENDIX

Mathematical Formulation of Plasticity Models

A.1 Krieg (1975) [7]

A.1.1 The Loading Surface:

$$(\underset{\sim}{s} - \underset{\sim}{\alpha}) : (\underset{\sim}{s} - \underset{\sim}{\alpha}) - R^2 = 0$$

A.1.2 The Limit Surface:

$$(\underset{\sim}{s}^* - \underset{\sim}{\alpha}^*) : (\underset{\sim}{s}^* - \underset{\sim}{\alpha}^*) - R^{*2} = 0$$

A.1.3 The Flow Rule:

$$\dot{\underset{\sim}{e}}_p = \frac{\underset{\sim}{c} : (\underset{\sim}{s} - \underset{\sim}{\alpha})}{R^2 + \frac{P}{3} \left(\frac{R}{R_o}\right) \underset{\sim}{\eta} : (\underset{\sim}{s} - \underset{\sim}{\alpha})} (\underset{\sim}{s} - \underset{\sim}{\alpha})$$

where

$$\underset{\sim}{\eta} = \left(\frac{R^*}{R} - 1\right) (\underset{\sim}{s} - \underset{\sim}{\alpha}) + \underset{\sim}{\alpha}^* - \underset{\sim}{\alpha}$$

A.1.4 Hardening Rules For The Yield Surface:

$$\dot{R} = \frac{\sqrt{2/3}\ \beta p G |\dot{\underset{\sim}{e}}_p|}{R R_o} \underset{\sim}{\eta} : (\underset{\sim}{s} - \underset{\sim}{\alpha})$$

$$\dot{\underset{\sim}{\alpha}} = \sqrt{2/3}\,\frac{(1-\beta)pG|\dot{\underset{\sim}{e}}_p|}{R_o}\,\underset{\sim}{n}$$

where

$$|\dot{\underset{\sim}{e}}_p| = (\tfrac{2}{3}\,\dot{\underset{\sim}{e}}_p : \dot{\underset{\sim}{e}}_p)^{1/2}$$

A.1.5 Hardening Rules For The Limit Surface:

$$\dot{R}^{\star} = \sqrt{2/3}\,Gk\gamma|\dot{\underset{\sim}{e}}_p|$$

$$\dot{\underset{\sim}{\alpha}}^{\star} = Gk(1-\gamma)\dot{\underset{\sim}{e}}_p/1.5$$

A.1.6 Notation:

$\underset{\sim}{s}$	Deviatoric Stress Tensor for the Loading Surface
$\underset{\sim}{\alpha}$	Tensor of the Center of the Loading Surface
R	Radius of the Loading Surface
$\underset{\sim}{s}^{\star}$	Deviatoric Stress Tensor for the Limit Surface
$\underset{\sim}{\alpha}^{\star}$	Tensor of the Center of the Limit Surface
$R^{\star}$	Radius of the Limit Surface
$\underset{\sim}{e}$	Total Deviatoric Strain Tensor
$\underset{\sim}{e}_p$	Plastic Strain Tensor

A.1.7 Material Constants:

G	Shear Modulus
R_o	Radius of Initial Loading Surface
p	Metelastic Coefficient
k	Asymptotic Plastic Stiffness
β	Isotropic Proportioning Factor for the Loading Surface
g	Isotropic Proportioning Factor for the Limit Surface

A.2 Drucker and Palgen (1981) [9]

A.2.1 The Yield Surface:

$$\frac{1}{2}(\underset{\sim}{s} - \underset{\sim}{s}^c):(\underset{\sim}{s} - \underset{\sim}{s}^c) - k^2 = 0$$

A.2.2 The Flow Rule:

$$\dot{\underset{\sim}{\varepsilon}}^p = B\left(\frac{J_2}{\sigma^2}\right)^N (\underset{\sim}{s} - \underset{\sim}{s}^c)\ [(\underset{\sim}{s} - \underset{\sim}{s}^c):\dot{\underset{\sim}{s}}]$$

where

$$J_2 = \frac{1}{2}\underset{\sim}{s}:\underset{\sim}{s}$$

A.2.3 Hardening Rules:

$$\sigma = \sigma^{*} \left[1 \pm \alpha \exp\left(-\frac{W^{pc}}{W_o}\right)\right]$$

$$\dot{\underset{\sim}{s}}^{c} = \frac{1}{2k^2} (\underset{\sim}{s} - \underset{\sim}{s}^{c}) \left[(\underset{\sim}{s} - \underset{\sim}{s}^{c}):\underset{\sim}{s}\right]$$

and

$$W^{pc} = \int_t (\underset{\sim}{s} - \underset{\sim}{s}^{c}):\dot{\underset{\sim}{\varepsilon}}_p \, dt$$

A.2.4 Notation:

$\underset{\sim}{s}$	Deviatoric Stress Tensor
$\underset{\sim}{s}^{c}$	Tensor of the Center of the Yield Surface
$\underset{\sim}{\varepsilon}^{p}$	Plastic Strain Tensor

A.2.5 Material Constants:

k	Yield Stress in Simple Shear
Wo, α, B, N, σ^{*}	Constants

A.3 McDowell (1985) [10]

A.3.1 The Yield Surface:

$$\frac{3}{2} (\underset{\sim}{s} - \underset{\sim}{\alpha}):(\underset{\sim}{s} - \underset{\sim}{\alpha}) - R^2 = 0$$

A.3.2 The Limit Surface:

$$\frac{3}{2}\,(\underset{\sim}{s}^* - \underset{\sim}{\alpha}^*):(\underset{\sim}{s}^* - \underset{\sim}{\alpha}^*) - R^{*2} = 0$$

A.3.3 The Flow Rule:

$$\dot{\underset{\sim}{\varepsilon}}_p = \frac{1}{h}\,(\dot{\underset{\sim}{s}}:\underset{\sim}{n})\underset{\sim}{n}$$

where

$$h = k\left[1 + \frac{91960}{k}\left(\sinh\left\{\frac{|\underset{\sim}{s}^* - \underset{\sim}{s}|}{|\underset{\sim}{s}_0^* - \underset{\sim}{s}_0|}\right\}^{1.1}\right)\right],$$

$$\underset{\sim}{n} = \frac{\underset{\sim}{s} - \underset{\sim}{\alpha}}{|\underset{\sim}{s} - \underset{\sim}{\alpha}|}\,,$$

and

$$\dot{k} = \mu[k(\phi,q) - k]\,\psi_k\,\dot{n}$$

$$\bar{k}(\phi,q) = \phi[\bar{k}(1,q) - \bar{k}(0,q)] + k(0,q)$$

ψ_k = experimentally determined function

A.3.4 Hardening Rules For The Yield Surface:

$$\dot{R} = \mu[\bar{R}(\phi,q) - R]\,\psi\,\dot{n}$$

$$\dot{\underset{\sim}{\alpha}} = \frac{[(\underset{\sim}{s} - \underset{\sim}{\alpha}):\dot{\underset{\sim}{s}} - (2/3)R\dot{R}]\,(\underset{\sim}{s}^* - \underset{\sim}{s})}{(\underset{\sim}{s} - \underset{\sim}{\alpha}):(\underset{\sim}{s}^* - \underset{\sim}{s})}$$

where

$$\psi = u[\overline{R}^* (\phi,q) - R],$$

$$\underset{\sim}{s}^* = \underset{\sim}{\alpha}^* + (\underset{\sim}{s} - \underset{\sim}{\alpha}) \frac{R^*}{R},$$

$$\overline{R}(\phi,q) = \phi[\overline{R}(1,q) - \overline{R}(0,q)] + \overline{R}(0,q),$$

$$\dot{\eta} = (\dot{\underset{\sim}{\varepsilon}}_p : \dot{\underset{\sim}{\varepsilon}}_p)^{1/2}$$

and

$$\dot{\phi} = \mu^* (1 - J - \phi)\, \dot{\eta}\, u(1 - J - \phi_{limit}),$$

in which

$$J = \left| \frac{\frac{d}{dt} (\varepsilon_1 - \varepsilon_3)}{g[(\dot{\varepsilon})_1 - (\dot{\varepsilon})_3]} \right|,$$

$$u(x) = \begin{cases} 1 & \text{if } x \geq 0 \\ 0 & \text{if } x < 0, \end{cases}$$

$$g(x) = \begin{cases} 1 & \text{if } x = 0 \\ x & \text{if } x \neq 0, \end{cases}$$

ε_1 and ε_3 are the largest and smallest principal strains and $(\dot{\varepsilon})_1$ and $(\dot{\varepsilon})_3$ are the largest and smallest principal strain rates.

A.3.5 Hardening Rules For The Limit Surface:

$$\dot{R}^* = \mu \left[\bar{R}^* (\phi,q) - R^*\right] \psi^* \dot{\eta}$$

$$\dot{\underset{\sim}{\alpha}}^* = \kappa \, \dot{\eta} \, \underset{\sim}{n}$$

where

$$\psi^* = u[\bar{R} (\phi,q) - R^*],$$

$$\bar{R}^* (\phi,q) = \phi[\bar{R}^*(1,q) - \bar{R}(0,q)] - \bar{R}^*(0,q)$$

A.3.6 Definition and Changing Rules Of A Strain Memory Surface

$$F = \frac{2}{3} (\underset{\sim}{\varepsilon}^p - \underset{\sim}{\alpha}^p):(\underset{\sim}{\varepsilon}^p - \underset{\sim}{\alpha}^p) - q^2$$

$$\dot{q} = [\frac{1}{2} u(F) \, \Gamma - \Lambda(q)] \, \dot{\eta}$$

$$\dot{\underset{\sim}{\alpha}}^p = \frac{u(F)}{2} (\dot{\underset{\sim}{\varepsilon}}^p : \underset{\sim}{n}^*) \, \underset{\sim}{n}^*$$

and

$$\Gamma = \underset{\sim}{n}^* : \underset{\sim}{n} + \sqrt{6}\Lambda(q)$$

$\underset{\sim}{n}^*$ = unit normal tensor of the strain surface

$\Lambda(q)$ = experimentally determined function

A.3.7 Notation:

$\underset{\sim}{s}$	Deviatoric Stress Tensor for the Loading Surface
$\underset{\sim}{\alpha}$	Tensor for the Center of the Loading Surface
R	Radius of the Loading Surface
$\underset{\sim}{s}^*$	Deviatoric Stress Tensor for the Limit Surface
$\underset{\sim}{\alpha}^*$	Tensor for the Center of the Limit Surface
R^*	Radius of the Limit Surface
$\underset{\sim}{\varepsilon}_p$	Plastic Strain Tensor
$\underset{\sim}{\alpha}^p$	Tensor for the Center of the Strain Memory Surface
q	Radius of the Strain Memory Surface

A.3.8 Material Constants:

$k, \mu, \mu^*, \bar{R}(1,q), \bar{R}^*(1,q), \bar{k}(1,q),$

$\bar{R}(0,q), \bar{R}^*(0,q), \bar{k}(0,q)$

A.4 Naghdi and Nikkel (1986) [11]

A.4.1 The Loading Surface:

$$g = 4\mu^2 \left[\underset{\sim}{\gamma} - \left(1 + \frac{\hat{\alpha}}{4\mu}\right)\underset{\sim}{\gamma}^p\right]:\left[\underset{\sim}{\gamma} - \left(1 + \frac{\hat{\alpha}}{4\mu}\right)\underset{\sim}{\gamma}^p\right] - k \qquad \text{(strain space)}$$

$$f = (\underset{\sim}{\tau} - \frac{1}{2}\,\hat{\alpha}\underset{\sim}{\gamma}^{p}):(\underset{\sim}{\tau} - \frac{1}{2}\,\hat{\alpha}\underset{\sim}{\gamma}^{p}) - k \qquad \text{(stress space)}$$

where

$$\hat{\alpha} = \frac{(\alpha_o - \alpha_s)\ k + \alpha_s k_o - \alpha_o k_s}{k_o - k_s}$$

A.4.2 The Flow Rule:

$$\dot{\underset{\sim}{\gamma}}^{p} = \begin{cases} 0 & \text{if } g < 0 \text{ or } g = 0 \text{ and } \hat{g} \leq 0 \\ \dfrac{\hat{g}}{\Gamma+\Lambda}\,(2\underset{\sim}{\tau} - \hat{\alpha}\underset{\sim}{\gamma}^{p}) & \text{if } g = 0 \text{ and } \hat{g} > 0 \end{cases}$$

where

$$\hat{g} = 4\mu(\underset{\sim}{\tau} - \frac{1}{2}\,\hat{\alpha}\underset{\sim}{\gamma}^{p}):\dot{\underset{\sim}{\gamma}} \qquad \text{when } g = 0,$$

$$\Lambda = 8\mu k > 0,$$

$$\Gamma = 2\hat{\alpha}k + 2\Big[1 + \Big(\frac{\alpha_o - \alpha_s}{k_o - k_s}\Big)\ (\underset{\sim}{\tau} - \frac{\hat{\alpha}}{2}\,\underset{\sim}{\gamma}^{p}):\underset{\sim}{\gamma}^{p}\Big]$$

$$[\hat{\beta}\ \underset{\sim}{\tau} + \hat{\eta}\ \underset{\sim}{\gamma}^{p}] : [\underset{\sim}{\tau} - \frac{\hat{\alpha}}{2}\,\underset{\sim}{\gamma}^{p}]$$

A.4.3 Hardening Rules:

$$\dot{k} = [\hat{\beta}(k)\underset{\sim}{\tau} + \hat{\eta}(k)\underset{\sim}{\gamma}^p]:\underset{\sim}{\gamma}^p$$

where

$$\hat{\beta} = \left(\frac{k - k_s}{k_o - k_s}\right) \beta,$$

$$\hat{\eta} = \left(\frac{k - k_s}{k_o - k_s}\right) \eta$$

A.4.4 Notation:

$\underset{\sim}{\tau}$	Deviatoric Stress Tensor
$\underset{\sim}{\gamma}$	Total Deviatoric Strain Tensor
$\underset{\sim}{\gamma}^p$	Plastic Strain Tensor

A.4.4 Material Constants:

μ	Shear Modulus
α_o, α_s, β	Constants
ko, ks, η	

A.5 Banallal and Marquis (1987) [12]

A.5.1 The Flow Rule:

$$\dot{\underset{\sim}{\varepsilon}}^p = \frac{3}{2} \frac{\underset{\sim}{s} - \underset{\sim}{x}}{J_2(\underset{\sim}{s}-\underset{\sim}{x})} \dot{p}$$

where

$$\dot{p} = u\{[\frac{J_2(\underset{\sim}{s}-\underset{\sim}{x}) - R - K}{K}]^n\}$$

$$J_2 = [\frac{3}{2}(\underset{\sim}{s}-\underset{\sim}{x}):(\underset{\sim}{s}-\underset{\sim}{x})]^{\frac{1}{2}}$$

in which

$$u(x) = \begin{cases} 1 & \text{if } x = 0 \\ x & \text{if } x \neq 0, \end{cases}$$

A.5.2 Hardening Rules:

$$\dot{R} = \gamma(Q - R)\,\dot{p}$$

$$\dot{\underset{\sim}{x}} = c\,[\frac{2}{3}\,a\,\dot{\underset{\sim}{\varepsilon}}^p - \phi(p)\,\underset{\sim}{x}\dot{p}]$$

where

$$\dot{Q} = D(A)\,[Q_{AS}(A) - Q]\,\dot{p},$$

$$\phi(p) = \phi_\infty + (1 - \phi_\infty)\exp(-\overline{W}p),$$

$$D(A) = (d - f)\,A + f,$$

$$Q_{AS}(A) = \frac{gAQ_\omega + (1 - A)\,Q_o}{gA + (1 - A)}$$

$$A = \sin^2(\alpha)$$

in which

$$\alpha = \cos^{-1} \left[\frac{\dot{\underset{\sim}{\varepsilon}}^{p} : \dot{\underset{\sim}{s}}}{(\dot{\underset{\sim}{\varepsilon}}^{p} : \dot{\underset{\sim}{\varepsilon}}^{p})(\dot{\underset{\sim}{s}} : \dot{\underset{\sim}{s}})}\right]$$

A.5.3 Notation:

$\underset{\sim}{s}$	Deviatoric Stress Tensor
$\underset{\sim}{x}$	Tensor of the Center of the Loading Surface
$\underset{\sim}{\varepsilon}^{p}$	Plastic Strain Tensor

A.5.3 Material Constants:

$k, \gamma, K, \alpha, n, c, Q_o, Q_\infty, g, d, f, \phi_o, \phi_\infty$

VITA

Shiing-Hwa Doong was born on November 15, 1959 in Taiwan, The Republic of China. He was educated at Cheng Kung Senior High School in Taipei, Taiwan. He attended the National Cheng-Kung University and received a B.S. Degree in Hydraulic Engineering in May 1981. From 1981 to 1983, he served as a training officer in the military of Taiwan. In August 1983, Shiing-Hwa came to the United States and started his graduate studies in the University of California, Berkeley where he received a M.S. Degree in Civil Engineering. In January 1985, he joined the Sargent & Lundy Association in Chicago and worked as a Structural Engineer for one year. He entered the University of Illinois at Urbana-Champaign to pursue his doctoral degree in Mechanical Engineering in January 1986. During the majority of his graduate education in the University of Illinois, he was supported as a research assistant by the Department of Energy. Shiing-Hwa will join the Material Research Laboratory at the University of Illinois as a post-doctoral researcher in July of this year.